Institut für Konstruktion und Entwurf
Stahl- Holz- und Verbundbau
Universität Stuttgart

Stability of steel plates under combined loading

Benjamin Braun

Mitteilungen

Oktober 2010 Nr. 2010-3

Stability of steel plates under combined loading

Von der Fakultät Bau- und Umweltingenieurwissenschaften
der Universität Stuttgart zur Erlangung der Würde eines Doktors der
Ingenieurwissenschaften (Dr.-Ing.) genehmigte Abhandlung

Vorgelegt von

Benjamin Thorsten Braun

aus Stuttgart

Hauptberichter:	Prof. Dr.-Ing. Ulrike Kuhlmann
Mitberichter:	Prof. Dr. Bernt Johansson
	Prof. Dr. Joël Raoul
Tag der mündlichen Prüfung:	13. Oktober 2010

Institut für Konstruktion und Entwurf der Universität Stuttgart

2010

Mitteilungen des Instituts für Konstruktion und Entwurf; Nr. 2010-3

Benjamin Braun — Stability of steel plates under combined loading

Herausgeber — Prof. Dr.-Ing. Ulrike Kuhlmann
Pfaffenwaldring 7
70569 Stuttgart
Germany
Telefon: +49 (0)711 - 685 66245
Telefax: +49 (0)711 - 685 66236

Redaktion — Dipl.-Ing. Bernadette Froschmeier

D 93

ISSN 1439-3751

Vollkommenheit entsteht nicht dann, wenn man nichts mehr hinzuzufügen hat, sondern wenn man nichts mehr wegnehmen kann.

Antoine de Saint-Exupéry
Terre des Hommes (1939), III: L'Avion, S. 60

Vorwort

Die vorliegende Arbeit entstand während meiner Tätigkeit als wissenschaftlicher Mitarbeiter am Institut für Konstruktion und Entwurf der Universität Stuttgart. Frau Professorin Ulrike Kuhlmann, Direktorin des Instituts, danke ich sehr herzlich für das entgegengebrachte Vertrauen und die Übernahme des Hauptberichts. Darüber hinaus bedanke ich mich recht herzlich für ihre stetige Unterstützung und die Förderung meines Forschungsaufenthalts an der Luleå Tekniska Universitet, Schweden.

Mein aufrichtiger Dank gilt auch Herrn Professor Bernt Johansson, Luleå Tekniska Universitet, Schweden, und Herrn Professor Joël Raoul, École Nationale des Ponts et Chaussées (ENPC), Paris, Frankreich, für ihr Interesse an meiner Arbeit, die kritische Durchsicht und die Übernahme des Mitberichts.

Ein Teil dieser Arbeit stützt sich auf experimentelle und theoretische Untersuchungen, die im Rahmen des Forschungsprojekts „Competitive Steel and Composite Bridges for Improved Steel Plated Structures“ (COMBRI) durchgeführt wurden. Ich bedanke mich für die finanzielle Unterstützung durch den Research Fund for Coal and Steel (RFCS), Brüssel, Belgien, und die inspirierende Zusammenarbeit mit allen am Projekt beteiligten Partnern.

Zu großem persönlichem Dank verpflichtet bin ich dem Deutschen Akademischen Auslandsdienst (DAAD) für die finanzielle Unterstützung meines richtungsweisenden Forschungsaufenthalts an der Luleå Tekniska Universitet, Schweden. An dieser Stelle danke ich Herrn Professor Schew-Ram Mehra, stellvertretender Leiter des Lehrstuhls für Bauphysik der Universität Stuttgart, für die Erstellung des Gutachtens zu meiner Person. Des Weiteren bedanke ich mich recht herzlich bei der Deutschen Forschungsgemeinschaft (DFG) für die finanzielle Unterstützung zur Teilnahme an zwei Konferenzen in Brisbane und Sydney, Australien.

Ein Dank gilt auch meinen Kolleginnen und Kollegen am Institut für Konstruktion und Entwurf für die Anregungen und die gute Zusammenarbeit. Dies gilt insbesondere denjenigen, ohne die die Zeit nur halb so schön gewesen wäre.

Ein ganz besonderer Dank gilt meinen Eltern und meiner Frau für ihre stetige Unterstützung und ihr Vertrauen, sowie der Geduld und Toleranz bei der Anfertigung dieser Arbeit.

Stuttgart, im Juni 2010 Benjamin Braun

Kurzfassung

Ziel der Arbeit ist es, das Interaktionsverhalten stabilitätsgefährdeter, stählerner Platten für ausgewählte Beanspruchungskombinationen zu analysieren und Bemessungsgleichungen zu entwickeln, die Unzulänglichkeiten von EN 1993-1-5:2006 beheben.

- **Platten unter biaxialem Druck und Anwendung der Methode der reduzierten Spannungen basierend auf einem einzigen Plattenschlankheitsgrad.** Bislang wurde die Interaktionsgleichung für biaxial druckbeanspruchte Platten lediglich anhand sehr weniger Ergebnisse überprüft und im Vergleich zu den bewährten Regelungen nach DIN 18800-3:1990 weicht sie deutlich ab. Das Interaktionsverhalten wird daher für die Basislastkombination „biaxialer Druck“ untersucht und die Plausibilitätskriterien zur Übertragbarkeit der Ergebnisse z.B. auf die Beanspruchungskombination Querspannung (patch loading) und Biegespannung werden diskutiert. Eine Modifikation der Interaktionsgleichung wird vorgeschlagen.
- **Interaktion zwischen Querbelastung, Biegemoment und Querkraft in Stegblechen von I-Trägern (F-M-V) und Anwendung der Methode der wirksamen Breiten**. Für die Interaktion zwischen Querbelastung und Querkraft wird derzeit keine Bemessungsgleichung angeboten. Einige wenige Untersuchungen in der Literatur zeigen jedoch eine gegenseitige Beeinflussung der beiden Beanspruchungsarten. Experimentelle und numerische Untersuchungen werden durchgeführt, um das Stabilitätsverhalten zu analysieren und ein Interaktionskriterium herzuleiten, das abschließend um den Biegemomenteneinfluss ergänzt wird.

Die Ergebnisse dieser Arbeit ermöglichen die zuverlässige und sichere Anwendung der Methode der reduzierten Spannungen basierend auf einem einzigen Plattenschlankheitsgrad als Nachweisverfahren für biaxial druckbeanspruchte Platten. Der Vorschlag erweitert zudem das bestehende Bemessungsverfahren um die Möglichkeit, günstig wirkende Randlagerungseffekte der Platte bei der Ermittlung der elastisch kritischen Spannungen zu berücksichtigen. Dies stellt einen wesentlichen Beitrag für einen numerisch gestützt zu führenden Nachweis in Zukunft dar. Für die Methode der wirksamen Breiten wird für den Nachweis der F-V-Interaktion eine Bemessungsgleichung vorgeschlagen, die mit der vorhandenen F-M-Interaktionsgleichung harmonisiert wird, um auch den Biegemomenteneinfluss erfassen zu können.

Schlagwörter:
Stabilität, Plattenbeulen, Interaktion, Stahlbau

Abstract

The objective of this work is to analyse the stability behaviour of steel plates under selected load combinations and to develop design rules which resolve shortcomings of EN 1993-1-5:2006.

- **Plates under biaxial compression and application of the reduced stress method based on a single plate slenderness.** The interaction equation was checked with merely few results for plates under biaxial compression so far. However, in comparison to the proven rules of DIN 18800-3:1990 it shows significant discrepancies. The stability behaviour is studied for the basic load combination "biaxial compression" and the plausibility criteria for the transferability of the results e.g. to the load combination of transverse stress (patch loading) and bending stress are discussed. A modification of the interaction equation is proposed.
- **Plate I-girder webs under transverse patch loading, bending moment and shear force (F-M-V) and application of the effective width method**. At present there is no interaction criterion for the load combination of transverse patch loading and shear force. However, a few studies from literature show that these two loadings interact. Experimental and numerical studies are carried out in order to analyse the stability behaviour and to develop an interaction criterion which is finally enhanced with the effect of bending moment.

The results of this work enable a reliable and safe application of the reduced stress method based on a single plate slenderness as verification method for plates under biaxial compression. Besides that, the proposal adds the possibility to take into account favourable edge boundary conditions for the determination of the elastic critical stresses. This essentially contributes to a numerically assisted verification procedure in the future. For the effective width method an interaction equation is proposed for the load combination "transverse patch loading and shear force (F-V)" which is harmonised with the existing F-M interaction equation to take also into account the effect of bending moment.

Keywords:
stability, plate buckling, interaction, steel structures

Contents

Notations **V**

1 Introduction **1**
1.1 Motivation . . . 1
1.2 Objective and scope . . . 2
1.3 Outline . . . 3

2 Stability behaviour of steel plated structures and design methods **5**
2.1 General . . . 5
2.2 Stability behaviour due to basic load effects . . . 6
2.2.1 Longitudinal stresses . . . 6
2.2.2 Shear stresses . . . 8
2.2.3 Transverse stresses (patch loading) . . . 9
2.3 Design methods of selected standards . . . 10
2.3.1 Prerequisite: Linear buckling theory . . . 10
2.3.2 DIN 18800-3:1990 . . . 15
2.3.3 DNV-RP-C201:2002 . . . 19
2.3.4 EN 1993-1-5:2006 . . . 24
2.3.4.1 General . . . 24
2.3.4.2 Reduced stress method . . . 26
2.3.4.3 Effective width method . . . 31
2.3.5 Comparison and evaluation of design methods . . . 36
2.4 Recent research works on patch loading resistance . . . 39
2.4.1 General . . . 39
2.4.2 Davaine (2005) . . . 40
2.4.3 Gozzi (2007) . . . 40
2.4.4 Clarin (2007) . . . 41
2.5 Summary . . . 42

3 Review and evaluation of earlier work **43**
3.1 General . . . 43
3.2 Plates under biaxial compression . . . 43
3.2.1 Becker et al. (1970/1977) . . . 43
3.2.2 Frieze et al. (1977) . . . 47
3.2.3 Valsgard (1978/1979) . . . 48

3.2.4 Dier and Dowling (1979/1980) . . . 51
3.2.5 Jungbluth and Kubsch (1980) . . . 53
3.2.6 Harding (1983) . . . 53
3.2.7 Narayanan and Shanmugan (1983) . . . 56
3.2.8 Stonor et al. (1983) . . . 56
3.2.9 Dinkler and Kröplin (1984) . . . 59
3.2.10 Davidson et al. (1989) . . . 59
3.2.11 Guedes Soares and Gordo (1995) . . . 61
3.2.12 Cui et al. (2002) . . . 63
3.2.13 Evaluation of results . . . 64
3.3 Girders subjected to transverse patch loading and shear force . . . 67
3.3.1 General . . . 67
3.3.2 Elgaaly (1975) . . . 69
3.3.3 Oxfort, Weber and Gauger (1981/1989) . . . 69
3.3.4 Roberts and Shahabian (2000) . . . 70
3.3.5 Evaluation of results . . . 71
3.4 Summary . . . 74

4 Experimental studies 77
4.1 Test programme . . . 77
4.2 Test specimens . . . 77
4.2.1 Dimensions . . . 77
4.2.2 Material properties . . . 78
4.2.3 Geometric imperfections . . . 78
4.3 Test set-up . . . 80
4.3.1 General . . . 80
4.3.2 Loading device . . . 81
4.3.3 Measuring devices . . . 81
4.4 Test procedure . . . 83
4.4.1 General . . . 83
4.4.2 Girder SP 600 . . . 83
4.4.3 Girder SP 1200 . . . 85
4.5 Test results . . . 86
4.6 Summary . . . 88

5 Theoretical studies 91
5.1 General . . . 91
5.2 Input data of the finite element analysis . . . 92
5.2.1 Modelling . . . 92
5.2.1.1 Geometry . . . 92
5.2.1.2 Material properties . . . 92
5.2.1.3 Loading and boundary conditions . . . 94
5.2.1.4 Imperfections . . . 95

5.2.2 Discretisation . . . 97
5.2.3 Numerical analyses . . . 99
5.2.3.1 Linear bifurcation analysis . . . 99
5.2.3.2 Nonlinear buckling analysis . . . 100
5.3 Verification of the numerical model . . . 102
5.3.1 General . . . 102
5.3.2 Recalculation of buckling curves . . . 102
5.3.2.1 Plates under compression . . . 102
5.3.2.2 Plates under compression susceptible to column-like buckling . . . 105
5.3.3 Recalculation of own experiments . . . 106
5.3.4 Recalculation of experiments from literature . . . 109
5.3.5 Conclusions . . . 112
5.4 Plate stability under biaxial compression . . . 113
5.4.1 General . . . 113
5.4.2 Structural behaviour . . . 113
5.4.3 Effect of imperfections . . . 115
5.4.4 Effect of edge boundary conditions . . . 117
5.4.5 Conclusions . . . 117
5.5 Girder web stability under transverse patch loading and shear force . . . 125
5.5.1 General . . . 125
5.5.2 Structural behaviour . . . 127
5.5.3 Effect of slenderness ratio . . . 130
5.5.4 Effect of end-post condition . . . 130
5.5.5 Effect of loading length . . . 132
5.5.6 Effect of longitudinal stiffener . . . 133
5.5.7 Conclusions . . . 140
5.6 Summary . . . 141

6 Proposal and justification of improved design rules for EN 1993-1-5:2006 143
6.1 General . . . 143
6.2 On the general formulation of an interaction equation . . . 143
6.3 On the choice of a verification point . . . 146
6.4 Reduced stress method . . . 148
6.4.1 General . . . 148
6.4.2 Evaluation of current design rules . . . 148
6.4.3 Proposal for improved design rules . . . 153
6.5 Effective width method . . . 164
6.5.1 General . . . 164
6.5.2 Evaluation of current proposals . . . 167
6.5.2.1 Transverse patch loading and shear force . . . 167
6.5.2.2 Transverse patch loading and bending moment . . . 169

6.5.3 Proposal for improved design rules . . . 179
6.5.3.1 Transverse patch loading and shear force (F-V) . . . 179
6.5.3.2 Enhancement of the F-V proposal with bending moment . 185
6.6 Conclusions . . . 188

7 Summary and outlook 191
7.1 Summary . . . 191
7.2 Outlook . . . 192

A Specimen data of girders under transverse patch loading and shear force 205
A.1 Girders without longitudinal stiffeners . . . 205
A.2 Girders with longitudinal stiffeners . . . 208

B Specimen data of girders under transverse patch loading and bending moment 211
B.1 Girders without longitudinal stiffeners . . . 211
B.2 Girders with longitudinal stiffeners . . . 216

C Proposal for a modification of EN 1993-1-5:2006 225
C.1 Reduced stress method . . . 225
C.2 Effective width method . . . 226

Notations

General definitions

- Compressive stresses are taken as positive unless otherwise stated
- The x-direction is the longitudinal direction of the plate, i.e. usually the long dimension
- The y- or z-direction is the transverse direction of the plate, i.e. usually the short dimension
- An unconstrained edge boundary condition defines an edge which is free to move in-plane
- A constrained edge boundary condition defines an edge which remains straight

Roman letters

a	length of plate, subpanel or stiffened panel; web length
b	width of plate, subpanel or stiffened panel
b_1	clear height of the directly loaded subpanel under patch loading
C_x	see ρ_x
C_τ	see χ_w
D	$= [E \cdot t^3]/[12 \cdot (1 - \nu^2)]$, flexural rigidity of a plate strip of unit width
E	Young's modulus, elastic modulus
e_N	shift of the position of the neutral axis
F	transverse force (patch loading)
f_y	characteristic yield strength
h_w	web height
$I_{s\ell,1}$	second moment of area of the longitudinal stiffener
k	buckling coefficient
K	Gaussian curvature
l	see b
M	bending moment
N	axial force, normal force
R_{cr}	elastic critical buckling strength
R_u	ultimate buckling strength

R_y	yield strength
s	see b
s_s	patch loading length
t	plate thickness
V	shear force
u	displacement
w_0	initial geometric imperfection amplitude

Greek letters

α	$= a/b$, panel aspect ratio
α; α_p	imperfection factor used in buckling curves
γ_M	partial factor for materials
ε	strain
η	utilisation factor
κ	see ρ
κ_K	see χ_c
κ_{PK}	see ρ_c
$\overline{\lambda}$	slenderness
$\overline{\lambda}_c$	$= \sqrt{f_y/\sigma_{cr,c}}$, column slenderness
$\overline{\lambda}_F$	$= \sqrt{F_y/F_{cr}}$, slenderness for patch loading
$\overline{\lambda}_p$	$= \sqrt{f_y/\sigma_{cr,p}} = \sqrt{\alpha_{ult,k}/\alpha_{cr}}$, plate slenderness
$\overline{\lambda}_{p0}$	plateau length
$\overline{\lambda}_w$	$= \sqrt{f_y/\tau_{cr}}$, plate slenderness for shear stress
ν	Poisson's ratio, taken as 0.3 throughout this work
$\rho(\overline{\lambda})$	buckling curve function
ρ	reduction factor
ρ_c	interpolated reduction factor taking column-like buckling into account
σ	stress
σ_1	principal tensile stress
σ_2	principal compressive stress
σ_c	compressive residual stress
$\sigma_{cr,p}$	elastic critical plate-buckling stress
$\sigma_{cr,c}$	elastic critical column-buckling stress
σ_E	Euler stress
σ_{Ki}	see $\sigma_{cr,c}$
σ_{Pi}	see $\sigma_{cr,p}$
σ_t	tensile residual stress
χ_c	reduction factor for column-like buckling
χ_w	reduction factor for shear stress
τ	shear stress

Subscripts

0	single loading direction
avg	average
c	referring to a column
comp	compressive
d	design value
Ed	load value (EN rules)
eff	effective cross-section properties
exp	experimental value
f	flange
k	characteristic value
min	minimum value
num	numerical value
p	referring to a plate
P,R,d	design value taking buckling into acount (DIN rules)
Rd	design value taking buckling into acount (DNV rules)
Sd	load value (DNV rules)
tens	tensile
τ	shearing direction
w	web
x	longitudinal direction
y	see z; yield
z	transverse direction

Acronyms

BSK	Boverkets handbok om Stålkonstruktioner
COV	coefficient of variation
DIN	Deutsches Institut für Normung
DNV	Det Norske Veritas
EBC	European buckling curve
EN	European standard
FEA	finite element analysis
FEM	finite element method
GMNIA	geometrically and materially nonlinear analysis with imperfections included
LA	linear elastic analysis
LBA	linear bifurcation analysis
LVDT	linear variable displacement transducer
MNA	materially nonlinear analysis
RFCS	Research Fund for Coal and Steel
SP	shear- and patch loading

1 Introduction

1.1 Motivation

Steel plated structures are used in many fields of application including plate and box girder bridges or heavy crane runway beams, but also ships, offshore platforms, power and chemical plants. During their lifetime, these structures are subjected to various types of loading in construction and final stages. Most of them are operational (servicability limit states) but in some cases may be extremal (ultimate limit states). The loadings often induce a complex state of stress in the plate. In civil engineering application such a highly demanding design situation is patch loading of a girder, as it occurs e.g. during incremental launching of a bridge girder or when wheel loads act on a crane runway beam. As the position of the load introduction changes continuously, stiffeners cannot be provided at all positions so that panels are prone to buckling. Moreover, these panels are usually not only loaded by a transverse force but also in combination with bending moment and shear force. The loading in such a plate can be decomposed into three basic load effects: transverse loading, bending moment and shear force, see Fig. 1.1. It can be seen that transverse loading and bending moment is a specific loading type of a biaxial compression state on which this work has one focus.

In EN 1993-1-5 [46] the interaction formulas of design methods are either not fully validated or not complete. The reduced stress method according to Chapter 10, EN 1993-1-5 [46], provides an interaction equation which is based on a single plate slenderness. It was checked with merely few results for plates under biaxial compression so far. However, in comparison to the proven rules of DIN 18800-3 [28], it shows significant discrepancies which require clarification. The interaction criterion related to the effective width method

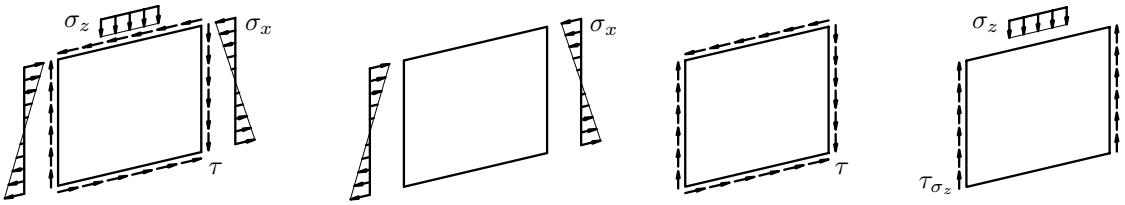

(a) Combined loading (b) Bending stress (c) Shear stress (d) Transverse stress

Figure 1.1: Plate under combined loading (a) and basic load effects (b-d)

according to Sec. 7.2, EN 1993-1-5 [46], addresses the interaction of transverse loading and bending moment, but transverse loading and shear force is not accounted for. However, a small experimental study in [115] shows that these two loadings interact so that the development of an interaction criterion is necessary. Both shortcomings are the motivation of this work in order to provide safe and reliable design rules for the interaction under biaxial compression and under transverse loading, bending moment and shear force.

1.2 Objective and scope

The objective of this work is to analyse the stability behaviour of steel plated structures under selected load combinations and to develop design rules which resolve shortcomings of current EN 1993-1-5 [46].

- **Plates under biaxial compression and application of the reduced stress method based on a single plate slenderness.** The interaction equation was checked with merely few results for plates under biaxial compression so far. However, in comparison to the proven rules of DIN 18800-3 [28], it shows significant discrepancies. The stability behaviour is studied for the basic load combination biaxial compression and the plausibility criteria for the transferability of the results e.g. to the load combination of transverse stress (patch loading) and bending stress are discussed. The results should enable a reliable and safe application of the reduced stress method based on a single plate slenderness as verification method for plates under biaxial compression. Besides that, the proposal should add the possibility to take into account favourable edge boundary conditions for the determination of the elastic critical stresses in order to facilitate numerically assisted verification procedures.
- **Plate I-girder webs under transverse patch loading, bending moment and shear force (F-M-V) and application of the effective width method.** At present there is no interaction criterion for the load combination of transverse loading and shear force. However, a few studies in literature show that these two loadings interact [115]. Experimental and numerical studies are carried out in order to analyse the stability behaviour and to develop an interaction criterion which should be finally enhanced with the effect of bending moment.

This work focuses on plate buckling effects of steel plates under biaxial compression in general and plate I-girder webs with transverse patch loading as leading loading. Transverse loading is understood herein as patch loading along one part of the edge only.

1.3 Outline

Chapter 2 provides a concise overview of the stability behaviour of steel plated structures due to basic load effects. Relevant knowledge and terms about load-carrying mechanisms in plates subjected to longitudinal stresses, shear stresses and transverse stresses (patch loading) are introduced with regard to the interpretation of earlier work and experimental and theoretical studies about the interaction behaviour in Chapters 3 to 5.

Besides that, characteristics of different standards and design methods, such as the reduced stress method and the effective width method, are presented. Especially the design rules of EN 1993-1-5 [46] are compared and reasons are given to improve them. Current developments in patch loading resistance models are also shortly presented.

Chapter 3 reviews earlier work about plates under biaxial compression and plate I-girder webs under transverse patch loading and shear force. Other interaction cases such as transverse patch loading and bending moment are intentionally omitted because they have been comprehensively covered in other works [24, 77, 114]. Together with the collected experimental and numerical data from literature which is given in Appendices A and B, this state of the research is used to identify shortcomings which are then studied with own experiments, Chapter 4, and theoretical studies, Chapter 5.

Chapter 4 summarises the results from the own experimental study which complements the existing studies in the field of interaction between transverse patch loading and shear force.

In **Chapter 5** numerical studies based on the finite element method are carried out. Besides the recalculation of buckling curves, selected experiments from literature and from Chapter 4 are used to verify the chosen numerical modelling. Parameter studies are conducted to analyse systematically the stability behaviour of plates under biaxial compression and plate I-girder webs under transverse patch loading and shear force.

In **Chapter 6** improved design rules are proposed for plates under biaxial compression and application of the reduced stress method based on a single plate slenderness, and for plate I-girder webs under transverse patch loading, bending moment and shear force and application of the effective width method. Both proposals are verified based on the experimental and numerical database which has been established in Chapters 4 and 5. Their impact on EN 1993-1-5 [46] is formulated as modification of the existing design rules in Appendix C.

In **Chapter 7** a summary of the work is given. An outlook stipulates topics for future research work.

2 Stability behaviour of steel plated structures and design methods

2.1 General

This work focuses on plate buckling effects of cross-sectional elements under in-plane loadings. These loadings can be stresses in longitudinal and transverse direction, shear stresses and stresses induced by patch loading. As the buckling process is a highly complex process which involves nonlinear stress distributions, load shedding effects between cross-sectional elements and effects of boundary conditions, this chapter gives an overview of relevant knowledge and design methods of selected standards.

Section 2.2 introduces the nonlinear stability behaviour of plates and plated structures due to basic load effects. Relevant effects which are necessary for the understanding of later chapters are explained in a concise manner. The interaction behaviour is not adressed here since it is reviewed in Chapter 3.

In Sec. 2.3 the design methods of selected standards are presented. The shortcomings of EN 1993-1-5 [46] which are one motivation of this work are identified. After a brief aside about linear buckling theory, the methods which are provided in current standards DIN 18800-3 [28], EN 1993-1-5 [46] and offshore design code DNV-RP-C201 [33] are described. The focus is on biaxial compression and interaction between transverse patch loading, bending moment and shear force. Whereas all standards contain a design method based on the reduced stress method, EN 1993-1-5 comprises also the effective width method and recommendations for the application of numerical methods.

Section 2.4 summarises recent developments in patch loading resistance models which are most likely to be used in the future and which are relevant for the evaluation of the proposals in Chapter 6.

In order to prevent this chapter from becoming unmanagable in length, only the minimal necessary effort is made to introduce the knowledge which is the basis of this work later on. Readers interested in pursuing any of these points further are urged to consult e.g. [7, 38, 67, 90] in which much of the basic knowledge is presented in far greater detail.

2.2 Stability behaviour due to basic load effects

2.2.1 Longitudinal stresses

In contrast to columns and shells, steel plated cross-sections under longitudinal stress can possess a significant postcritical strength reserve which results from favourable membrane actions perpendicular to the loading direction and from load shedding to cross-sectional elements which are less utilised.

Plate-like behaviour. Figure 2.1 illustrates the postcritical strength reserve from membrane actions for a square plate under uniform compression. Before buckling of the plate occurs, the compressive stresses are equally distributed over the plate width, see Fig. 2.1a. Both geometric and material imperfections may influence the onset of buckling. Residual stresses usually occur as compressive stresses in mid-plate which in turn leads to a loss of stiffness. Due to the higher stiffness near the edges, the applied stresses redistribute nonlinearly and reach higher stress values there. Tensile membrane stresses occur perpendicular to the loading direction which can be assessed by large deflection theory. However, for high slendernesses the amount of these stabilising membrane stresses also depends on the edge boundary conditions. The two extremal edge configurations "unconstrained" and "constrained" are shown at the top in Figs. 2.1b and 2.1c. For the unconstrained case, there is no in-plane restraint and it depends on the plate's edge stiffness to which amount tensile stresses develop. For the constrained case, edges are assumed to remain straight as it is e.g. the case for subpanels in multi-stiffened panels.

Column-like behaviour. The favourable plate-like behaviour relies on the double curvature of the plate after the onset of buckling. However, if the deformed plate curvature becomes developable, i.e. the Gaussian curvature K of the plate approaches zero ($K \to 0$), the favourable effect of the tensile membrane stresses is reduced. Such a single curvature occurs depending on the geometry of the plate or the stiffness ratio from loaded and unloaded direction e.g. due to stiffening. Figure 2.2 shows these two cases when column-like behaviour is likely to occur.

Plated cross-section behaviour. Each single plate is usually bounded by one or more cross-sectional elements. In a plated structure, the individual plates may have different levels of utilisation so that the load shedding of stresses from a highly utilised cross-sectional element to less utilised ones may further increase the resistance. In such a case, it is required that the material allows for large strains without loosing strength.

Effect of stiffeners. Generally, it can be distinguished between weak stiffeners which buckle themselves under loading and strong stiffeners which enforce buckling of the subpanels instead. Subpanel buckling can be treated similar to buckling of a single plate element. In case of stiffener buckling it has to be distinguished between the minimum stiffener's stiffness based on a bifurcation analysis and the minimum stiffener's stiffness when loading up to ultimate load is considered. The objective of a stiffener is to increase the resistance. Thus, modern stiffeners are usually strong and possess a closed cross-

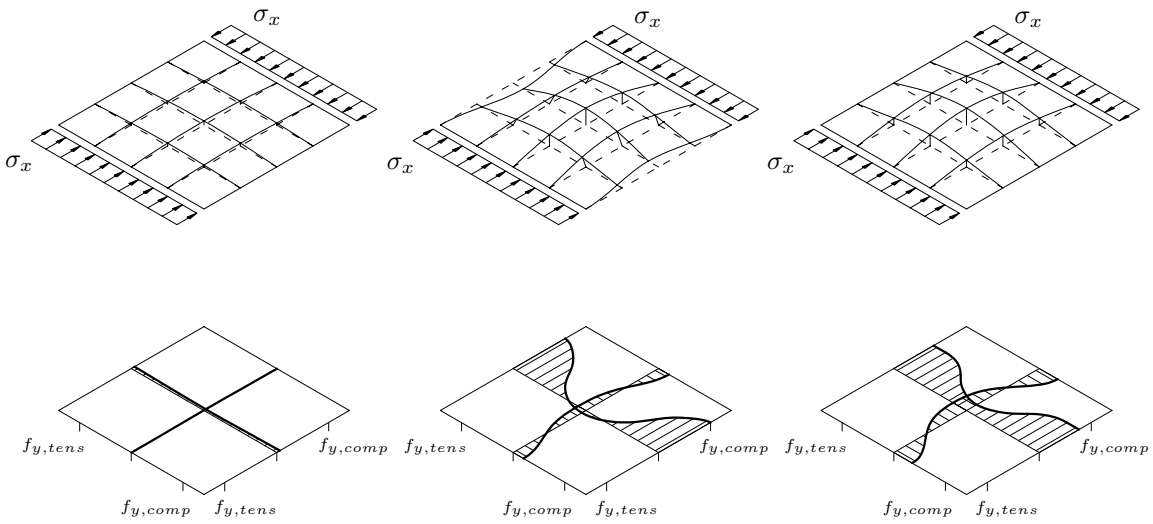

(a) stress distribution before buckling

(b) stress distribution at ultimate load with **unconstrained** edge boundary condition of the unloaded edges

(c) stress distribution at ultimate load with **constrained** edge boundary condition of the unloaded edges

Figure 2.1: Stability behaviour of a single plate ($b/t = 100$, $f_y = 355$ MPa)

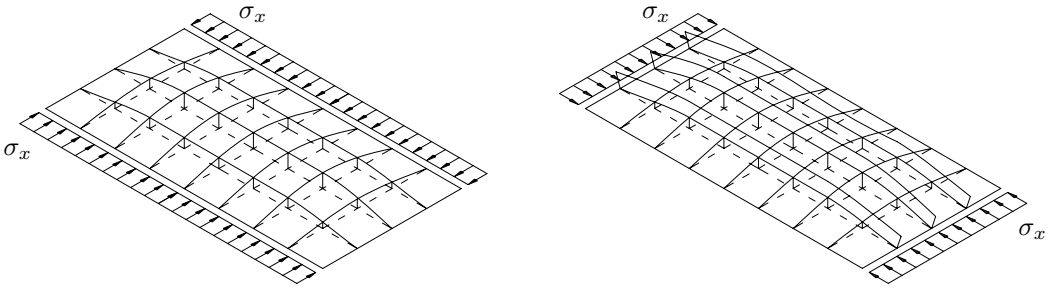

(a) small panel aspect ratio

(b) stiffened panel

Figure 2.2: Examples of column-like buckling of a plate

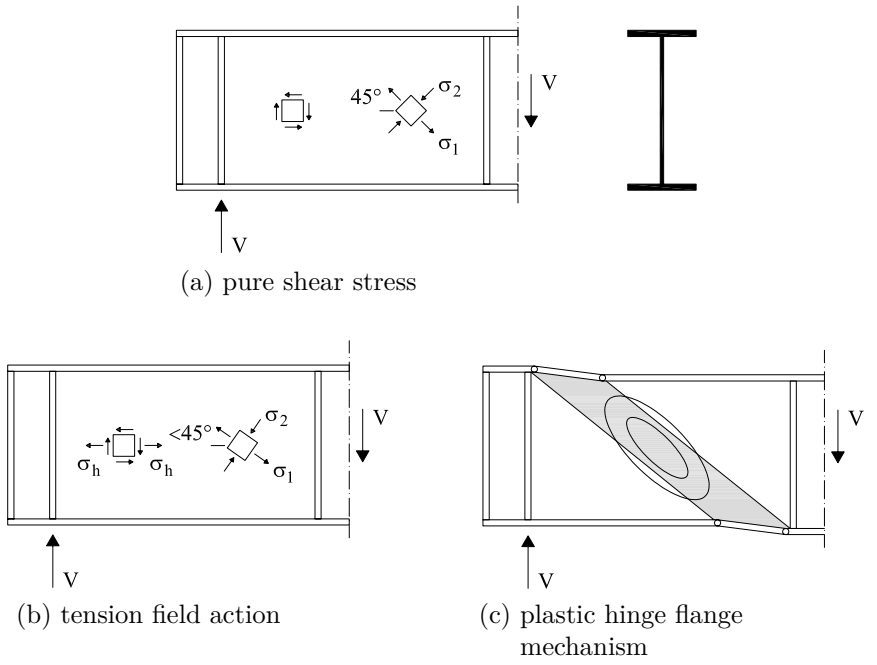

Figure 2.3: Stress states and collapse behaviour of an I-plate girder subjected to shear

section with a substantial torsional rigidity. In case load shedding is taken into account, the stiffener has to be able to sustain the additional compressive strain without failure.

2.2.2 Shear stresses

The behaviour of plates under shear comprises two phenomena: the state of pure shear stress and the tension field. Prior to buckling, pure shear stresses occur in the plate. When these shear stresses are transformed into principal stresses, they correspond to principal tensile stresses σ_1 and principal compressive stresses σ_2 with equal magnitude and inclined by 45° with regard to the longitudinal axis of the girder. In this case only constant shear stresses occur at the edges, see Fig. 2.3a.

As for plates subjected to longitudinal compressive stress, slender plates under shear possess a postcritical strength reserve. After buckling, the plate reaches the post-critical stress state while a shear buckle forms in the direction of the principal tensile stresses σ_1. Due to buckling no significant increase of the stresses in the direction of the principal compressive stresses σ_2 is possible whereas the principal tensile stresses may still increase. As a result, stress values of different magnitude occur (tension > compression), which lead to a rotation of the stress field for equilibrium reasons and which is denoted tension field action, see Fig. 2.3b. The development of such a tensile force is only possible if the boundary elements, mainly the flanges, provide a sufficient anchorage for the axial forces. The maximum amount of axial force which can be carried depends on the extensional stiffness and flexural rigidity of the boundary element. When reaching ultimate load a plastic hinge mechanism forms in the flange, see Fig. 2.3c.

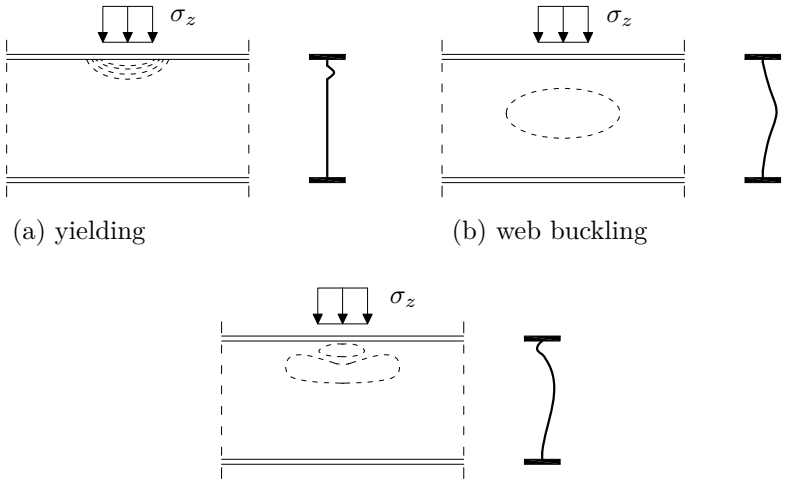

(a) yielding (b) web buckling

(c) web crippling

Figure 2.4: Collapse modes of girders under transverse patch loading

2.2.3 Transverse stresses (patch loading)

The behaviour of plates under transverse stress can be described with the phenomena which were introduced in Sec. 2.2.1 presuming that the whole edge is loaded. Due to their geometry, such plates are often prone to column-like buckling.

However, transverse loading may also describe a concentrated load which is partially applied perpendicular to the panel edge in the plane of the plate. This loading is referred to as "patch loading". In civil engineering application such a highly demanding design situation occurs e.g. during incremental launching of a bridge girder or when the wheel loads act on a crane runway beam. As the position of the load introduction changes continuously, stiffeners cannot be provided at all positions so that panels are prone to buckling. Due to the nature of the load application, flanges are often existent through which the load is applied. The flanges effect the load-carrying behaviour to a great extent and in some cases a plastic hinge flange mechanism develops in the loaded flange which increases the resistance. The collapse behaviour of girders under transverse patch loading may be characterised by the three failure types yielding, buckling or crippling of the web, see Fig. 2.4. In reality, however, an accurate separation of these phenomena is neither possible nor feasible.

It should be noted that in case of transverse patch loading the assumption that the loaded edges remain straight is usually not true because the loaded flange deforms.

2.3 Design methods of selected standards

2.3.1 Prerequisite: Linear buckling theory

Although the elastic critical buckling load has been the starting point for an understanding of plate buckling behaviour, it turned out that the linear buckling theory alone is not an appropriate predictor for the ultimate buckling strength according to nonlinear buckling theory. Some plates possess a considerable post-critical strength reserve whereas others are affected by detrimental column-like behaviour. Since linear buckling theory assumes a perfect geometry and linear material behaviour, the elastic critical buckling load can be explicitely mathematically defined. This makes it today yet well-suited as input parameter for the common approach to determine the ultimate buckling strength via buckling curves, see Eq. 2.1.

$$\overline{\lambda} = \sqrt{\frac{R_y}{R_{cr}}} \quad \rightarrow \quad R_{ult} = \rho(\overline{\lambda}) \cdot R_y \tag{2.1}$$

where

R_y	yield strength
R_{ult}	ultimate buckling strength
R_{cr}	elastic critical buckling strength
$\overline{\lambda}$	slenderness
$\rho(\overline{\lambda})$	buckling curve

The elastic critical buckling stress is usually defined as the product of buckling coefficient and Euler stress, see Eq. 2.2. It should be noted that some design methods use the elastic critical force F_{cr} or the minimum load amplifier α_{cr} which factors the applied load to the elastic critical load of the plate. The Euler stress refers to a transverse plate strip of unit width and length equal to the plate width. With Poisson's ratio $\nu = 0.3$ and the elastic modulus of $E = 210$ GPa, the Euler stress can be written according to Eq. 2.3.

$$\sigma_{cr} = k \cdot \sigma_E \tag{2.2}$$

where

σ_{cr}	elastic critical buckling stress
k	buckling coefficient
σ_E	Euler stress

$$\sigma_E = \frac{\pi^2 \cdot D}{b^2 \cdot t} = \frac{\pi^2 \cdot E}{12 \cdot (1 - \nu^2)} \cdot \left(\frac{t}{b}\right)^2 = \tag{2.3a}$$

$$= 189.800 \cdot \left(\frac{t}{b}\right)^2 = \tag{2.3b}$$

$$\cong 0.9 \cdot E \cdot \left(\frac{t}{b}\right)^2 \tag{2.3c}$$

where

D	$= [E \cdot t^3] / [12 \cdot (1 - \nu^2)]$, flexural rigidity of a plate strip of unit width
b	plate width
t	plate thickness
E	elastic modulus
ν	Poisson's ratio

The buckling coefficient and the elastic critical buckling load are the key parameters for the determination of the slenderness. For that reason, formulas and buckling charts are provided for common cases e.g. in literature [70, 71] and even standards. They often assume simply supported boundary conditions and, although not always explicitly stated, design methods often presume these simply supported boundary conditions for the calculation of the elastic critical buckling load. Today however, advanced software tools enable the user not only to determine the elastic critical buckling load for almost arbitrary geometries and stiffener arrangements but also to take favourable restraints from edge boundary conditions into account.

In the following, the interaction behaviour of different load components and edge boundary conditions according to linear buckling theory is illustrated. Figures 2.5 to 2.8 show interaction surfaces and planes for the load case "biaxial compression and shear". Panel aspect ratios of $\alpha = 1$ and $\alpha = 3$ are considered. It can be shown that the type of rotational edge boundary condition, i.e. hinged and clamped, does not significantly effect the interaction behaviour. Instead the panel aspect ratio plays an important role. For a square plate ($\alpha = 1$) the eigenmode shape is a one-wave mode regardless what the main loading direction is. For a rectangular plate (e.g. $\alpha = 3$) the number of halfwaves depends on the main loading direction and changes from one wave in the short direction to three waves in the long direction. Other aspect ratios may be considered accordingly. As a result, interaction for non-square plates is more favourable than for square plates. The load case "transverse patch loading with bending and shear" is shown in Figs. 2.9 and 2.10. It can be shown that a similar interaction behaviour is observed as for biaxial uniform compression.

The in-plane membrane restraint condition only effects large deformations and thus it is not relevant in linear buckling theory.

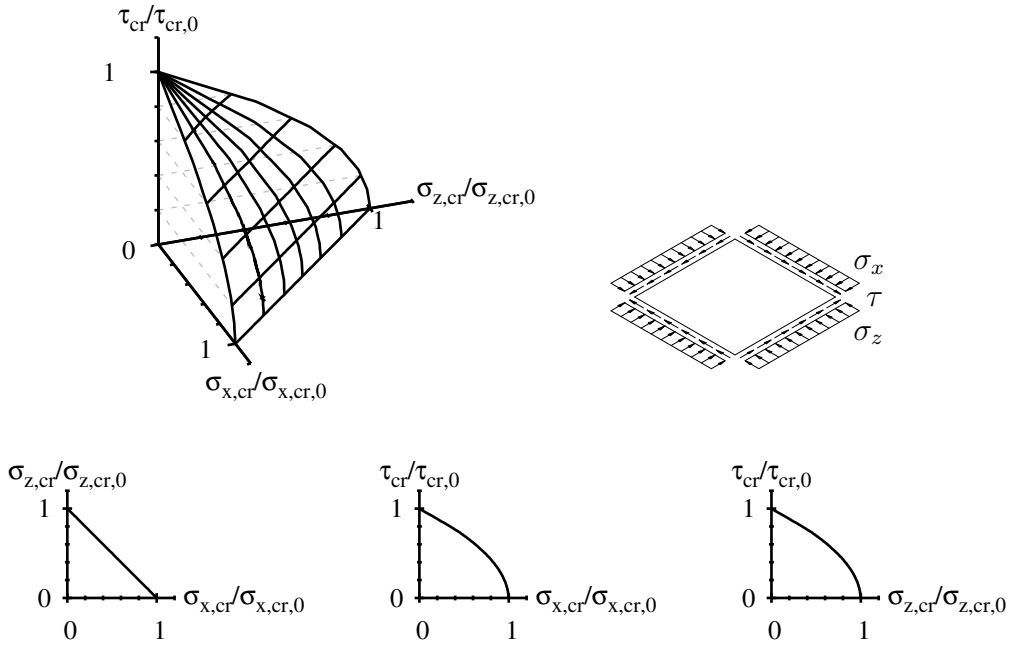

Figure 2.5: Normalised interaction surface and planes for biaxial compression and shear ($\alpha = 1$, all edges **hinged**)

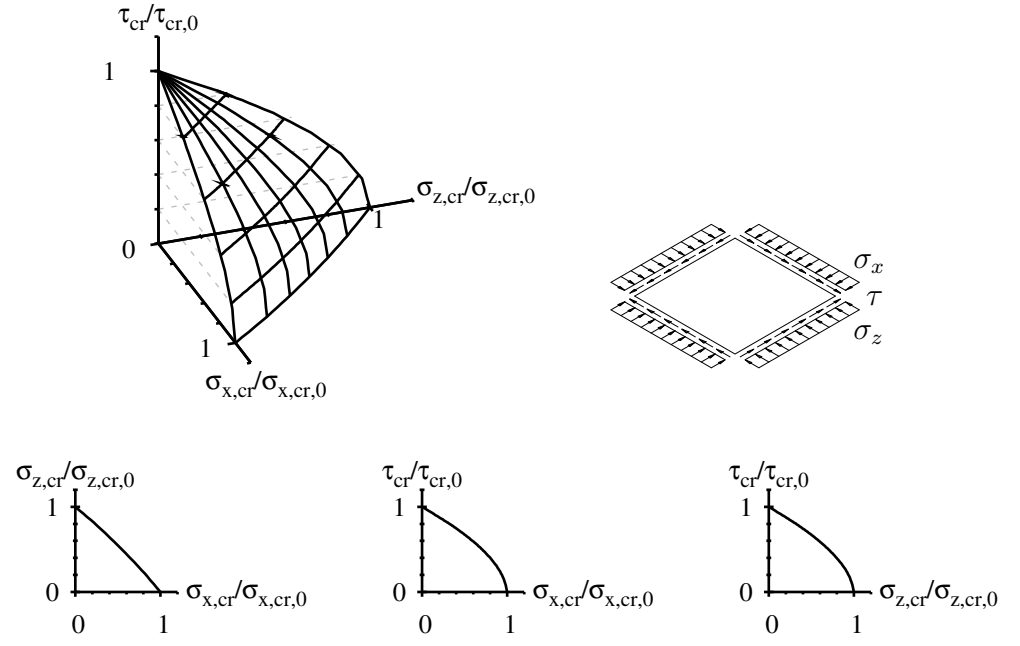

Figure 2.6: Normalised interaction surface and planes for biaxial compression and shear ($\alpha = 1$, all edges **clamped**)

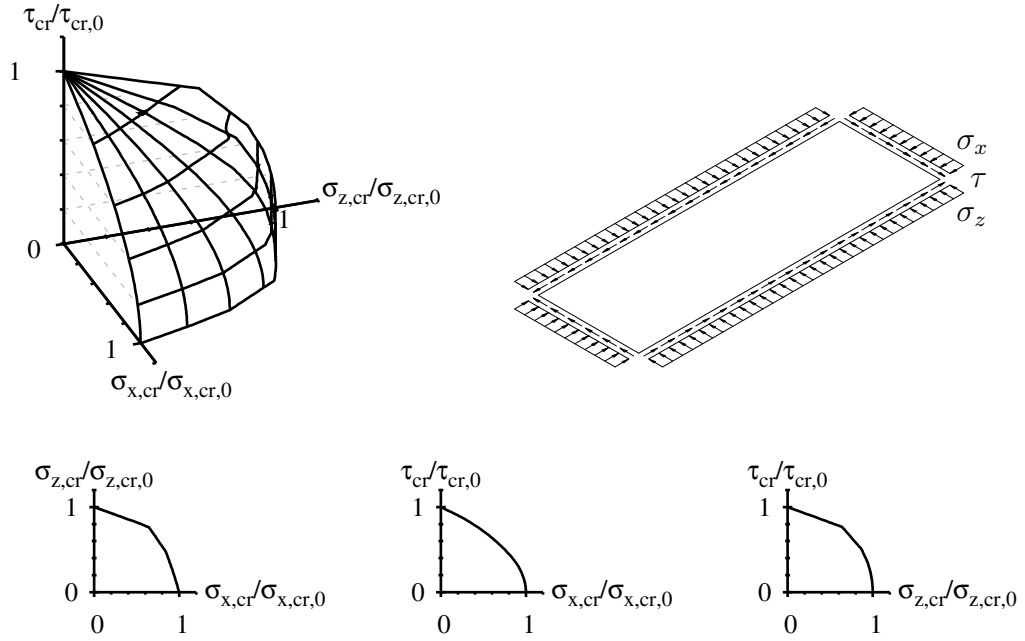

Figure 2.7: Normalised interaction surface and planes for biaxial compression and shear ($\alpha = 3$, all edges **hinged**)

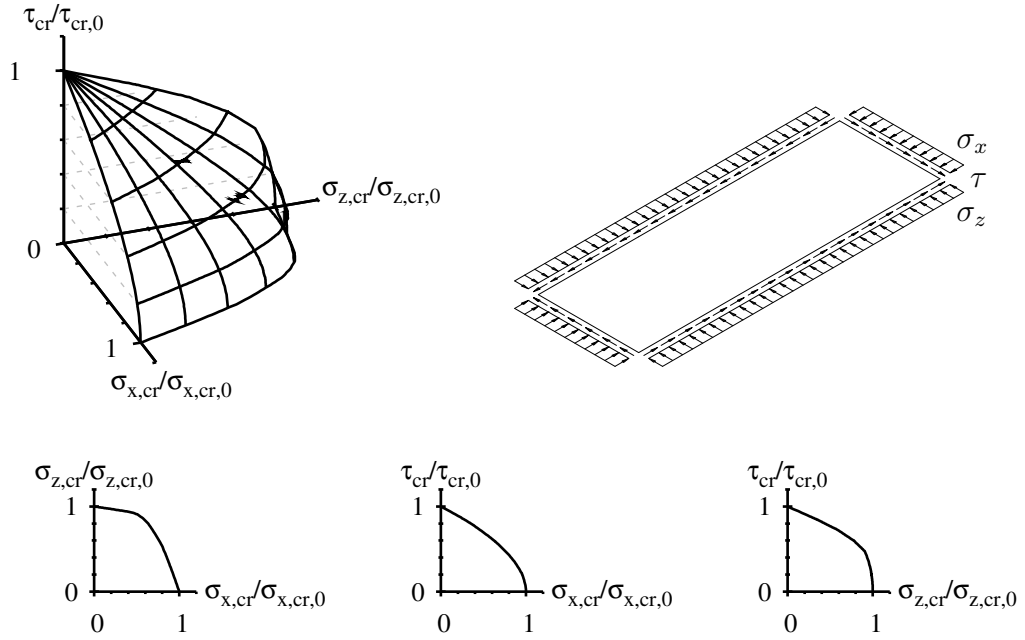

Figure 2.8: Normalised interaction surface and planes for biaxial compression and shear ($\alpha = 3$, all edges **clamped**)

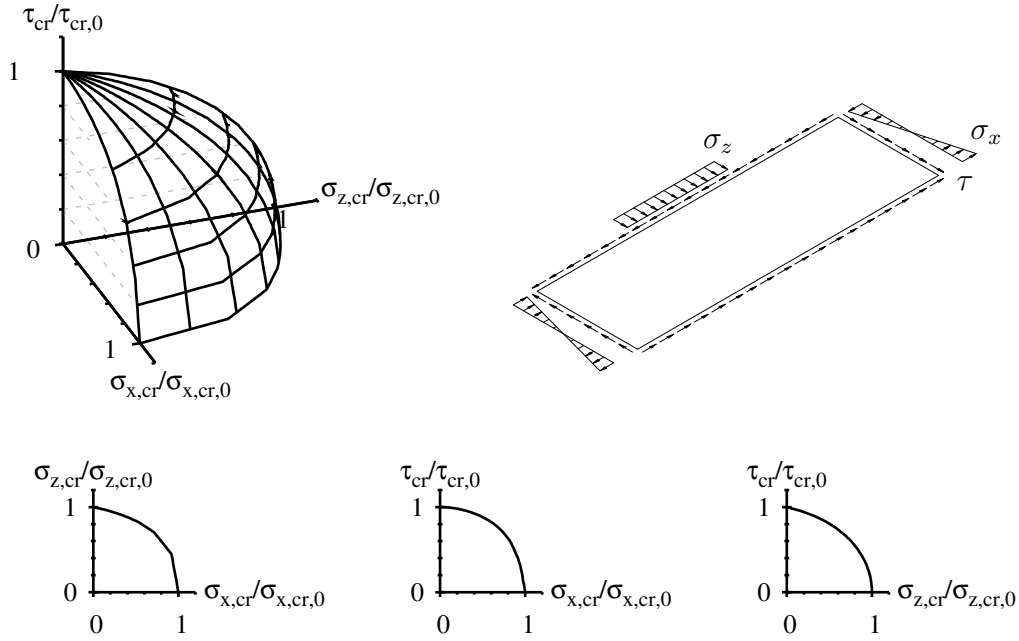

Figure 2.9: Normalised interaction surface and planes for transverse patch loading with bending and shear ($\alpha = 3$, all edges **hinged**, $s_s/h_w = 0.67$)

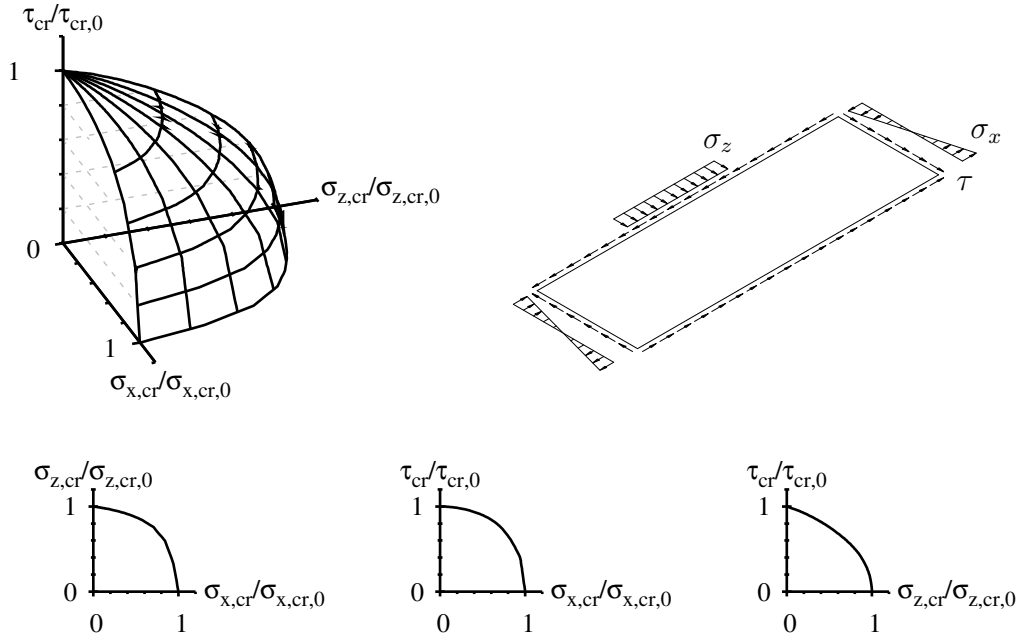

Figure 2.10: Normalised interaction surface and planes for transverse patch loading with bending and shear ($\alpha = 3$, all edges **clamped**, $s_s/h_w = 0.67$)

2.3.2 DIN 18800-3:1990

The interaction criterion according to DIN 18800-3 [28] is given in Eq. 2.4.

$$\left(\frac{|\sigma_x|}{\sigma_{xP,R,d}}\right)^{e_1} + \left(\frac{|\sigma_y|}{\sigma_{yP,R,d}}\right)^{e_2} - V \cdot \left(\frac{|\sigma_x \cdot \sigma_y|}{\sigma_{xP,R,d} \cdot \sigma_{yP,R,d}}\right) + \left(\frac{\tau}{\tau_{P,R,d}}\right)^{e_3} \leq 1 \tag{2.4}$$

where

σ; τ	design load values
$\sigma_{P,R,d}$; $\tau_{P,R,d}$	design resistance values
κ	reduction factors
e_1	$= 1 + \kappa_x^4$
e_2	$= 1 + \kappa_y^4$
e_3	$= 1 + \kappa_x \cdot \kappa_y \cdot \kappa_\tau^2$
V	$= (\kappa_x \cdot \kappa_y)^6$ when σ_x and σ_y are both compression, else $V = \frac{\sigma_x \cdot \sigma_y}{\lvert\sigma_x \cdot \sigma_y\rvert}$

The exponents $e_{i=1,2,3}$ and the factor V were calibrated from comparisons with test results and numerical calculations, see [78–80]. In Fig. 2.11 the interaction equation is evaluated for panels with aspect ratios $\alpha = 1$ and $\alpha = 3$ under biaxial loading and longitudinal stress with shear. Under biaxial compression, the curves stretch between the equivalent stress hypothesis as upper bound limited by material law and a straight line as lower bound limited by linear buckling theory. The parameters e and V are chosen such that for slender plates the linear interaction governs. It should be noted that Eq. 2.4 does not account for the positive stabilising influence of tensile stresses.

In Fig. 2.12 the procedure to determine the interaction curves is shown for the simple case of a square plate under biaxial compression. Firstly, the slendernesses $\overline{\lambda}_{xP}$ and $\overline{\lambda}_{yP}$ are determined, i.e. each basic loading direction is considered individually. With these slendernesses, the reference strengths $\sigma_{P,R,d}$ and $\tau_{P,R,d}$ are determined according to Eq. 2.5 based on the reduction factors from Tables 2.1 and 2.2.

$$\sigma_{P,R,d} = \kappa \cdot \frac{f_y}{\gamma_M} \; ; \; \tau_{P,R,d} = \kappa_\tau \cdot \frac{f_y}{\sqrt{3} \cdot \gamma_M} \tag{2.5}$$

where

κ; κ_τ	reduction factors according to Tables 2.1 and 2.2
f_y	yield strength
γ_M	material partial safety factor

For the design values a material partial safety factor of $\gamma_M = 1.1$ is used. Based on the reduction factors for each relevant loading direction, interaction is accounted for according to Eq. 2.4. The reduction curves are summarised in Fig. 2.14. DIN 18800-3 distinguishes between subpanels as well as plates with and without longitudinal stiffeners.

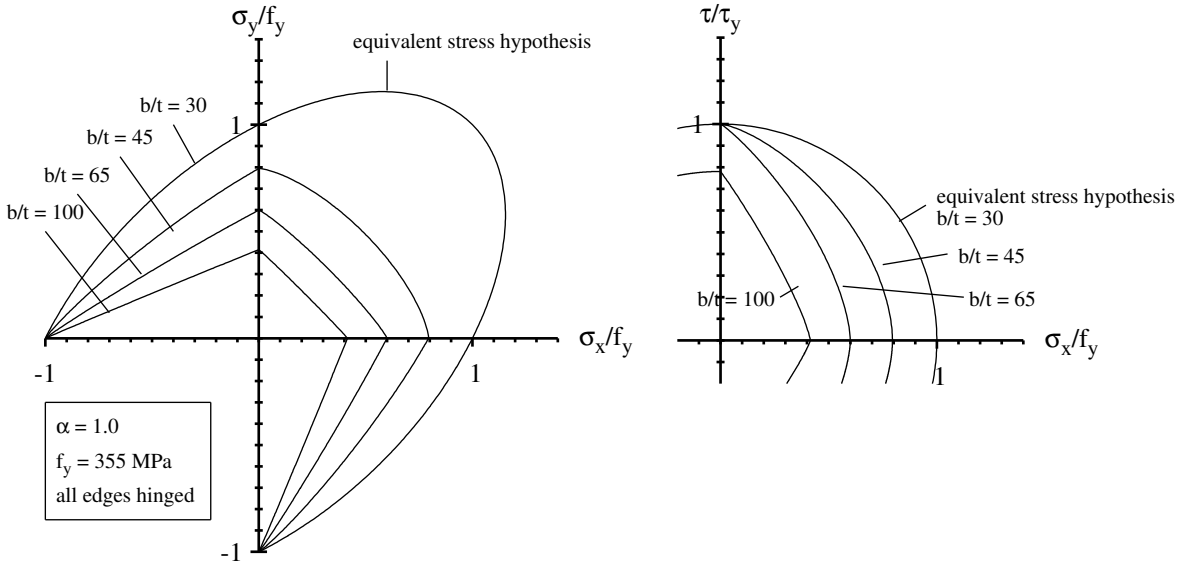

(a) panel aspect ratio $\alpha = 1$

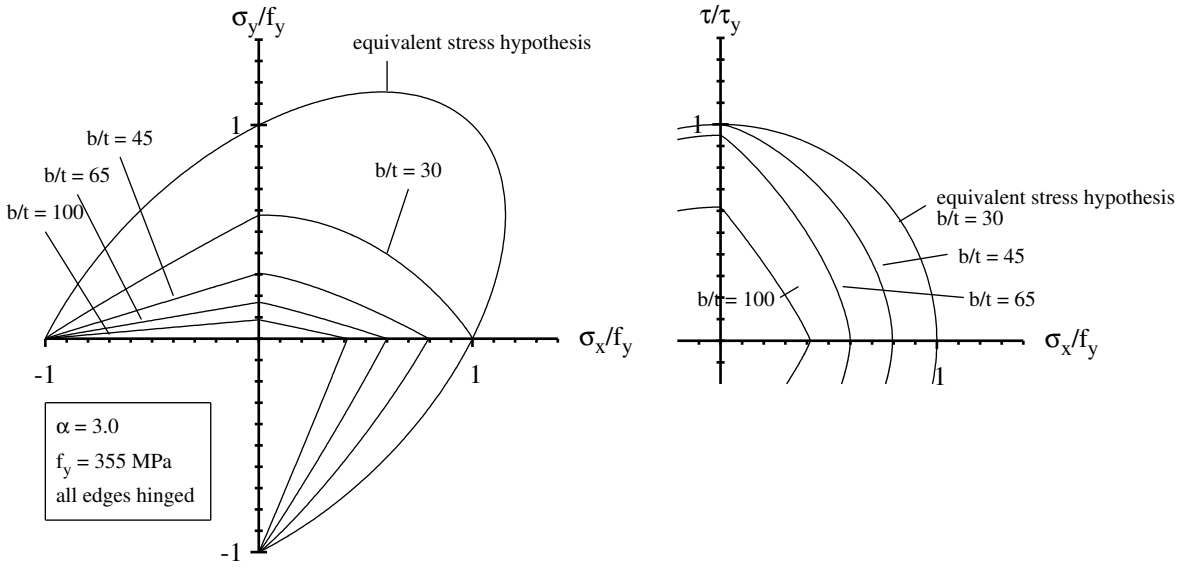

(b) panel aspect ratio $\alpha = 3$

Figure 2.11: Interaction curves according to DIN 18800-3 [28]

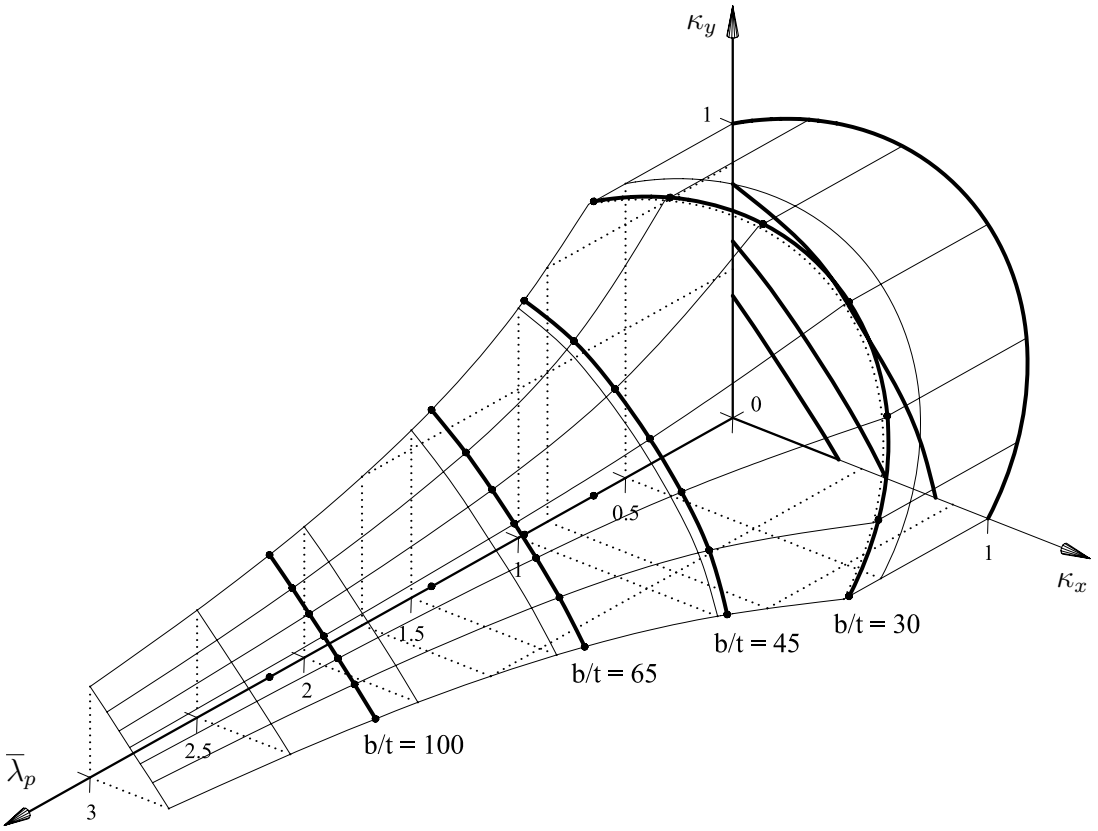

Figure 2.12: Interaction scheme according to DIN 18800-3 [28]
($\alpha = 1$, $f_y = 355\,\mathrm{MPa}$)

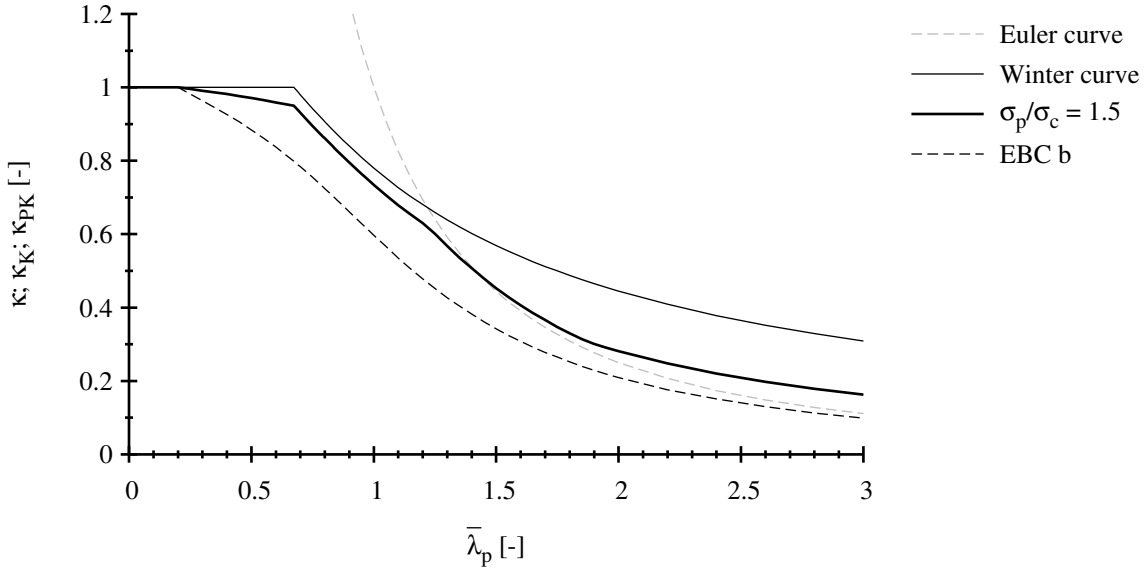

Figure 2.13: Interpolation scheme to account for column-like buckling according to DIN 18800-3 [28]

For stiffened plates under longitudinal stress, $c = 1.25 - 0.25 \cdot \psi \leq 1.25$, whereas for subpanels, $c = 1.25 - 0.12 \cdot \psi_T \leq 1.25$, so that for uniform compression an increase of 13% may always be accounted for which is based on the in-plane membrane restraint of subpanels. Besides that, ψ_T is allowed to be the edge stress ratio of the stiffened panel where the subpanel is a part of. However, the factor c is limited to an upper value of $c = 1.25$.

The postcritical strength reserve of plates under shear is only considered for plates without longitudinal stiffener. It can be shown in Fig. 2.14 that for plates with longitudinal stiffeners, the postcritical strength reserve is not accounted for.

Column-like buckling is accounted for by the interpolation between plate-buckling and column-buckling curve, see Fig. 2.13. The interpolation function according to Eq. 2.6 is used.

$$\kappa_{PK} = \left(1 - \rho^2\right) \cdot \kappa + \rho^2 \cdot \kappa_K \tag{2.6}$$

where

$$\rho = \frac{\Lambda - \sigma_{Pi}/\sigma_{Ki}}{\Lambda - 1} \geq 0$$

$$\Lambda = \bar{\lambda}_p^2 + 0.5$$

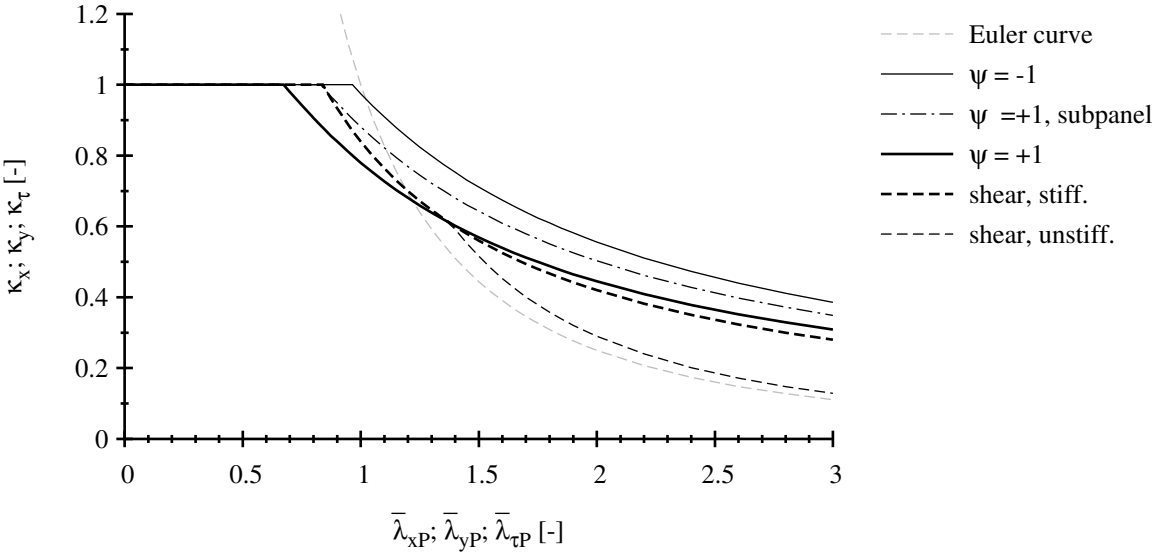

Figure 2.14: Overview of reduction curves according to DIN 18800-3 [28]

As column-buckling curve, European Buckling Curve b (EBC b) is used. For high slendernesses, the reduction becomes more severe, see Eq. 2.6.

$$\chi_c = \frac{1}{\phi + \sqrt{\phi^2 - \overline{\lambda}_p^2}} \leq 1.0 \tag{2.7}$$

where

$$\phi = 0.5 \cdot (1 + \alpha \cdot (\overline{\lambda}_p - 0.2) + \overline{\lambda}_p^2)$$

2.3.3 DNV-RP-C201:2002

The interaction criterion according to DNV-RP-C201 [33] is given in Eq. 2.8. DNV-RP-C201 is part of the offshore codes published by Det Norske Veritas (DNV) and it provides recommended practice for the buckling strength of plated structures. The interaction criterion is applied only to unstiffened plates. Stiffened panels are covered in terms of stiffener checks using effective widths. Another common type of loading on offshore structures are lateral loadings which are not treated here.

For tensile stress components, the interaction equation is fully affine to the equivalent stress hypothesis. For biaxial compression, the factor c_i is used to reduce the curvature. For a b/t-ratio (here: s/t) greater than 120 the interaction curve becomes circular. In Fig. 2.15 the interaction equation is evaluated for panels with aspect ratios $\alpha = 1$ and $\alpha = 3$ under biaxial loading and longitudinal stress with shear. For stocky plates under biaxial compression, the resistance is reduced in comparison to a plate under uniaxial compression with the same b/t-ratio. It should be noted that Eq. 2.8 does not account

Table 2.1: Plate-buckling reduction factors for subpanels and panels without longitudinal stiffeners according to DIN 18800-3 [28]

loading	reduction factor
longitudinal stresses (subpanel)	$\kappa = c \cdot \left(\frac{1}{\overline{\lambda}_p} - \frac{0.22}{\overline{\lambda}_p^2}\right) \leq 1$ where $c = 1.25 - 0.12 \cdot \psi_T \leq 1.25$; ψ_T is the stress ratio of the relevant stiffened panel
longitudinal stresses (panel without longitudinal stiffeners)	$\kappa = c \cdot \left(\frac{1}{\overline{\lambda}_p} - \frac{0.22}{\overline{\lambda}_p^2}\right) \leq 1$ where $c = 1.25 - 0.25 \cdot \psi \leq 1.25$
shear stresses	$\kappa_\tau = \frac{0.84}{\overline{\lambda}_p} \leq 1$

Table 2.2: Plate-buckling reduction factors for panels with longitudinal stiffeners according to DIN 18800-3 [28]

loading	reduction factor
longitudinal stresses	$\kappa = c \cdot \left(\frac{1}{\overline{\lambda}_p} - \frac{0.22}{\overline{\lambda}_p^2}\right) \leq 1$ where $c = 1.25 - 0.25 \cdot \psi \leq 1.25$
shear stresses	$\kappa_\tau = \frac{0.84}{\overline{\lambda}_p} \leq 1$ for $\overline{\lambda}_p \leq 1.38$ $\kappa_\tau = \frac{1.16}{\overline{\lambda}_p^2}$ for $\overline{\lambda}_p > 1.38$

for the positive stabilising influence of tensile stresses.

$$\left(\frac{\sigma_{x,Sd}}{\sigma_{x,Rd}}\right)^2 + \left(\frac{\sigma_{y,Sd}}{\sigma_{y,Rd}}\right)^2 - c_i \cdot \left(\frac{\sigma_{x,Sd}}{\sigma_{x,Rd}}\right) \cdot \left(\frac{\sigma_{y,Sd}}{\sigma_{y,Rd}}\right) + \left(\frac{\tau_{Sd}}{\tau_{Rd}}\right)^2 \leq 1.0 \tag{2.8}$$

where

σ_{Sd}; τ_{Sd}	design load values	
σ_{Rd}; τ_{Rd}	design resistance values	
c_i	$= 1 - \frac{1}{120} \cdot \frac{s}{t}$	for $s/t \leq 120$
	$= 0$	for $s/t > 120$
	when $\sigma_{x,Sd}$ and $\sigma_{y,Sd}$ are both compression, else $c_i = 1.0$	

In Fig. 2.16 the procedure to determine the interaction curve is shown for the simple case of a square plate under biaxial compression. The procedure is analogous to the one of DIN 18800-3 [28], i.e. the input parameteres are the individual slendernesses but then a different interaction criterion is used. The reference strengths $\sigma_{x,Rd}$, $\sigma_{y,Rd}$ and τ_{Rd} are determined according to Eq. 2.9 based on the reduction factors in Table 2.3. For the design values, a material partial safety factor of $\gamma_M = 1.15$ is used.

$$\sigma_{x,Rd} = C_x \cdot \frac{f_y}{\gamma_M} \; ; \; \sigma_{y,Rd} = \frac{\sigma_{y,R}}{\gamma_M} \; ; \; \tau_{Rd} = C_\tau \cdot \frac{f_y}{\sqrt{3} \cdot \gamma_M} \tag{2.9}$$

where

C_x; C_τ	reduction factors
f_y	yield strength
γ_M	material partial safety factor

The reduction curves are summarised in Fig. 2.17. For longitudinal stresses, the Winter curve is used for uniform compression and the stress ratio is accounted for. In-plane restraints are not taken into account.

In case of pure column-buckling, DNV-RP-C201 uses a reduction curve for $\overline{\lambda}_p < 2.0$ similar to European Buckling Curve a (EBC a). For $\overline{\lambda}_p \geq 2.0$ it differs marginally. The reduction curve is given in Eq. 2.12. Interpolation between plate-like and column-like buckling is accounted for by Eq. 2.11 and is shown in Fig. 2.18. It should be noted that the interpolation function is appropriately adjusted for typical plates of ships with large panel aspect ratios but that it leads to odd results when it is applied to plates approaching a square geometry.

$$\sigma_{y,Rd} = \frac{\sigma_{y,R}}{\gamma_M} \tag{2.10}$$

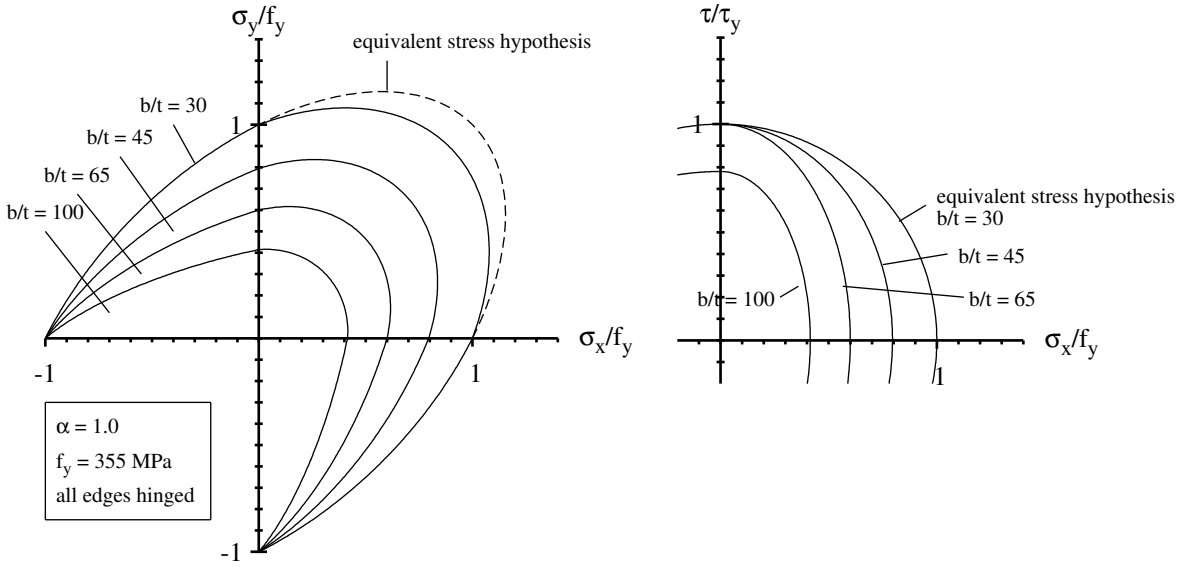

(a) panel aspect ratio $\alpha = 1$

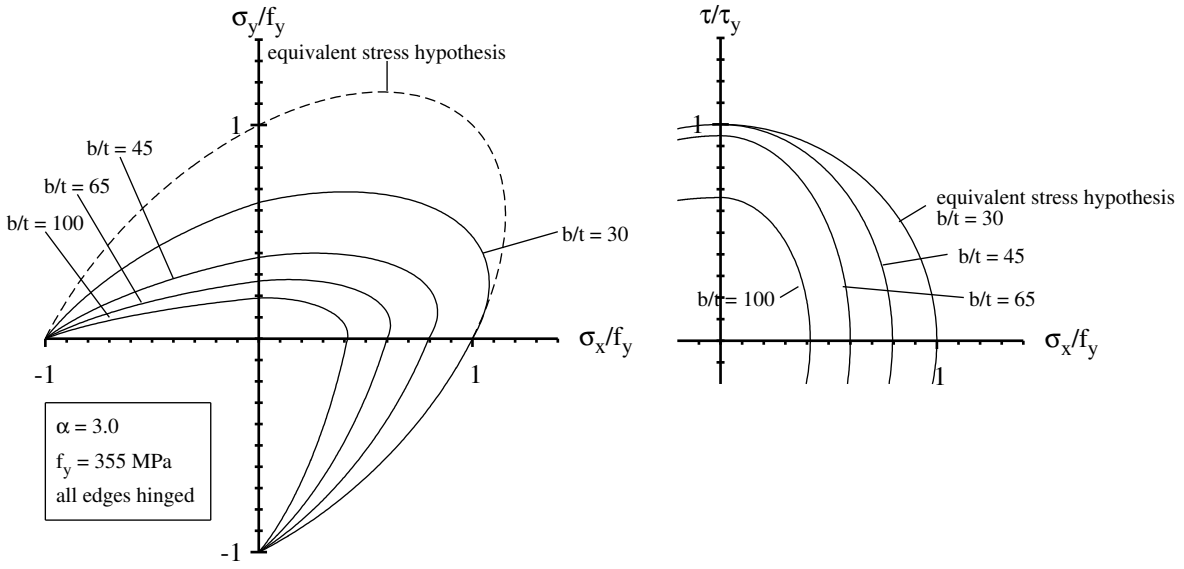

(b) panel aspect ratio $\alpha = 3$

Figure 2.15: Interaction curves according to DNV-RP-C201 [33]

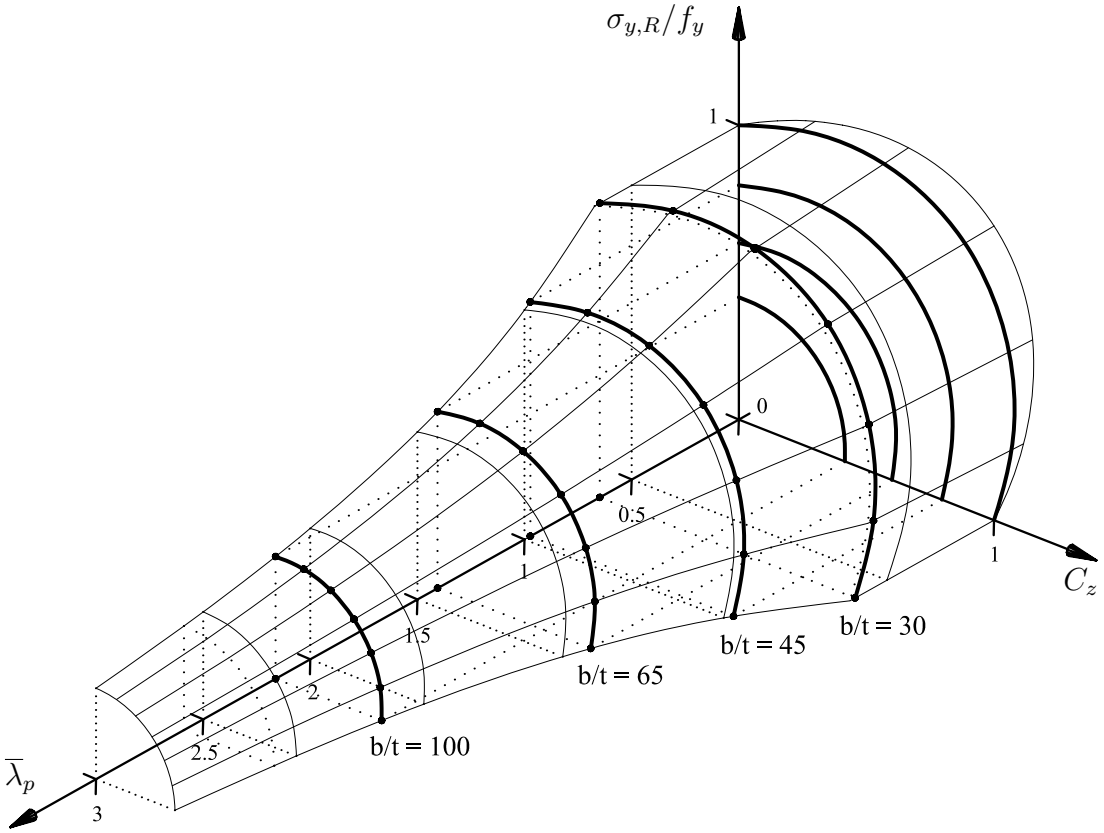

Figure 2.16: Interaction scheme for according to DNV-RP-C201 [33]
($\alpha = 1$, $f_y = 355\,\mathrm{Mpa}$)

$$\sigma_{y,R} = \left[\frac{1.3 \cdot t}{l} \cdot \sqrt{\frac{E}{f_y}} + \kappa \cdot \left(1 - \frac{1.3 \cdot t}{l} \cdot \sqrt{\frac{E}{f_y}}\right)\right] \cdot f_y \tag{2.11}$$

$$\kappa = 1.0 \qquad \text{for } \overline{\lambda}_c \leq 0.2 \tag{2.12a}$$

$$\kappa = \frac{1}{2 \cdot \overline{\lambda}_c^2} \cdot \left(1 + \mu + \overline{\lambda}_c^2 - \sqrt{\left(1 + \mu + \overline{\lambda}_c^2\right)^2 - 4 \cdot \overline{\lambda}_c^2}\right) \tag{2.12b}$$

$$\text{for } 0.2 < \overline{\lambda}_c < 2.0$$

$$\kappa = \frac{1}{2 \cdot \overline{\lambda}_c^2} + 0.07 \quad \text{for } \overline{\lambda}_c \geq 2.0 \tag{2.12c}$$

where

$$\mu = 0.21 \cdot (\overline{\lambda}_c - 0.2)$$

2.3.4 EN 1993-1-5:2006

2.3.4.1 General

In EN 1993-1-5 [46] the designer may choose, considering national allowance, mainly between two different types of design methods: the reduced stress method based on a single plate slenderness and the effective width method. In addition, a verification methodology based on the finite element method (FEM) is also given. FEM is the most versatile verification method and it can be used for the determination of the "real" buckling resistance by means of a nonlinear analysis considering imperfections and local plastification as well as for the calculation of elastic critical stress values by means of a linear bifurcation analysis. For further information on principles when applying the finite element method, the reader is referred to Sec. 5.2.

Table 2.3: Plate-buckling reduction factors for subpanels according to DNV-RP-C201 [33]

loading	reduction factor	
longitudinal stresses	$C_x = \frac{\overline{\lambda}_p - 0.055 \cdot (3+\psi)}{\overline{\lambda}_p^2}$	
shear stresses	$C_\tau = 1.0 - 0.625 \cdot \left(\overline{\lambda}_w - 0.8\right)$	for $\overline{\lambda}_w \leq 1.2$
	$C_\tau = \frac{0.9}{\overline{\lambda}_w}$	for $\overline{\lambda}_w > 1.2$

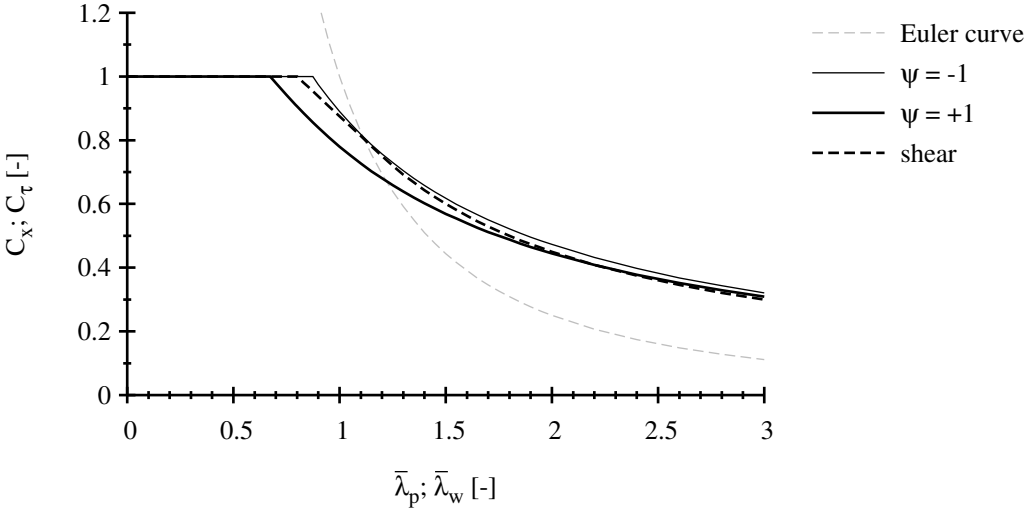

Figure 2.17: Overview of reduction curves according to DNV-RP-C201 [33]

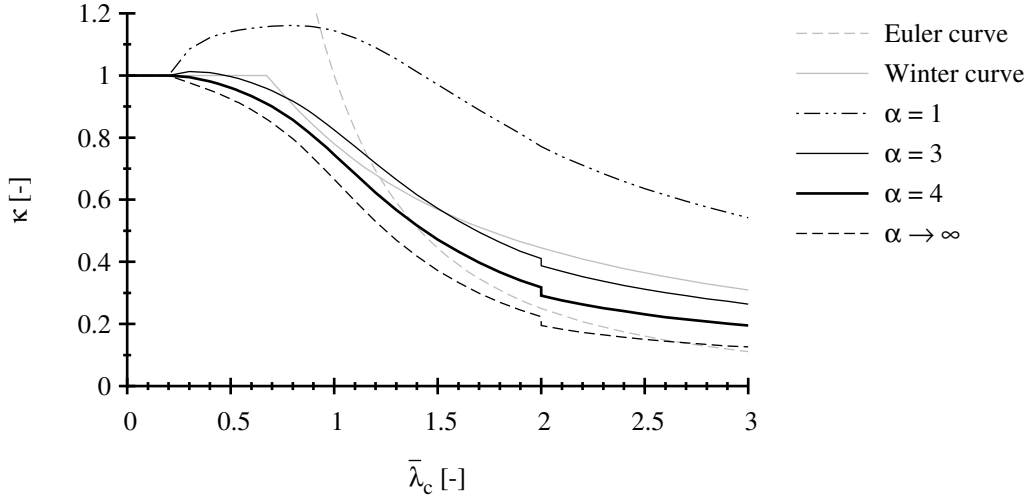

Figure 2.18: Interpolation scheme to account for column-like buckling according to DNV-RP-C201 [33]

The reduced stress method abstains from load shedding between cross-sectional elements but it fully accounts for the postcritical strength reserve in a single plate element. The general format facilitates its use not only for buckling verifications of standard geometries but also for serviceability verifications and for the design of non-uniform members such as haunched beams, webs with openings and plates with non-orthogonal stiffeners.

The effective width method, informally comprising resistance models for shear force and transverse patch loading, is very efficient for standard geometries because it accounts not only for the postcritical strength reserve in a single plate element but also for the load shedding between cross-sectional elements. The behaviour of each stability load case is addressed separately due to its complexity and the single verifications are joined in an interaction check in the end. In Chapter 7, EN 1993-1-5 [46], the interaction between axial force, bending moment and shear force as well as between transverse patch loading and bending moment is covered.

2.3.4.2 Reduced stress method

The interaction criterion according to Chapter 10, EN 1993-1-5 [46] is given in Eq. 2.13. EN 1993-1-5 also gives a simplified verification format according to Eq. 2.14 if the minimum reduction factor is used.

$$\left(\frac{\sigma_{x,Ed}}{\sigma_{x,Rd}}\right)^2 + \left(\frac{\sigma_{z,Ed}}{\sigma_{z,Rd}}\right)^2 - \left(\frac{\sigma_{x,Ed} \cdot \sigma_{z,Ed}}{\sigma_{x,Rd} \cdot \sigma_{z,Rd}}\right) + 3 \cdot \left(\frac{\tau_{Ed}}{\tau_{Rd}}\right)^2 \leq 1 \tag{2.13}$$

$$\sigma_{eq,Ed} = \sigma_{x,Ed}^2 + \sigma_{z,Ed}^2 - \sigma_{x,Ed} \cdot \sigma_{z,Ed} + 3 \cdot \tau_{Ed}^2 \leq \rho_{min} \cdot \frac{f_y}{\gamma_{M1}} \tag{2.14}$$

where

σ_{Ed}; τ_{Ed}	design load values
σ_{Rd}; τ_{Rd}	design resistance values
ρ_c; χ_w	reduction factors
f_y	yield strength
γ_M	material partial safety factor
ρ_{min}	$= \min(\rho_{x,c}; \rho_{z,c}; \chi_w)$

The interaction criterion has been proposed by Scheer and Nölke [110, 111] and it is based on the equivalent stress hyopthesis. It uses a single slenderness which is determined based on the complete stress field. In contrast to DIN 18800-3 [28] and DNV-RP-C201 [33], the slendernesses are not individually determined on the basis of the maximum compressive stresses so that on the basis of the complete stress field also tensile stresses are taken into account. In Fig. 2.19 the interaction equation is evaluated for panels with aspect ratios $\alpha = 1$ and $\alpha = 3$ under biaxial loading and longitudinal stress with shear.

Under biaxial compression, the curves are favourable but they lead to strange curvatures for high slendernesses. It becomes evident for non-square plates for which the resistance increases when the loading switches from compression-tension to biaxial compression. Eq. 2.13 has been compared to test results and numerical calculations [67] but it should be noted that information lacks on the biaxial loadings.

In Fig. 2.20 the procedure to determine the interaction curve is shown for the simple case of a square plate under biaxial compression. The procedure uses the single slenderness $\overline{\lambda}_p$ which is determined based on the complete stress field, i.e. each loading is assigned an individual slenderness. With this slenderness, the reference strengths σ_{Rd} and τ_{Rd} are determined according to Eq. 2.15 based on the reduction factors in Table 2.4 or based on Table 2.5 with Eq. 2.16 alternatively. For the design values, the material partial safety factor γ_{M1} is given in the relevant application standard and it is recommended to be taken as $\gamma_{M1} = 1.1$.

$$\sigma_{Rd} = \rho \cdot \frac{f_y}{\gamma_{M1}} \; ; \; \tau_{Rd} = \chi_w \cdot \frac{f_y}{\sqrt{3} \cdot \gamma_{M1}} \tag{2.15}$$

The reduction curves are summarised in Fig. 2.21. In Chapter 10, EN 1993-1-5, the reduction factors may either be determined from Chapters 4 and 5 or from Annex B. Reduction factors according to Chapters 4 and 5 utilise as much of the postcritical strength reserve as possible. In contrast to this, Annex B provides buckling curves on the basis of a generalised format which do not account for the postcritical strength reserve to such an extent as Chapters 4 and 5 do. On the other hand, they are in favour of a reduced number of buckling curves. Chapter 4 uses the Winter curve for longitudinal stresses and the stress ratio is accounted for. In-plane restraints are not taken into account. In case of shear stresses, it is distinguished between non-rigid and rigid end-post conditions. Annex B is based on the general equation according to Eq. 2.16 and the values from Table 2.5.

$$\rho = \frac{1}{\phi_p + \sqrt{\phi_p^2 - \overline{\lambda_p}}} \tag{2.16}$$

where

$\phi_P \quad = 0.5 \cdot \left(1 + \alpha_P \cdot \left(\overline{\lambda}_p - \overline{\lambda}_{p0}\right) + \overline{\lambda}_p\right)$

α_p; $\overline{\lambda}_{p0}$ according to Table 2.5

Column-like buckling is accounted for by the interpolation between the relevant plate buckling and column-buckling curve. Fig. 2.22 shows the interpolation for a plate without longitudinal stiffeners and plate-buckling curve according to Chapter 4 and Annex B. The interpolation for a plate with longitudinal stiffeners is shown in Fig. 2.25, Sec. 2.3.4.3.

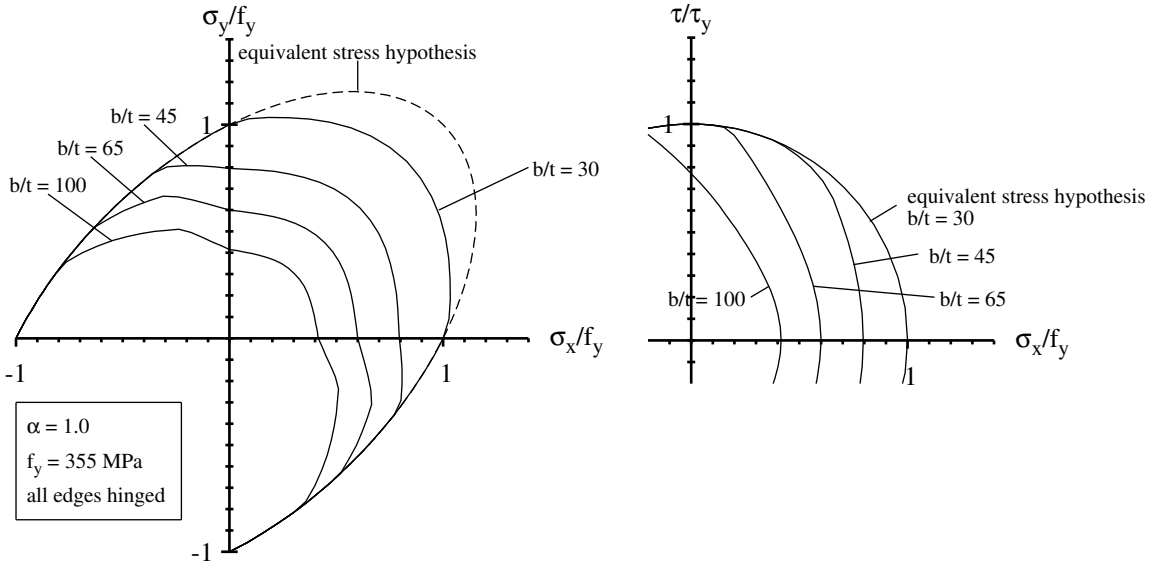

(a) panel aspect ratio $\alpha = 1$

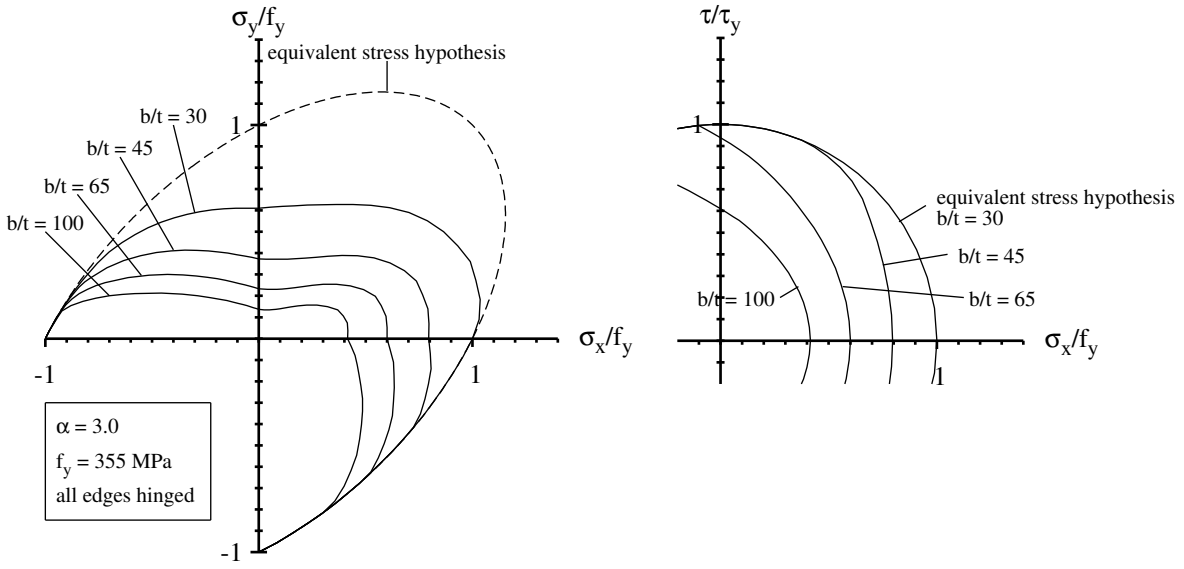

(b) panel aspect ratio $\alpha = 3$

Figure 2.19: Interaction curves according to Chapter 10, EN 1993-1-5 [46]

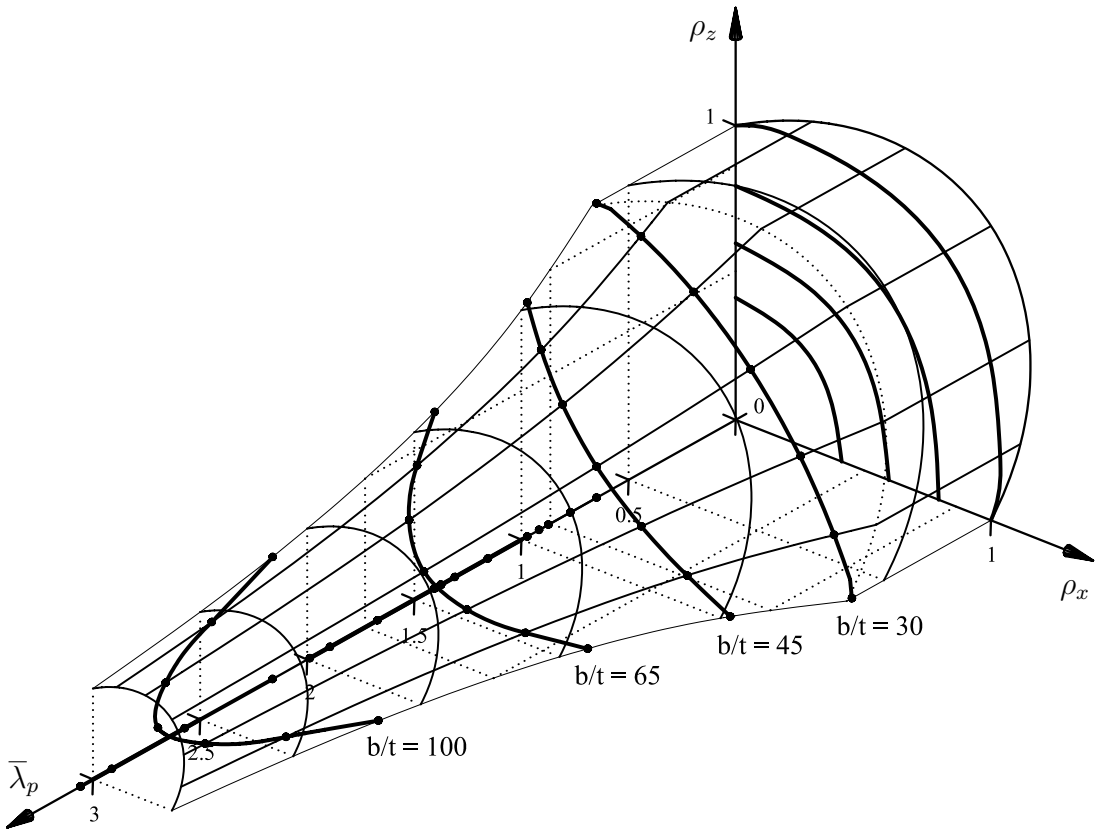

Figure 2.20: Interaction scheme according to Chapter 10, EN 1993-1-5 [46] ($\alpha = 1$, $f_y = 355\,\mathrm{MPa}$)

Table 2.4: Plate-buckling reduction factors according to Chapters 4 and 5, EN 1993-1-5 [46]

loading	reduction factor
longitudinal stresses	$\rho = \frac{\overline{\lambda}_p - 0.055\cdot(3+\psi)}{\overline{\lambda}_p^2}$
shear stresses (non-rigid end-post)	$\chi_w = \frac{0.83}{\overline{\lambda}_p} \leq \eta$
shear stresses (rigid end-post)	$\chi_w = \frac{0.83}{\overline{\lambda}_p} \leq \eta$ for $\overline{\lambda}_p < 1.08$ $\chi_w = \frac{1.37}{0.7+\overline{\lambda}_p}$ for $\overline{\lambda}_p \geq 1.08$

Table 2.5: Values α_p and $\overline{\lambda}_{p0}$ according to Annex B, EN 1993-1-5 [46], for welded cross-sections

loading	α_p	$\overline{\lambda}_{p0}$
longitudinal stresses for $\psi \geq 1$	0.34	0.70
longitudinal stresses for $\psi < 1$	0.34	0.80
shear stresses	0.34	0.80
transverse stresses	0.34	0.80

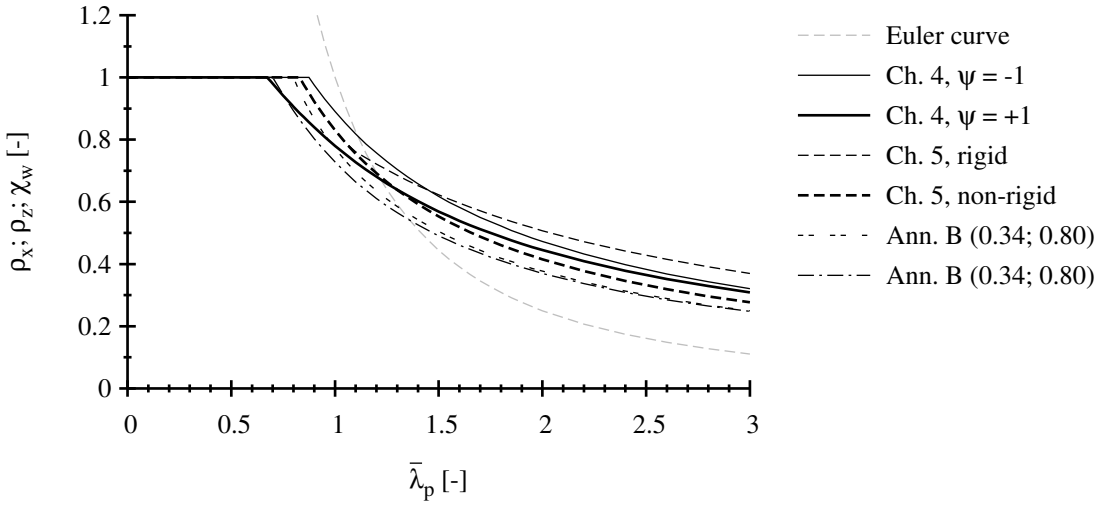

Figure 2.21: Overview of reduction curves according to Chapter 10, EN 1993-1-5 [46]

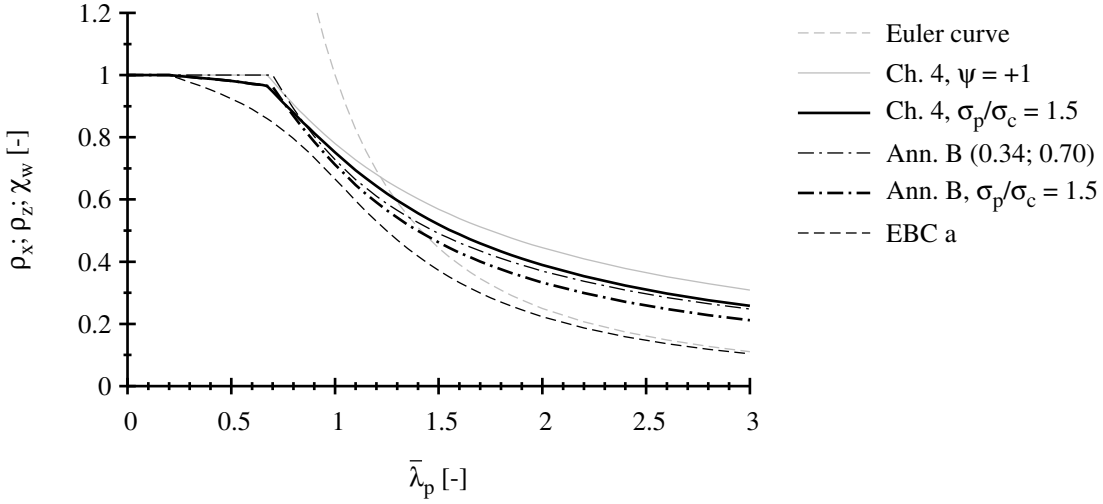

Figure 2.22: Interpolation scheme to account for column-like buckling according to EN 1993-1-5 [46] (plate without longitudinal stiffeners)

The following interpolation function is used:

$$\rho_c = (\rho - \chi_c) \cdot \xi \cdot (2 - \xi) + \chi_c \tag{2.17}$$

where $\xi = (\sigma_{cr,p}/\sigma_{cr,c}) - 1$

As column-buckling curve, European Buckling curve a (EBC a) is used for plates without longitudinal stiffeners. For plates with longitudinal stiffeners, an increased imperfection value α_e should be used which is calculated based on EBC b for closed-section stiffeners and on EBC c for open-section stiffeners.

$$\chi_c = \frac{1}{\phi + \sqrt{\phi^2 - \overline{\lambda}_c^2}} \leq 1.0 \tag{2.18}$$

where $\phi = 0.5 \cdot (1 + \alpha_e \cdot (\overline{\lambda}_c - 0.2) + \overline{\lambda}_c^2)$

2.3.4.3 Effective width method

Chapter 7, EN 1993-1-5 [46], covers the interaction between axial force, bending moment and shear force in webs and between transverse patch loading and bending moment. The interaction between axial force, bending moment and shear force in flanges is treated in Sec. 5.4, EN 1993-1-5, which deals with the contribution of the flanges to the shear resistance.

The interaction criterion between axial force, bending moment and shear force according to Sec. 7.1, EN 1993-1-5, is given in Eq. 2.19. It becomes relevant if the applied bending moment is larger than the moment resistance of the cross-section consisting of the effective area of the flanges alone, see Fig. 2.23.

$$\overline{\eta}_1 + \left(1 - \frac{M_{f,Rd}}{M_{pl,Rd}}\right) \cdot [2 \cdot \overline{\eta}_3 - 1]^2 \leq 1.0 \qquad \text{for} \qquad M_{Ed} \geq M_{f,Rd} \tag{2.19}$$

where

$\overline{\eta}_1$	$= M_{Ed}/M_{pl,Rd}$, utilisation factor of the plastic bending moment resistance
$\overline{\eta}_3$	$= V_{Ed}/V_{bw,Rd}$, utilisation factor of the web shear resistance
M_{Ed}	design bending moment
$M_{f,Rd}$	design plastic bending moment resistance, cross-section consisting of the effective area of the flanges alone
$M_{pl,Rd}$	design plastic bending moment resistance, cross-section consisting of the effective area of the flanges and the gross web area
V_{Ed}	design shear force
$V_{bw,Rd}$	design web shear resistance

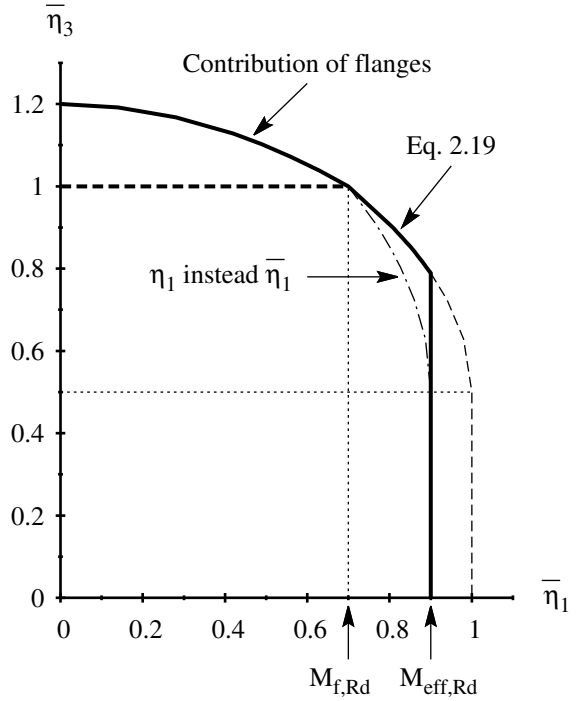

Figure 2.23: Interaction between axial force, bending moment and shear force according to Sec. 7.1, EN 1993-1-5 [46]

The interaction criterion between transverse patch loading and bending moment according to Sec. 7.2, EN 1993-1-5, is given in Eq. 2.20, see Fig. 2.24.

$$\eta_2 + 0.8 \cdot \eta_1 \leq 1.4 \tag{2.20}$$

where

η_1	$= M_{Ed}/M_{el,Rd}$, utilisation factor of the elastic bending moment resistance
η_2	$= F_{Ed}/F_{Rd}$, utilisation factor of the transverse patch loading resistance
M_{Ed}	design bending moment
$M_{el,Rd}$	design elastic bending moment resistance
F_{Ed}	design transverse patch loading
F_{Rd}	design transverse patch loading resistance

Both interaction curves were fit empirically to test results and numerical calculations [67]. The input parameters come from individual checks for basic load cases which are shortly summarised below. For both interaction criteria, the individual checks have to be fulfilled as well.

For longitudinal stresses the verification is done in the basis of the effective cross-section. In the end, axial force and bending moment are elastically verified against this

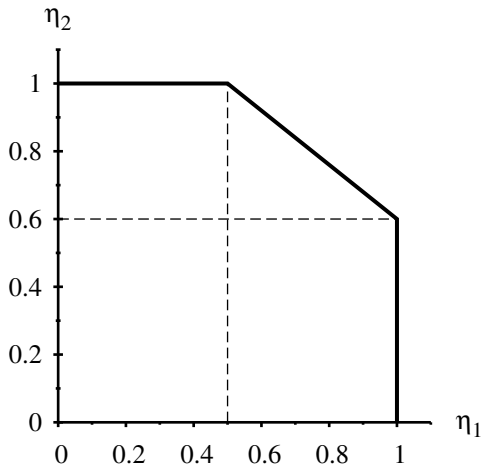

Figure 2.24: Interaction between transverse loading, bending moment and axial force according to Sec. 7.2, EN 1993-1-5 [46]

effective cross-section according to Eq. 2.21. It should be noted that it is shown in [86] that effective width method and reduced stress method have a commen basis. When a single plate element is considered both methods lead to the same level of utilisation if the same buckling curves are used.

$$\eta_1 = \frac{N_{Ed}}{A_{eff} \cdot f_y/\gamma_{M0}} + \frac{M_{Ed} + N_{Ed} \cdot e_N}{W_{eff} \cdot f_y/\gamma_{M0}} \tag{2.21}$$

where

N_{Ed}	design axial force
M_{Ed}	design bending moment
e_N	shift of the position of the neutral axis
$A_{eff}; W_{eff}$	effective cross-section properties
f_y	yield strength
γ_{M0}	material partial safety factor

The gross cross-section A_c is reduced by the reduction factors according to Table 2.4 based on Eq. 2.22 for panels without longitudinal stiffeners and based on Eq. 2.23 for panels with longitudinal stiffeners. Column-like buckling is accounted for as described in Sec. 2.3.4.2. Fig. 2.25 shows the interpolation scheme, focusing on the different column-buckling curves used for plates with longitudinal stiffeners. For plates with longitudinal stiffeners see Fig. 2.21.

$$A_{c,eff} = \rho \cdot A_c \tag{2.22}$$

$$A_{c,eff} = \rho_c \cdot A_{c,eff,loc} + \sum_m b_{m,edge,eff} \cdot t \tag{2.23}$$

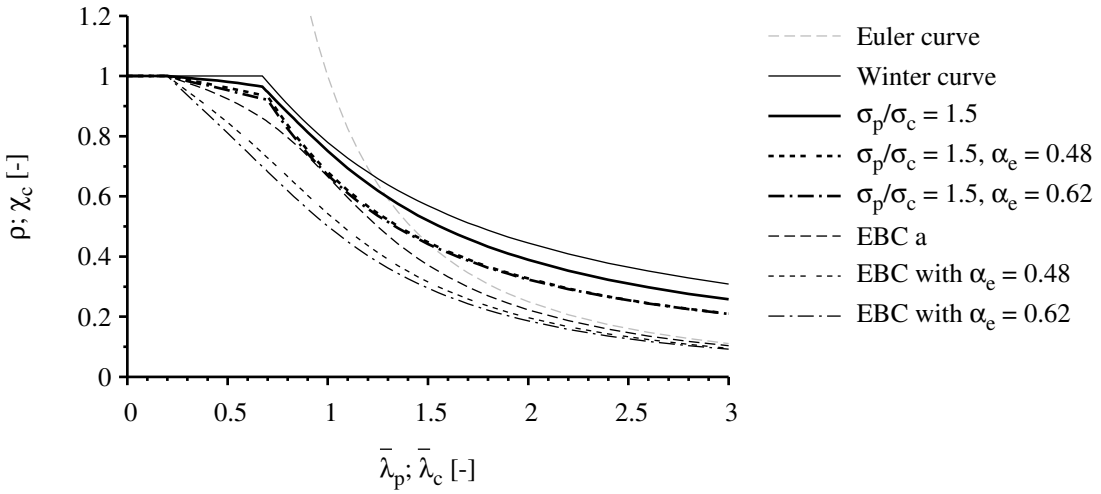

Figure 2.25: Interpolation scheme to account for column-like buckling according to EN 1993-1-5 [46] (plate with longitudinal stiffeners)

The shear resistance is given in Eq. 2.24. It is composed of the contribution from the web and from the flanges according to Eqs. 2.25 and 2.26.

$$\eta_3 = \frac{V_{Ed}}{V_{bw,Rd} + V_{bf,Rd}} \leq h_w \cdot t_w \cdot \frac{\eta \cdot f_{yw}}{\sqrt{3} \cdot \gamma_{M1}} \tag{2.24}$$

where

V_{Ed} design shear force
$V_{bw,Rd}$ design shear resistance, contribution from the web
$V_{bf,Rd}$ design shear resistance, contribution from the flanges

$$V_{bw,Rd} = \chi_w \cdot h_w \cdot t_w \cdot \frac{f_{yw}}{\sqrt{3} \cdot \gamma_{M1}} \tag{2.25}$$

$$V_{bf,Rd} = \frac{b_f \cdot t_f^2 \cdot f_{yf}}{c \cdot \gamma_{M1}} \cdot \left[1 - \frac{M_{Ed}}{M_{f,Rd}}\right] \tag{2.26}$$

The verification against transverse patch loading is determined according to Eq. 2.27.

$$\eta_2 = \frac{F_{Ed}}{F_{Rd}} \leq 1.0 \tag{2.27}$$

where

F_{Ed} design transverse patch loading
F_{Rd} design transverse patch loading resistance

The transverse patch loading resistance is calculated according to Eq. 2.28. Herein the

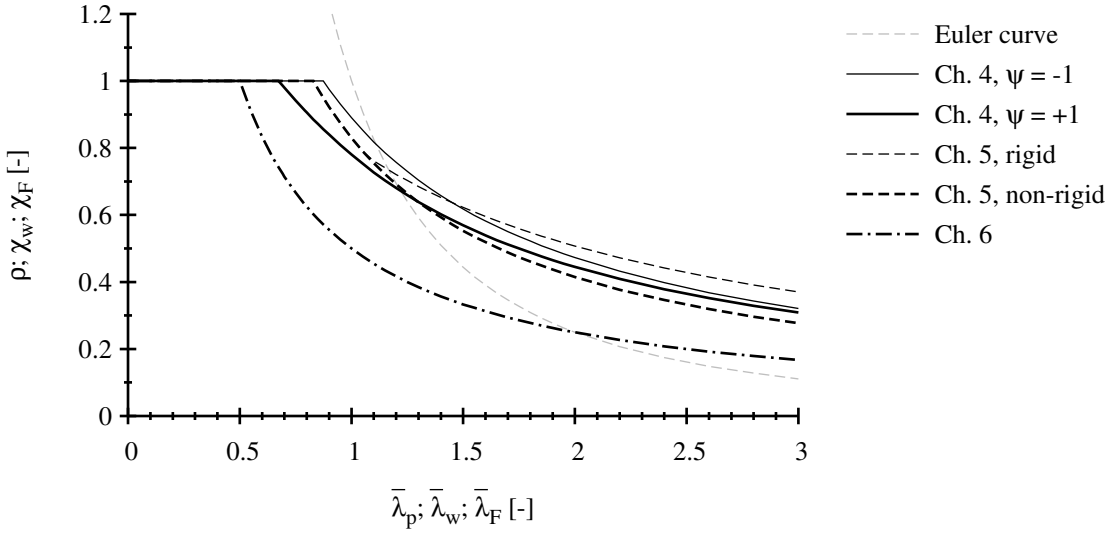

Figure 2.26: Overview of reduction curves according to Chapters 4 to 6, EN 1993-1-5 [46]

yield load F_y is reduced by the reduction factor χ_F which is determined based on the slenderness $\overline{\lambda}_F$. This slenderness is calculated from the elastic critical load F_{cr} according to Eq. 2.29 and the yield load F_y according to Eq. 2.30.

$$F_{Rd} = \chi_F \cdot \frac{F_y}{\gamma_{M1}} = \chi_F \cdot \ell_y \cdot t_w \cdot \frac{f_{yw}}{\gamma_{M1}} \tag{2.28}$$

where

F_y	yield load
χ_F	$= 0.5/\overline{\lambda}_F \leq 1.0$, reduction factor, see Fig. 2.26
ℓ_y	effective loaded length
t_w	web thickness
f_{yw}	web yield strength
γ_{M1}	material partial safety factor

$$F_{cr} = 0.9 \cdot k_F \cdot E \cdot \frac{t_w^3}{h_w} \tag{2.29}$$

$$F_y = \ell_y \cdot t_w \cdot f_{yw} \tag{2.30}$$

The improvement of the transverse patch loading resistance according to Chapter 6, EN 1993-1-5, has been the subject of recent researches, see Davaine [24], Gozzi [56], Clarin [19] and Chacon [16]. The proposals directly effect the reference strength which are used in the interaction criteria and in later studies so that they will be discussed separately in Sec. 2.4. All reduction curves used with the effective width method are summarised in Fig. 2.26.

2.3.5 Comparison and evaluation of design methods

The reduced stress method based on individual plate slendernesses has been implemented in proven standards DIN 18800-3 [28] and DNV-RP-C201 [33] but it has some known drawbacks. One is the missing consideration of the stabilising influence of tensile stresses in a stress field with stress gradients comprising both compression and tension. The other one is the "incompatibility" with advanced software tools when edge boundary conditions other than hinged are considered for the determination of the elastic critical stresses. In Chapter 10, EN 1993-1-5 [46] a modified verification procedure based on a single plate slenderness is provided which is capable to consider at least the effect of tensile stresses. Whereas the consideration of tensile stresses succeeds with a rather simple interaction shape which is affine to the equivalent stress hypothesis, a comparison of the results for plates under biaxial compression detects significant discrepancies e.g. to proven standard DIN 18800-3 [28]. In Figs. 2.27 and 2.28 the interaction curves of DIN 18800-3 [28], DNV-RP-C201 [33] and Chapter 10, EN 1993-1-5 [46], are compared for plates under biaxial loading with b/t-ratios equal to 30, 45, 65 and 100. In Fig. 2.27 results are given for square plates ($\alpha = 1$) and in Fig. 2.28 for rectangular plates ($\alpha = 3$). It can be shown that the curves are significantly different which negligibly depends on the reference strength. The reference strength e.g. for square plates is the Winter curve in all cases. For rectangular plates the reference strength accounts for column-like buckling and in this case it differs, even though marginally, with increasing slenderness. A comparison of the interaction curve shapes leads to the following conclusions:

DIN 18800-3 [28] rules are conservative in the medium to high slenderness range and all curves have a minor almost linear curvature. It is therefore astonishing that for biaxial compression and when the slenderness approaches the border to Class 3 cross-sections, a stability-induced reduction of the uniaxial loading load case is not required. As a result, in this slenderness range DIN 18800-3 is more favourable than the other rules and allows the application of the equivalent stress hypothesis.

DNV-RP-C201 [33] rules are significantly more favourable in the medium to high slenderness range. Also with tensile stresses present, the curves are somewhat more favourable than DIN 18800-3 but it can be said that this positive influnce is negligible. In general, it is felt that the curve shapes have been adjusted such that exponents and factors provide a simple interaction equation.

In case of biaxial compression the rules of Chapter 10, EN 1993-1-5 [46], are similar to DNV-RP-C201 rules. However, EN 1993-1-5 accounts for the positive influence of tensile stresses which leads to a significant increase of resistance and which is only limited by plastic-destabilising effects represented by sharp bends in the curve (see $\odot$ in Figs. 2.27 and 2.28). When the biaxial load case changes from compression-tension to biaxial compression, it is eye-catching and not plausible why the resistance is not monotonically decreasing (see $\otimes$ in Figs. 2.27 and 2.28). For high slendernesses, even an increase in resistance may be observed. However, for biaxial compression and approaching the border to Class 3 cross-sections, Chapter 10, EN 1993-1-5, leads to the most conservative results.

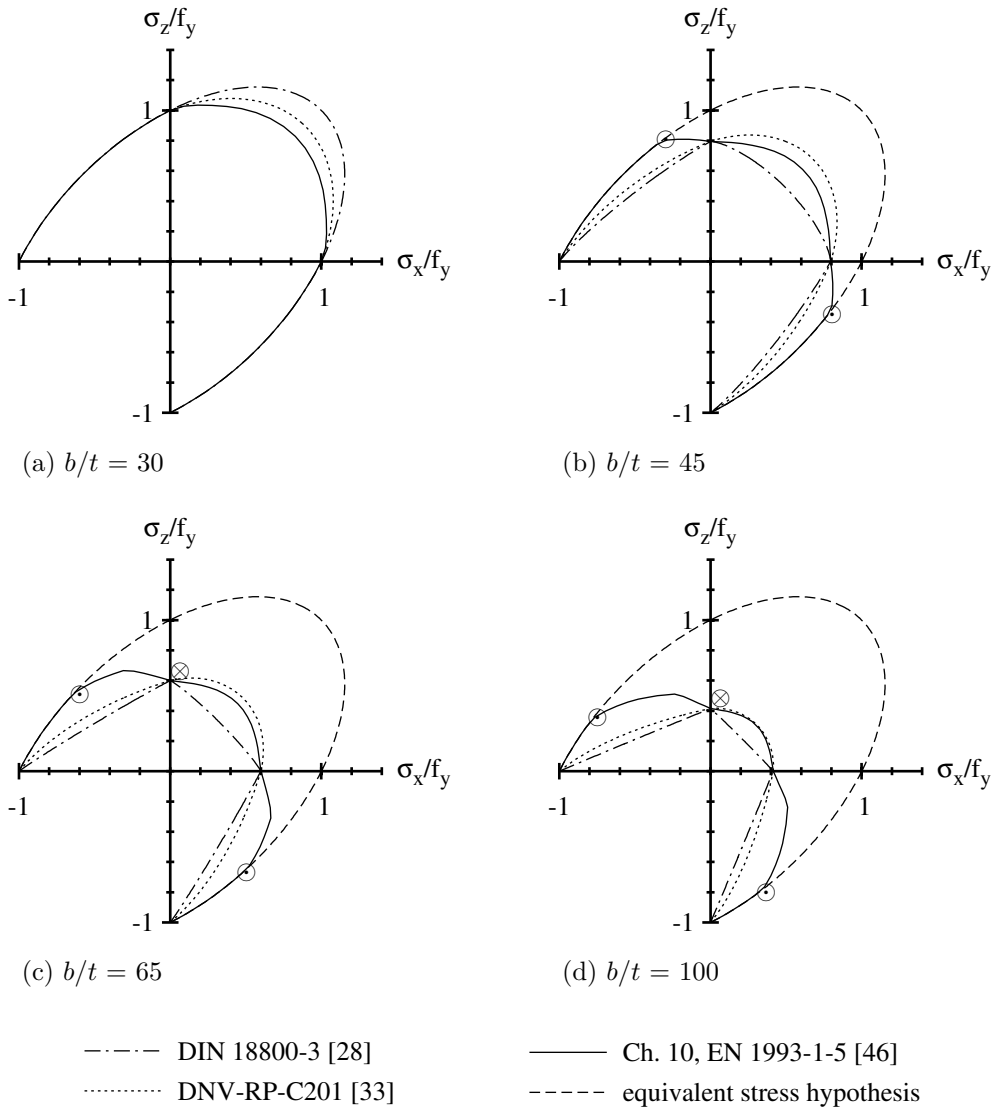

Figure 2.27: Comparison of interaction rules for biaxial loading ($\alpha = 1$, $f_y = 355\,\mathrm{MPa}$)

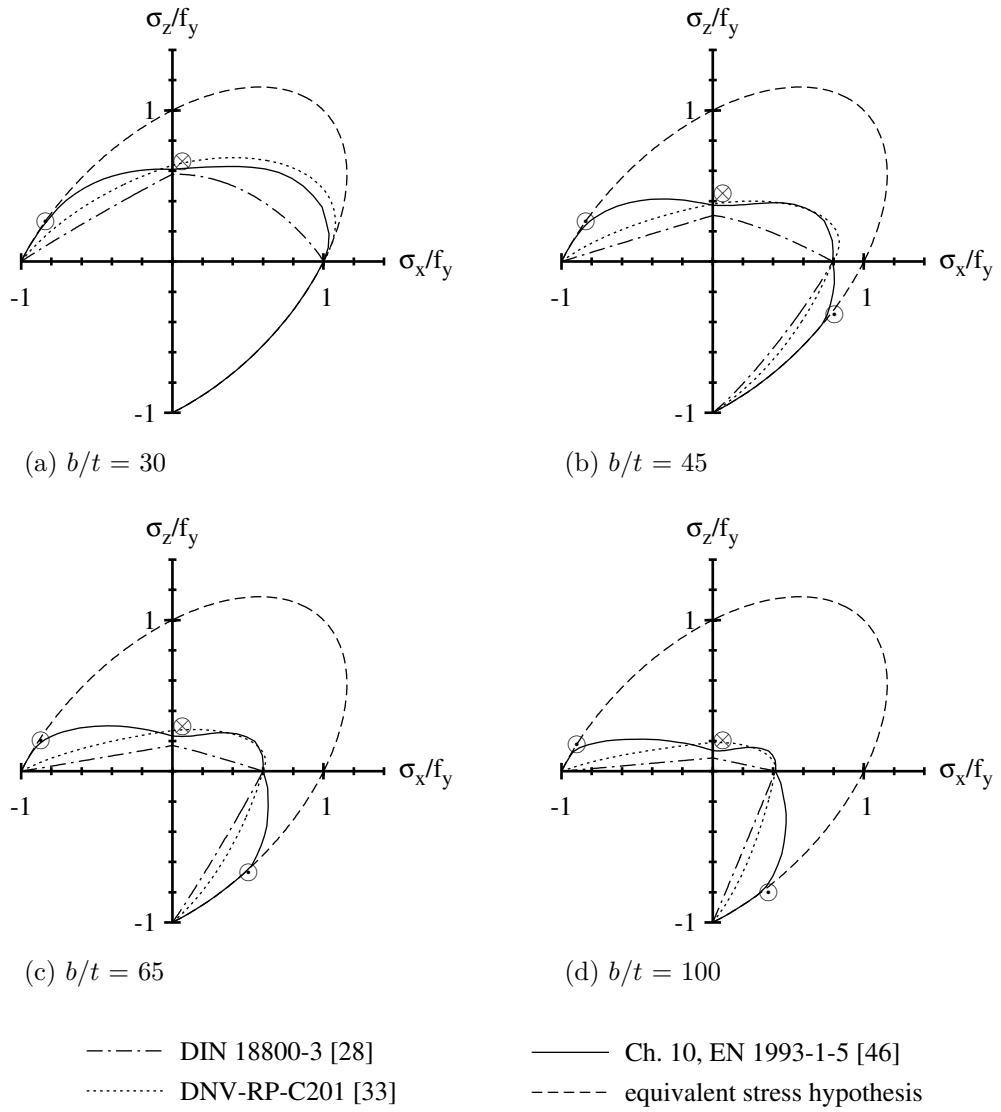

(a) $b/t = 30$ (b) $b/t = 45$

(c) $b/t = 65$ (d) $b/t = 100$

Figure 2.28: Comparison of interaction rules for biaxial loading ($\alpha = 3$, $f_y = 355\,\mathrm{MPa}$)

It was shown that Chapters 4 to 5, EN 1993-1-5 [46], provide the effective width method for standard geometries and load cases. Interaction is accounted for axial force, bending moment and shear force as well as transverse patch loading and bending moment. Other interaction cases such as biaxial compression are usually determined based on the reduced stress method. At present there is no interaction criterion for the load combination of transverse loading and shear force. Further studies will have to clarify if there is a need for the development of such an interaction criterion.

2.4 Recent research works on patch loading resistance

2.4.1 General

Patch loading on which this work focuses as leading loading is a specific load case which in civil engineering is important for the launching of bridges and the introduction of wheel loads in crane runway beams. A large number of research work has been recently carried out since the patch loading resistance models of current EN 1993-1-5 [46] have several shortcomings. For girders without longitudinal stiffeners, the effect of long loading lengths was not checked. For girders with longitudinal stiffeners, calculated results were contradictory to experiments and simulations because only the first eigenvalue is used in the determination of the buckling coefficient k_F. As a result, if the longitudinal stiffener moves away from the loaded flange, the depth of the indirectly loaded subpanel decreases, the critical load F_{cr} according to Chapter 6, EN 1993-1-5 [46] increases and finally the resistance F_R increases which is contradictory to the fact that the web is less stiffened at this position for patch loading. Mainly in the COMBRI research project [72] several aspects concerning an improvement of the patch loading resistance model of EN 1993-1-5 [46] have been studied and proposals were developed. In the successive valorisation project COMBRI+ [73] these proposals have been prepared for an implementation for standardisation as given below.

- The proposal according to Davaine [24] may be used as Nationally Determined Parameter (NDP) because it improves current Chapter 6, EN 1993-1-5 [46] for girders with longitudinal stiffeners as summarised in Sec. 2.4.2.
- The proposals according to Gozzi [56] and Clarin [19] may be used for the next revision of Eurocode because no national choice is allowed for this purpose in Chapter 6, EN 1993-1-5 [46]. The work of Gozzi [56] addresses girders without longitudinal stiffeners, see Sec. 2.4.3. The work of Clarin [19] is based on the proposal of Gozzi [56] but covers girders with longitudinal stiffeners, see Sec. 2.4.4.

In adddition to the models above, it is shown by Chacon [16] that the yield strength ratio between flanges and web of a hybrid girder has less influence on its resistance to patch loading than assumed in current Chapter 6, EN 1993-1-5 [46]. As a consequence, a proposal is made to account for hybrid girders by simplifying the coefficient m_1 in the

determination of the yield load F_y. However, hybrid girders are not within the scope of this work so that the proposal of Chacon [16] is not presented here in detail. Instead the reader is referred to [16–18] for further information.

Since this work focuses on the interaction behaviour with patch loading as the leading load, the improved patch loading resistance models of Davaine [24], Gozzi [56] and Clarin [19] will be considered as future choices for the reference strength. The consideration is mandatory in order to provide state-of-the-art interaction equations.

2.4.2 Davaine (2005)

Chapter 6, EN 1993-1-5 [46] uses the elastic critical load F_{cr} of the first web buckling mode which usually corresponds to a buckling of the indirectly loaded subpanel. As the shape of this buckling mode is not directly related to the collapse shape, it makes sense to introduce the one-wave buckling mode localised in the directly loaded subpanel according to Eq. 2.31.

$$F_{cr,2} = \left[0.8 \cdot \frac{s_s + 2 \cdot t_f}{a} + 0.6\right] \cdot \left(\frac{a}{b_1}\right)^{0.6 \cdot \frac{s_s + 2 \cdot t_f}{a} + 0.5} \cdot \frac{\pi^2 \cdot E}{12 \cdot (1 - \nu^2)} \cdot \frac{t_w^3}{h_w} \tag{2.31}$$

The elastic critical load of the first web buckling mode according to Eq. 2.29 is taken as $F_{cr,1}$. $F_{cr,2}$ from Eq. 2.31 is then interpolated with $F_{cr,1}$ to determine F_{cr} according to Eq. 2.32.

$$\frac{1}{F_{cr}} = \frac{1}{F_{cr,1}} + \frac{1}{F_{cr,2}} \tag{2.32}$$

As a consequence of the modified elastic critical load a new calibration of the reduction factor which relates the resistance to the slenderness was conducted. It is suggested to use the general format of Eq. 2.16 which follows Annex B, EN 1993-1-5 [46], as a basis for the calibration of the resistance function. The parameters α_0 and $\overline{\lambda}_0$ were calibrated using the experimental data collected in [57] for girders with longitudinal stiffeners and the numerical database built in [24] which is especially dedicated to bridge girders. The parameters were calibrated to $\alpha_0 = 0.21$ and $\overline{\lambda}_0 = 0.8$.

2.4.3 Gozzi (2007)

The equation of the yield load F_y in Chapter 6, EN 1993-1-5 [46] is based on a four plastic hinges mechanism of the loaded flange which is partly supported by the web. It includes the parameter m_2 which comes from an assumed T-section at the outer plastic hinges in the flange. However, the relevance of this parameter and the effect of the loading length has been questioned e.g. in [24] and thus an investigation was carried out by means of nonlinear finite element analyses in [56]. Various simulations were performed on

I-girders with the web restrained against out of plane deformations. The effective loaded length ℓ_y from the numerical analyses was integrated over the part of the web which is in compression and then compared to ℓ_y from EN 1993-1-5. All simulations showed that the consideration of m_2 overstimated ℓ_y but without m_2 the agreement was good. Hence, the parameter m_2 was removed which gave a new expression for the yield resistance according to Eq. 2.33.

$$F_y = f_{yw} \cdot t_w \cdot \left[s_s + 2 \cdot t_f \cdot \left(1 + \sqrt{\frac{f_{yf} \cdot b_f}{f_{yw} \cdot t_w}} \right) \right] \leq f_{yw} \cdot t_w \cdot a \tag{2.33}$$

As a consequence of the modified yield load a new calibration of the reduction factor which relates the resistance to the slenderness was conducted. It was suggested to use the general format of Eq. 2.16 which follows Annex B, EN 1993-1-5 [46], as a basis for the calibration of the resistance function. The slenderness $\overline{\lambda}_F$ has been determined with both hand calculation and advanced software. Then α_0 and $\overline{\lambda}_0$ were calibrated to fit the test results in the best possible way. A total of 190 tests with a negligible bending moment influence ($M_E/M_R \leq 0.4$) were used for the calibration and the best fit was found when α_0 and $\overline{\lambda}_0$ is set to 0.5 and 0.6 respectively. The reduction factor is determined according to Eq. 2.16 and has an upper limit of 1.2 instead of 1.0.

2.4.4 Clarin (2007)

When determining the elastic critical load F_{cr} according to current Chapter 6, EN 1993-1-5 [46], only buckling of the web panel as a whole is considered, see also Sec. 2.4.2. In contrast to this, tests show that buckling of the directly loaded subpanel is commonly experienced in experiments. It was shown that Davaine [24] presented a buckling coefficient for the directly loaded subpanel as introduced in Eq. 2.31. The approach of Clarin [19] is to use the minimum value of the buckling coefficient based on Eqs. 2.29 and 2.31 according to Eq. 2.34.

$$F_{cr} = \min \ (F_{cr,1}; F_{cr,2}) \tag{2.34}$$

For the new elastic critical load F_{cr} the reduction curve developed for girders without longitudinal stiffeners according to Gozzi [56] is adopted. The proposed design model was statistically evaluated with experiments summarised in [57] and simulations carried out by Davaine [24].

2.5 Summary

The complex nature of buckling phenomena under combined loading becomes evident when the nonlinear buckling due to basic load effects is analysed. Nevertheless, modern standards such as DIN 18800-3 [28], DNV-RP-C201 [33] and EN 1993-1-5 [46] provide efficient calculation procedures which are based upon the reduced stress method in case of both standard and arbitrary geometries as well as the effective width method in case of standard geometries.

Based on the comparison and evaluation of interaction criteria the following summary and imperatives for further work can be drawn:

- **Plates under biaxial compression and application of the reduced stress method based on a single plate slenderness.** The interaction equation based on a single plate slenderness shows significant discrepancies for the results of plates under biaxial compression in comparison with proven standard DIN 18800-3 [28]. A clarification of the background and a possible correction is required. Having the influence of edge boundary conditions in mind, not only their effect on the interaction criterion will have to be analysed, but also the plausibility criteria for the transferability of the results to the load combination of transverse stress (patch loading) and bending stress have to be reassessed.
- **Plate I-girder webs under transverse patch loading, bending moment and shear force (F-M-V) and application of the effective width method.** At present there is no interaction criterion for the load combination of transverse patch loading and shear force. Further studies will have to clarify if there is a need for the development of such an interaction criterion. Since this work focuses on the interaction behaviour with patch loading as the leading load, the improved patch loading resistance models of Davaine [24], Gozzi [56] and Clarin [19] will be considered as future choices for the reference strength. The consideration is mandatory in order to provide state-of-the-art interaction equations.

3 Review and evaluation of earlier work

3.1 General

In Chapter 2 shortcomings of current EN 1993-1-5 [46] have been identified for plates under biaxial compression and plate I-girder webs under transverse patch loading and shear force. In this chapter, earlier work on plates under biaxial compression and on girders under transverse patch loading and shear force is reviewed and evaluated.

It should be noted that plates under biaxial compression are a typical component of ship structures and many studies have their origin in this field. Plates under biaxial compression have been quite extensively studied in the 1970s and 1980s. Some experimental studies exist but the majority of the works are of theoretical nature due the effort which has to be undertaken for the experimental accomplishment, especially in the definition of the edge boundary conditions. Nevertheless, the results have been transferred to other fields of application and extended to other load cases such as transverse patch loading and bending moment presuming reasons of plausibility. Section 3.2 summarises the results of earlier work on plates under biaxial compression.

The interaction between transverse patch loading and shear force in plate I-girder webs is rarely governing and the decisive load combination is usually the interaction between transverse patch loading and bending moment. Nevertheless, it will be shown that the effect of shear forces onto transverse patch loading is not negligible. Section 3.3 summarises the results of earlier work on girders under transverse patch loading and shear force.

The interaction case "transverse patch loading and bending moment" which is also relevant for this work is not reassessed. Instead the reader is referred to literature where the results have been already summarised in detail, see e.g. [24, 77, 114].

3.2 Plates under biaxial compression

3.2.1 Becker et al. (1970/1977)

In 1970 and 1977, Becker et al. [5, 6] conducted two test series on steel plates under biaxial compression with regard to ship hull girders which marks the beginning of tests on plates under biaxial compression. The specimens were square sheet metal tubes with a side aspect ratio of $\alpha = 3$ which has been found to be representative for ship plating with aspect ratios of $\alpha \geq 3$. Tubes have been chosen because it was felt that the continuity across

Table 3.1: Main characteristics of the tests done by Becker et al. (1970/1977) [5, 6]

parameter	first test series (1970)	second test series (1977)
α	3.0	3.0
b/t	30; 50; 70; 90	30; 70
t	0.762 mm	0.635 mm
f_y	270 MPa (mild steel)	680 MPa (stainless steel 4130)
E	200 GPa	203 GPa
w_0	not measured	not measured
residual stresses	yes	yes
rotational restraint	$\approx$ simply supported	$\approx$ simply supported
in-plane restraint	not specified	not specified

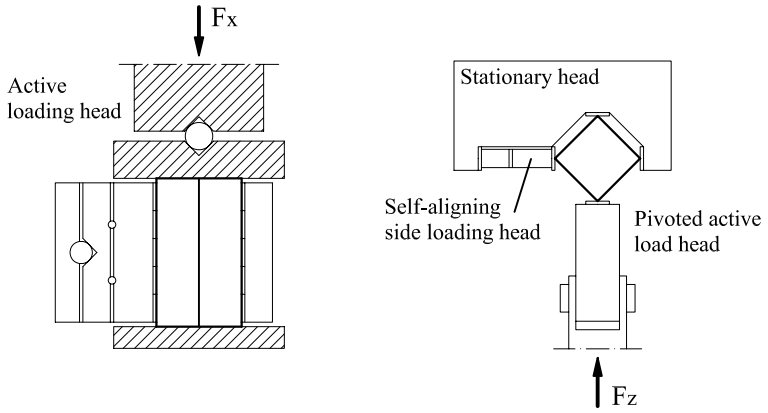

(a) Side view (b) Top view

Figure 3.1: Test set-up from Becker et al. (1970/1977) [5, 6]

each edge can simulate very well the behaviour of plates in a ship hull girder and each specimen provides information about four plates. The tubes were loaded longitudinally by applying loads to their ends through welded stiff plates which restrained the out-of-plane displacements of each plate element. Transversely, four equal inward loads along the corners of the tube were applied by applying the load to two opposed corners of the tube and the adjacent corners reacting against the fixed frame, see Fig. 3.1. All edges were assumed as hinged boundary conditions which is formally not fully correct but the influence of the stiff end plates was found to be negligible for the studied aspect ratio. In some cases the specimens have been stress-relieved by normalisation. Residual stresses were measured in all cases but no initial geometric imperfections were recorded.

In the first test series, the boundary conditions were not clearly represented when only transverse loading was applied. In that case, on the one hand, the tube could slide over the end plates without any effective restraint of the shape, on the other hand, the longitudinal elongation was restrained which de facto led to a biaxial state of stress. Thus, when a

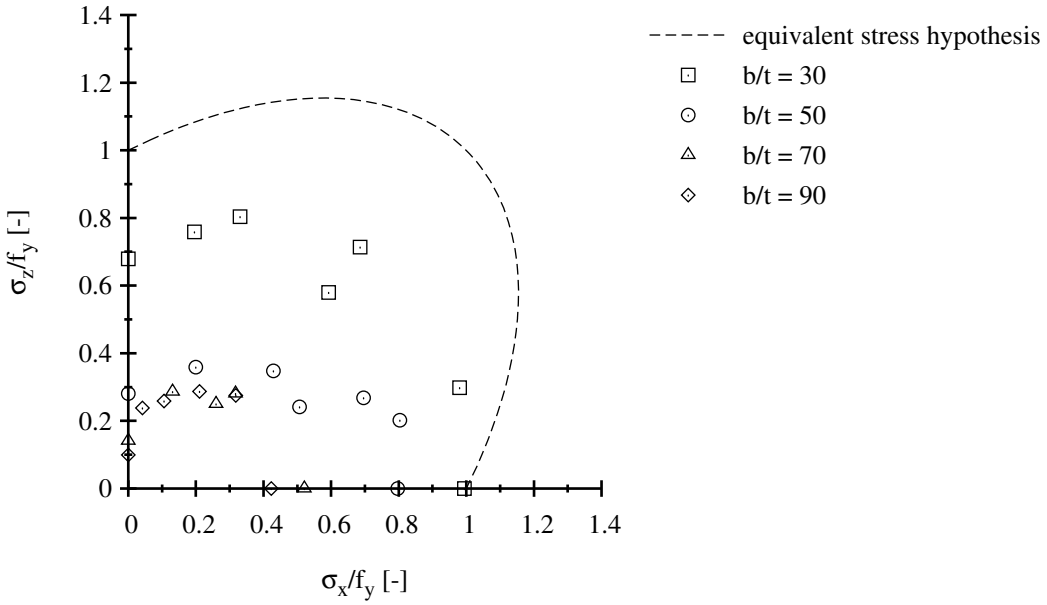

Figure 3.2: First test series from Becker (1970) [6] ($\alpha = 3$, $f_y = 270\,\mathrm{MPa}$)

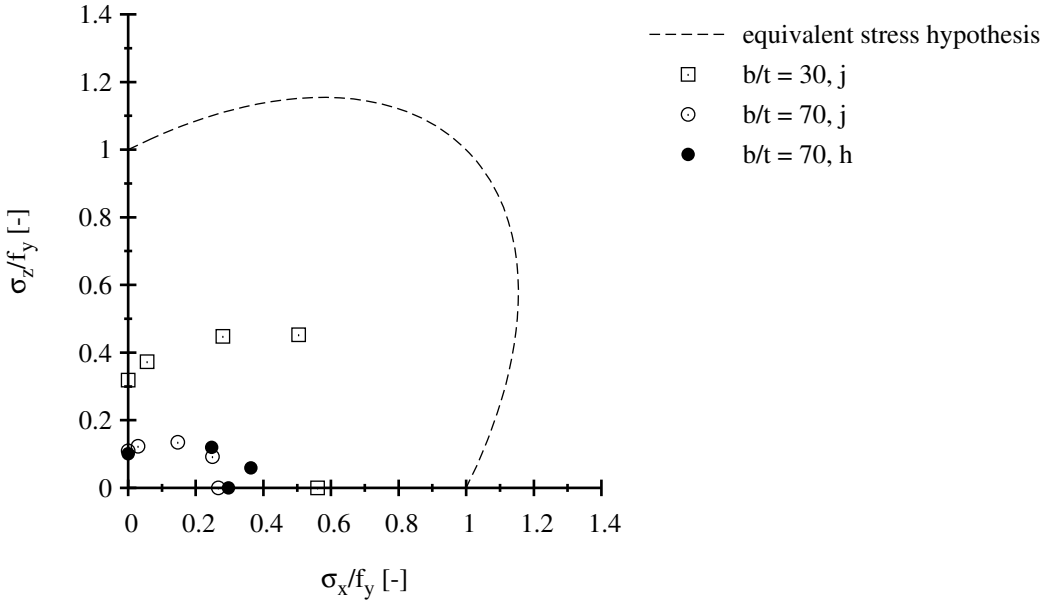

Figure 3.3: Second test series from Becker (1977) [5] ($\alpha = 3$, $f_y = 680\,\mathrm{MPa}$)

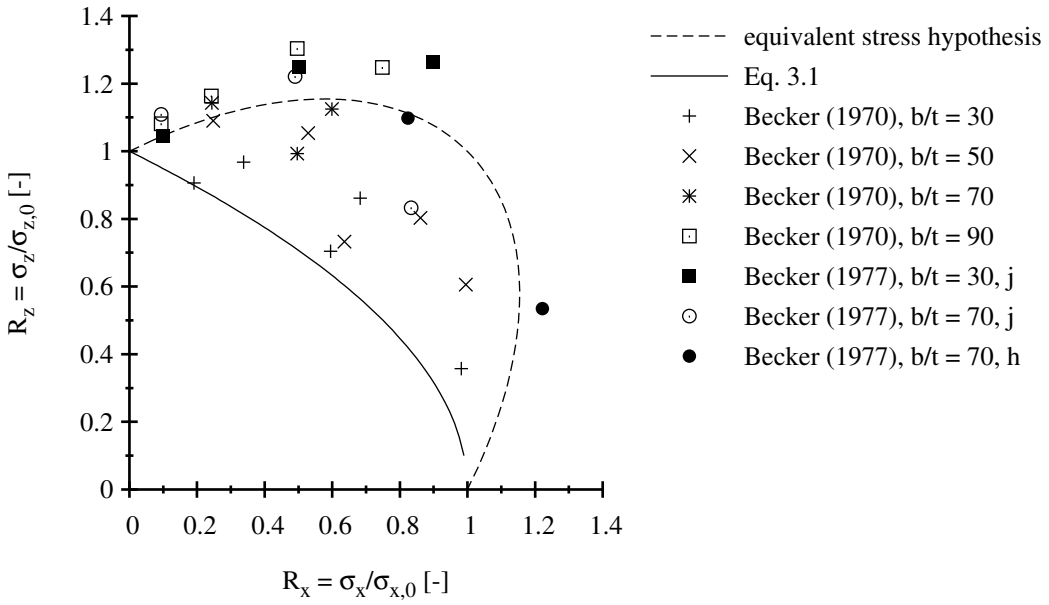

Figure 3.4: Normalised test results from Becker et al. (1970/1977) [5, 6] ($\alpha = 3$) and interaction curve proposal by Faulkner et al. [50]

second test series on high strength stainless steel was carried out, the opportunity was taken to identify the influence of the boundary conditions. The longitudinal loads were applied similarly as in the first test series. However, end plates were fitted in the tube to maintain the shape of the ends when only transverse loading was applied, without restraining the longitudinal elongation.

A considerable scatter is found in the experimental data of the first test series, see Fig. 3.2, which is due to difficulties with a proper control of the boundary conditions. In that way the low resistances when only transverse loading is applied can be explained. Buckling due to a biaxial state of stress contributes to a reduced resistance in the transverse direction. However, the difficulty which arises for the transverse resistance does not really question the results under combined loading. The experiments of the second test series are more consistent, see Fig. 3.2. However, stainless steels are used for which the yield strength could not distinctively be determined.

In a later publication [4], Becker presents the relation of these results to design and amends them with considerations on the minimum weight optimisation of ship structures. Although a design proposal for interaction is not made, the major conclusion is drawn that "the efficient design of biaxially loaded structures may employ an appropriate interaction law which is a function of [the slenderness, A. N.] β " [4]. Besides that it is stated that biaxially loaded plates possess only a reduced or no postcritical strength reserve at all. Finally, Becker gives an overview in [4] on the test results according to Fig. 3.4 with the following normalising strengths ρ_x according to Becker and Colao [5] and ρ_z based on extrapolated values as roughly described in Becker [4].

Based on the first test series by Becker et al. [6], Faulkner et al. [50] proposed Eq. 3.1

Table 3.2: Main characteristics of the simulations done by Frieze et al. (1977) [52]

parameter	Frieze et al. (1977)
α	1.0
b/t	20; 30; 40; 60; 80
t	not available
f_y	251 MPa (mild steel)
E	210 GPa
material model	elastic-perfectly plastic
w_0	b/240 to b/60 (slenderness dependent)
residual stresses	no
rotational restraint	simply supported
in-plane restraint	constrained

in 1973 for the design of plates with an aspect ratio of $\alpha = 3$, see Fig. 3.4. Although the results show a significant scatter, this parabolic interaction curve has been adopted also in the DNV offshore design code [32] of 1977.

$$R_x + R_y^2 = 1.0 \tag{3.1}$$

3.2.2 Frieze et al. (1977)

Frieze et al. [52] carried out a theoretical pilot study on plates under biaxial compression which is part of a larger study on plates under uniaxial compression. They used an elasto-plastic large deflection analysis method based on finite difference procedure to study plate behaviour in which displacements i.e. strains are prescribed. In [60] this analysis method has been compared and confirmed by other large deflection elasto-plastic procedures. For uniaxial compression, the method was applied to study extensively the influence of initial deformations, residual stresses and edge boundary conditions. In the frame of the pilot study, interaction curves for the design of square plates under biaxial compression were proposed.

The influence of aspect ratio and initial imperfections was also adressed briefly. Aspect ratios of $\alpha = 1$ and 3 were directly compared. The conclusion was drawn that square plate data could not be used to predict the strength and stiffness of a rectangular plate in the transverse direction which is nowaydays known as column-like buckling. On the other hand, it could be shown that in the longitudinal direction the strength may be higher than for square plates. The influence of initial imperfections has been studied for $b/t = 60$ ($\overline{\lambda} = 1.091$) with sine-shape and imperfection amplitudes from $w_0 = $ b/320 to b/40. It was found, similar to the uniaxial tests, that with increasing amplitude the ultimate load decreases. Parameters of the study are given in Table 3.2.

Based on a parameter study the interaction curves according to Fig. 3.5 have been

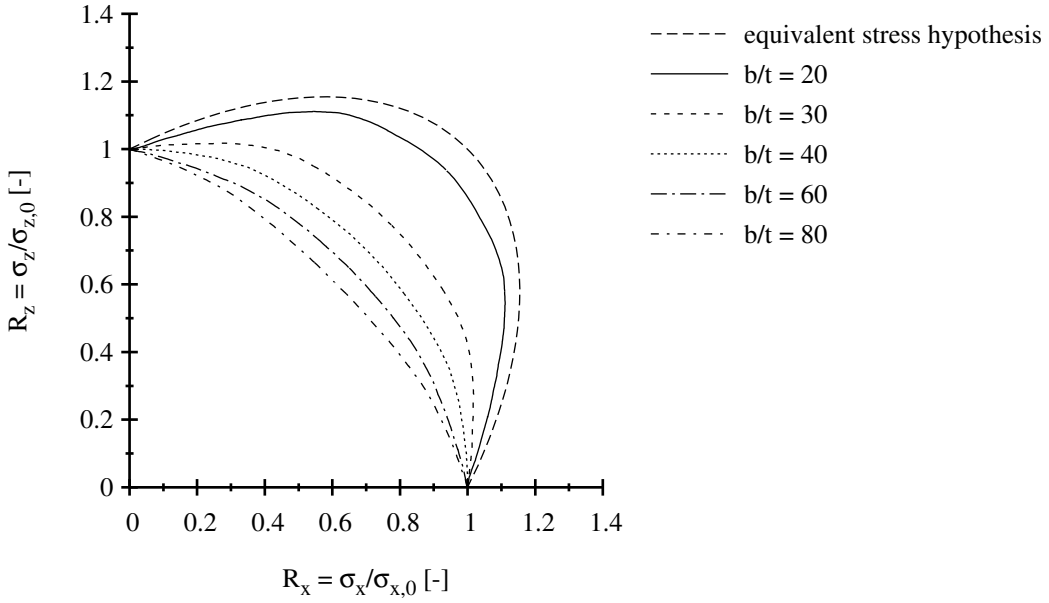

Figure 3.5: Normalised interaction curves proposed by Frieze et al. (1977) [52] ($\alpha = 1$, $f_y = 251\,\mathrm{MPa}$)

derived for the design of square plates. The evaluation of interaction was done based on ρ_x and ρ_z derived from their own study [52] on uniaxially compressed plates. Because the plates are square and all edges constrained, i.e. they remain straight in-plane, the same reduction curve is used for ρ_x and ρ_z. In Fig. 3.5 the biaxial data are normalised with the corresponding uniaxial data. For stocky plates with $\overline{\lambda} < 0.526$, which corresponds to $b/t \approx 30$ here, it is stated that membrane action is predominant so that the ultimate load behaviour is rather influenced by material behaviour than buckling, leading to higher strengths for biaxial compression.

3.2.3 Valsgard (1978/1979)

Valsgard [121] conducted a theoretical study on plates under biaxial compression. The results have been published in [122] together with a study on column-like behaviour of transversely compressed plates. For calculation nonlinear shell analysis programs based on both the finite difference method and the finite element method were used and validated against each other and other available design data mainly for the uniaxial direction. Valsgard conducted four series in which mainly the slenderness was varied, see Table 3.3. From the study, it is concluded that neither residual stresses nor initial geometric imperfections significantly change the shape of the biaxial interaction curve provided that they are limited to reasonable margins.

Moreover, alternative loading sequences have been studied which take into account a non-proportional loading such as compressing the plate firstly in transverse direction, keeping this value constant and applying the compression in the longitudinal direction

Table 3.3: Main characteristics of the simulations done by Valsgard (1978/1979) [121]

parameter	Valsgard (1978/1979)
α	3.0
b/t	40; 50; 67; 89
t	20; 16; 12; 9
f_y/f_u	320 MPa / 340 MPa
E	not available
material model	tri-linear
w_0	b/200
residual stresses	no
rotational restraint	simply supported
in-plane restraint	constrained

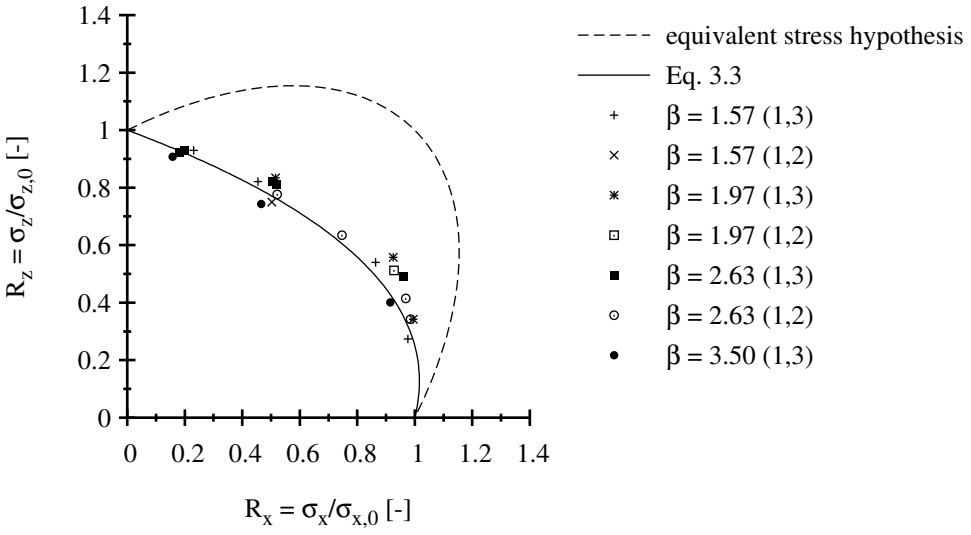

Figure 3.6: Normalised interaction curve proposed by Valsgard (1980) [121] ($\alpha = 3$)

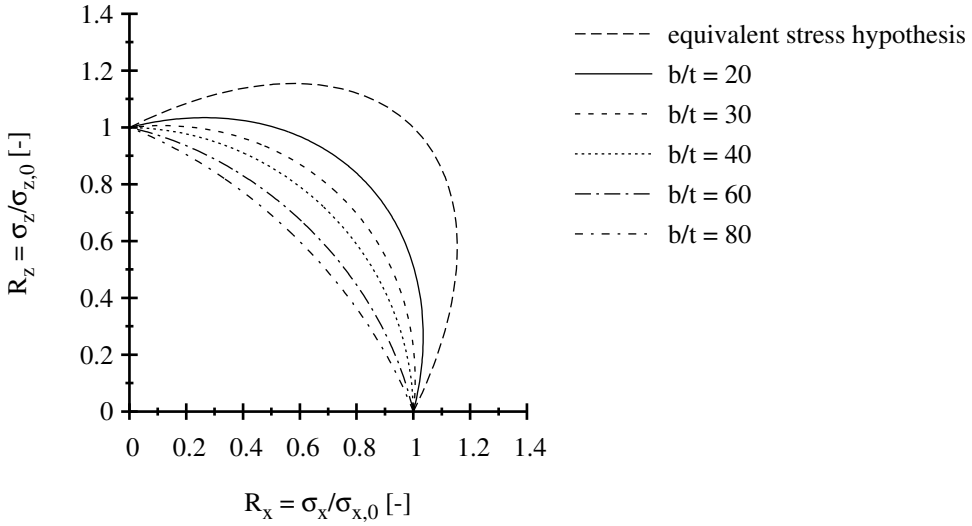

Figure 3.7: Normalised interaction curves proposed by Valsgard (1980) [121] ($\alpha = 1$), similar parameters as for Frieze et al. (1977) [52], see Fig. 3.5

secondly or vice versa. An extensive analysis was carried out showing that in both ways the buckling pattern develops favourably and tends to increase the resistance. Thus, a conservative prediction of a biaxial design formula has to based on proportional loading.

Finally, Valsgard proposes a general form of an interaction equation according to Eq. 3.2. For aspect ratios $\alpha \geq 3$, the parameters e and η have been determined by curve fitting to numerical calculations by Valsgard [122] which results in $e = 1$ and $\eta = 0.25$, see Eq. 3.3. The influence of slenderness was found to be small in the studied range so that constant parameters were defined. For plates with an aspect ratio of $\alpha = 1$, the slenderness dependent interaction curve proposed by Frieze et al. [52], see Sec. 3.2.2, has been approximated on the basis of Eq. 3.2 resulting in Eq. 3.4 with an exponential function for $\overline{\eta}$. For intermediate aspect ratios a linear interpolation for both parameters is proposed. In general, it is concluded that both parameters are dependent on aspect ratio and slenderness.

$$R_x^e - \eta \cdot R_x \cdot R_y + R_y^2 \leq 1.0 \tag{3.2}$$

$$R_x - 0.25 \cdot R_x \cdot R_y + R_y^2 \leq 1.0 \qquad \text{for } \alpha \geq 3 \tag{3.3}$$

$$R_x^2 - \overline{\eta} \cdot R_x \cdot R_y + R_y^2 \leq 1.0 \qquad \text{for } \alpha = 1 \tag{3.4}$$

where

$$\overline{\eta} = 3.2 \cdot e^{-0.35 \cdot \beta} - 2$$

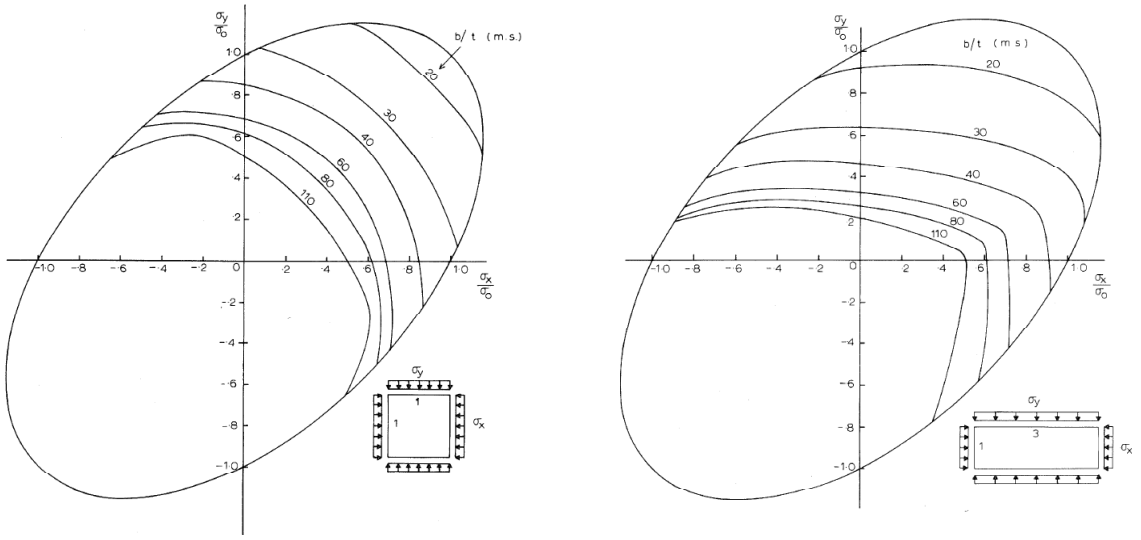

(a) $\alpha = 1$ (b) $\alpha = 3$

Figure 3.8: Numerical results by Dier and Dowling (1979/1980) [27]

3.2.4 Dier and Dowling (1979/1980)

Dier and Dowling conducted an extensive study on plates under biaxial loading, mainly compression-compression, but also considering compression-tension and lateral pressure, which led to two research reports [26, 36]. In [36] only plates under biaxial in-plane loading with an aspect ratio of $\alpha = 3$ were studied. In [26] it was extended to square plates and lateral loading. The results have been published later in part by Dier and Dowling [27]. The theoretical studies have been conducted on the basis of the finite difference method. The main focus was on the level of initial geometric imperfections and residual stresses. The geometric imperfections have a single wave in transverse direction and three waves in longitudinal direction. The initial imperfection amplitude was scaled with factors 3 and 0.25 to study the influence of amplitude. It was found "that interaction curves are very similar in shape for any given plate" [27]. Also the level of residual stress with a compressive stress of $0.2 \cdot f_y$ was scaled with factors 2 and 0.25.

Moreover, alternative loading sequences have been studied which take into account a non-proportional loading such as compressing the plate firstly in transverse direction, keeping this value constant and applying the compression in the longitudinal direction secondly or vice versa. An extensive analysis was carried out showing that in both ways the buckling pattern develops favourably and tends to increase the resistance. Thus, a conservative prediction of a biaxial design formula has to based on proportional loading. Dier and Dowling studied also the effect of aspect ratio on column-like behaviour. It is shown that an aspect ratio of $\alpha = 3$ represents very well plates with larger aspect ratios.

The results of the numerical calculations are drawn in the form of interaction curves. In Fig. 3.8 curves are shown for aspect ratios $\alpha = 1$ and $\alpha = 3$. These curves were compared

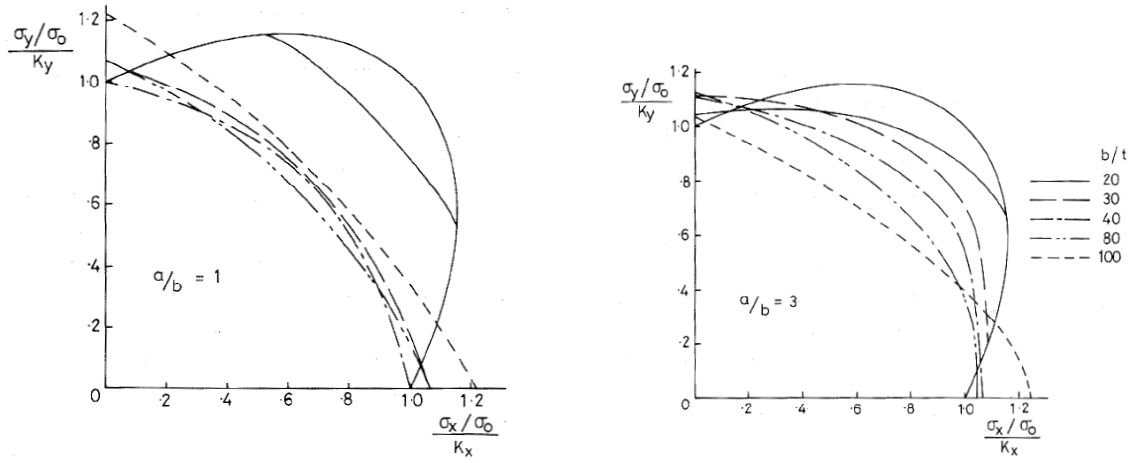

(a) $\alpha = 1$ (b) $\alpha = 3$

Figure 3.9: Normalised numerical results by Dier and Dowling (1979/1980) [27]

to experimental results by Becker et al. [6], see Sec. 3.2.1, and they were later confirmed independently by Isami [63].

For square plates, Dier and Dowling propose Eq. 3.5. As normalising strengths, values from own calculations in the uniaxial longitudinal and transverse direction are used. A single interaction curve with a constant η is proposed although it is recognised that slender plates have straighter interaction curves than stocky plates. To account for stocky plates, it is proposed to allow the reduction factor ρ to become greater than unity. Conservatism is ensured by applying the equivalent stress hypothesis at the same time. It is not mentioned but implicitely assumed that the reduction factor requires also a modification for slender plates in order to use Eq. 3.5, see Fig. 3.9. After all, Dier and Dowling recognise by themselves that the drawback of this approach would be that it is not logical for the designer to understand but the only way to use a single interaction curve for simplicity.

$$R_x^2 + 0.45 \cdot R_x \cdot R_y + R_y^2 = 1.0 \text{ for } \alpha = 1 \tag{3.5}$$

For plates with an aspect ratio of $\alpha \geq 3$, it is proposed that R_x^2 to the second power is kept for the sake of simplicity. η is proposed to be adjusted but neither further studies are undertaken nor a proposal is made. Comparing the diagrams in Fig. 3.9, it can be seen that only for medium slendernesses a common interaction curve is reasonable. As soon as the slenderness becomes small or high, η requires adjustment. For plates with an aspect ratio of $\alpha \geq 3$, Dier and Dowling propose to give η as a function of the slenderness. This is not consistent with the chosen procedure for square plates and to the proposal of Valsgard, see Sec. 3.2.3.

Table 3.4: Main characteristics of the simulations done by Dier and Dowling (1983) [27]

parameter	Dier and Dowling (1983)
α	3.0
b/t	20 to 120
t	12 mm to 2 mm
f_y	245 MPa (mild steel)
E	205 GPa
material model	elasto-plastic
loading type	prescribed displacements
w_0	slenderness and aspect ratio dependent
residual stresses	yes
rotational restraint	simply supported
in-plane restraint	constrained

3.2.5 Jungbluth and Kubsch (1980)

In [68] Jungbluth and Kubsch carried out a theoretical study and interaction curves were proposed. The study was based on the finite element method which was implemented in a program system by Dumont [40]. In total, 35 results were calculated of which four concerned biaxial compression only and 35 results biaxial compression and shear force. The program was verified later on also in a study on buckling loads of unstiffened plate elements taking into account geometric imperfections and residual stresses [69].

As [68] is an unpublished paper, the data are taken from Lindner and Habermann [78]. Edge boundary conditions are given as constrained which is contradictory to Fig. 3.10 where they have been drawn in relation to interaction curves. The information can be doubted in so far as in the later study [69] the edge boundary condition is unrestrained.

3.2.6 Harding (1983)

Harding [61] conducted a general theoretical study on plates taking into account uniaxial and biaxial compression as well as shear. Results of computer simulations and analysis of design codes are presented. For the numerical study a finite difference large deflection elasto-plastic method was applied. An extensive study on the effect of aspect ratio, edge boundary condition, geometric imperfection and residual stress is conducted for the uniaxial compression case. For the biaxial case, Table 3.6 summarises the main characteristics. The imperfection sensitivity was studied and also the residual stress level was varied. As can be seen in Fig. 3.12 the influence of geometric imperfections is large for medium slender plates, but the shape of the interaction curve is not influenced.

It can be cited that “for the stocky panels a biaxial effect induces stress levels greater than yield in certain areas while the circular yielding interaction controls general be-

Table 3.5: Main characteristics of the simulations done by Jungbluth and Kubsch (1980) [68]

parameter	Jungbluth and Kubsch (1980)
α	1.0
b/t	100
t	not specified
f_y	240 MPa
E	not available
material model	not specified
w_0	b/200
residual stresses	yes
rotational restraint	simply supported
in-plane restraint	constrained (reported, but unconstrained assumed)

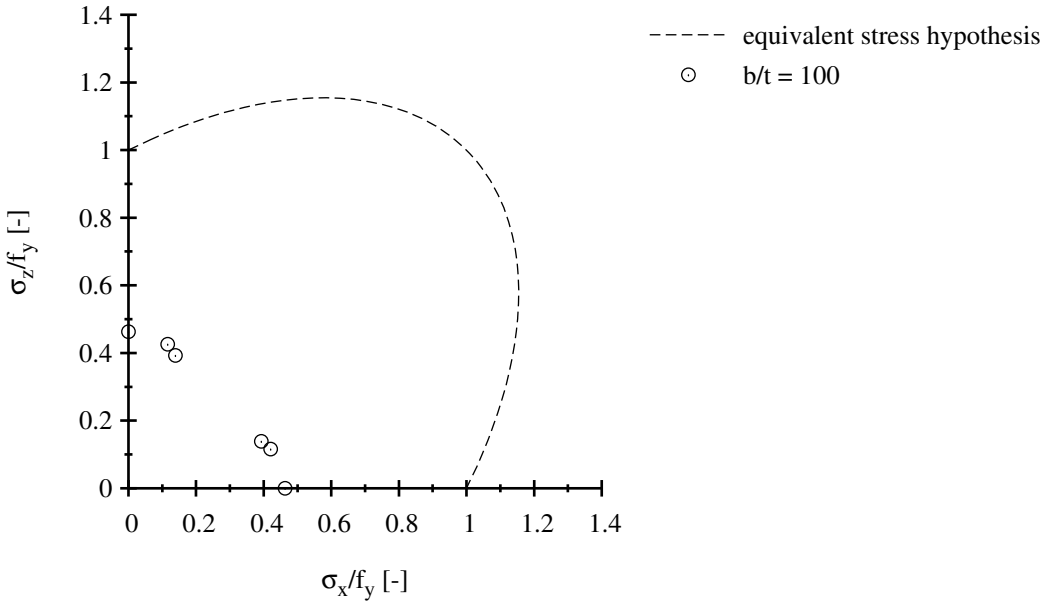

Figure 3.10: Numerical results by Jungbluth and Kubsch (1980) [68] ($\alpha = 1$, $f_y = 240\,\mathrm{MPa}$)

Table 3.6: Main characteristics of the simulations done by Harding (1983) [61]

parameter	Harding (1983)
α	3.0
b/t	20; 30; 50; 80; 120
t	not specified
f_y	245 MPa (mild steel)
E	205 GPa
material model	elasto-plastic
loading type	prescribed displacements
w_0	slenderness and aspect ratio dependent
residual stresses	yes
rotational restraint	simply supported
in-plane restraint	unrestrained

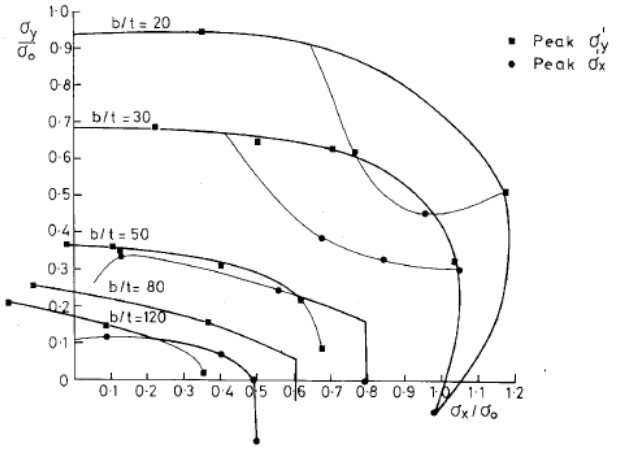

Figure 3.11: Interaction curves proposed by Harding (1983) [61] ($\alpha = 3$, $f_y = 245\,\mathrm{MPa}$)

haviour. For the slender panels behaviour is much closer to a straight line reflecting elastic buckling influences" [61, Sec. 8.4.4]. In Fig. 3.11 tentative interaction curves are drawn against the calculated results.

Harding [61] imposed displacements, i.e. ϵ_x/ϵ_y-ratios, onto the edges which per se assumes that the edges remain straight. The specialty of the calculations done with imposed displacements is that σ_x peaks at a different strain than σ_y. Two points are obtained which lead to two different "peak stress interaction curves", see Figs. 3.11 and 3.12. It is justifiable to take the interaction curve obtained from the rising curve which corresponds to the outside interaction curve because if the stress in one direction dominates, the weaker stress peak occurs significantly earlier than the one of the stronger component but without leading to immediate failure.

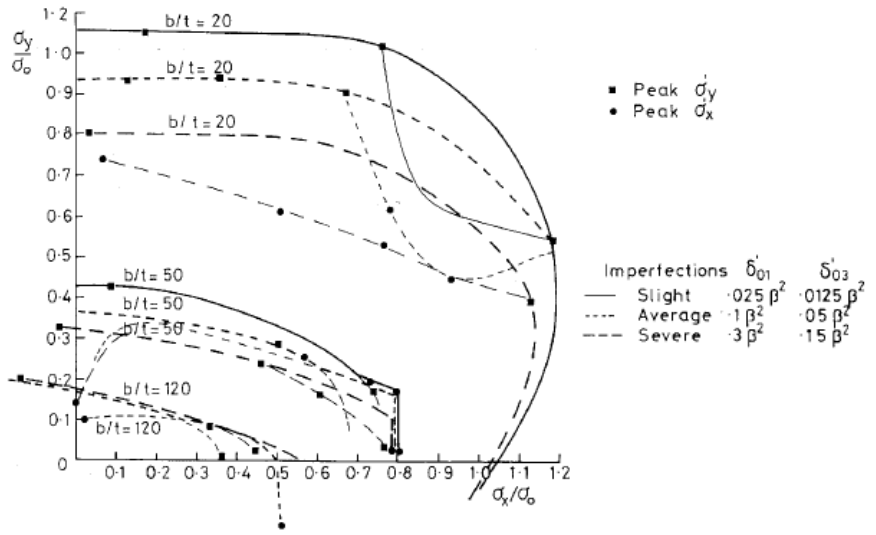

Figure 3.12: Influence of imperfections by Harding (1983) [61] ($\alpha = 3$, $f_y = 245\,\mathrm{MPa}$)

3.2.7 Narayanan and Shanmugan (1983)

Narayanan and Shanmugan [85] conducted a theoretical study for square plates and developed an approximate analysis method to account for interaction. The calculation was based on the energy method. Comparison was made with more accurate calculation methods and it could be shown that the results are sufficiently good. The extensively studied and documented parameters are aspect ratio, initial imperfection, loading ratio and slenderness. Interaction curves for different sets of boundary conditions are provided according to Figs. 3.13 and 3.14.

3.2.8 Stonor et al. (1983)

Stonor et al. [118] conducted an experimental test series on long plates ($\alpha = 4$ and 6) under biaxial compression which has been published later by Bradfield et al. [11]. The test layout of the biaxially loaded plates is shown in Fig. 3.15. In the longitudinal direction the shortening curve for each plate under loading was measured. Out-of-plane deformations were recorded in order to identify the failure buckling mode. The loading was composed of a dominant longitudinal compression together with a small transverse compressive loading. Thus, the failure mode was expected to resemble the uniaxial loading case. Tests were performed both under constant transverse loading and under proportional loading to study the effect of different loading paths.

Plates of aspect ratio $\alpha = 4$ and 6 with simply supported edge boundary conditions were tested. The plate thickness was 6 mm and steel grade BS 4360, Grade 50B. The longitudinal loading was applied as prescribed displacement to the short edges. The transverse loading was a constant force per unit length applied to the longer edges, over

Table 3.7: Main characteristics of the simulations done by Narayanan and Shanmugan (1983) [85]

parameter	Narayanan and Shanmugan (1983)
α	1.0
b/t	30; 40; 50; 60; 80; 100
t	not specified
f_y	245 MPa (mild steel)
E	205 GPa
material model	elastic-perfectly plastic
loading type	not specified
w_0	slenderness and B.C. dependent
residual stresses	no
rotational restraint	simply supported and clamped
in-plane restraint	constrained

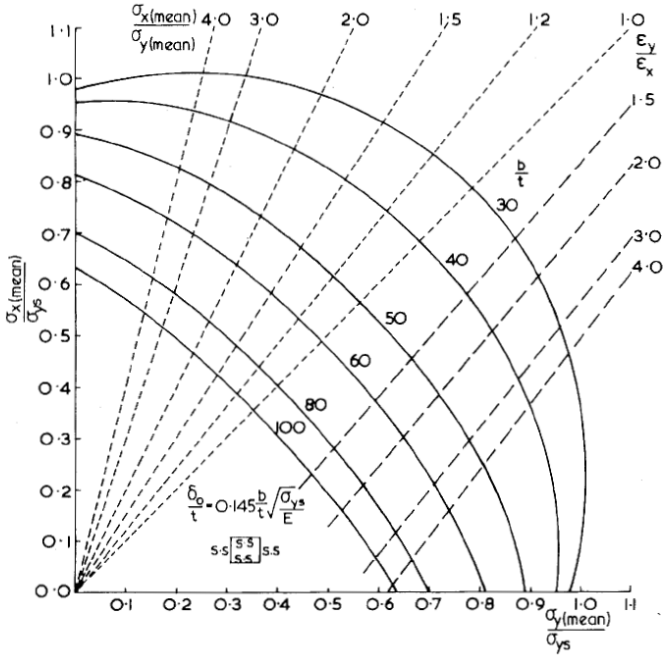

Figure 3.13: Interaction curves with **hinged** edges proposed by Narayanan and Shanmugan (1983) [85] ($\alpha = 1$, $f_y = 245\,\mathrm{MPa}$)

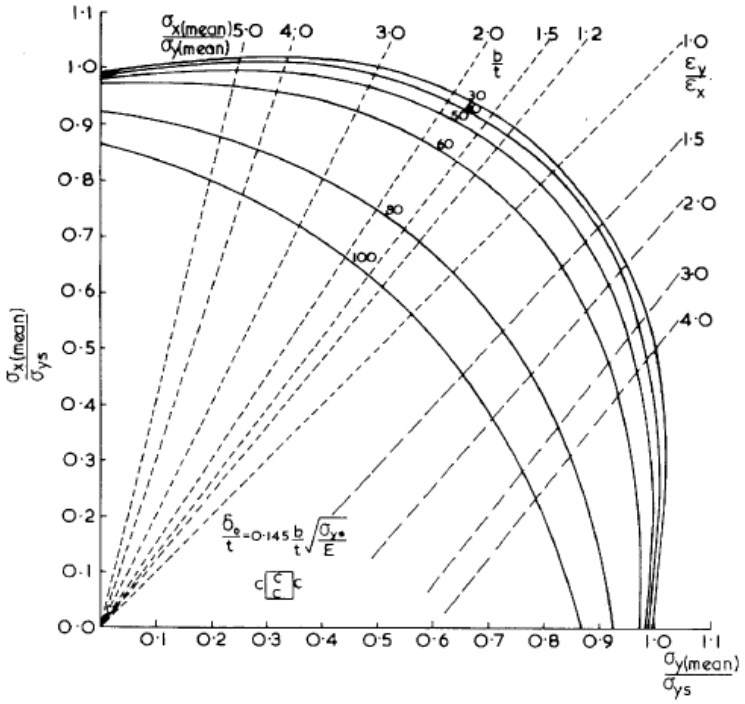

Figure 3.14: Interaction curves with **clamped** edges proposed by Narayanan and Shanmugan (1983) [85] ($\alpha = 1$, $f_y = 245\,\mathrm{MPa}$)

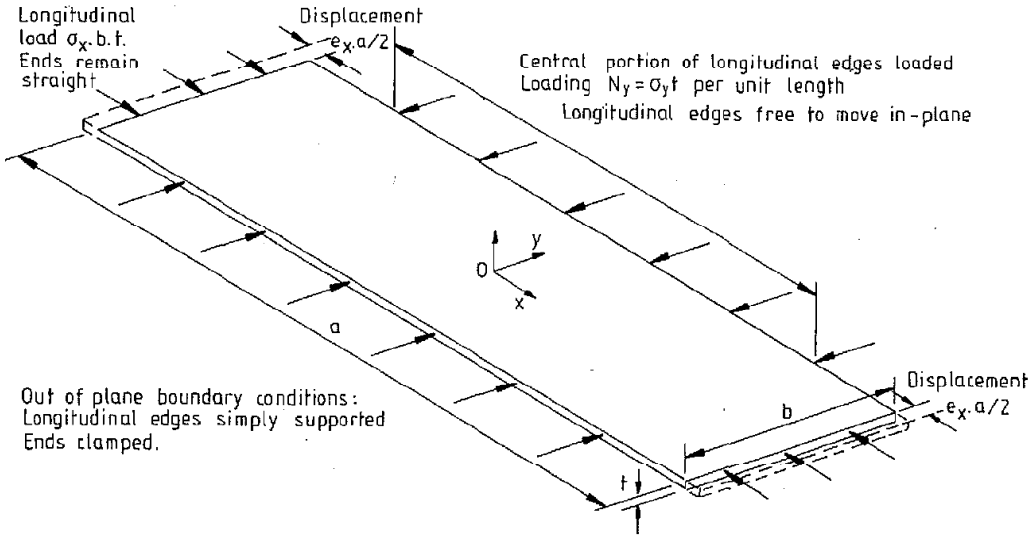

Figure 3.15: Test layout according to Stonor et al. (1983) [118]

Table 3.8: Main characteristics of the tests done by Stonor et al. (1983) [118]

parameter	Stonor et al. (1983)
α	4.0; 6.0
b/t	35; 45; 55
t	6 mm
f_y	369 MPa
E	not specified
w_0	not available
residual stresses	with and without
rotational restraint	simply supported
in-plane restraint	unrestrained

a length of $2 \cdot b$ and $4 \cdot b$. The longitudinal load was applied through a stiff wedge-jack and a set of discrete fingers was used to restrain the out-of-plane displacements of the longitudinal edges. The edges were flexible in the x- and y-directions to avoid the transfer of the longitudinal loads into their supports and to allow inward and outward in-plane movement of the longitudinal edges. Thus, the short edges remain straight during loading whereas the longer edges are allowed to move in-plane. An initial out-of-plane imperfection was introduced by using an hydraulic jack carrying a small cap as load spreader. All plates failed by the formation of a single large buckle at the centre, corresponding to the position of the initial dent. For the plates with a b/t-ratio of 35 the buckle length is about the plate width but for plates with $b/t = 45$ and 55 this length grows to $1.3 \cdot b$.

In the view of all uncertainties in the test results, Stonor et al. [118] propose Eq. 3.6 as lower bound curve.

$$R_x^{1.5} + R_y^{1.5} = 1.0 \tag{3.6}$$

3.2.9 Dinkler and Kröplin (1984)

Dinkler and Kröplin [31] carried out a theoretical study on square plates based on the finite element method. In total, 27 results were calculated of which six concerned biaxial compression alone and 15 concerned the biaxial loading case “compression-tension”, see Fig. 3.17. Six results also consider an additional shear force. Edge boundary conditions were constrained. For further parameters see Table 3.9.

3.2.10 Davidson et al. (1989)

Davidson et al. [25] conducted an extensive theoretical study in order to determine the ultimate strength of rectangular plates under longitudinal, transverse and biaxial compression in ship structures. The study was based on an elasto-plastic numerical analysis.

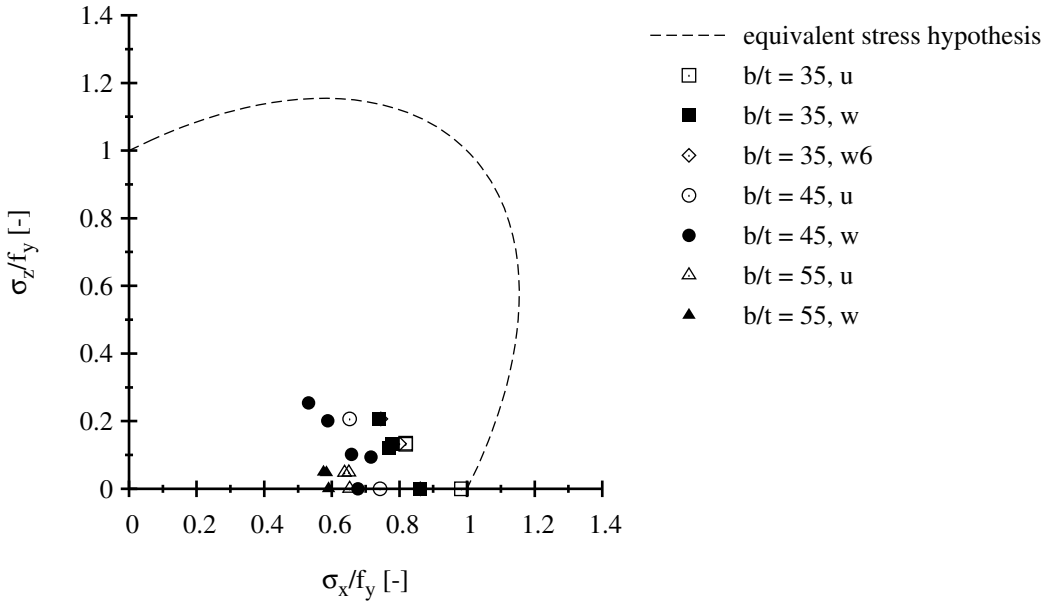

Figure 3.16: Tests from Stonor et al. (1983) [118] ($\alpha = 4$ and 6, $f_y = 369\,\mathrm{MPa}$)

Table 3.9: Main characteristics of the simulations done by Dinkler and Kröplin (1980) [31]

parameter	Dinkler and Kröplin (1984)
α	1.0
b/t	55; 110
t	not specified
f_y	240 MPa
E	not available
material model	not specified
w_0	b/250
residual stresses	not specified
rotational restraint	simply supported
in-plane restraint	constrained

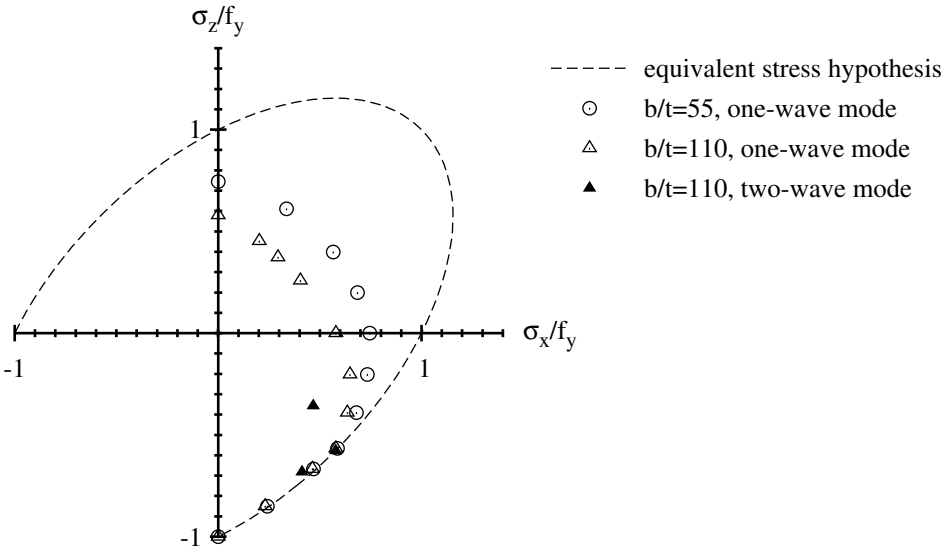

Figure 3.17: Numerical results from Dinkler and Kröplin (1984) [31]
($\alpha = 1$, $f_y = 240\,\mathrm{MPa}$)

The focus was on the reference strengths since it was recognised that the significance of the interaction diagram mainly depends on this input value.

The analysis of the existing interaction equations according to Fig. 3.18 shows that these design models are not satisfactory, since they are limited to specific geometries or they do not describe the effect of mode changes. Moreover, it is found that interaction curves ranging from stocky to slender panels are not very realistic. For that reason a high number of parameters was varied, see Table 3.10.

3.2.11 Guedes Soares and Gordo (1995)

Guedes Soares and Gordo [59] reassessed existing results and design methods for plates subjected to biaxial compression, taking into account lateral pressure in a separate chapter. Existing experimental results from Becker et al. [6], Becker and Colao [5], Stonor et al. [118] were considered as well as numerical results from Dier and Dowling [26]. The results were systematically analysed and normalised with:

- yield strength
- ρ_x according to Faulkner [49] and ρ_z according to Valsgard [121]
- strength predictions taking into account residual stresses

A characterisation of the data points led to the conclusion that stocky plates fail in the plastic range which is governed by the equivalent stress hypothesis. The stocky range is assumed to be $\beta < 1.3$ and the slender range $\beta > 1.3$ where β =1.3 corresponds approximately to a b/t-ratio of 30.

A comparison with existing interaction equations from code rules and e.g. Faulkner

Table 3.10: Main characteristics of the simulations done by Davidson et al. [25]

parameter	Davidson et al. [25]
α	1.0; 3.0
b/t	40 to 180
t	not specified
f_y	245 MPa
E	not specified
material model	elasto plastic
w_0	b/200
residual stresses	not specified
rotational restraint	simply supported
in-plane restraint	constrained

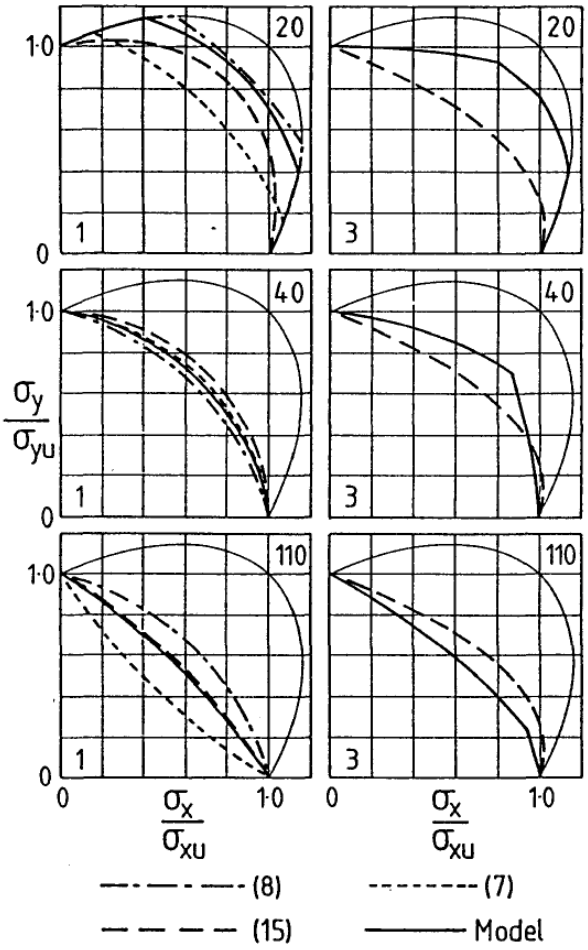

Figure 3.18: Biaxial interaction curves proposed by Davidson et al. [25] in comparison to (7) Dier and Dowling [26], (8) Dier and Dowling [27] and (15) Valsgard [122] (left column: $\alpha = 1$, right column: $\alpha = 3$)

et al. [50] shows that the model uncertainty level is satisfactory so that the interaction curve from BS 5400 is used and validated. Further improvement seems to be difficult.

Although the bias is reduced, the mean value for slender plates looks alright. But if for high slendernesses the interaction is more severe and for low slendernesses it is the opposite, the mean value may be still alright but not the description in dependence on the slenderness. Unfortunately, no deviation of results from the interaction curve is shown before the correction for residual stress is applied.

Finally, the revalidated and proposed interaction curve for all panel aspect ratios is according to Eq. 3.7.

$$R_x^2 + R_y^2 = 1.0 \tag{3.7}$$

3.2.12 Cui et al. (2002)

Cui et al. [22] conducted a theoretical study on plates under biaxial compression and small lateral pressure. For calculation they used the "simplified analytical method" proposed by Fujita et al. [53, 54] which combines elastic large deflection theory and rigid-plastic analysis based on kinematically admissible collapse mechanisms. This method has been generalised and validated for plates subjected to uniaxial compression by Cui and Mansour [23]. It takes into account geometric and material imperfections. Cui et al. applied this method to plates subjected to biaxial compression and small lateral pressure in order to validate it for combined loading and to propose an interaction equation for plates subjected to biaxial compression. Lateral pressure was assumed to be small in order to be able to apply the simplified analytical method and it was substituted by an equivalent geometric imperfection so that its influence plays only a minor role here.

In a first step, the method was validated against the experimental results for combined loading from Becker [4]. Experimental results from Paik and Pedersen [91] and Max [83] have been used to revalidate it for the uniaxial compression case. All recalculations show that the simplified analytical method is sufficiently accurate to determine the ultimate strength of plates subjected to biaxial compression and small lateral pressure.

On the basis of a parameter study the influence of various parameters is assessed. It is found that the findings for uniaxial compression as reported in Cui and Mansour [21] hold true for biaxial compression as well. Thus, in the following the relevant aspects for biaxial compression are summarised only: For the effect of transverse compression on the longitudinal strength "it can be seen that as the transverse stress increases, the longitudinal ultimate strength decreases almost linearly" [22, Sec. 4.1] which is independent from the studied slenderness. Besides that, it is shown that the effect of lateral pressure is small in this study [22, Sec. 4.2].

The background of the study were ship structures and for the choice of parameters a floating production and storage facility (FPSO) is referenced. Parameters of the study are given in Table 3.11.

Table 3.11: Main characteristics of the simulations done by Cui et al. (2002) [22]

parameter	Cui et al. (2002)
α	3.0
b/t	$\beta = 2.0$ to 3.5 ($\approx b/t = 49$ to 86)
t	not specified
f_y	330 MPa
E	200 GPa
w_0	slenderness dependent
residual stresses	yes
rotational restraint	simply supported
in-plane restraint	not specified

Based on the parameter study the interaction equation according to Eq. 3.8 has been derived by curve fitting. Here, the evaluation is done based on ρ_x according to an own curve-fitted reduction curve [22] and ρ_z according to Valsgard [121].

$$R_x^2 + 0.1135 \cdot R_x \cdot R_y + R_y^2 = 1.0 \tag{3.8}$$

Finally, the proposal has been drawn against other normalised interaction curves by Faulkner, Stonor and Dier and Dowling. It can be shown that they fit to these proposal as well and, by doing this, that the simplified analytical method is revalidated as calculation tool.

3.2.13 Evaluation of results

Tables 3.12 and 3.13 summarise the experimental and numerical studies on plates under biaxial compression. From the large number of studies on plates under biaxial compression relevant aspects which effect the results are given below.

- **Slenderness.** Studied slendernesses cover the practical application range of mild steel up to a b/t-ratio of 120. Stocky plates may still benefit from the favourable material behaviour under biaxial compression which allows stress levels close to the equivalent stress hypothesis. However, the more slender a plate becomes, the higher the influence of elastic buckling is. As a result the interaction curve shapes range from the equivalent stress hypothesis to almost a straight line which reflects elastic buckling.
- **Aspect ratio.** Studied aspect ratios comprise square plates with $\alpha = 1$ and rectangular plates with $\alpha = 3$ which represent typical bounds of plate behaviour. If only a single load direction of the rectangular plate is considered, the longitudinal direction (assumed to be the long edge) shows plate-like behaviour whereas the transverse direction (assumed to be the short edge) is governed by column-like behaviour. In

the studies, an aspect ratio of $\alpha = 3$ could be confirmed as representative for plates with aspect ratios $\alpha \geq 3$. Plate-like and column-like behaviour influence directly the basic reduction factors and thus the reference strengths, which have been used as normalising strengths in some cases. As a result, interaction curves for plates with increasing aspect ratio loose their symmetry to the bisector of the first quadrant. Linear interpolation between interaction curves developed for an aspect ratio of $\alpha = 1$ and $\alpha = 3$ has been often proposed for intermediate values.

- **Geometric imperfection.** Geometric imperfection shape and amplitude have been a main issue for the theoretical studies and efforts have been undertaken to determine the imperfection sensitivity. It was shown by Narayanan and Shanmugan [85] that the amplitude does not alter the interaction curve shape. Imperfection shapes have a significant influence on non-square plates because the number of halfwaves in the longitudinal directions differs from that in the transverse direction. In the longitudinal direction it depends on the length of the plate how many halfwaves appear. In the transverse direction it is usually a single halfwave which occurs. Thus, for a rectangular plate two imperfection shapes based on the basic loading are reasonable. It is found that for column-like buckling a single halfwave in both directions governs the plate resistance. For plate-like buckling the multi-halfwave configuration is more appropriate. Other shapes tend to stiffen the plate, thus leading to an overestimation of the ultimate resistance.
- **Residual stress distribution.** The influence of residual stresses has been accounted for in most of the studies and different levels of residual stress have been analysed. Some influence is found for stocky to medium slendernesses but the use of equivalent geometric imperfections is considered as sufficient.
- **Rotational edge restraint.** Each plate which is part of a steel plated structure possesses some amount of rotational edge restraint. These edge restraints can be usually idealised on the safe side as simply supported boundary conditions. The opposite to this is a fully clamped boundary condition. Rotational edge restraints influence the plate resistance and for clamped boundary conditions higher ultimate resistances may be reached. These effects are usually covered by the reduction factor determined for basic loading. Although the edge restraints effect the interaction curve shape, the use of appropriate reduction curves may cover their influence as it can be concluded from Narayanan and Shanmugan [85], i.e. clamping has a similar effect as if a lower slenderness would be chosen.
- **In-plane edge restraint.** In-plane edge restraints are usually provided when a plate is joined with an adjacent element. For stocky plates, there is no influence because the in-plane stiffness of the plate itself is high. For slender plates, the in-plane restraint may significantly increase the plate resistance. This effect is rarely accounted for.
- **Load application.** In both the experimental and the numerical studies displacement-controlled boundary conditions, i.e. ϵ_x/ϵ_y-ratios, have been used almost without

Table 3.12: Overview of experimental studies on plates under biaxial compression

main reference	year	α [-]	b/t [-]	f_y [MPa]
Becker et al. [6]	1970	3	30; 50; 70; 90	270
Becker and Colao [5]	1977	3	30; 70	680
Stonor et al. [118]	1983	4; 6	35; 45; 55	369

Table 3.13: Overview of numerical studies on plates under biaxial compression

main reference	year	α	b/t [-]	f_y [MPa]
Frieze et al. [52]	1977	1	20 to 80	251
Valsgard [121]	1978	3	40 to 89	320
Dowling et al. [36]	1979	3	20 to 120	245
Dier and Dowling [26]	1980	1 and 3	40 to 80	245
Jungbluth [68]	1980	1	100	240
Harding [61]	1983	3	20 to 120	245
Narayanan and Shanmugan [85]	1983	1	30 to 100	245
Dinkler and Kröplin [31]	1984	1	55 and 110	240
Davidson et al. [25]	1989	1 to 10	18 to 180	n.a.
Cui et al. [22]	2002	3	n.a.	330

exception because other boundary conditions were difficult to define at that time. However, imposed displacements per se assume that the edges remain straight which is true for a large number of applications but extraordinary shapes or certain applications may not follow this. It is e.g. not true for patch loading where the loaded edges usually deform in-plane.

A comparison of interaction curve proposals is difficult since it strongly depends on the reference strengths. Sometimes reduction curves have been used, sometimes customised reference values from tests were taken. The reference strengths used for plate-like and column-like behaviour are summarised in Figs. 3.19 and 3.20. Despite the various number of reference strengths, it can be shown that the reference strengths which have been chosen in the standards today represent an upper bound to all the curves, i.e. the reference strengths we are using now are more favourable in comparison to the ones which were used in former times. If it is assumed that the interaction criteria were proposed based on conservative reference strengths, the curve shapes are more favourable than in case the "real" reference strengths for biaxial loading were used. In turn, the curve shapes should stay or become more severe if the reference strength is improved. To make this point clearer, take an example as follows: if an almost linear interaction is predicted based on a conservative reference strength, the interaction curve usually cannot become more favourable with a more favourable reference strength but most likely the opposite trend may be observed instead.

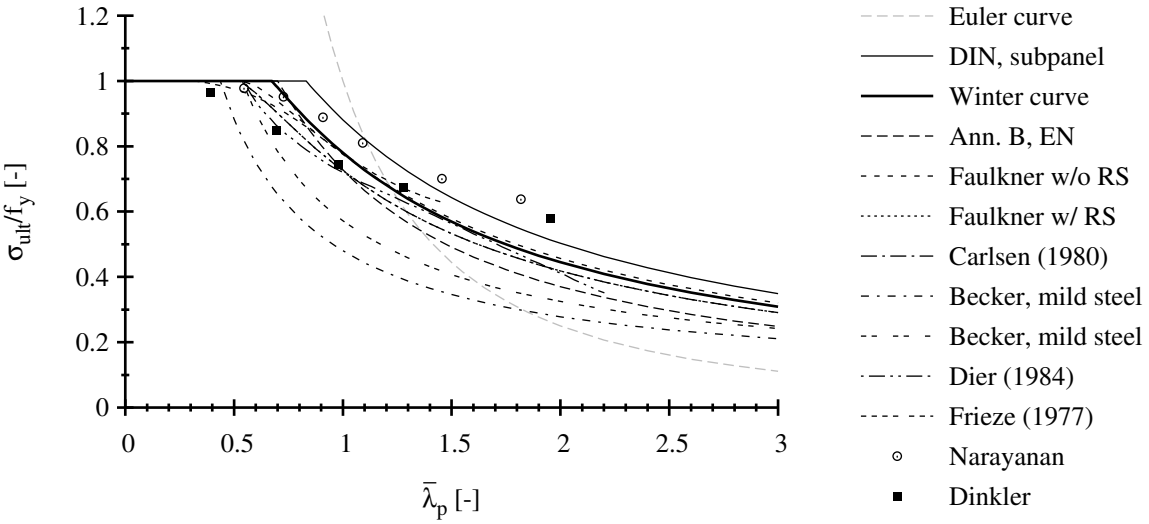

Figure 3.19: Comparison of reference strengths for plate-like behaviour

Although experimental and numerical studies from literature have been summarised and a lot of knowledge has been gained, it does not resolve the discrepancies which have been identified between Chapter 10, EN 1993-1-5 [46], DIN 18800-3 [28] and DNV-RP-C201 [33]. Nevertheless, the summary is of great help for the definition of the boundary conditions of the numerical parameter studies.

3.3 Girders subjected to transverse patch loading and shear force

3.3.1 General

A review of published studies on the interaction between transverse patch loading and shear force shows that only few data are available in general and for plated girders in particular. Early studies were conducted on beams with cold-formed hat sections and hot rolled sections.

Zoetemeijer [126] studied the influence of shear stresses on the transverse patch loading resistance of hot rolled sections of type IPE 240, HEA 240, HEA 300 and HEA 500. The yield strength of the beams varied between 286 MPa and 425 MPa. Background of the study is the bearing capacity of beam-to-column connections in which beams are connected to each side of the column having asymmetric loading or different height of the beams so that there is no equal shear force. Although the webs are not as slender in order to be in line with the objective of this work, the drawn conclusion is yet interesting. A comparison of the results led to the conclusion that the "shearing stresses caused by the lateral force (transverse patch loading, A.N.) itself have no influence on the collapse load of the laterally applied force. Shear stresses have an important influence if the shearing

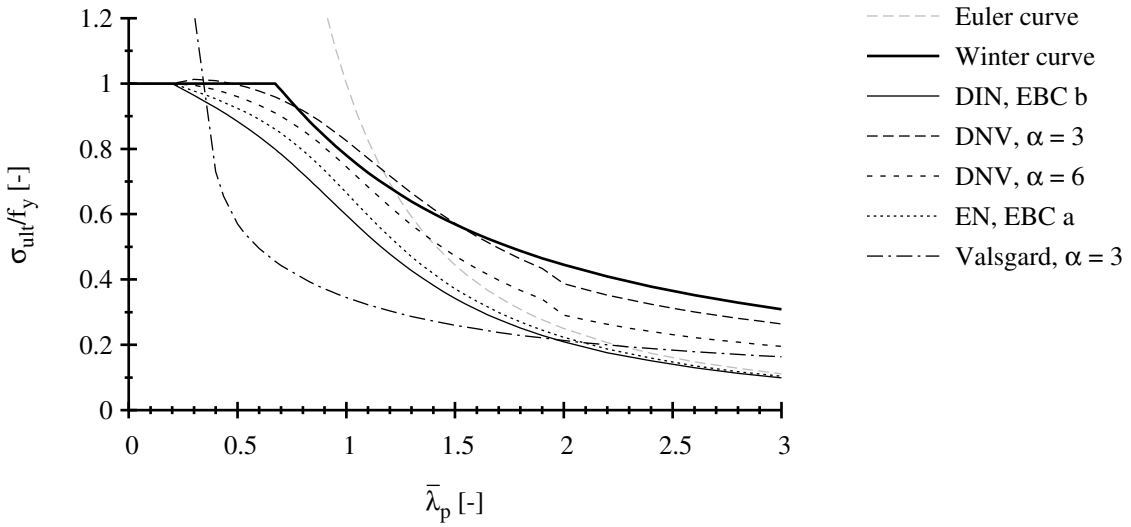

Figure 3.20: Comparison of reference strengths for column-like behaviour

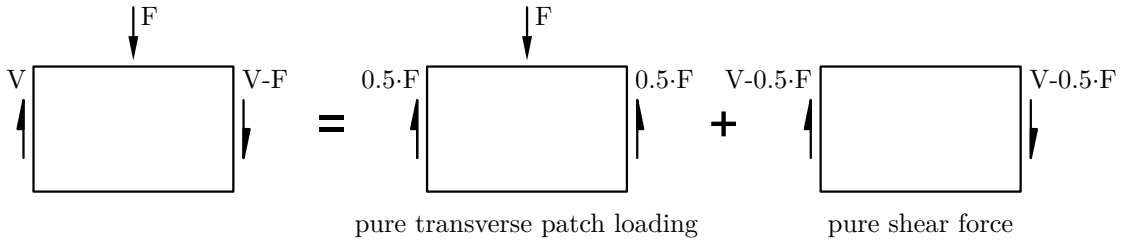

Figure 3.21: Subdivision into basic load cases

force does not reverse at the lateral compression force" [126]. The observation is traced back to the fact that the onset of buckling induced by the shear stresses is increased by the transverse patch loading and Eq. 3.9 was derived.

$$\left(\frac{V - 0.5 \cdot F}{V_R}\right)^2 + \left(\frac{F}{F_R}\right)^2 \leq 1.0 \tag{3.9}$$

Since the transverse patch loading already induces a shear force for reasons of equilibrium, all further studies have in common that they subdivide the combined loading into two basic load cases. Thus, the influence of additional shear stresses which are not caused by the transverse patch loading can be better accounted for and a regular transverse patch loading verification does not require an interaction check. Figure 3.21 shows the two basic load cases pure transverse patch loading and pure shear force which in combination lead to the considered type of interaction. In the following the component (V-0.5·F) is called "average shear force".

In Secs. 3.3.2 to 3.3.4, studies on girders with slender webs are presented in detail.

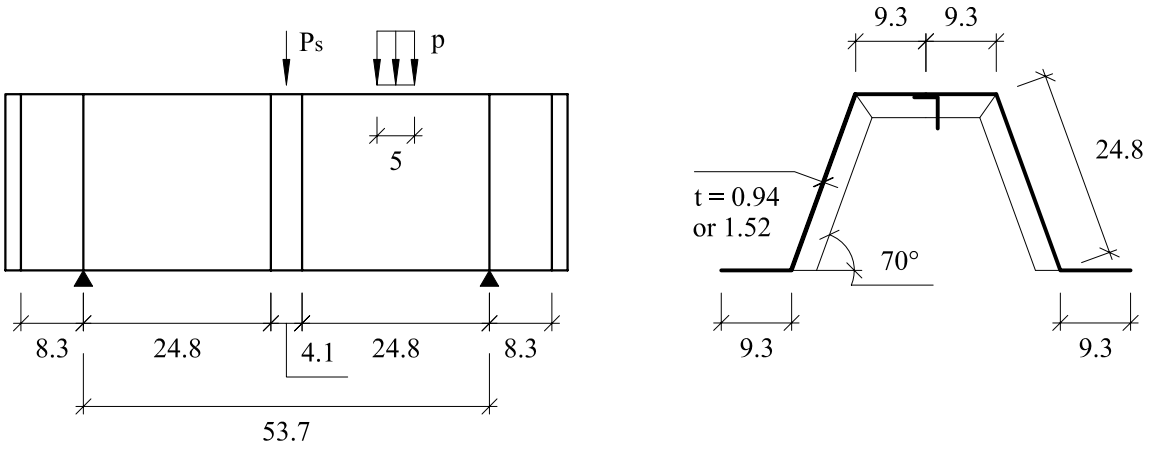

Figure 3.22: Tests from Elgaaly (1975) [41], dimensions in [mm]

3.3.2 Elgaaly (1975)

In 1975, Elgaaly [41] published the earliest known experimental study on the interaction between transverse patch loading and shear force on 11 beams made of cold-formed hat sections with slightly inclined webs, see Fig. 3.22. The relevant panels had an aspect ratio of $\alpha = 1$, b/t-ratio of 200 and 325 and the yield strength was either 228 or 274 MPa. The girders were simply supported and strengthened by diaphragms at the supports and at the load introduction at mid-span. Outer diaphragms were intended to serve as rigid end-posts for the anchorage of the tension field stresses. In order to avoid buckling of the slender top flange, a logitudinal stiffener was bolted to the flange as shown in Fig. 3.22. The girders were loaded with a concentrated load P_s at mid-span and a transverse patch loading p with $s_s/h_w = 0.2$ in each panel adjacent to mid-span, one at a time, so that in total 18 test results could be gained. The variation of the shear force level was achieved by varying the magnitude of P_s so that also in case of pure patch loading the induced shear stresses were not equally distributed to the edges. The behaviour of the basic load cases was confirmed by comparison to other studies on transverse patch loading [105] and Basler's shear theory. Based on the test series, Eq. 3.10 is proposed.

$$\left(\frac{V - 0.5 \cdot F}{V_R}\right)^{1.8} + \left(\frac{F}{F_R}\right)^{1.8} \leq 1.0 \tag{3.10}$$

3.3.3 Oxfort, Weber and Gauger (1981/1989)

In 1981, Oxfort and Weber [89] conducted three tests on steel plated girders to study the influence of shear force on the transverse patch loading resistance, which was extensively studied in a preceding study [88]. The tests were done in the frame of a test programme in which also the interaction between transverse patch loading and bending moment was studied. The relevant panels had an aspect ratio of $\alpha \approx 1.5$, b/t-ratio of 113 and 162.5

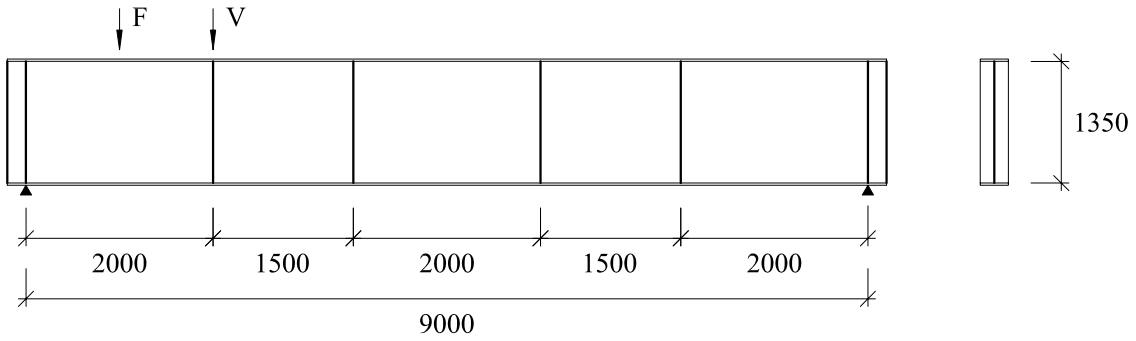

Figure 3.23: Tests from Oxfort, Weber and Gauger (1981/1989) [87, 89], dimensions in [mm]

and the yield strength varied between 210 and 312 MPa. As shown in Fig. 3.23, the girders were simply supported and assembled with friction grip bolts. The girders were loaded with a transverse patch load F in the middle of the panel near the support and an additional shear force V was applied at the adjacent transverse stiffener.

Based on [89], Oxfort and Gauger [87] propose to avoid high levels of shear force according to Eq. 3.11 when transverse patch loading is present. From the test results it was concluded that a high shear force has no influence on the transverse patch loading resistance, it was however questioned if in turn a high level of transverse patch loading has an influence on the shear resistance. Thus, the proposal can be traced back to general thoughts about the Cardiff model for the shear resistance which was used here. The preliminary approach was then to say that the capacity of the flanges is already used up by the transverse patch loading and it does not contribute to the tension field action anymore. Due to the small number of tests and since no tests with a high level of transverse patch loading were done, it becomes obvious that an assertive conclusion cannot be drawn.

$$\frac{V - 0.5 \cdot F}{V_R} \leq 0.8 \tag{3.11}$$

3.3.4 Roberts and Shahabian (2000)

In 2000, Roberts and Shahabian conducted a comprehensive study on steel plated girders subjected to transverse patch loading and shear force which has been published in several journals [102, 103]. The test series comprised 12 short-span girders which were tested twice giving in total 24 test results. The relevant panels had an aspect ratio between $\alpha = 1$ and 2, b/t-ratios between 150 and 300 and the yield strength varied between 236 and 343 MPa. As shown in Fig. 3.24, the girders were simply supported. At the supports rigid end-posts exist for the anchorage of the tension field stresses. The girders were loaded with a transverse patch load F in the middle of the panel near the support and an additional shear force V at mid-span. The load was applied via a spreader beam which

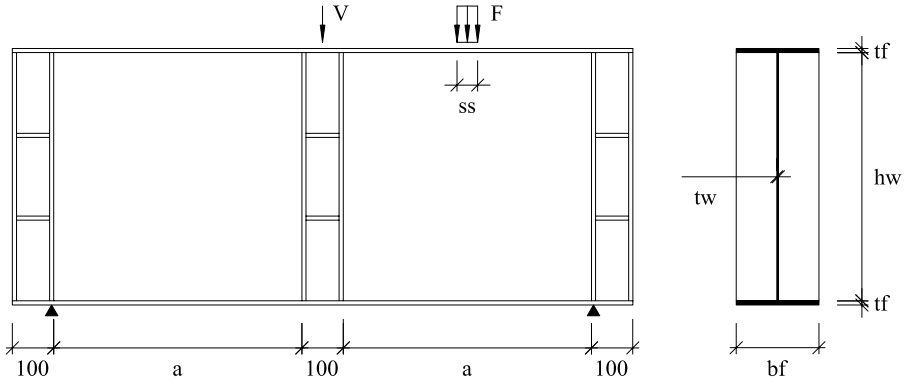

Figure 3.24: Tests from Roberts and Shahabian (2000) [102, 103], dimensions in [mm]

Table 3.14: Dimensions of the test girders from Roberts and Shahabian (2000) [102, 103]

series	web			flanges		loading length
	a [mm]	h_w [mm]	t_w [mm]	b_f [mm]	t_f [mm]	s_s [mm]
PG 1	600	600	4.1	200	12.5	50
PG 2	900	900	3.1	300	10.2	50
PG 3	900	600	3.2	200	10.2	50
PG 4	1000	500	1.9	200	10	50
PG 5	600	600	3.03	150	10	50

was used to achieve the relevant ratio of transverse patch loading to shear force. Based on the test series, Eq. 3.12 was proposed.

$$\left(\frac{V - 0.5 \cdot F}{V_R}\right)^2 + \frac{F}{F_R} \leq 1.0 \tag{3.12}$$

3.3.5 Evaluation of results

In Fig. 3.25 all test results and the proposed interaction equations are summarised in an interaction diagram based on the average shear component $(V - 0.5 \cdot F)$. The reference strengths F_R and V_R are taken from corresponding experiments of the basic load cases transverse patch loading and shear force. Only for the tests from Oxfort and Weber, the reference strengths are based on theoretical resistance models according to Rockey's and Basler's theory, since no experimental reference strengths were provided at that time. It can be noticed that the interaction equations of Zoetemeijer [126] and Elgaaly [41] are both symmetric whereas Roberts and Shahabian [102, 103] propose a curve which is symmetric to the x-axis but not to the y-axis. For the stocky webs tested by Zoetemeijer [126] the symmetric interaction curve is reasonable. In case of slender webs, buckling is irrespective of the direction of shear, but if the transverse patch loading is tensile

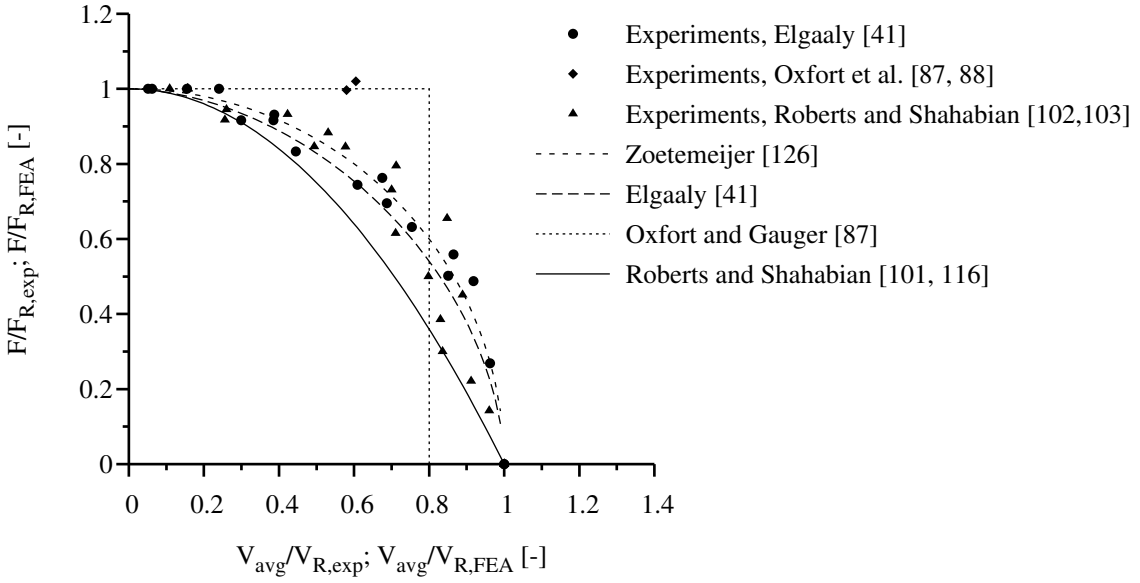

Figure 3.25: F-V interaction equation models from literature, F_R and V_R according to experiments, F_R and V_R of Oxfort et al. [87, 89] according to Rockey's and Basler's theory

instead of compressive, an increase in resistance is noticed which is only limited by plastic-destabilising effects and material yield. The tests by Elgaaly [41] confirm their symmetric proposal, although the general thoughts would rather expect a curve similar in shape as the one proposed by Roberts and Shahabian [102, 103]. Although the slendernesses studied by Elgaaly [41] and Roberts and Shahabian are in the same range, Roberts and Shahabian find not only a stronger interaction but they also propose an asymmetric interaction curve. Oxfort and Gauger [87] studied slender plated girders as well but the three test results without experimentally based reference strengths are not very conclusive.

In Fig. 3.26 all test results and the proposed interaction equations are summarised in an interaction diagram based on the average shear force component $(V - 0.5 \cdot F)$ and the reference strengths F_R and V_R are determined according to Chapters 5 and 6, EN 1993-1-5 [46]. It is shown that the deviation of resistance model leads to an increase in the data scatter. For the shear force resistance model, mean value and variation are low whereas the model for patch loading gives very conservative results over all experimental tests. As a result, the data scatter is widely dispersed which may lead to the conclusion that interaction has not to be considered. However, a refinement of the theoretical resistance models may shift the data closer to the interaction equation so that interaction becomes relevant. Further studies will have to discuss this point.

In general, it can be said that the conclusions which have been drawn on the basis of studies on cold-formed trapezoidal beams and hot rolled sections cannot easily be transferred to steel plated sections with slender webs. The recommendation of Oxfort and Gauger [87] is not assertive since it is derived from three tests only. For high levels of shear force it is overconservative whereas for high levels of patch loading the interaction

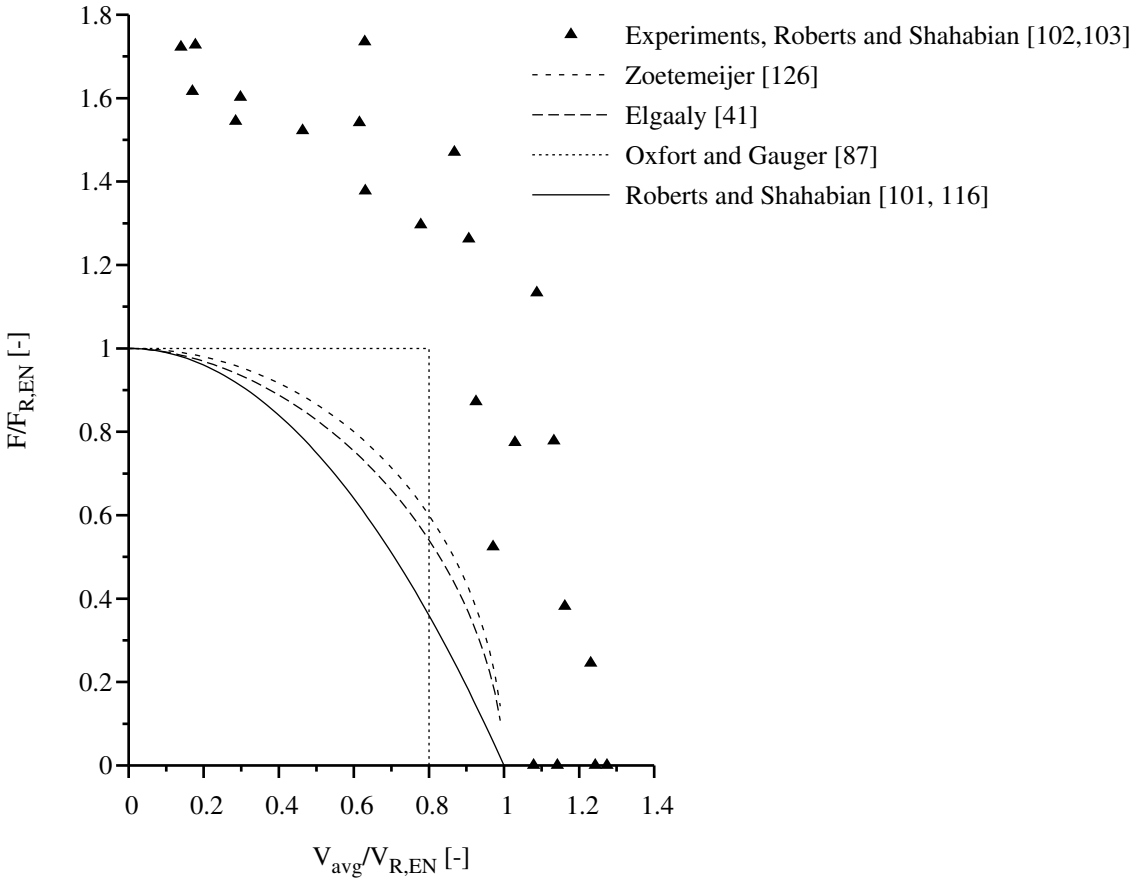

Figure 3.26: F-V interaction equation models from literature, F_R and V_R according to Chapters 5 and 6, EN 1993-1-5 [46]

behaviour is clearly underestimated. The proposed interaction equation of Roberts and Shahabian [102, 103] gives the best fit because it has been calibrated on the largest set of test results for steel plated girders. However, it is currently limited to the parameters which have been experimentally studied so that further studies are required.

3.4 Summary

For plates under biaxial compression a large number of studies mainly from the 1970s and 1980s exists and various parameters have been studied which provide a comprehensive insight into the stability behaviour. Nevertheless, further work is mandatory for certain points which become relevant for the procedure of the reduced stress method based on a single plate slenderness according to Chapter 10, EN 1993-1-5 [46]. The focus lies on the following questions:

- The procedure of the reduced stress method according to Chapter 10, EN 1993-1-5, is based on a single plate slenderness. Discrepancies between DIN 18800-3 [28] and Chapter 10, EN 1993-1-5 [46], have been pointed out in Sec. 2.5. The review of earlier work does not clarify the disrcepancies but it gives useful information on the effect of relevant parameters. Further work is necessary to evaluate the applicability of the reduced stress method based on a single plate slendernes.
- The so far claimed plausibility to transfer the results from biaxial compression to transverse patch loading and bending moment requires a clear assignment in such a way that the biaxial compression case sometimes relies on favourable boundary effects which cannot be accounted for in case of patch loading. Further insight when the reduced stress method is applied to biaxial compression and to transverse patch loading and bending moment has to be gained.
- Mainly theoretical studies were undertaken which is due to the fact that boundary conditions are difficult to define in tests in which usually displacement-controlled edge boundary conditions have to be used. Advanced software allows for a load-controlled edge boundary condition which gives more choice to study edge boundary conditions in general. Together with the exising studies, a final assertive evaluation will be drawn.

For the interaction of transverse patch loading and shear force, further work is mandatory and it will focus on the following questions:

- The proposals for an interaction equation are based on few results. For slender plate I-girders only the proposal of Roberts and Shahabian [102, 103] is reasonable. However, some parameters are not considered and their influence is not negligible such as long loading lengths and panels with longitudinal stiffeners. In order to propose an interaction equation for practical application, further studies are necessary.
- In order to extend the parameter range, a high number of test results is required which cannot be based on experiments alone. For numerical studies, a recalculation

of well-documented tests is the basis for further work so that own experimental studies will be conducted.

- Results of the so far used subdivision into the basic load cases transverse patch loading and average shear force show that for this decision of the verification point interaction has to be considered. The average shear force component has been adopted from literature but other verification points such as the maximum shear force are imaginable. Further insight into the choice of the verification will have to be gained before a final conclusion is drawn.

4 Experimental studies

4.1 Test programme

The test programme intends to quantify the effect of shear force on the patch loading resistance for welded plate I-girders and to serve as basis for the verification of the numerical model which is used to recalculate the tests and for further parameter studies. The review of earlier work in Sec. 3.3 clearly shows that an interaction between transverse patch loading and shear force exists. However, the need for further experimental studies is not only based on the fact that only few experimental studies could be gathered but also that contradictory conclusions were drawn. For these reasons, an own test programme is carried out. The test specimens are based upon typical plate I-girder geometries which can be found in bridge construction. Steel grade S 355 was chosen. The ratio of transverse patch loading F and shear force V is chosen such that the relevant F-V-ratio is met. Further information about the dimensions, material properties and geometric imperfections of the test specimens is given in Sec. 4.2. Sections 4.3 to 4.5 summarise the test procedure including test set-up and results.

The experimental studies were sponsored by a financial grant from the Research Fund for Coal and Steel (RFCS) in the frame of the research project "Competitive Steel and Composite Bridges by Improved Steel Plated Structures" (COMBRI) [72]. They were carried out with the collaboration of the author at Luleå Tekniska Universitet, Sweden.

In order to prevent this chapter from becoming unmanagable in length, only the minimal necessary effort is made to report about the experimental studies. Readers interested in pursuing any of these points further are urged to consult the test report [13] in which the experiments are presented in far greater detail.

4.2 Test specimens

4.2.1 Dimensions

The general layout of the two test girders is given in Fig. 4.1 with dimensions according to Table 4.1. Both girders are double-symmetric and the web slenderness h_w/t_w as key parameter in the experimental studies varies from 100 to 200. Transverse stiffeners and end-plates possess the same width and thickness as the flanges. The girders are denoted SP 600 and SP 1200 according to the height of their web.

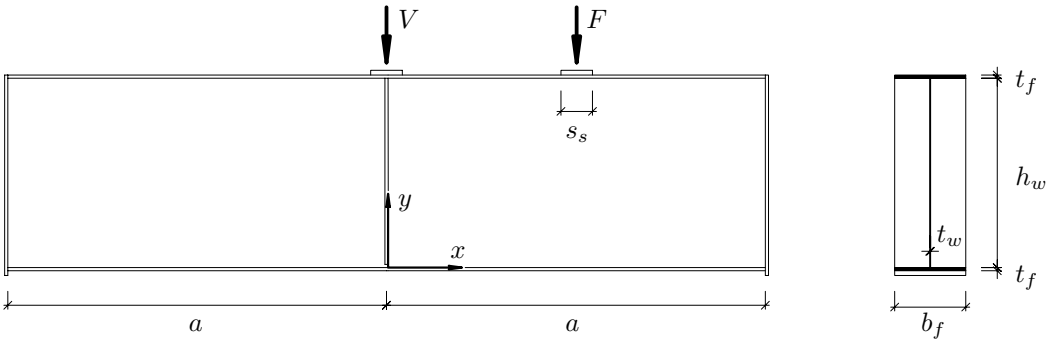

Figure 4.1: General layout of the test girders

Table 4.1: Dimensions of the test girders

girder	web			flanges		loading length
	a [mm]	h_w [mm]	t_w [mm]	b_f [mm]	t_f [mm]	s_s [mm]
SP 600	2390	600	6	450	20	200
SP 1200	2390	1200	6	450	20	200

4.2.2 Material properties

The mechanical steel properties were determined from uniaxial tensile coupon tests. Three individual coupon tests were conducted both along and transverse the rolling direction of each steel plate which was used for flanges, stiffeners and webs. Yield strength, ultimate strength and elastic modulus were averaged over the individual coupon tests according to Table 4.2. These results are used for the realculation of the test girders in order to verify the numerical model, see Sec. 5.3.3.

The test report [13] gives further details about the coupon tests.

4.2.3 Geometric imperfections

The geometric variations from the perfect web flatness were measured with a movable LVDT device (**L**inear **V**ariable **D**isplacement **T**ransducer). In Figs. 4.2 and 4.3, the geometric imperfections are shown with reference to a xy-plane which is defined by the bottom flange and the upper left point of the web panel near the top flange.

Table 4.2: Mechanical steel properties of the test specimens

cross-sectional element	yield strength f_y [MPa]	ultimate strength f_u [MPA]	elastic modulus E [MPa]
flange, stiffener	354	519	186 139
web	383	543	176 938

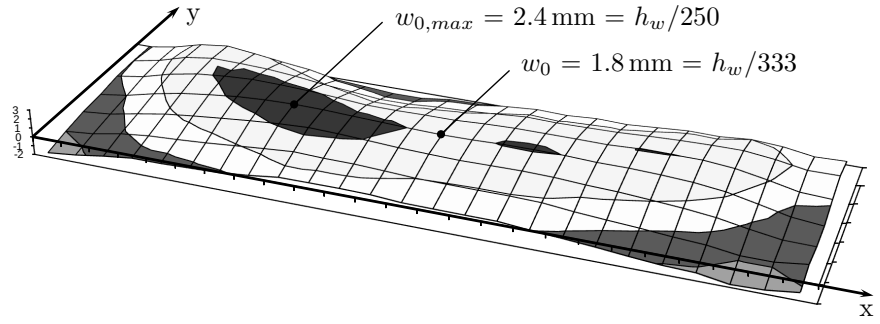

Figure 4.2: Geometric imperfection of test girder SP 600

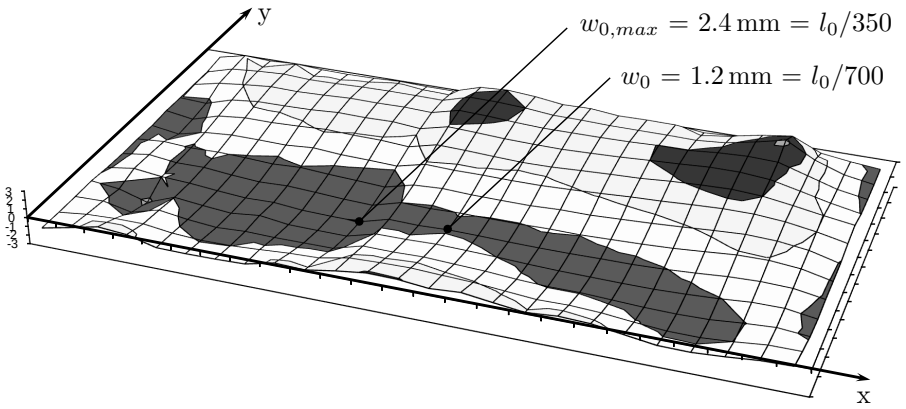

Figure 4.3: Geometric imperfection of test girder SP 1200 (gauge length $l_0 = 0.7 \cdot h_w$)

The imperfection shape of girder SP 600 over the web height resembles a C-shape. The imperfection amplitude has a maximum value of $h_w/250$ and a value of $h_w/333$ at the centerline underneath the loading device. The imperfection shape varies along the relevant web panel of the test girder according to Fig. 4.2.

The imperfection shape of girder SP 1200 over the web height resembles a S-shape. The imperfection amplitude has a maximum value of $l_0/350$ belonging to a gauge length of $l_0 = 0.7 \cdot h_w$. At the centerline underneath the loading device the value becomes $l_0/700$. The imperfection shape varies along the relevant web panel of the test girder according to Fig. 4.3.

For both girders the measured geometric imperfections are significantly smaller than the allowable geometric tolerances according to the Swedish design code BSK 07 [14] and EN 1090-2 [45], see Table 4.3. It should be noted that in BSK 07 the allowable fabrication tolerance depends on the plate slenderness.

Table 4.3: Comparison of measured geometric imperfections and fabrication tolerances

geometric imperfection	SP 600	SP 1200
measured (maximum)	$h_w/250$	$l_0/350$
measured (at centerline)	$h_w/333$	$l_0/700$
allowable, BSK 07 [14]	$h_w/160$	$h_w/80$
allowable, EN 1090-2 [45]	$h_w/100$	$h_w/100$

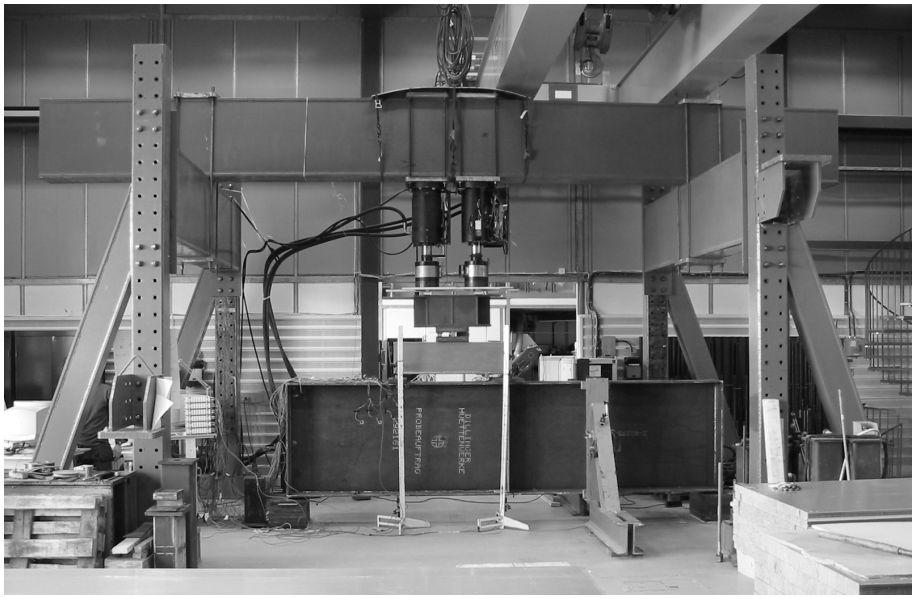

Figure 4.4: Test rig, backside

4.3 Test set-up

4.3.1 General

The tests are performed in a test rig as shown in Fig. 4.4 consisting of two portal frames and a main girder. Two hydraulic cylinders with a capacity of 1 000 kN each are attached to the main girder. The shear force V is applied at half the span length L whereas the patch load F is introduced at the centerline of one of the adjacent web panels.

The test girders are simply supported on bearing plates. This is realised by an outstand of the end-post exceeding the bottom flange with a height of 30 mm in the vertical direction. In order to avoid any kind of introduction of normal forces into the girder a teflon-coated plate on a stainless steel plate is used to create a support that is able to move without restraint in the horizontal direction.

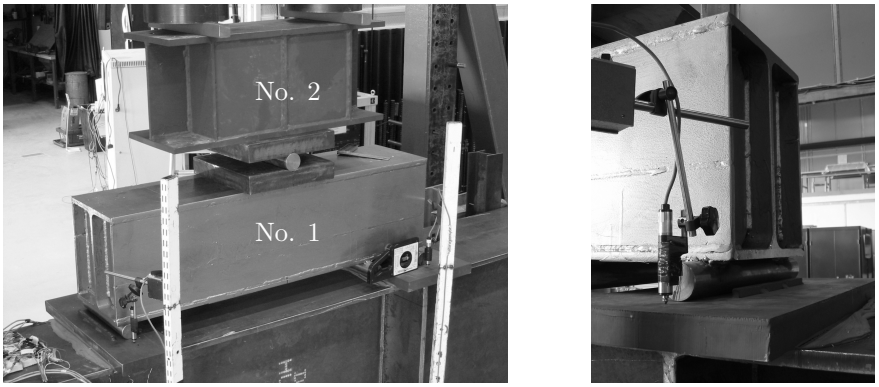

(a) Loading device (b) LVDT location

Figure 4.5: Load introduction devices (a) and LVDT on top of the loading plate (b)

4.3.2 Loading device

Transverse patch loading and shear force are applied at two different locations at the top flange of the girder. The jack force is equally distributed by a spreader beam (designated "No. 1" in Fig. 4.5a) via rollers to the loading plates on the top flange. The way how the load is applied and the design of the loading devices are assumed to prevent a rotation of the top flange along its longitudinal axis. The load plate for the transverse loading is 200 mm wide whereas the load plate for introduction of the shear force measures 330 mm.

Due to technical limitations two hydraulic cylinders with a capacity of 1 000 kN each are used to reach the ultimate load of girder SP 1200. Both hydraulic actuators are combined by means of a second beam (designated "No. 2" in Fig. 4.5a) which applies the combined load via a roller to the aforementioned spreader beam.

4.3.3 Measuring devices

During the test procedure, displacements and strains are recorded.

At certain load increments, displacements of the full panel are measured. Intermediate measurements at smaller load increments are carried out for the vertical line of the grid at the centerline of the relevant panel (x = 1 195 mm). The measuring grid is shown in Fig. 4.6 for girder SP 1200. In the horizontal x-direction and the vertical y-direction an equal spacing of 100 mm between each point has been predefined. The edge distances around the panel are set to 30 mm which is as close as the LVDT can get to flanges and stiffeners.

A movable LVDT device for the measurement of the horizontal displacements is initially used to determine the geometric imperfections. During the test procedure, web panel deformations are recorded. For both measurements a steel bar is applied to the flanges guiding the LVDT along a vertical path and assuring a measurement perpendicular to the steel bar at each point.

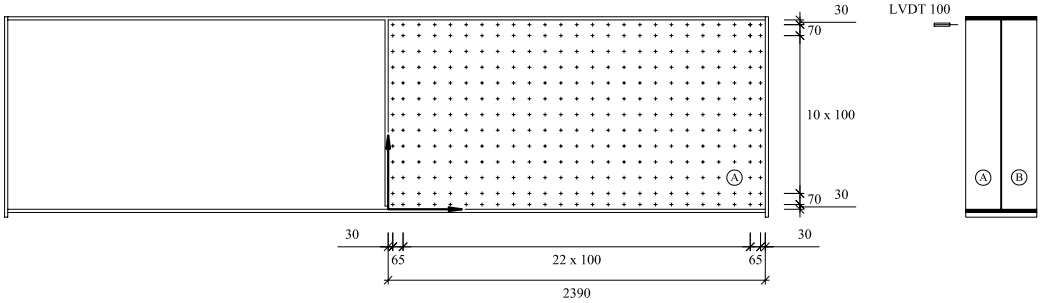

Figure 4.6: Measuring grid (SP 1200), dimensions in [mm]

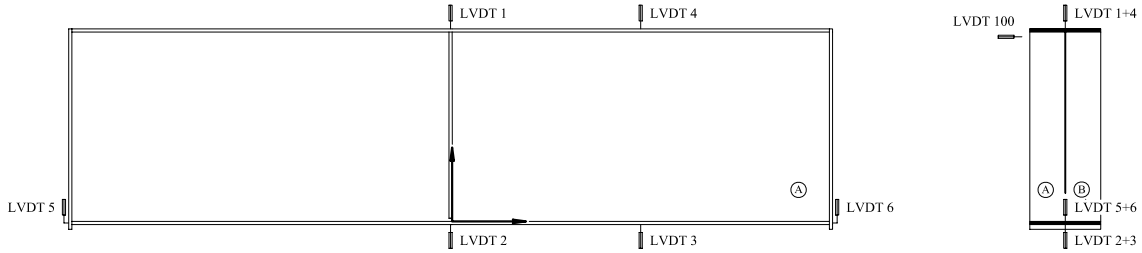

Figure 4.7: Location of the LVDTs (SP 1200)

Vertical displacements are measured during the test procedure with LVDTs at six locations according to Fig. 4.7. LVDT 5 and LVDT 6 account for settlement of the supports during the experimental procedure.

Strains are measured continuously during the test procedure. Both girders are equipped with monoaxial strain gauges and triaxial rosette gauges for strain measurements at selected points. The basic layout is shown in Fig. 4.8 for girder SP 1200.

On each side of the web panel three monoaxial strain gauges are applied in the vertical direction underneath the patch load to log its strains. Four triaxial rosette gauges are applied asymmetrically on each side of the web panel to account for the interaction between transverse loading and shear force. One triaxial rosette gauge is placed in the upper corner at each side of the web panel to record the anchoring of the tension field.

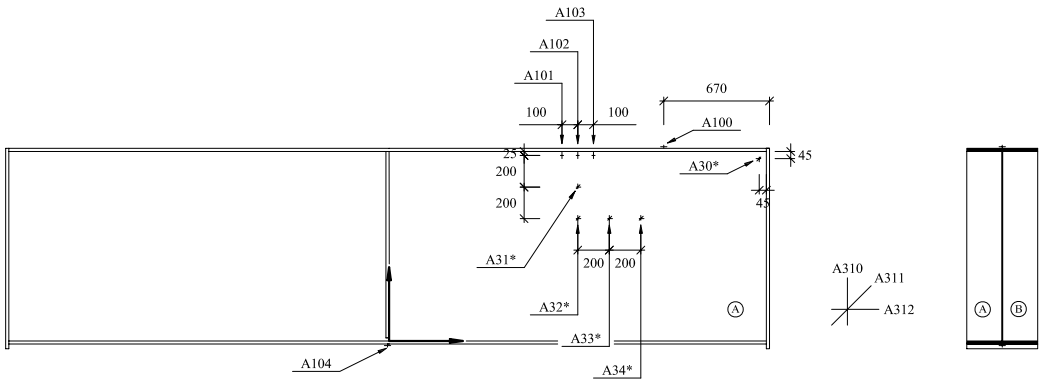

Figure 4.8: Basic layout of strain gauges (SP 1200), dimensions in [mm]

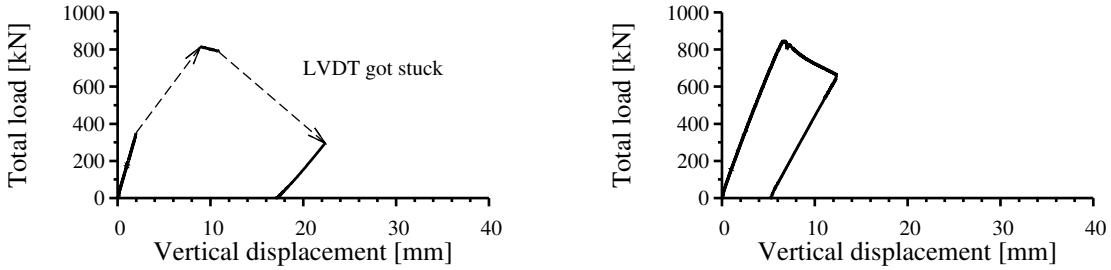

(a) Transverse patch loading (b) Shear force

Figure 4.9: Load-displacement-curves of girder SP 600

A monoaxial strain gauge is applied on both the top and the bottom flange. On the top flange the strain gauge is placed at a location where a plastic hinge due to the shear loading is assumed to occur. The strain gauge at the bottom flange is placed at mid-span to record strains due to bending.

4.4 Test procedure

4.4.1 General

Before the test procedure is started the geometric imperfections are determined and the girder is preloaded with approximately 15 % of the predicted ultimate load.

During the test procedure a constant vertical displacement rate of 0.005 mm/sec is used for the hydraulic cylinders to assume for static loading conditions until ultimate load is reached. Afterwards the rate is increased to 0.02 mm/sec. At load increments of 100 kN the loading is stopped and the web panel deformations are measured at the centerline (x = 1 195 mm). A full panel measurement is conducted at the following load steps:

- SP 600: 500 kN, 700 kN, 830 kN (ultimate load) and after unloading
- SP 1200: 600 kN, 700 kN, 900 kN, 1 030 kN (ultimate load) and after unloading

Strains and vertical displacements are continuously recorded during the test procedure.

4.4.2 Girder SP 600

The imperfection shape of girder SP 600 resembles a C-shape over the web height in the positive z-direction of the web panel and an unsymmetrical “halfwave” along the panel length. During loading a constant increase of the web panel deformation is observed. A deformed shape is first noticeable to the eye at around $F = 450\,\text{kN}$. The ultimate load $F_{ult} = 846\,\text{kN}$ is reached at a vertical displacement of $u_y = 6.5\,\text{mm}$.

A three-dimensional plot with the corresponding plan view is shown in Fig. 4.11 at

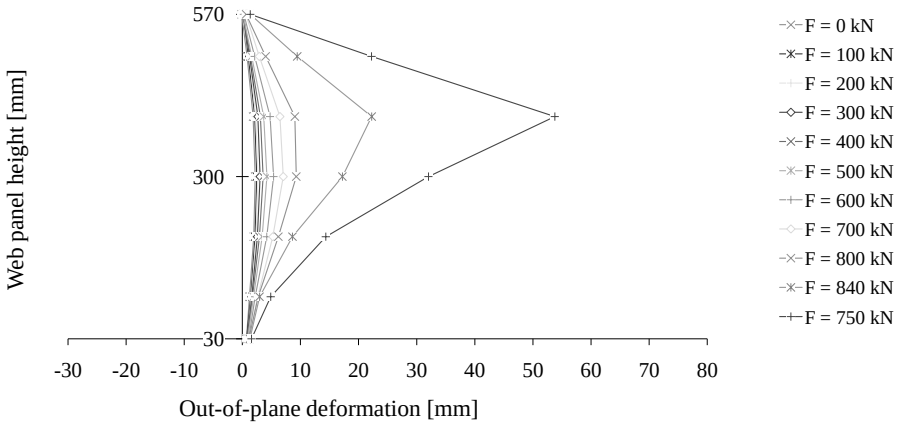

Figure 4.10: Lateral web deformation of girder SP 600

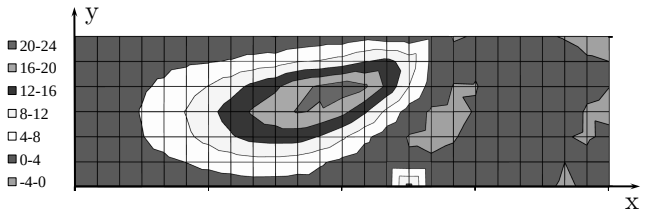

Figure 4.11: Web panel deformation at ultimate load for girder SP 600

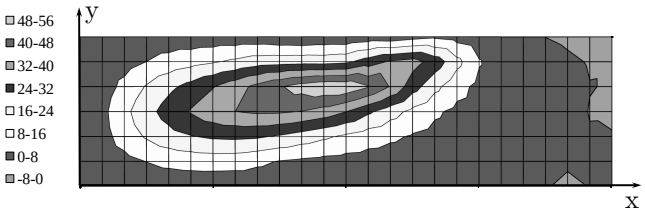

Figure 4.12: Web panel deformation after unloading for girder SP 600

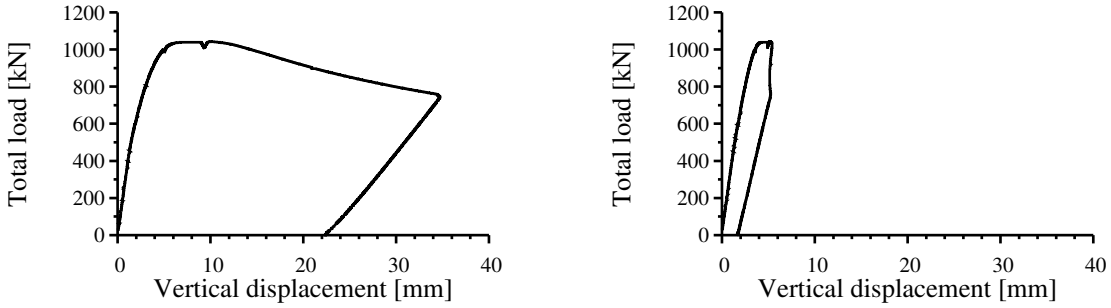

(a) Transverse patch loading (b) Shear force

Figure 4.13: Load-displacement-curves of girder SP 1200

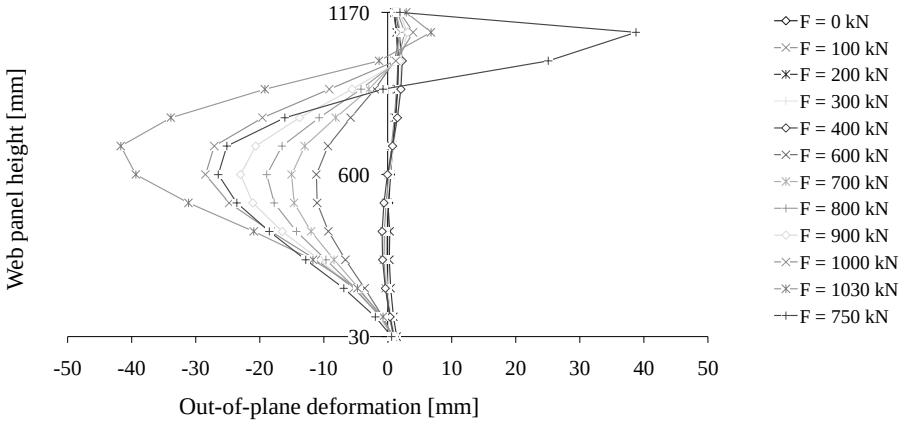

Figure 4.14: Lateral web deformation of girder SP 1200

ultimate load and in Fig. 4.12 after unloading. It can be seen that the initial imperfection shape is replaced by a typical web buckle underneath the patch load which is however influenced by the additional shear force. This is evident due to the diagonalisation of the out-of-plane deformation shape. In the post-ultimate range the deformations increase and a patch loading-like failure dominates.

4.4.3 Girder SP 1200

The imperfection shape of girder SP 1200 consists of two half-waves (S-shape) over the web height and an unsymmetrical "halfwave" along the web panel length. At a load of $F = 400\,\text{kN}$ the initial imperfection shape changes to one halfwave (C-shape) in the negative z-direction, see Fig. 4.14. A deformed shape is first noticeable to the eye at around $F = 500\,\text{kN}$. As soon as ultimate load is reached almost no further deflection of the girder at mid-span is noticed. The ultimate load $F_{ult} = 1\,030\,\text{kN}$ is reached at a vertical displacement of $u_y = 5.0\,\text{mm}$.

Figures 4.15 and 4.16 show a three-dimensional plot with the corresponding plan view for girder SP 1200 at ultimate load and after unloading. At ultimate load a combination of

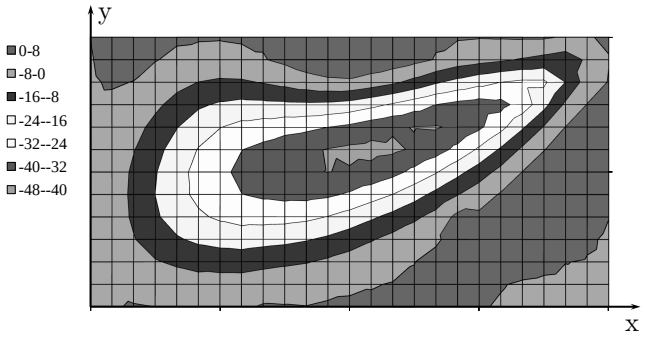

Figure 4.15: Web panel deformation at ultimate load for girder SP 1200

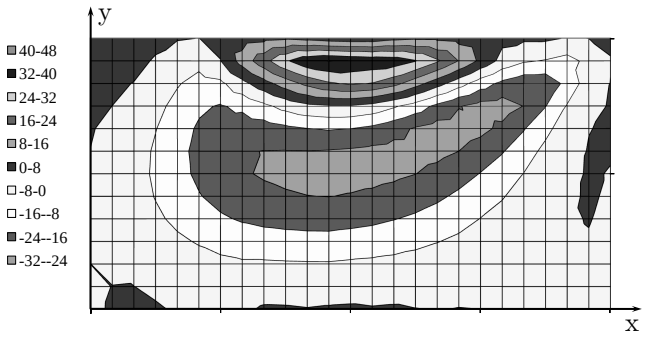

Figure 4.16: Web panel deformation after unloading for girder SP 1200

shear force and patch load buckling is found. In the post-ultimate range, the deformations show a patch loading failure which is influenced but not dominated by the additionally present shear force.

4.5 Test results

Both girders are equipped with monoaxial strain gauges and triaxial rosette gauges according to the layout in Fig. 4.8. The results of the strain measurements are presented here for selected points. From the measured surface strains the membrane strains at the web panel mid-plane are calculated assuming a linear strain distribution over the web panel thickness. For the rosette gauge measurements, principal strains are calculated.

The comparison of monoaxial strain gauges (A100) located at the top flange shows that the upper surface of the flange is subjected to compressive strains until ultimate load is reached. After that point tensile strains develop due to the patch loading failure which induces a curvature on the upper flange due to the buckling of the web panel, see Fig. 4.17.

The comparison of the monoaxial strain gauges (A101/B101 to A103/B103) located on the web panel directly underneath the patch loaded top flange shows that the plastic membrane strain is exceeded shortly before or at the same time ultimate load is reached,

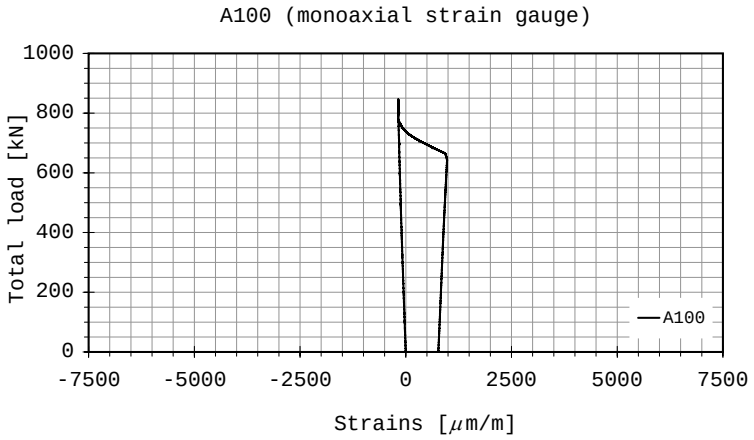

Figure 4.17: SP 600 - Strain gauge A100 (top flange)

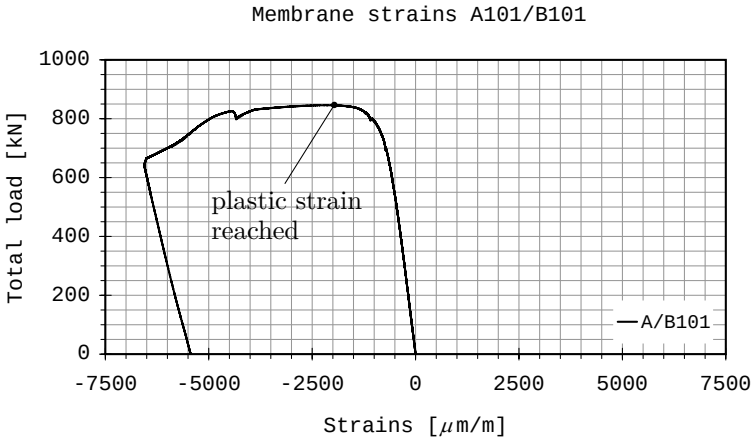

Figure 4.18: SP 600 - Strain gauge A101/B101

see Fig. 4.18. The local buckling of the web panel can be followed by the development of tensile and compressive strains on the surfaces of each web panel of girders SP 600 and SP 1200.

The comparison of the web panel strains measured by the triaxial rosette gauges (A31*/B31* to A34*/B34*) shows that all membrane strains stay below uniaxial plastic strain limits until ultimate load is reached. This applies for both ϵ_x in the horizontal direction and ϵ_y in the vertical direction. On the surfaces of the web panels higher strains are measured due to the deformation of the web panel and the onset of buckling. Tensile and compressive strains correspond to local bending effects which are induced by the deformation of the web panel.

For both girders compressive strains ϵ_y in the vertical direction are measured decreasing from a maximum value at rosette gauges A31*/B31* located at the centerline of the patch loading to zero at rosette gauges A34*/B34*, see Fig. 4.19. On the other hand, the developing tension field is confirmed by membrane shear strains ϵ_{xy} at rosette gauges A34*/B34*. Here, the principal membrane strains are zero so that a pure shear state of

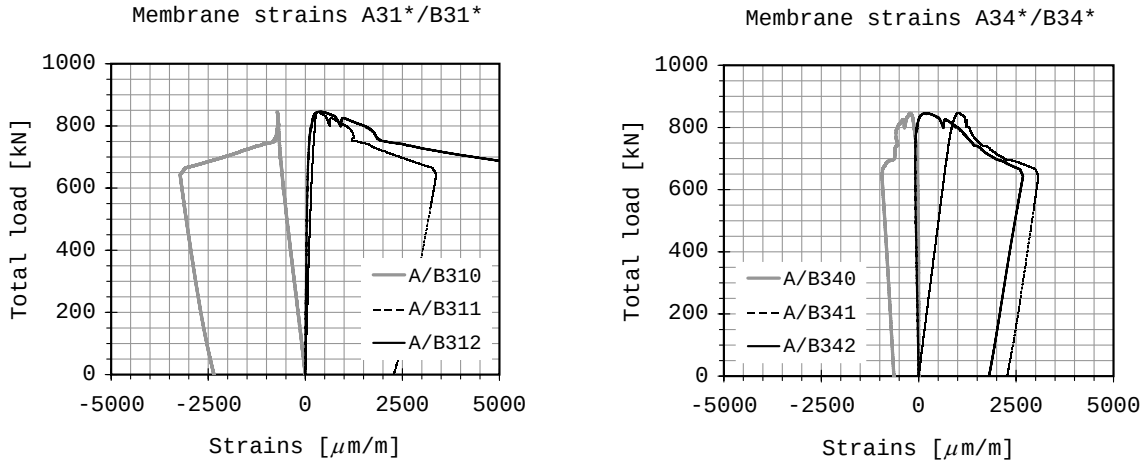

(a) Dominating compressive stresses in y-direction (see A/B310)

(b) Pure shear state of stress (see A/B341)

Figure 4.19: SP 600 - Strain gauges A31*/B31* and A34*/B34*

stress exists. The surface strains ϵ_y exceed plastic strain in the vertical direction due to the high curvature of the deformed web panel shape. In the horizontal direction smaller strains ϵ_x occur which is due to the smaller curvature in this direction.

For girder SP 1200, the initial web panel S-shape changes to a C-shape at a total load of about $F = 400\,\text{kN}$, see Fig. 4.14. This change causes a sharp bend in the load-strain-curves accounting for the altered web panel shape. The membrane strains are not affected.

For girder SP 600, the analysis of the triaxial rosette gauges (A30*/B30*) located in the upper corner above the support shows the development of tensile strains ϵ_{xy} in the direction of the assumed anchoring of the tension field. But strains clearly stay below plastic strain limits when ultimate load is reached. The almost uniform distribution of strains throughout the thickness of the web plate corresponds to the observation that the web panel remains plane next to the vertical end-post. In contrast to this, although barely noticeable, SP 1200 developed a folding of the web panel which leads to local bending moments over the web thickness. Up to ultimate load plastic strain is not reached but the strains increase significantly after ultimate load has been passed.

4.6 Summary

Test girder SP 600 fails due to a combination of shear force and patch loading which is confirmed by the analysis of strains and deformation shapes. Vertical displacements both at the load introduction of the patch loading and at the load introduction of the shear force increase after ultimate load has been reached. Test girder SP 1200 shows also some influence from the combined loading although not as distinctive as girder SP 600. No further vertical displacement is recorded at the load introduction of the shear force after

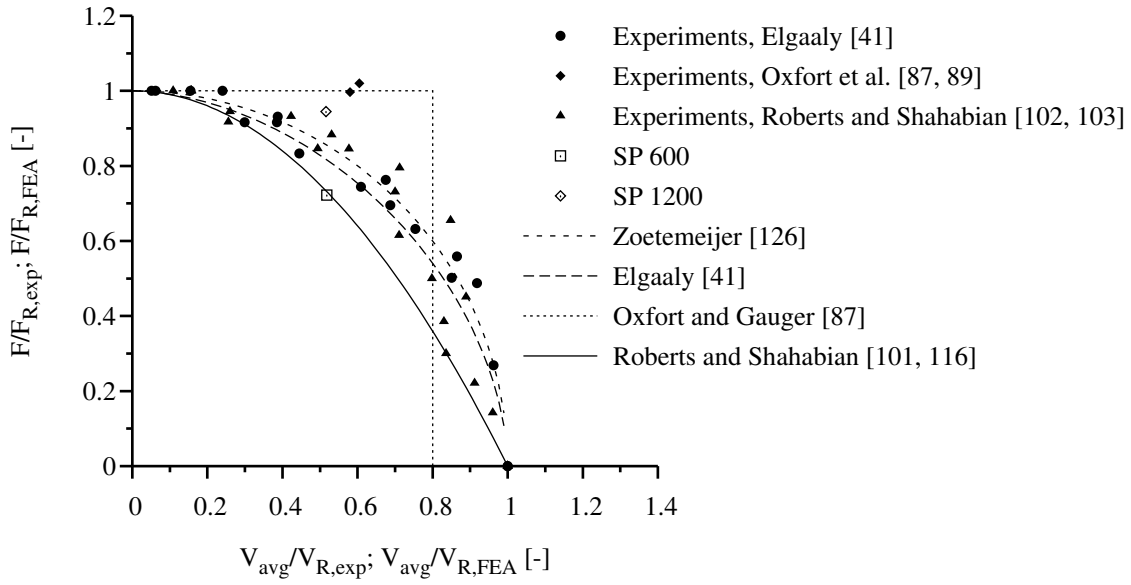

Figure 4.20: Comparison of experiments and interaction equation models, F_R and V_R according to experiments or based on FEA

ultimate load has been reached. It can be concluded that at this point the patch loading capacity has been reached.

In Fig. 4.20, the results of girders SP 600 and SP 1200 are compared to experiments from literature and in Fig. 4.21 comparison is made to EN 1993-1-5 [46]. Both diagrams are given in the same scale along with the proposals for interaction equations taken from literature and introduced in Sec. 3.3. The proposal of Zoetemeijer [126] does not meet the requirements of steel plated girders because it was proposed for hot rolled sections. In fact, Oxfort and Gauger [87] dealt with slender girders but at that time few test results were available so that only a vague recommendation could be given to avoid high levels of shear in combination with patch loading. The test results do not confirm this proposal. Roberts and Shahabian [102, 103] defined an interaction equation based on a comprehensive experimental tests series. A comparison with the own experimental studies shows that the results of the girders SP 600 and SP 1200 are covered within the existing data scatter and that they are on the safe side with regard to the proposed interaction equation by Roberts and Shahabian [101, 116]. For SP 600 with a longer relative loading length $s_s/h_w = 0.33$ a stronger interaction is found than for SP 1200 with a shorter relative loading length of $s_s/h_w = 0.17$.

The evaluation of test results based on the reference strengths according to experiments or FEA shows that there is an interaction between transverse loading and shear force. On the other hand, the evaluation of test results with regard to Chapters 5 and 6, EN 1993-1-5 [46], identifies that due to the limited number of test results and the uncertainties of the theoretical resistance models data points do not fall in the interaction range.

If the test results are compared based on the reference strengths according to Chapters 5 and 6, EN 1993-1-5 [46], the uncertainty of the corresponding engineering model leads

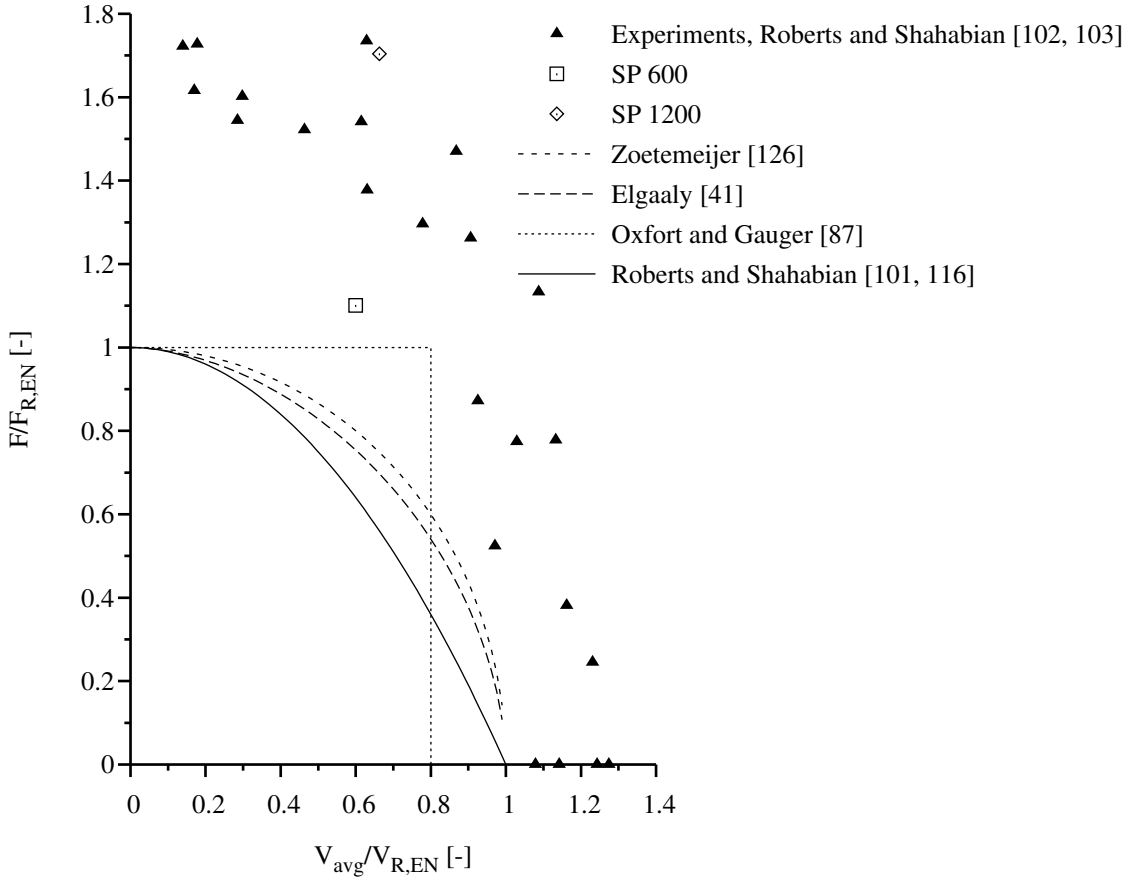

Figure 4.21: Comparison of experiments and interaction equation models, F_R and V_R according to Chapters 5 and 6, EN 1993-1-5 [46]

to a wide scatter of the data points. For the theoretical shear force model mean value and variation are quite low whereas the model for patch loading gives very conservative results over all experimental tests. As a result, the data scatter is widely dispersed which may lead to the conclusion that interaction has not to be considered. However, a refinement of the theoretical resistance models shifts the data closer to the interaction equation so that interaction becomes relevant. Further investigations are necessary to clarify in detail the influence of parameters such as loading length, slenderness ratio, ratio of shear force to patch loading, end-post condition and longitudinal stiffeners. The consideration of this influence will be further studied with the help of numerical investigations, see Sec. 5.5, which are based on the tests performed herein.

5 Theoretical studies

5.1 General

Within the scope of this work, experimental studies are often laborious and for reasons of size and costs they are not feasible to conduct. And although it is recognised that experiments should be the basis of each theoretical work, it becomes obvious that some aspects, e.g. certain loading scenarios and boundary conditions, cannot be studied very well or not at all due to limitations of the test set-up. A way to overcome such difficulties is the application of a numerical method. Here, the finite element method, also known as finite element analysis, is used (FEM/FEA).

FEM has establised itself as numerical analysis method because it offers versatility and physical appeal. FEA is nowadays used in many fields of application not only for stress analysis but e.g. also for heat transfer and magnetic fields. The basic idea behind is to approximate a structure in a piecewise way, element by element, i.e. finite elements. Thus, it should be clear that FEA is always an approximation to the exact solution.

In this work, general-purpose FEA software ANSYS releases 10.0 and 11.0 [1] was used. In Sec. 5.2 choices with regard to aspects of modelling, discretisation and numerical analyses are explained. Subjects such as material properties, boundary conditions, type of elements and the effect of imperfections are addressed. Background information on FEM however will be only given where it appears necessary. In general, principles of FEA are presumed to be known and will not be repetitively explained here. For further reading, the reader is referred e.g. to the textbooks of Bathe [3], Zienkiewicz and Taylor [124, 125] and Cook et al. [20] which allow for a comprehensive in-depth knowledge. In Sec. 5.3, the steps which were undertaken to verify the numerical model are given. Besides the recalculation of own experiments, known results from literature and buckling curves are used as basis for comparison.

The numerical model is then used to carry out systematic parameter studies in order to enhance the parameter range. These studies can be subdivided into studies on plates under biaxial compression and plate I-girders under transverse patch loading and shear force of which the behaviour is studied in Sec. 5.4 for single plates and in Sec. 5.5 for plate I-girders.

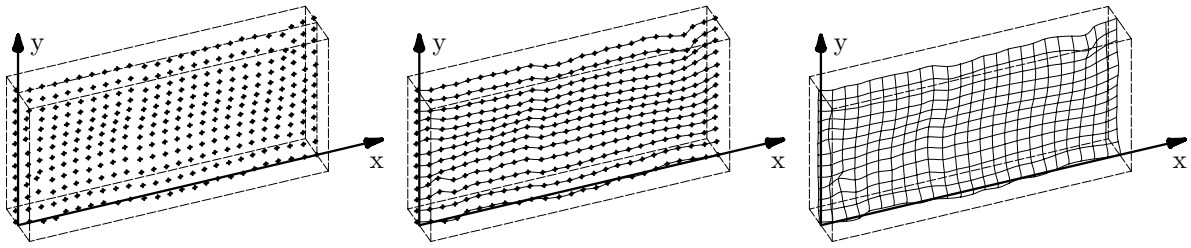

(a) processing of measured data points (b) spline fitting (c) surface generation

Figure 5.1: Parametric solid modelling technique

5.2 Input data of the finite element analysis

5.2.1 Modelling

5.2.1.1 Geometry

In order to build the numerical model, the geometry is processed on the basis of the parametric solid modelling technique. This means the attributes of the geometry are parametrised and allocated with numerical values so that these values can be changed easily. All cross-sectional elements of the numerical models have in common that the dimensions are large in two directions and small in the third direction. Thus, the geometry is degenerated in terms of the midsurface which is then discretised with shell elements, see Sec. 5.2.2.

Figure 5.1 shows exemplarily how the parametric modelling technique is applied to process the measured web geometry of test girder SP 1200. In order to simulate the geometric web imperfections correctly, the measured data points are attributed to a referential plane by processing them with MathCAD software [82]. Spline functions are then fit through the data points and used as guiding lines for the surface generation.

For the initial geometry of the numerical models in case of the parameter studies a functional description of the geometric web imperfection is used such as sine functions. Imperfections of longitudinal stiffeners are modelled accordingly.

5.2.1.2 Material properties

The correct representation of material behaviour is of utmost importance because it is one of the most influential parameters. The mechanical properties of steel are characterised by elastic modulus, yield strength, ultimate strength and strain hardening behaviour. It is common to assume isotropic material with identical values of mechanical properties in all directions so that the input can be based on uniaxial stress-strain data.

Recommendations for material models are given in Annex C.6, EN 1993-1-5 [46], and

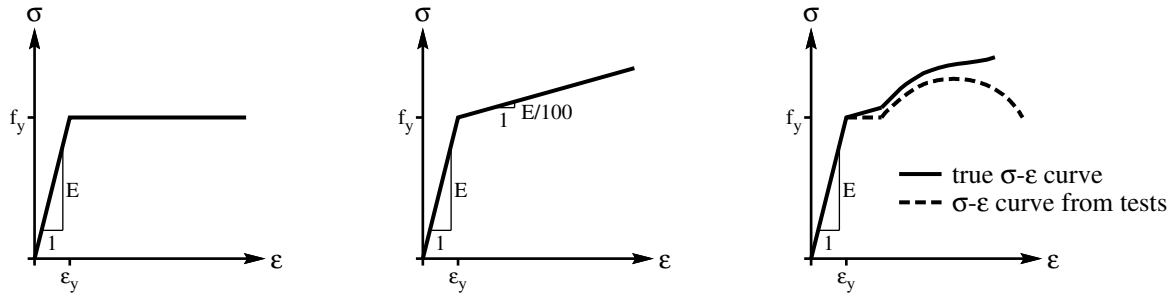

(a) bilinear stress-strain curve without strain hardening

(b) bilinear stress-strain curve with strain hardening

(c) true stress-strain curve based on tests

Figure 5.2: Material models according to Annex C.6, EN 1993-1-5 [46]

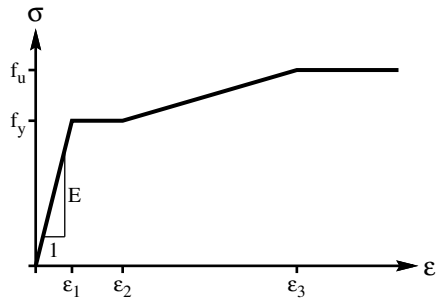

$$\varepsilon_1 = \frac{f_y}{E}$$

$$\varepsilon_2 = 0.025 - 5 \cdot \frac{f_y}{E}$$

$$\varepsilon_3 = 0.02 + 50 \cdot \frac{f_u - f_y}{E}$$

Figure 5.3: Material model according to BSK 07 [14]

in Swedish Steel Standard BSK 07 [14]. Basically, EN 1993-1-5 provides three material models, see Fig. 5.2. The bilinear stress-strain curves are intended for calculations for which no stress-strain data are explicitely available. If strain hardening is neglected a yield plateau is theoretically assumed, see Fig. 5.2a. For reasons of numerical convergence, it might be useful to define a nominal plateau slope with a small value of $E/10\,000$. Whether strain hardening is considered or not depends on the required accuracy. In case it is considered, EN 1993-1-5 proposes a simple approximation with a slope of $E/100$ which has proven to be a reasonable value for a wide range of steel grades for strains up to 5 %, see Fig. 5.2b. If material properties from tests are available, the stress-strain curve can be followed one-to-one. Then the stress-strain curve from tests should be transformed into the true stress-strain curve to account for the decrease of cross-sectional area near fracture, see Fig. 5.2c. BSK 07 offers a parametrised stress-strain curve according to Fig. 5.3. Since it is based on the values from elastic modulus, yield strength and ultimate strength, it allows a very simple though refined definition of the material behaviour.

Poisson's ratio is uniformly set to $\nu = 0.3$. The used material models are based on an isotropic hardening rule based on the theory of von-Mises-plasticity.

The recalculation of the experiments is based on the multilinear stress-strain curve

according to BSK 07, see Fig. 5.3. Characteristic values of elastic modulus, yield strength and ultimate strength are taken from the tensile coupon tests as given in Sec. 4.2.2. The true stress-strain curve is derived from the stress-strain data of the tests with Eq. 5.1 to account for the decrease of cross-sectional area near fracture. However, this effect is noticeable only when the strains at failure become really large which is not the case here.

$$\sigma_{true} = \sigma \cdot (1 + \varepsilon) \tag{5.1a}$$

$$\varepsilon_{true} = \ell n\,(1 + \varepsilon) \tag{5.1b}$$

In the parameter studies, nominal values of the yield strength are used and an elastic modulus of $E = 210\,\text{GPa}$ is assumed. The bilinear stress-strain curve with strain hardening according to EN 1993-1-5 is adopted, see Fig. 5.2b. Following the comments in [67], strain hardening is not neglected here because in a buckled plate besides primary membrane stresses, secondary bending stresses occur in both directions. Using a yield plateau results in an early loss of plate bending stiffness as soon as yielding of the primary stresses starts. Thus, plate buckling will occur too early which can be avoided when strain hardening is taken into account.

5.2.1.3 Loading and boundary conditions

Loading and boundary conditions have to be carefully chosen since they can have a relevant influence on the stability behaviour, see Sec. 2.2. General information is hard to give, since they strongly depend on the definition of the problem, so that more information is given in the relevant sections.

For the recalculation of experiments, the loading is chosen to represent the test set-up, see Sec. 4.3. The load plates are modelled by rigid regions, i.e. the degrees of freedom are coupled but a rigid body translation and rotation is possible. Support conditions are modelled as given. The boundary conditions of the plates are constituted by the continuity to adjacent cross-sectional elements.

For the parameter studies, plate elements are considered which usually represent one specific part of the whole structure. The proper choice of boundary conditions is of utmost importance. Upper and lower bounds are given by simply supported and clamped rotational restraint conditions as well as by unconstrained and constrained in-plane restraint conditions.

Loads are applied as line loads, for which the loaded edge is usually assumed to remain straight if the whole edge is loaded. For patch loading the edges move in-plane due to the nature of loading type. Both scenarios represent either uniform displacements or uniform loading.

5.2.1.4 Imperfections

If the buckling resistance of a steel plated structure is to be determined from numerical analysis without applying in addition any reduction factor, the use of imperfections becomes mandatory. Imperfections are unavoidable during fabrication and erection of real structures. In general, geometrical and material imperfections are distinguished. Geometric imperfections comprise e.g. initial deformations, shrinkage at welds and tolerances from nominal geometric values. Material imperfections comprise e.g. residual stresses due to fabrication and material inhomogenities. It should be clear that any imperfection modelling, however sophisticated it is, can represent only "substitute imperfections". This refers to certain effects such as material inhomogenities, loading and boundary inaccuracies which are not feasible to include and therefore they have to be somehow substituted in the numerical model. The state-of-the-art in imperfection modelling includes the modelling of initial deformations and residual stresses where relevant.

Initial deformations. Initial deformations have to catch the relevant instability modes. In steel plated structures, these imperfections can be local such as buckles in subpanels and twists of flanges or stiffeners. Global imperfections comprise bow of stiffeners or whole members. The most difficult task is to choose the imperfection shape and amplitude. A classification can be done as follows:

- **Realistic imperfections.** They correspond to the "real" imperfections of the structure. However, except for test girders and for systematically fabrication-induced imperfections in series products, this approach cannot be met in civil engineering structures because the imperfections are not known sufficiently well in advance.
- **Manually defined imperfections.** They correspond to the commonly observed imperfections during fabrication and are also called fabrication-oriented imperfections. They account for imperfections in real structures on a very simple basis. Often imperfection shapes are defined by functional descriptions such as sine functions.
- **Eigenmode-affine imperfections.** They are defined on a mathematical basis and the modelling methodology is very clear because the nonlinear buckling analysis is based on the imperfections coming from a linear bifurcation analysis (LBA) beforehand. The effort however can be large without getting appropriate results e.g. when only the first eigenmode is used, see Sec. 5.3.2.
- **Collapse-affine imperfections.** They correspond to the deformed shape at collapse and are assumed to lead to the lowest buckling resistance. The calculation effort is high, because a nonlinear buckling analysis has to be carried out beforehand for which the right choice of imperfection has to be made as well. Due to its worst case character, the amplitude needs to be scaled properly and it is often smaller than amplitudes for the other imperfections shapes mentioned above.

Based on Schmidt [113], a further differentiation should be done between worst-case and stimulating imperfections. Whereas worst-case imperfections should lead to the lowest buckling resistance in general, they are not directly linkable to the fabrication-induced

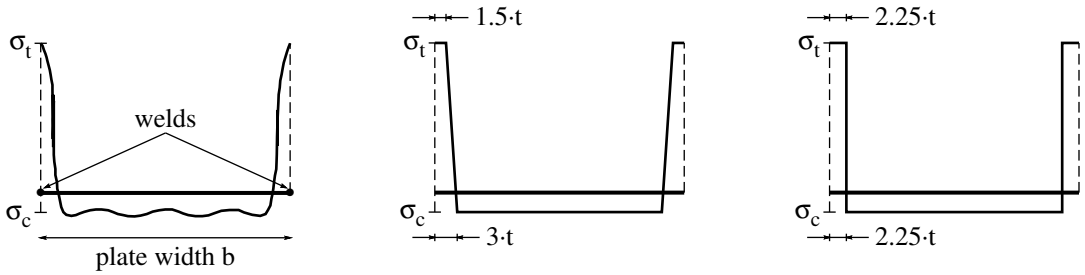

(a) as measured [38] (b) BSK 07 [14] (c) as implemented

Figure 5.4: Distribution of residual stresses

deformations. Stimulating imperfections should catch the stability behaviour of the structure sufficiently well to allow for a prediction of the ultimate load. Eigenmode-affine or collapse-affine imperfections are usually tried for worst-case imperfections, eigenmode-affine and fabrication-oriented imperfections may be used as stimulating imperfection. An evaluation of both concepts is given in Sec. 5.3.2.

For the recalculation of experiments realistic imperfection shapes and amplitudes are used since measured data are available. The implementation of the measured web geometry is explained in Sec. 5.2.1.1. For the recalculation of buckling curves and the parameter studies, further studies are given in the frame of the verification by buckling curves, see Sec. 5.3.2, from which some considerations will be given here. It becomes clear that for extensive parameter studies where a great number of fully nonlinear buckling analyses has to be performed, it is a feasible decision to choose an as simple equivalent geometric imperfection pattern as possible. Its function should be to "stimulate" the characteristic physical plate buckling behaviour. For that purpose it must only have a certain geometric similarity to the relevant imperfection shape. Thus, manually defined imperfection shapes are used. They are oriented at possible fabrication-induced shapes and do not represent the worst case but obviously they are able to represent well the ultimate loads in practice, see also the discussion by Ruff and Schulz [106, 107] and Rusch and Lindner [108].

Residual stresses. Residual stresses are mainly caused by welding and therefore present in most steel plated structures. Post-weld treatment methods such as anealling are often impractical and therefore not applied. Their distribution in idealised form is shown in Fig. 5.4, however, the level of residual stress depends on the heat input and weld size and scatters a lot. In Swedish Steel Standard BSK 07 [14], a recommendation for the consideration of residual stresses is given according to Fig. 5.4b. Alternatively, residual stresses can be taken into account by equivalent geometric imperfections as proposed in Annex C, EN 1993-1-5 [46].

Residual stresses were not measured for the experiments and therefore are not considered in the recalculation of tests. For the recalculation of buckling curves and in some of the parameter studies, residual stresses have been accounted for according to BSK 07 [14] with f_y in tension less than 500 MPa a which is based on [19], see Table 5.1. A simplified

Table 5.1: Residual stress values

residual stress	stress value [MPa]	mean width
σ_t	$f_y \leq 500\,\text{MPa}$	$2.25 \cdot t$
σ_c	equilibrating stress	$b - 4.5 \cdot t$

rectangular stress distribution has been used, in which the level of tensile residual stress is equal to the yield strength and the compressive stress is determined from equilibrium.

Comment on Annex C, EN 1993-1-5. Annex C.5, EN 1993-1-5, gives guidance on the use of imperfections and is introduced here shortly. It is said to use both geometric and structural imperfections which in practical terms comprises initial deformations and residual stresses. Eigenmode shapes with an amplitude of 80 % of the fabrication tolerances and manually defined imperfection shapes are recommended. For residual stresses a stress pattern corresponding to the mean expected values should be assumed. In fact, residual stresses have to be chosen by the engineer.

5.2.2 Discretisation

The geometric midsurface plane of the mathematical model is dicretised by dividing it into a mesh of finite elements of the chosen type. There are a number of shell elements with different features, ranging from elastic shell theory to nonlinear theory with large rotations and plasticity. Nonlinear buckling analysis of plates is based here upon small strain, large displacement analyses accounting for large rotations. Besides material nonlinearity, the geometrical nonlinear effect in the anaylsis of slender plates is caused by finite (large) rotations. The requirements imposed by the nonlinear analysis lead to the preselection of a shell finite element which accounts for nonlinear, large rotation, and even finite strain applications, plasticity and transverse shear deformation. These elements were also used for linear bifurcation analysis, e.g. to generate eigenmode-affine imperfection shapes. Because they perform similar well as purely elastic shell types, there was no need to change the shell type. In ANSYS the nonlinear shell types are denoted SHELL181 and SHELL281. This notation will be used here for reference, too. Both elements have six degrees of freedom at each node: translations in the x, y, and z axes, and rotations about the x-, y-, and z-axis. They differ in the type of shape function which is either a bilinear or a biquadratic shape function, see Fig. 5.5. SHELL281 is a serendipity element, i.e. without an interior node. The piecewise approximation of the mathematical model by finite elements inevitably leads to a discretisation error which should be reduced to a minimum. The accuracy of results may be increased according to [93] as follows:

- **h-method.** Overall refinement of the mesh density.
- **r-method.** Refinement of the mesh density in areas with high stress gradients.
- **p-method.** Increase of the polynomial degree of the element's shape function.

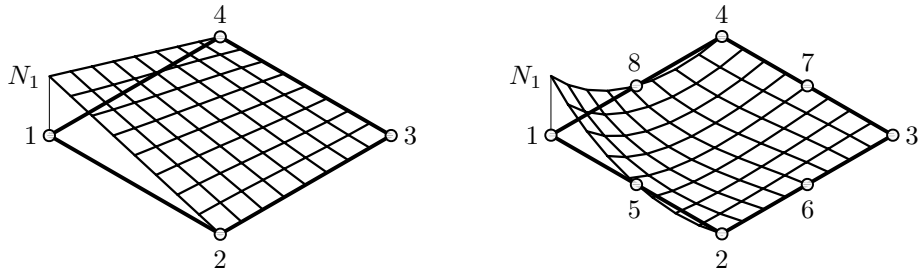

(a) four-node bilinear quadrilateral (SHELL181)

(b) eight-node biquadratic serendipity quadrilateral (SHELL281)

Figure 5.5: Shape functions of quadrilateral shell finite elements (showing a perspective view of the shape function N_1)

Here, the mesh density should be able to cover buckling shapes and stress gradients adequately. Figure 5.6 shows the results of a discretisation study on a square plate under bending for which finite elements with bilinear and biquadratic shape functions have been used. The deviation from the code rules is drawn over the number of elements per edge length. It can be shown that a refinement of the mesh density clearly leads to a reduction of the discretisation error. Besides that, it is found that biquadratic elements show a lower divergence and converge faster than bilinear elements.

According to Fig. 5.6d, firstly a linear elastic bifurcation analysis was carried out and the first eigenvalue was determined. The quadratic elements converge quickly whereas the linear elements require roughly twice the number of elements. Though it is difficult to give general recommendations, it can be concluded that a sufficient number to cover a buckling halfwave is a number of six elements for the linear shape function and a number of four elements in case the quadratic shape function is used.

Secondly, a nonlinear buckling analysis including imperfections was carried out. At ultimate state, a nonlinear stress distribution occurs which may require a finer mesh density in order to cover the stress gradient adequately. From Fig. 5.6e it can be shown that the quadratic element converges rapidly. In contrast to this, the linear element is not too bad, but it is slightly stiffer throughout which leads to slightly higher resistances.

In this work shell elements with biquadratic shape function are used for the analysis of plates due to the aforementioned advantages in comparison with linear elements. Since the analysis of plate I-girders chronologically took place before the parameter study on plates, shell elements with bilinear shape functions are used for the plate I-girders. The discretisation was done according to the recommendations for mesh density. The number of integration points is usually five over the thickness. It has been changed to nine in regions where high bending stresses over the thickness are expected.

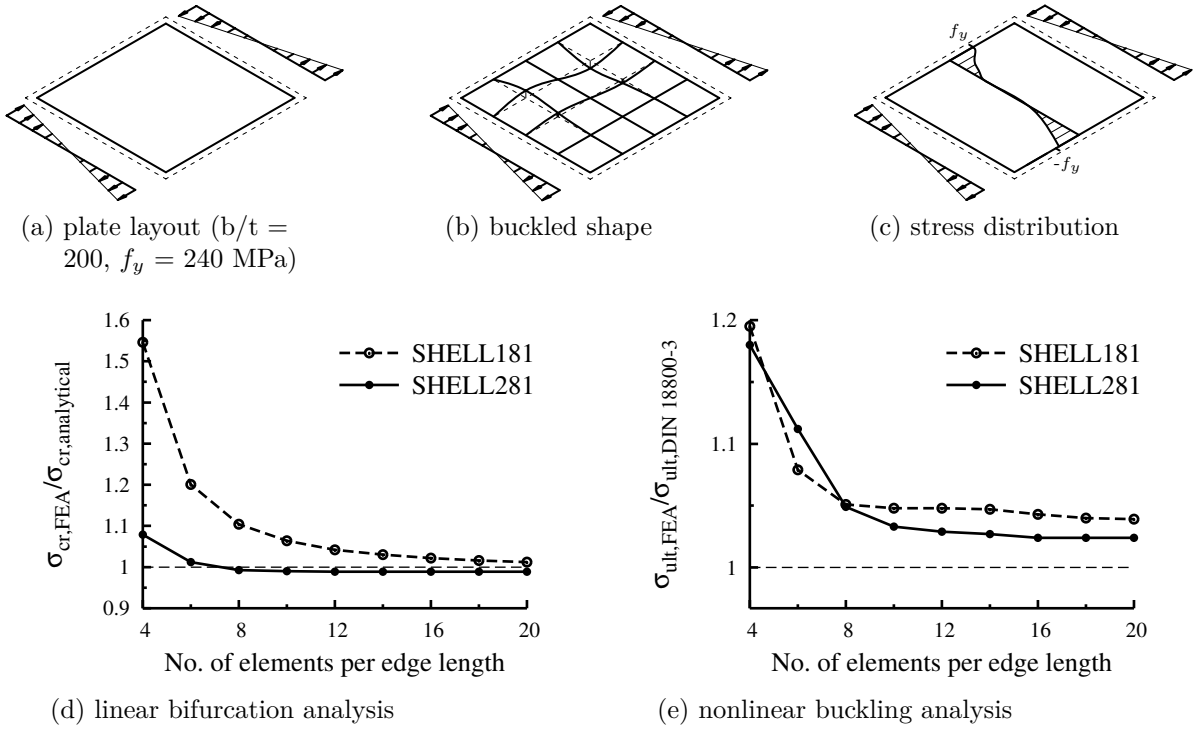

(a) plate layout (b/t = 200, f_y = 240 MPa)

(b) buckled shape

(c) stress distribution

(d) linear bifurcation analysis

(e) nonlinear buckling analysis

Figure 5.6: Discretisation study

5.2.3 Numerical analyses

5.2.3.1 Linear bifurcation analysis

A linear bifurcation analysis is based on perfect geometry, linear material behaviour and small deformations. Buckling occurs by bifurcation which means that a reference configuration of the geometry and an infinitesimally close deformed, i.e. buckled, configuration are both possible at the same load level. To determine the corresponding eigenvalues and eigenmodes, a linear analysis is sufficient to be carried out and the structure can be loaded by an arbitrary load $\{R\}_{ref}$. The associated stress stiffness matrix is $[K_\sigma]_{ref}$ and as the problem is presumed to be linear the conventional stiffness matrix $[K]$ is unaffected by the load level so that λ_{cr} can be introduced which changes the load level but not the distribution of stresses, see Eq. 5.2a. If buckling displacements $\{\delta D\}$ are introduced, see Eq. 5.2b, and both equations are subtracted from each other, Eq. 5.3 is the result, which is a classical eigenvalue problem.

$$\Big([K] + \lambda_{cr}\,[K_\sigma]_{ref}\Big)\,\{D\}_{ref} = \lambda_{cr}\,\{R\}_{ref} \tag{5.2a}$$

$$\Big([K] + \lambda_{cr}\,[K_\sigma]_{ref}\Big)\,\{D_{ref} + \delta D\} = \lambda_{cr}\,\{R\}_{ref} \tag{5.2b}$$

$$\Big([K] + \lambda_{cr}\,[K_\sigma]_{ref}\Big)\,\{\delta D\} = \{0\} \tag{5.3}$$

Thus, the elastic critical load $\{R\}_{cr}$ is determined based on the smallest root λ_{cr}. The eigenvector $\{\delta D\}$ associated with λ_{cr} is the eigenmode which can be scaled and used e.g. as geometric imperfection shape.

As eigenvalue and eigenmode extraction method, the block Lanczos method is chosen. It is well suited for solving large symmetric eigenvalue problems, with equivalent accuracy as the commonly used subspace iteration method. In contrast to the subspace iteration method, block Lanczos offers shorter run times though requiring more memory. In [12] it has been found that the block Lanczos method is better suited if many modes are extracted and that it is more robust if the model contains different types of elements such as shell and beam elements.

5.2.3.2 Nonlinear buckling analysis

A nonlinear buckling analysis is based on imperfect geometry, nonlinear material behaviour and large deformations. The nonlinear nature of the buckling problem requires an incremental and iterative approach as solution strategy. Geometric nonlinearity arises from deformations which become so large due to buckling that the equilibrium equations must be written with respect to the deformed geometry. Material nonlinearity comes from the material properties which are functions of the stress or strain, see Sec. 5.2.1.2. Generally spoken, the problem is nonlinear because the stiffness matrix $[K]$ is a function of the displacements $\{D\}$. Unlike in the linear case, information on $[K]$ is needed here to be able to solve for $\{D\}$ and the load $\{R\}$ is not known in advance. Principles of superposition do not hold true anymore, so that an iterative process is required to obtain the displacements and its associated stiffness matrix and load so that the product $[K]\{D\}$ is in equilibrium with $\{R\}$, see Eq. 5.4.

$$[K]\{D\} = \{R\} \tag{5.4}$$

The solution of the governing nonlinear equations can be achieved through an incremental approach, i.e. the correct solution is approximated by taking linear steps in the appropriate direction. To solve these equations within a step usually iterative Newton-Raphson based methods are applied. ANSYS offers different Newton-Raphson schemes: full, modified and using the initial stiffness matrix. Due to the required large deformation analysis, the full Newton-Raphson method is used here in which the tangent stiffness is updated at every equilibrium iteration. Figure 5.7a depicts the present explanations as a two-dimensional plot of load versus displacement. Loads are applied stepwise. The method starts with a trial based on the initial tangent stiffness k_{t0}. From this, the load imbalance vector $\{R\}_i$ is determined which is the difference between the applied loads and the loads evaluated based on the assumed solution. A new equilibrium iteration is performed to achieve a load imbalance vector close to zero depending on the convergence criteria. The characteristics of the full Newton-Raphson method is that the tangent stiffness is updated prior to each equilibrium iteration. This procedure is repeated within

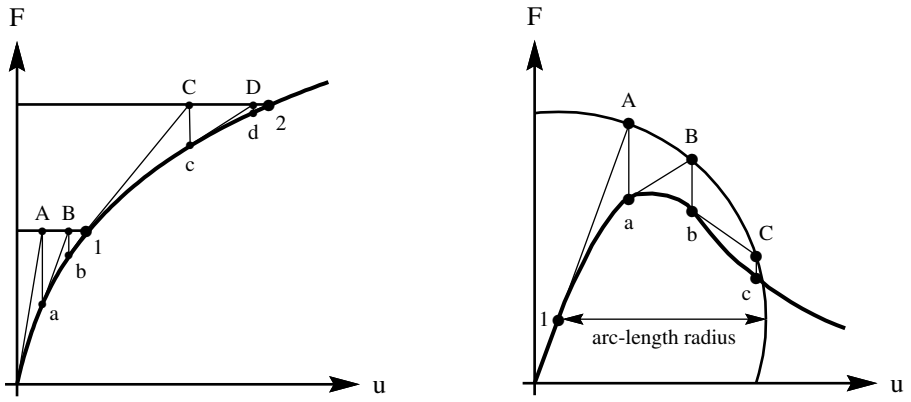

(a) full Newton-Raphson method

(b) arc-length method

Figure 5.7: Solution strategies

each substep until convergence is accomplished.

For a given load step these increments are named substeps in ANSYS. Only a single load step is used. Initial substep size is usually prescribed as $P/100$. Automatic time stepping has been used where appropriate, however, a maximum substep size of $P/10$ has been prescribed. Such an incremental form of the governing equations can be written according to Eq. 5.5, where $\{\Delta D\}$ and $\{\Delta R\}$ represent the unknown incremental displacement and load vectors. No line search methods are applied.

$$[K_t]\{\Delta D\} = \{\Delta R\} \tag{5.5}$$

Load control has been chosen due to the combined loading which is applied at the edges. In the vicinity of limit points where a maximum of the load-displacement curve is reached, the tangent stiffness becomes zero or negative when the descending load path is to be followed. In such cases regular load-controlled Newton-Raphson methods fail to converge. A method which usually succeeds and which has been used here is the arc-length method. As shown in Fig. 5.7b the load parameter is introduced as an additional variable. The increments of both displacements and load are adjusted in such a way that iterative steps cause points to lie on a curve of radius Δl centered at the initial point 1. The method prevents a doubling back on itself when the curve reaches a negative slope. The radius of the arc-length method has been prescribed within certain limits of the radius depending on the solution characteristics. The arc-length method is used here for cases where the tangent stiffness approaches zero due to the formation of plastic hinges in flanges or in cases where the descending load-displacement-path is followed in order to study the plate behaviour also in the postultimate range.

5.3 Verification of the numerical model

5.3.1 General

In order to verifiy the numerical model for parameter ranges which are not explicitly covered by the recalculation of experiments and to evaluate the reference strengths on which the interaction curves are based, the relevant buckling curves for the basic load cases from DIN 18800-3 [28], DNV-RP-C201 [33] and Chapter 10, EN 1993-1-5 [46] are recalculated. The findings of this section go beyond the aforementioned objectives insofar that they provide an extensive insight into the recalculability of buckling curves in terms of choice of boundary conditions, imperfection shape and amplitude as well as their effect and relevance on buckling resistance. This, in turn, supports the decisions taken for the numerical modelling in the frame of the parameter studies.

In the following, the calculated results are shown in comparison with their relevant buckling curve which allows for a visual evaluation of the results. It should be kept in mind that up to now, buckling curves have been established empirically based on experiments in which several effects influencing the buckling resistance cannot be fully controlled. This is in contrast to the possibilities numerical models offer where certain effects can be precisely defined and studied.

Also the experimental tests conducted by the author and well-documented tests from literature are recalculated. For a quantitive measure, an accompanying statistical evaluation is carried out in which regression and correlation coefficients are presented for the recalculation of experiments.

5.3.2 Recalculation of buckling curves

5.3.2.1 Plates under compression

The recalculability of the Winter curve for plates under uniform compression has already thoroughly been studied e.g. in [81] and [106]. Ruff and Schulz [106] concluded from their numerical studies that the Winter curve leads to unsafe results when the allowable fabrication tolerances (b/250) and residual stresses are used for imperfection modelling. This has been put into perspective in a comment [107] later on. However, the discrepancy and the resulting uncertainty was addressed in the frame of a DIBt research project [81] of which results were published by Rusch and Lindner [108]. Plates under uniform stress which were supported at four and three sides were studied. It is concluded that the discrepancy "can only be resolved, if stimulating imperfections are taken into account instead of worst-case imperfections. It is not considered necessary to tighten the current plate buckling curves used in the codes" [108] which is justified by the empirically established and proven-in-reality Winter curve. Finally, the recommended values for recalculation were:

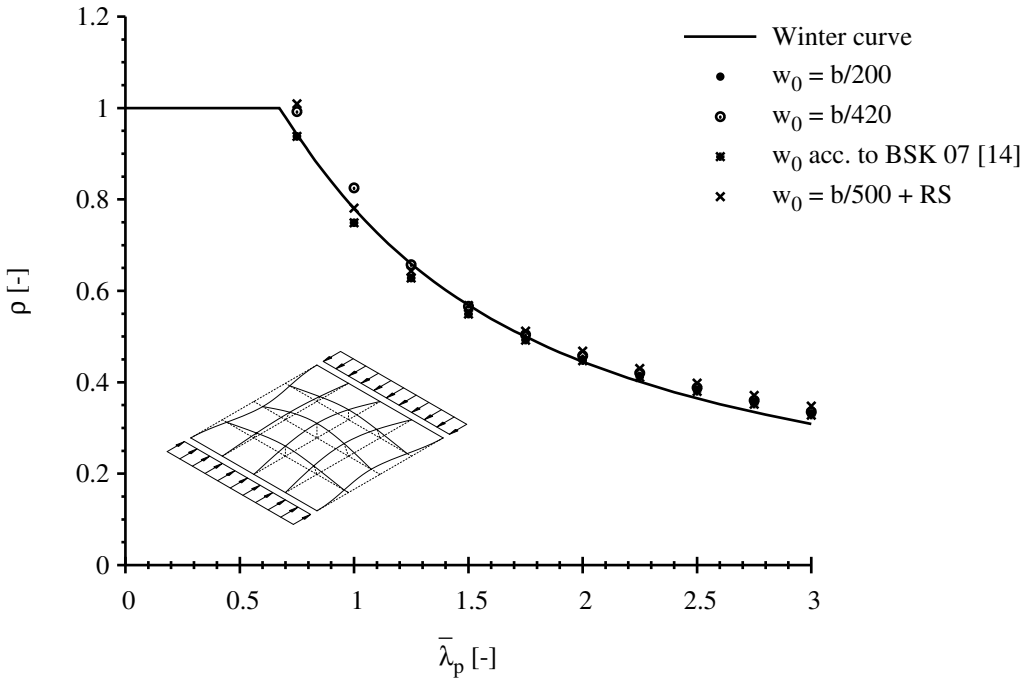

Figure 5.8: Comparison of simulations and the Winter curve ($\alpha = 1$, all edges hinged, loaded edges constrained and unloaded edges unconstrained)

- Equivalent geometric imperfection b/420, see also Usami [120]
- Geometric imperfection b/500 and residual stresses (RS) $\sigma_t = 0.5 \cdot f_y$ and $\sigma_c = -0.1 \cdot f_y$, see Rusch and Lindner [108]

The recalculation of the Winter curve with these two values is shown in Fig. 5.8. It can be concluded that a recalculation of the Winter curve is sufficiently well possible on the basis of hinged boundary conditions and unloaded edges free to move in-plane, i.e. unconstrained, and loaded edges remaining straight, i.e. constrained. In addition, the recommended imperfection according to Annex C, EN 1993-1-5 [46], and Swedish steel design standard BSK 07 [14] are also given in Fig. 5.8.

Although the Winter curve presumes that the loaded edges remain straight this cannot be assured for all kind of loadings. A transverse patch loading will inevitably cause the loaded edges to move in-plane, depending on the stiffness of the attached boundary element, e.g. flanges. It can be shown that for unconstrained loaded edges a recalculation of the buckling curve according to Annex B, EN 1993-1-5, with parameters $\alpha_p = 0.34$ and $\overline{\lambda}_p = 0.70$ is well possible based on an imperfection amplitude of b/200, see Fig. 5.9.

On the other hand, the assumption of the Winter curve that unloaded edges are free to move in-plane is on the safe side when e.g. inner subpanels of multi-stiffened panels are considered. Figure 5.10 compares numerical results to the Winter curve. It can be shown that for an increasing plate slenderness the membrane boundary condition becomes more important which leads to favourable results.

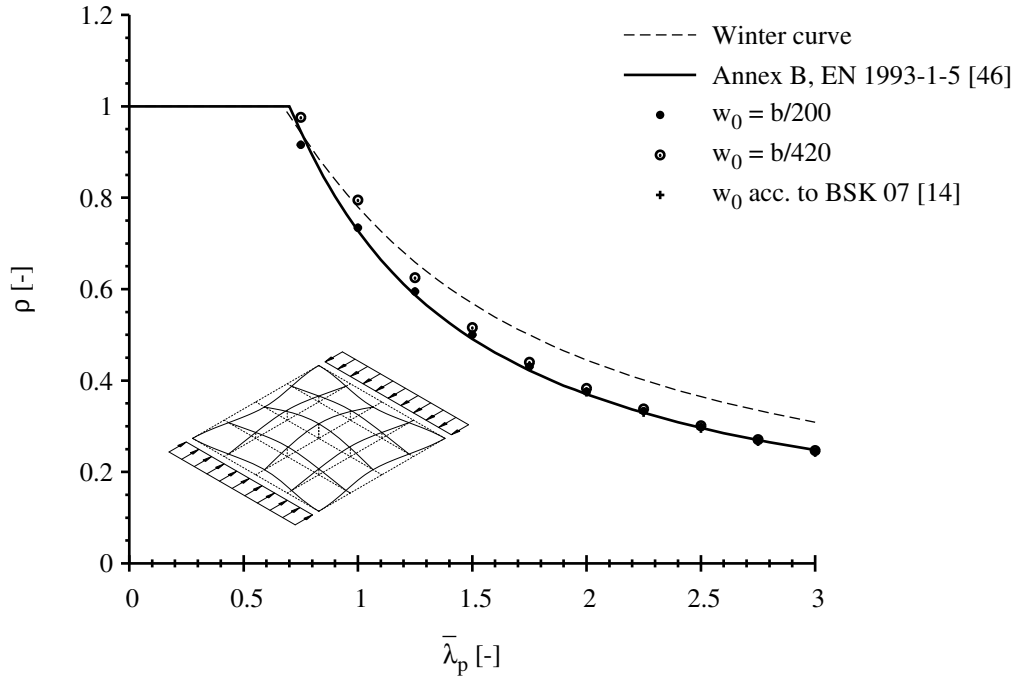

Figure 5.9: Comparison of simulations and the buckling curve according to Annex B, EN 1993-1-5 [46] ($\alpha = 1$, all edges hinged and unconstrained)

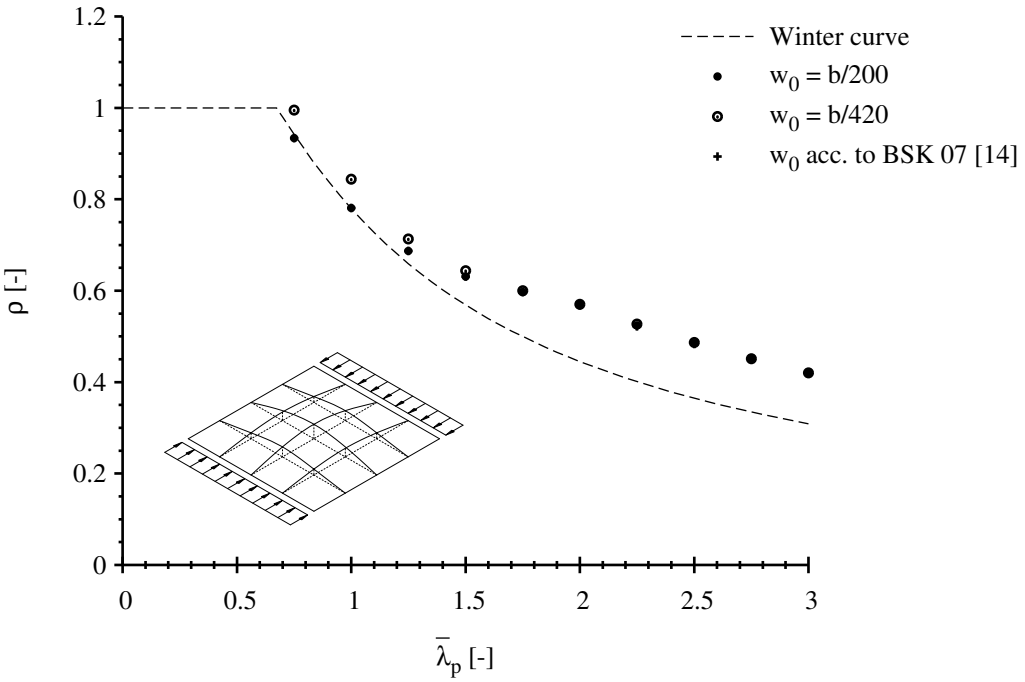

Figure 5.10: Results of simulations in case of a plate with constrained edges ($\alpha = 1$, all edges hinged and constrained)

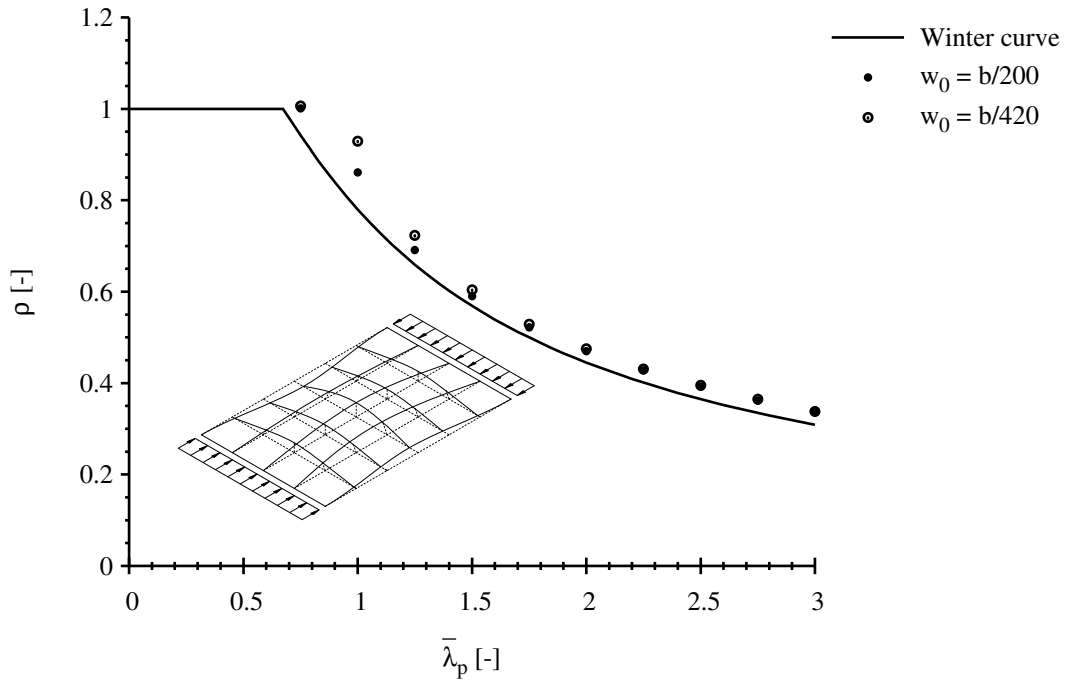

Figure 5.11: Comparison of simulations and the Winter curve ($\alpha = 1.4$, all edges hinged, loaded edges constrained and unloaded edges unconstrained)

The recalculations according to Figs. 5.8 to 5.10 are based on square plates. The advantage of a square plate is that the difference in imperfection shape between eigenmode and sine-imperfection becomes negligible. Starting from a panel aspect ratio of $\alpha = 1.4$ the eigenmode shape changes into a two-wave configuration. Imperfection measurements on such plates [51] however show that usually a single-wave mode further prevails. However, with this example configuration it can be shown that the resistance depends not only on imperfection amplitude and shape but also on panel aspect ratio. In Fig. 5.11, results of a plate with an aspect ratio of $\alpha = 1.4$ are given for which the eigenmode shape is still a one-halfwave mode. It can be shown that the resistance is increased so that the square plate can be considered as worst case. In reality however, square plates are rarely used in comparison to rectangular plates with larger aspect ratios so that nevertheless the Winter curve is generally applicable, which coincides with the conclusions drawn by Rusch and Lindner [108]. Taking the time into account when the Winter curve was established, it becomes clear that with numerical methods a perfect match cannot be achieved which makes it in turn however complex to draw conclusions e.g. for interaction cases.

5.3.2.2 Plates under compression susceptible to column-like buckling

The reduced postcritical strength reserve of plates which are susceptible to column-like buckling is accounted for by an interpolation between plate- and column-buckling curve. In EN 1993-1-5 [46] a quadratic interpolation function is used, see Sec. 2.3.4. In order to evaluate the quality of the results, the calculated results are compared to simulations as

Table 5.2: Comparison of ultimate loads

girder	$F_{ult,exp}$ [kN]	$F_{ult,FEA}$ [kN]	$F_{ult,FEA}/F_{ult,exp}$ [-]
SP 600	846	892	1.05
SP 1200	1030	1027	0.99

shown in Fig. 5.12. Plates with aspect ratios $\alpha = 1/2, 1/3$ and $1/6$ have been chosen as representative dimensions. Since the imperfection sensitivity of columns is higher than of plates, the sensitivity is studied by doubling and halving the imperfection amplitude according to EN 1993-1-5 so that besides b/200 the amplitudes b/100 and b/400 are studied.

It can be shown in Fig. 5.12 that in case of column-like behaviour a strong influence of the imperfection amplitude exists. Nevertheless, when evaluating the interpolation between plate- and column-like behaviour a linear relationship can be found, see Fig. 5.13, instead of the quadratic interpolation used in Sec. 4.5.4, EN 1993-1-5 [46]. It is eye-catching that the DNV interpolation performs sufficiently well for small panel aspect ratio but if a plate with $\alpha = 1/2$ is approached the results are far off, see Fig. 5.12a. The source of this oddity can be attributed to the fact that in ship building, which is the origin of the DNV rules, subpanel aspect ratios of 1/10 are commonly reached in the multi-stiffened segments. One should be aware of this fact when evaluating the DNV rules in case of column-like buckling. In reality the resistance is usually not overestimated since for ship plating both clamped and constrained boundary conditions can be usually assumed. As shown in Fig. 5.14 these edge restraints have a very favourable effect on the column-like resistance.

5.3.3 Recalculation of own experiments

The experiments which were introduced in Chapter 4 are recalculated numerically. Imperfections are taken as measured according to the shapes given in Sec. 4.2.3. Edge boundary conditions are defined by the continuity between web and flanges. The modelling is based on the parametric solid modelling technique, see Sec. 5.2.1.1.

Experimental and numerical ultimate loads are compared in Table 5.2. For both girders SP 600 and SP 1200 a good agreement between both types of ultimate loads is found. Figures 5.15 and 5.16 show the applied total load drawn over the vertical displacement of the LVDTs located at the load plate of the shear force introduction and at the load plate of the patch load introduction which correspond to LVDT 1 and LVDT 4 according to Fig. 4.7. It should be noted that in all cases the vertical displacement is corrected by the settlements of the supports during loading. Generally, a good agreement between relevant load-displacement curves is found.

In Figs. 5.17 and 5.18 the deformations of the web panels for the experimentally and

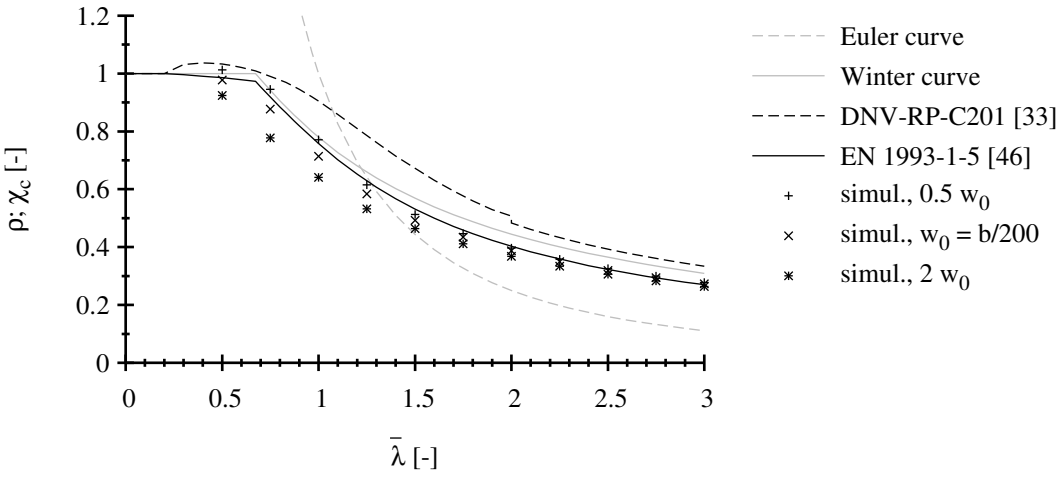

(a) $\alpha = 1/2$

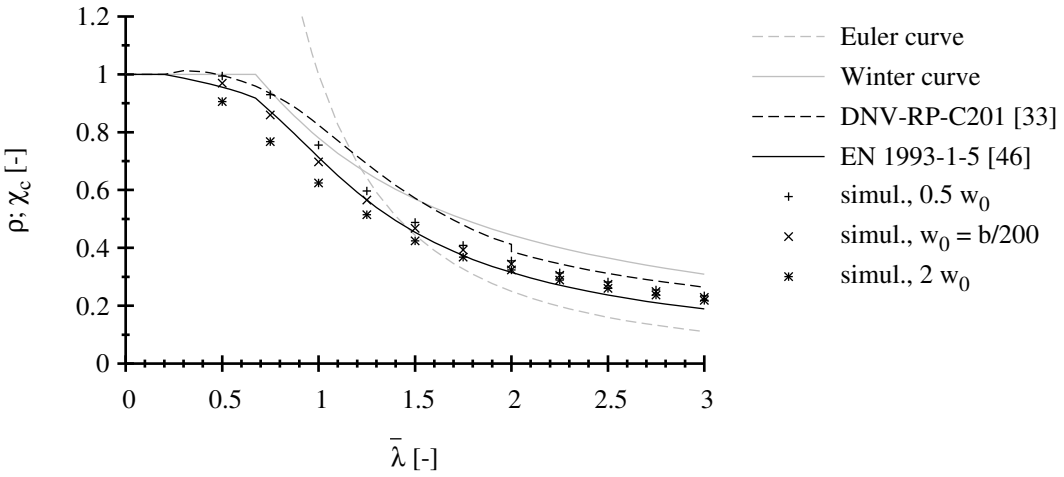

(b) $\alpha = 1/3$

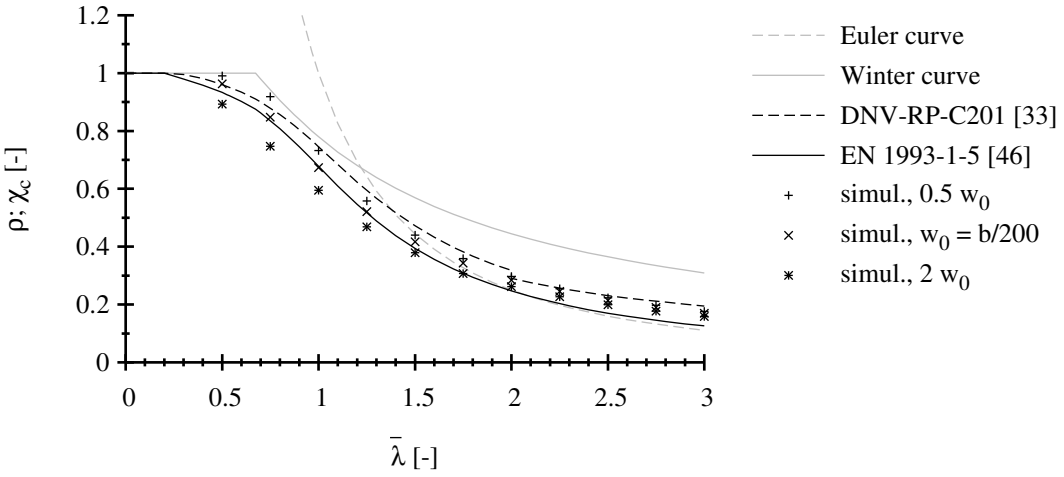

(c) $\alpha = 1/6$

Figure 5.12: Comparison of simulations and interpolated column-like buckling curves (all edges hinged, loaded edges constrained, unloaded edges unconstrained)

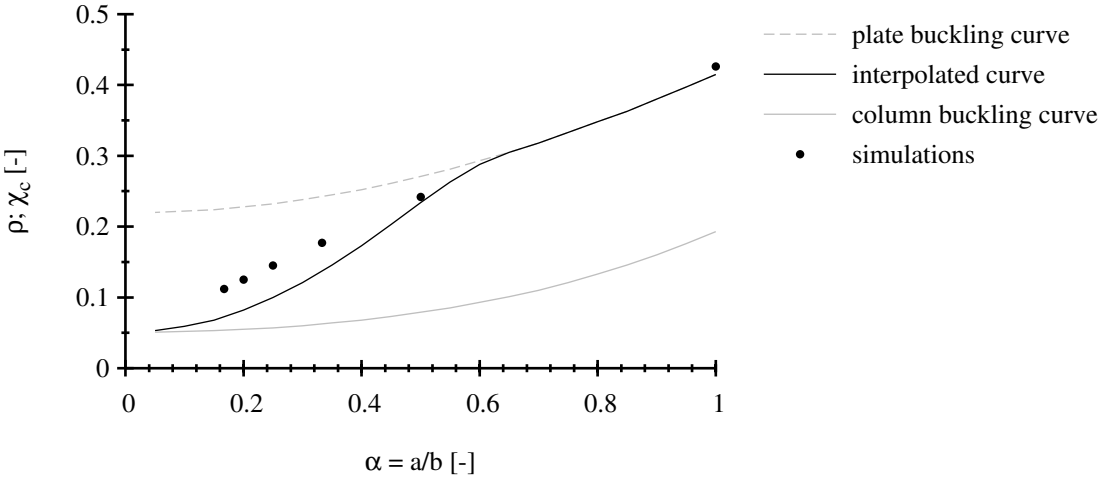

Figure 5.13: Evaluation of the interpolation function according to Sec. 4.5.4, EN 1993-1-5 [46]

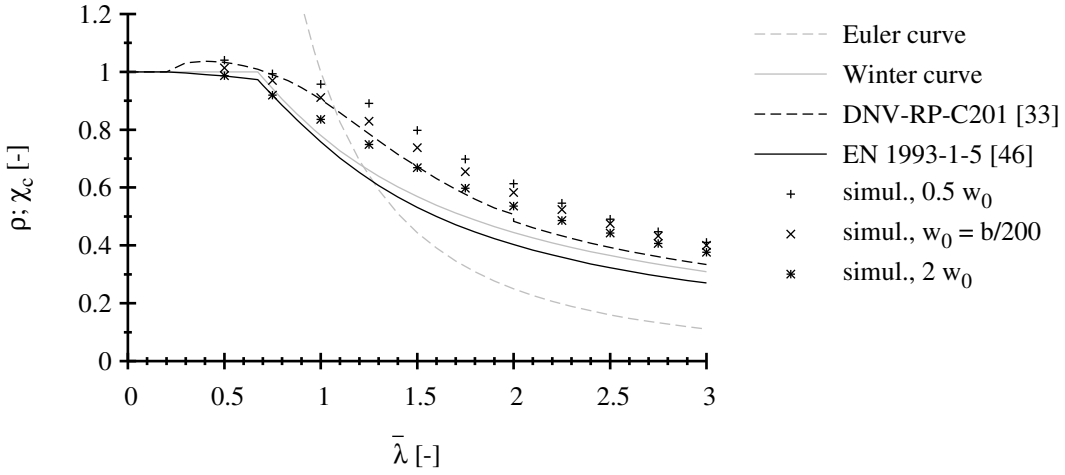

Figure 5.14: Comparison of simulations and interpolated column-like buckling curves ($\alpha = 1/2$, loaded edges clamped and constrained, unloaded edges hinged and unconstrained)

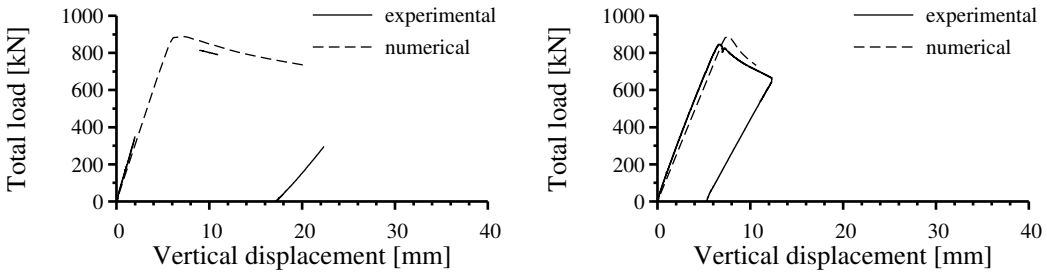

(a) transverse patch loading (b) shear force

Figure 5.15: SP 600 - Comparison of load-displacement-curves

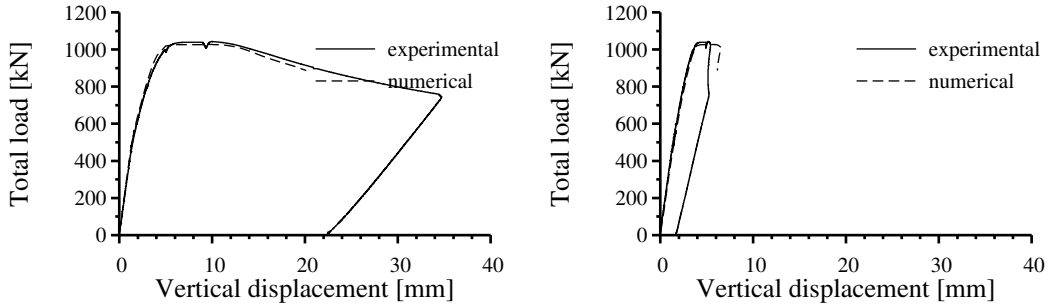

(a) transverse patch loading (b) shear force

Figure 5.16: SP 1200 - Comparison of load-displacement-curves

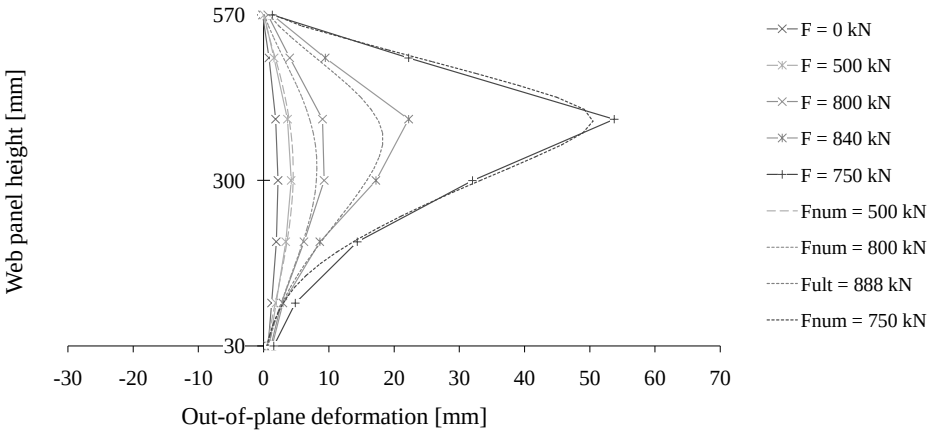

Figure 5.17: SP 600 - Comparison of lateral web deformations

numerically determined data are compared at different load levels. For girders SP 600 and SP 1200 the behaviour of the web panel and the magnitude of the deformation can be retraced very well up to ultimate load. Only in the post-ultimate range the numerically determined deformations of SP 1200 differ from the experimental ones but the deformed shape still develops in a similar way.

From the recalculation of the own tests it can be concluded that the finite element model is able to reproduce reliable numerical results. Both ultimate load and quality of the displacement behaviour show a good agreement. In order to allow for a better evaluation of the numerical model additional experimental tests from literature are recalculated in Sec. 5.3.4.

5.3.4 Recalculation of experiments from literature

The most comprehensive and well-documented test series in literature has been conducted by Roberts and Shahabian [101, 116] in the year 2000, see Sec. 3.3.4. Hereafter this series is numerically recalculated with the established finite element model which has

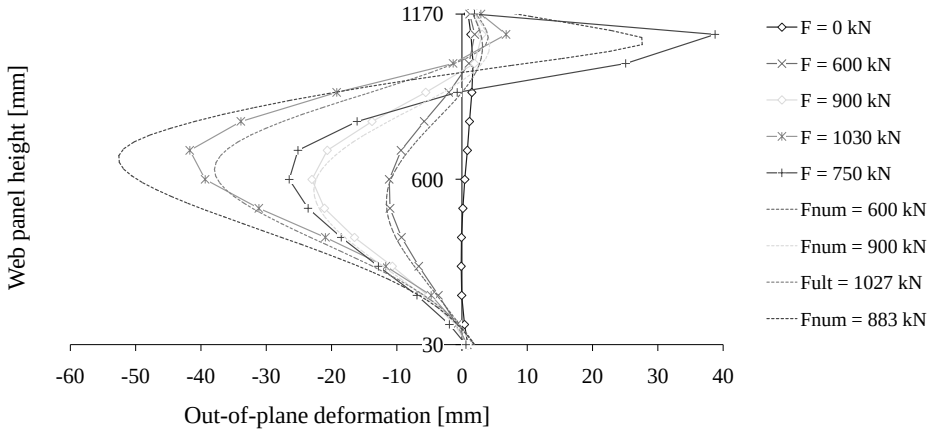

Figure 5.18: SP 1200 - Comparison of lateral web deformations

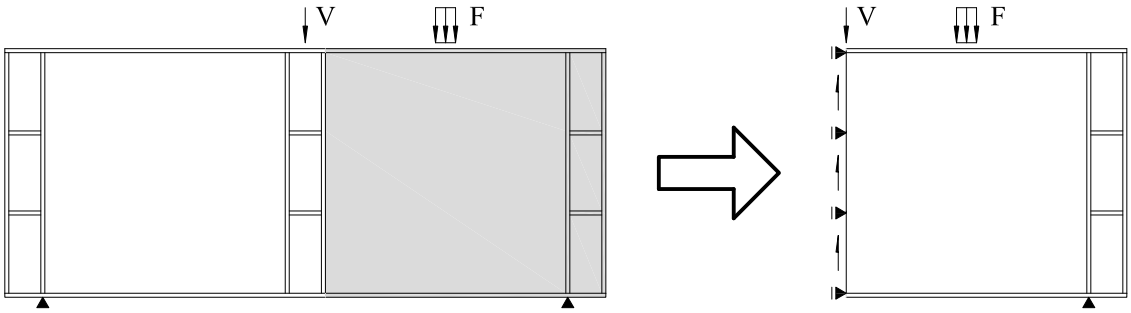

Figure 5.19: Transformation of real girder geometry into numerical model geometry and introduction of equilibrating shear stresses

been used to recalculate the own tests. However, in order to reduce calculation time in the light of the later parameter study, use is made of the girder symmetry as shown in Fig. 5.19. Imperfections are taken as sine-function with one halfwave in each direction and an amplitude of $b/200$. Edge boundary conditions are defined by the continuity between web and flanges.

Here it appears from the girder layout that the vertical stiffeners are designed as rigid end-posts with additional strength coming from smaller stiffeners welded between the two vertical end-stiffeners as shown in Fig. 5.19. For this reason, it has been studied in the frame of the recalculation of the tests if such a strengthened end-post can be represented in the numerical model by simple coupling equations. Fig. 5.20 shows the level of equivalence

Table 5.3: Statistical evaluation of the end-post representation in terms of R_e/R_t

end-post representation	mean value	standard deviation	COV
coupling equations	1.017	0.097	0.009
full shell model	0.960	0.062	0.004

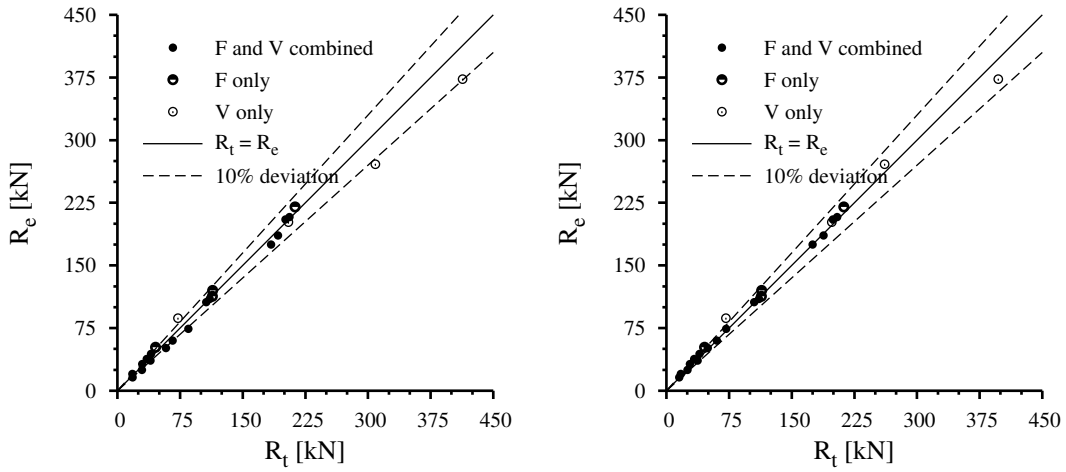

(a) coupling equations (b) full shell model

Figure 5.20: Comparison of the end-post representation in the numerical model

for the experimentally and numerically determined ultimate loads R_e and R_t with regard to the different end-post modelling. The ultimate loads correspond both to combinations of shear- and patch loading (shown by filled circles) and to the basic load cases "pure patch loading" (shown by half-filled circles) as well as "pure shear force" (shown by circles only). Data points above the angle bisector stand for an underestimation (= safe side) of the experimental ultimate load when recalculated numerically, whereas for data points below the angle bisector the experimental ultimate load is overestimated. The comparison of the two diagrams in Fig. 5.20 shows that rigid end-posts in reality cannot be represented with the help of simple coupling equations in the numerical model because the experimental ultimate load is overestimated in most cases. The design requirements formulated in Sec. 9.3.1, EN 1993-1-5 [46] give rules for the design of rigid end-posts which provide suffcient anchorage for the longitudinal portion of the tensile membrane stresses. However, in contrast to this, coupling equations neglect any beam-like behaviour and they substitute a rigid region which is too favourable with regard to the anchoring potential of real end-post configurations, see Fig. 5.20a. Therefore a fully modelled end-post condition with shell elements instead leads to better results, see Fig. 5.20b.

A statistical evaluation of the ratio of numerical to experimental ultimate load confirms that the full shell model gives more accurate results, see Table 5.3. For the full shell model not only the mean value but also the standard deviation is reduced resulting in a lower coefficient of variation (COV) so that the latter layout of the finite element model is validated and adopted for further studies.

5.3.5 Conclusions

The recalculation of buckling curves shows that the recalculability of plate-buckling curves is acceptable though knowing that a perfect accordance between empirically determined buckling curves and numerical results cannot be achieved. It turns out that the in-plane membrane restraint is an unused strength reserve for slender plates which cannot be assessed by elastic critical calculations. For this purpose an appropriate formulation of the buckling curve is required. In case of column-like buckling, the EN interpolation function is partly on the safe side in comparison to the studied parameters and literature. The DNV interpolation function has another background and should not be used for plates approaching square geometries. However, based on the general evaluation of the recalculations the applicability of the plate finite element model is considered as approved.

The recalculations of full girders show that good results are strongly dependent on the quality of the provided experimental records. The finite element model which has been established for the recalculation of the own experimental studies shows a good agreement between experimental and numerical data for both load and displacement behaviour. A further simplification of the numerical model which takes advantage of girder symmetry has been confirmed by recalculation of the experimental test series by Roberts and Shahabian [101, 116]. In addition to that, a study on the correct modelling of the end-post representation has been performed which shows that a further simplification for rigid end-posts with the help of coupling equations cannot be recommended. Based on the evaluation of the recalculations the applicability of the numerical full shell model is considered as approved.

Besides that, the following conclusions can be drawn from the recalculations in order to define the boundary conditions and scope of the parameter studies:

- **Imperfection shape.** The square plate is kept as reference configuration and worst case scenario since the difference between different mode shapes such as eigenmode and sine-imperfection becomes negligible. The imperfection shape becomes relevant when non-square plates are studied so that for rectangular geometries different halfwave configurations will be considered. Manually defined imperfections such as sine functions may be used since the difference to eigenmode shapes is small in case of biaxial compression.
- **Imperfection amplitude.** The amplitude has a large influence in the stocky to medium slenderness range. It was shown that the recalculation of buckling curves succeeds only with reduced amplitudes. As the agreement between buckling curves and simulations for the reference strength is not fully achievable, the two amplitude values $b/200$ and $b/420$ are kept for the parameter studies. The value $b/420$ turns out to be adequate in the stocky to medium slenderness range. For higher slendernesses the value $b/420$ is also used but it is found that the absolute value of the imperfection amplitude becomes less important there.
- **Residual stresses.** Residual stresses may be used but it is shown that they do not

significantly increase the quality of recalculation. Instead geometric imperfection and residual stresses have to be adjusted in every case such that a good agreement with the relevant buckling curve can be achieved. With regard to the parameter studies equivalent geometric imperfections are considered as sufficient.

- **Edge boundary conditions.** It is shown that the recalculation of buckling curves strongly depends on the choice of the relevant in-plane edge boundary condition. Rotational edge boundary conditions can be covered by taking them into account for the determination of the elastic critical stresses. For the parameter studies the main focus will be on unconstrained and constrained edge configurations.

In summary, the comparison shows that both buckling curves and experiments can be recalculated adequately so that the numerical model is approved and found to be well-suited for further parameter studies.

5.4 Plate stability under biaxial compression

5.4.1 General

Earlier work comprises a large number of studies which date back in the 1970s and 1980s, see Sec. 3.2. Later work mainly focused on summary and reevaluation of these studies. The evaluation of results in this work revealed a large knowledge base of studies on plates under biaxial compression, see Sec. 3.2.13. However, the large number of influential parameters led always to a discussion on the quality and usability of the results. For these reasons own simulations are carried out in the following which will be used for a reassessment of earlier work and on which a design proposal will be based in Sec. 6.4. Initially, the stability behaviour of biaxially loaded plates is studied. In the parameter study the key parameters are addressed as follows:

- Slenderness, i.e. b/t-ratio = 30, 45, 65 and 100
- Panel aspect ratio $\alpha = 1$ and 3
- Imperfection shape and amplitude
- Edge boundary conditions, both in-plane and rotational

5.4.2 Structural behaviour

On one side, it is agreed that stocky plates can reach the equivalent stress criterion which takes advantage of material behaviour. On the other hand, plates are more and more effected by stability with increasing slenderness. This should be reflected by the interaction curves but their comparison shows non-neglible discrepancies when comparing e.g. for slender plates the linear interaction according to DIN 18800-3 [28] with the circular-shaped interaction according to Chapter 10, EN 1993-1-5 [46], and DNV-RP-C201 [33].

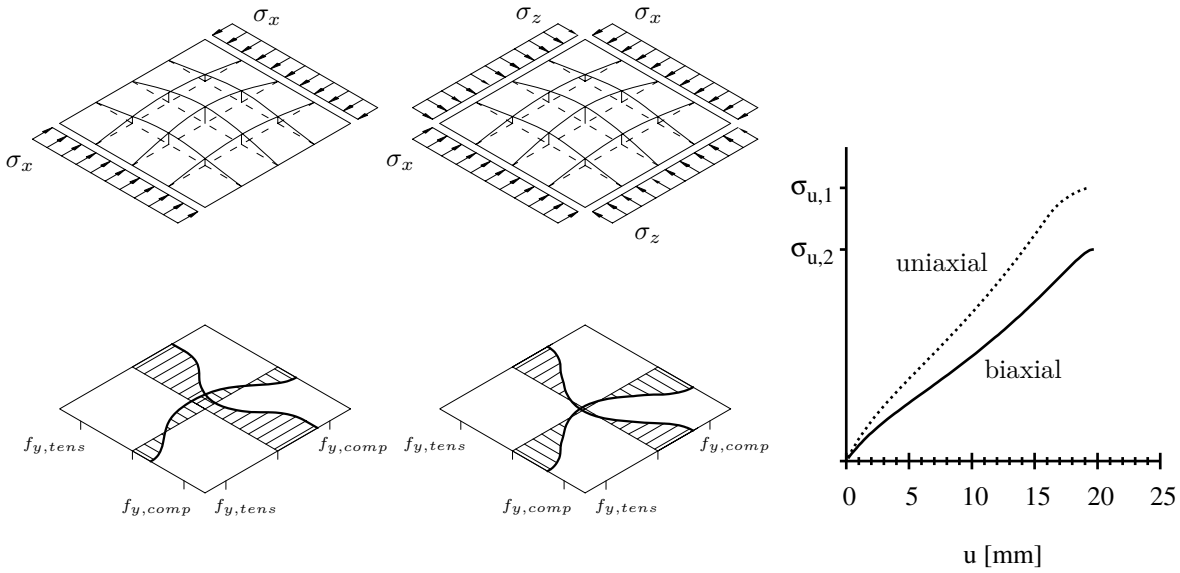

(a) stress distribution at ultimate load, uniaxial compression

(b) stress distribution at ultimate load, biaxial compression

(c) deformation at mid-plate

Figure 5.21: Comparison of the stability behaviour of a plate under uniaxial and biaxial compression (b/t =100, f_y = 355 MPa)

Since the documentation of background information and decisions taken is rather poor, the stability behaviour will be studied below. However, an evaluation of the results to design rules with regard to design rules will be done in Sec. 6.4.

The stability behaviour of a plate under uniaxial compression which has been studied in Sec. 2.2.1 is used here again to explain the stability behaviour of biaxially loaded plates. It has been shown that a plate possesses a significant postcritical strength reserve in case of plate-like behaviour which results from favourable tensile membrane stresses that develop perpendicular to the loading direction. Light will be shed on the fact when the second loading direction is also loaded in compression.

In Fig. 5.21 the stability behaviour of a square plate which is able to develop a post-critical strength reserve in both loading directions is compared under uniaxial and biaxial compression. For the uniaxial case, it was shown that tensile stresses develop perpendicular to the loading direction which attenuate the out-of-plane deformation of the plate. Figure 5.21b illustrates the same situation with compression also in the second loading direction. It can be shown that the compression nullifies the tensile stresses which leads to an increased deformation for the same load level, see Fig. 5.21c. Since the ultimate load is reached at about the same out-of-plane deformation, it becomes obvious that higher stresses can be attained if the tensile membrane component reduces the deviation forces.

The square plate is a special case because the imperfection shapes of its basic loadings coincide. Since plate-like behaviour can be accounted for both basic loading directions, the interaction criterion represents the worst case scenario because it has to take its

disappearance into account. The stability behaviour of plates with panel aspect ratios other than square is usually effected by column-like buckling which cannot benefit from favourable tensile membrane stresses. It will be shown in Sec. 5.4.3 that for rectangular plates the imperfection shape becomes important.

5.4.3 Effect of imperfections

For a non-square plate, the imperfection shape which leads to the smallest resistance depends on the number of halfwaves and the corresponding loading direction. Figure 5.22 shows two eigenmode imperfection shapes of a biaxially loaded plate with a panel aspect ratio of $\alpha = 3$. The three-halfwave mode results from a loading of the short edges (σ_x) and the one-halfwave mode from a loading of the long edges (σ_z). For each of the uniaxial loadings the corresponding mode leads to the smallest resistance. However, if the plate is biaxially loaded the shape strongly effects the structural behaviour. The inflexion points of the three-halfwave mode act like a stiffening of the plate which significantly increase the resistance when mainly the long edges are loaded, see the thick lines in Fig. 5.22a. On the other hand, the one-halfwave mode increases the resistance when mainly the short edges are loaded because the out-of-plane deformation usually prevents the plate from switching to its natural three-halfwave mode. In [36] a large number of initial mode shapes combinations were studied for panel aspect ratios of $\alpha = 3$ but they could not produce a smaller failure resistance than it was achieved with the three- and one-halfwave mode shapes. Therefore they will be used in the following study.

In Fig. 5.23 interaction curves are drawn over the stress ratio σ_x/σ_z each normalised with the yield strength. It can be shown that beyond the point where both curves intersect the resistance is clearly overestimated when the governing imperfection shape is not applied. For the three-halfwave mode the stiffening effect is quickly reached. In contrast to this, the one-halfwave mode can be applied for a wider range of stress ratios. However, it can be seen that it also overestimates the basic loading resistance when mainly the short edges are loaded. It can be shown that when the simulation results are considered up the intersection point of both lines, a safe estimate of the interaction behaviour can be made although the curvature is quite favourable. Measurements of occuring initial imperfection shapes of normally fabricated plates [51] support that the one-halfwave mode shape is the one which is most likely to occur in reality. Thus, the three-halfwave mode shape is usually on the safe side when the loading of the short edges begins to dominate. Nevertheless, the three-halfwave mode shape is used in the further studies to aim at a lower bound.

In Figs. 5.24 to 5.29 interaction curves with amplitudes of b/200 and b/420 are summarised. It can be shown that the imperfection amplitude has an influence in the small to medium slenderness range and become less important for large slendernesses. Similar conclusions were also drawn for the recalculation of the buckling curves.

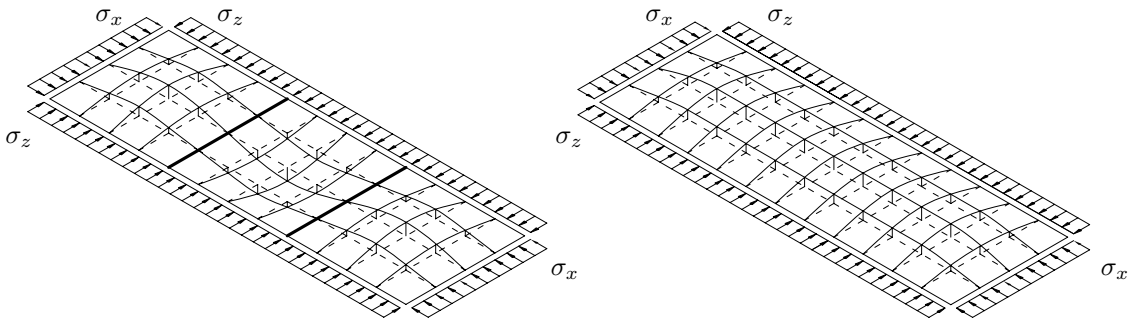

(a) three-halfwave mode (b) one-halfwave mode

Figure 5.22: Comparison of imperfection shapes

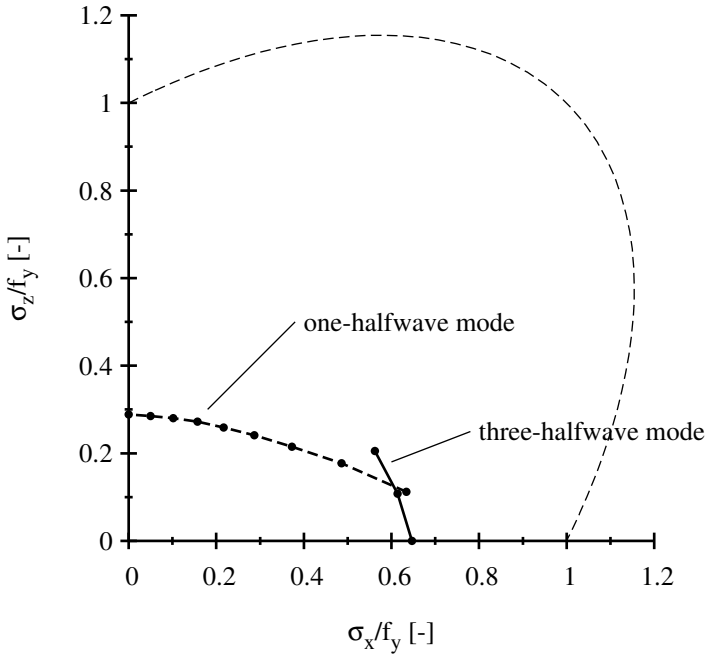

Figure 5.23: Effect of aspect ratio on the shape of interaction curves, exemplarily shown for an aspect ratio of $\alpha = 3$

5.4.4 Effect of edge boundary conditions

It was shown in Sec. 5.3.2 that the recalculability of buckling curves strongly depends on the choice of the relevant edge boundary conditions. A difficulty arises when the buckling curves of EN 1993-1-5 [46] have to be applied to biaxial loadings because the in-plane restraint condition is usually not fully applicable. The Winter curve presumes e.g. that loaded edges are constrained and the unloaded edges are unconstrained. However, biaxially loaded plates have all edges loaded and usually all edges are either constrained or unconstrained. It is therefore necessary that adequate reference strengths are used for the evaluation of the interaction behaviour with regard to the edge boundary conditions. In order to achieve a clear attribution of the behaviour to certain boundary conditions, all edges are taken as either constrained or unconstrained in the following study.

Effect of in-plane edge restraints. Figures 5.24 and 5.27 show the simulation results of a square and a rectangular plate with b/t-ratios of 30, 45, 65 and 100 for unconstrained and constrained boundary conditions. Constrained boundary conditions lead to an increase of the resistance for slender plates and they provide a strength reserve which is not considered in the buckling curves of EN 1993-1-5 [46]. Unconstrained boundary conditions represent a lower bound. For medium slenderness ranges constrained conditions show a slightly more favourable interaction behaviour.

Effect of rotational edge restraints. Figures 5.25 and 5.28 show the simulation results of a square and a rectangular plate with b/t-ratios of 30, 45, 65 and 100 for hinged and clamped boundary conditions. Clamped boundary conditions lead to an increase of the resistance. A strength reserve exists when hinged boundary conditions are assumed for the calculation of the elastic critical buckling stress but clamped conditions are present in reality. In general, hinged boundary conditions represent a lower bound.

In Figs. 5.26 and 5.29 the normalised values of the interaction curves are evaluated for plates with panel aspect ratios $\alpha = 1$ and $\alpha = 3$. Normalisation has to be understood in such a way that the simulation results refer to the reduced strength value of the corresponding uniaxial loading with same geometry and boundary conditions. Comparing the normalised values for the different in-plane edge restraints it can be shown that the deviation of the interaction behaviour in general is marginal. However, comparing the normalised values for the different rotational edge restraints it can be shown that the deviation is significant for small to medium slendernesses.

In both cases, it can be generally shown that with increasing plate slenderness the favourable biaxial state of stress on the material side vanishes and that for very slender plates the interaction behaviour approaches a linear interaction.

5.4.5 Conclusions

The studies on plates under biaxial compression follow up earlier work. It is shown that for slender plates of which the slenderness theoretically approaches infinity a linear in-

teraction is reached. For square plates such a linear relationship is true because the imperfection shapes of the basic loadings coincide. For non-square plates the imperfection shape significantly alters the interaction curve due to the stiffening effects of the different shapes. One- and three-halfwave mode shapes are used to describe the interaction behaviour. Since the resulting, favourable interaction behaviour relies on realistic imperfection shapes, it can be generally taken into account. It can be concluded that the panel aspect ratio is one of the most influential parameters for the interaction curvature.

Another important parameter which effects the interaction behaviour is the edge restraint, both in-plane and rotational. For high slendernesses, the in-plane restraint leads to favourable interaction curves in terms of absolute values. A normalisation however shows that the interaction shapes are very similar. This is an important observation since the slenderness is determined irrespective of the in-plane edge boundary condition which only becomes relevant in large deformation analysis. Thus, similar interaction curves can be drawn over the same slenderness for both unconstrained and constrained in-plane restraints. The rotational edge restraint is even more favourable both in absolute values and after normalisation. Since clamping effects can be accounted for in linear buckling theory, the slenderness becomes smaller and this positive influence on the interaction behaviour can be taken into account in the determination of the slenderness.

It is concluded and assumed for the studies in Chapter 6 that a precise assessment of the reference strength facilitates the use of few interaction curves which are then able to account for different edge boundary conditions. Current design rules will be improved with regard to the following objectives: sound representation of the interaction behaviour by using precise reference strengths and, by doing this, enabling the use of advanced software solutions in determining elastic critical buckling stresses which is especially of advantage in full building models where the individual panel is analysed as part of the whole structure.

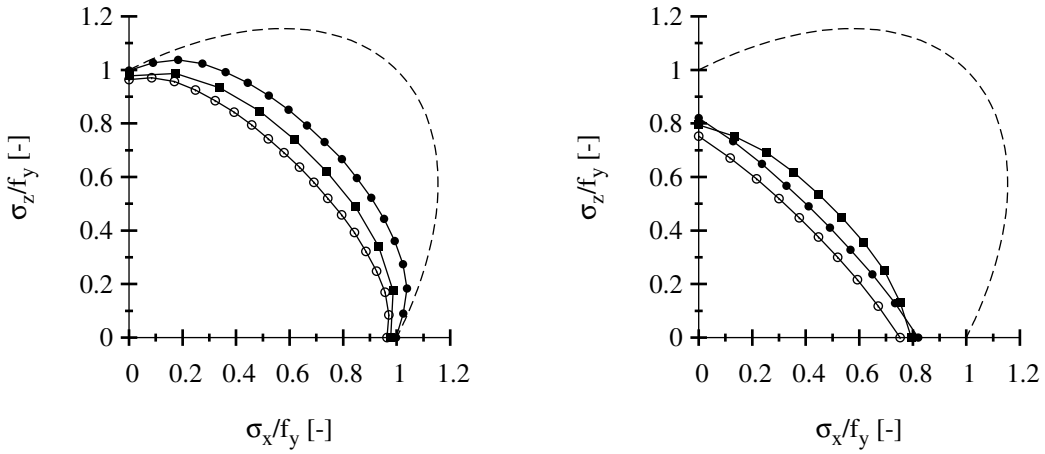

(a) $b/t = 30$

(b) $b/t = 45$

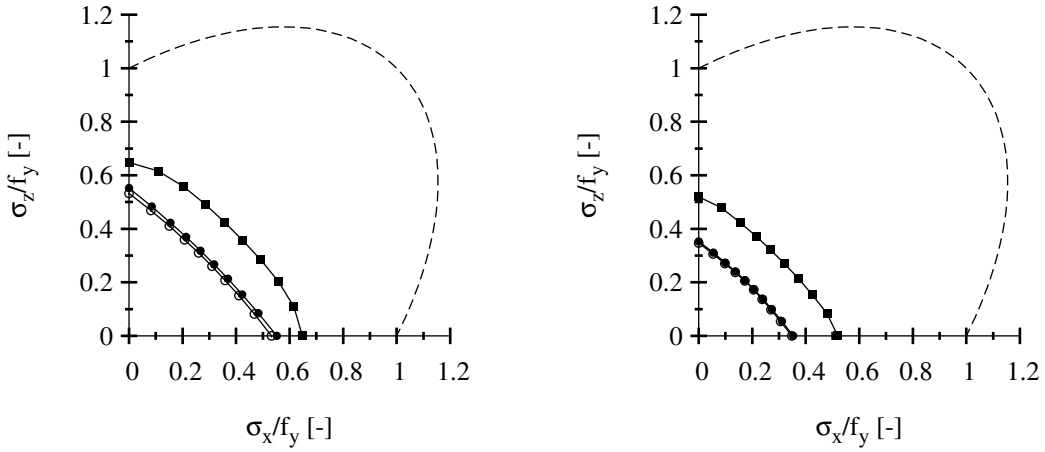

(c) $b/t = 65$

(d) $b/t = 100$

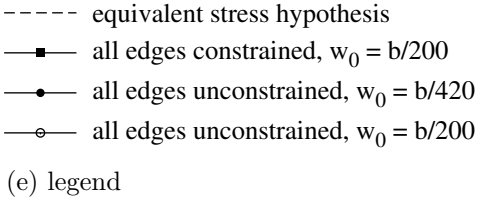

(e) legend

Figure 5.24: Effect of in-plane edge restraints ($\alpha = 1$, all edges hinged)

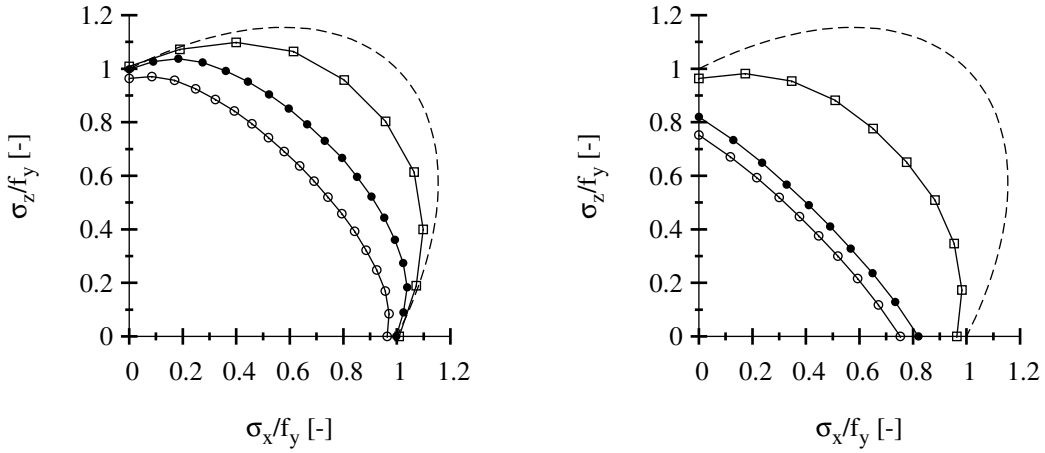

(a) $b/t = 30$

(b) $b/t = 45$

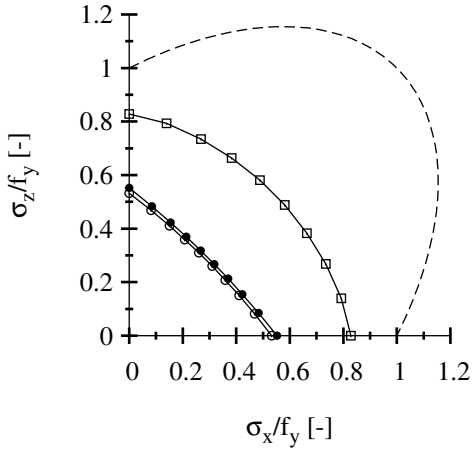

(c) $b/t = 65$

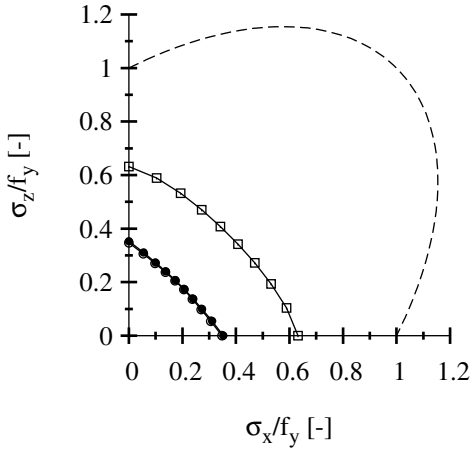

(d) $b/t = 100$

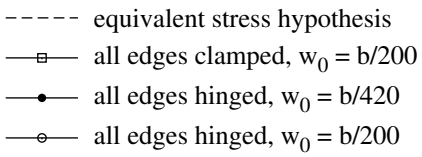

(e) legend

Figure 5.25: Effect of rotational edge restraints ($\alpha = 1$, all edges unconstrained)

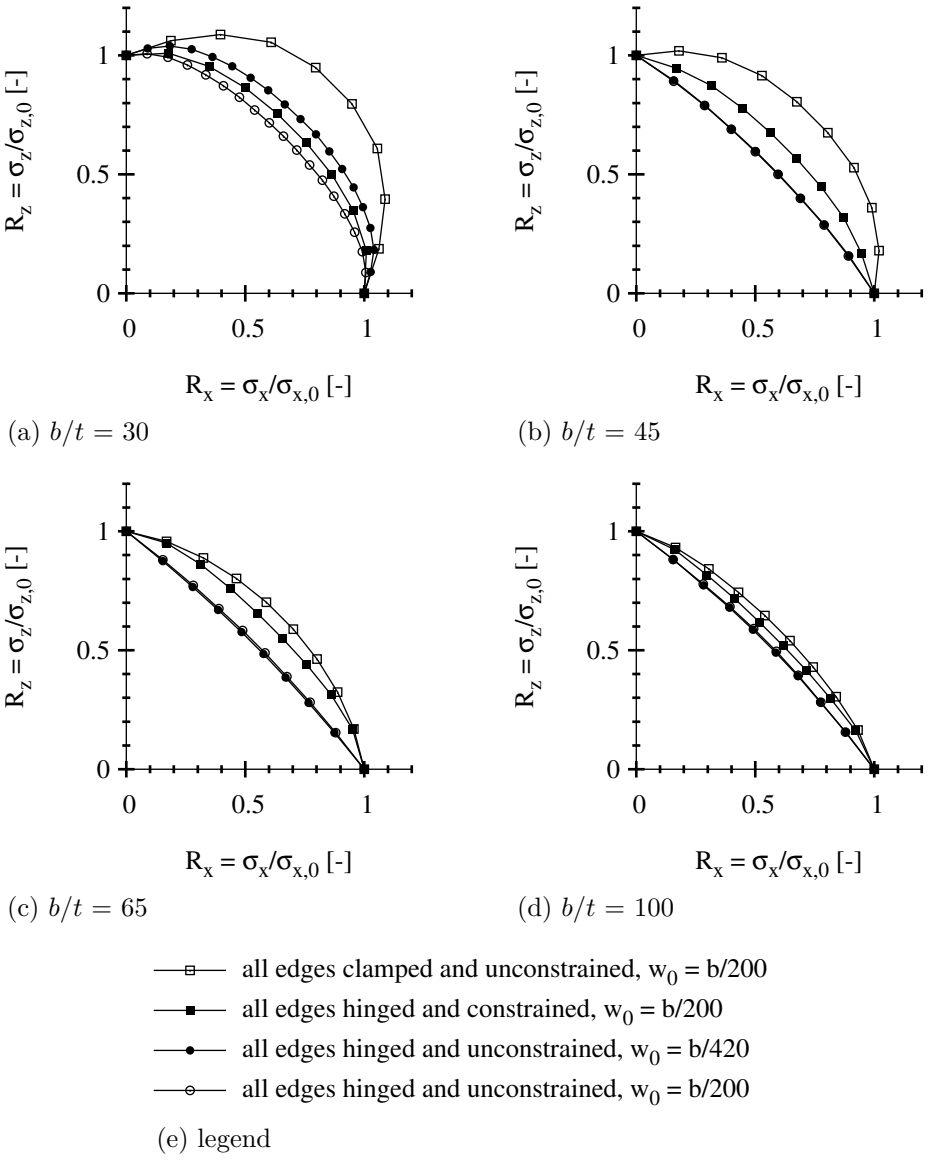

(a) $b/t = 30$ (b) $b/t = 45$

(c) $b/t = 65$ (d) $b/t = 100$

(e) legend

Figure 5.26: Effect of edge restraints, normalised values ($\alpha = 1$)

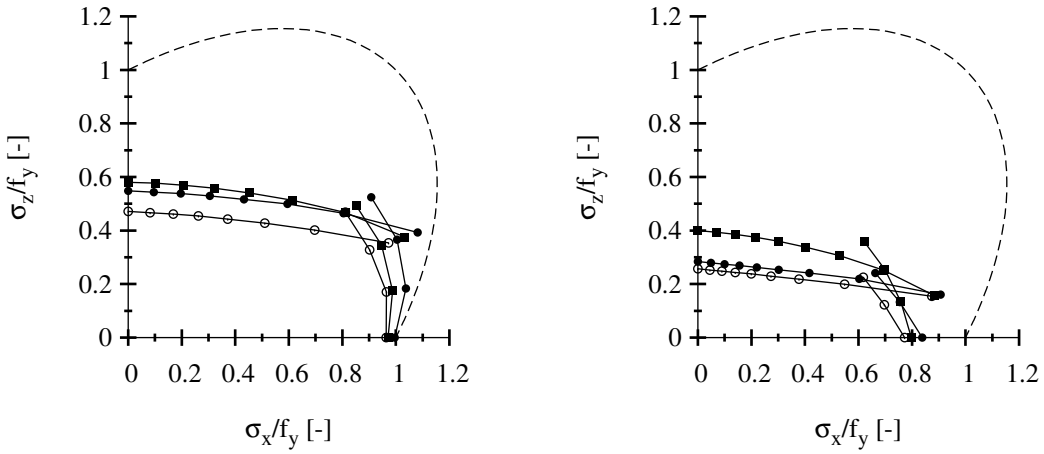

(a) $b/t = 30$

(b) $b/t = 45$

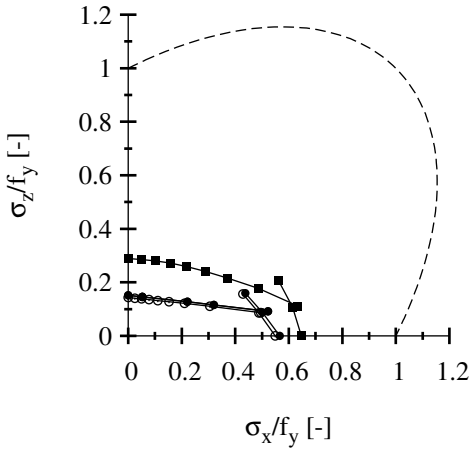

(c) $b/t = 65$

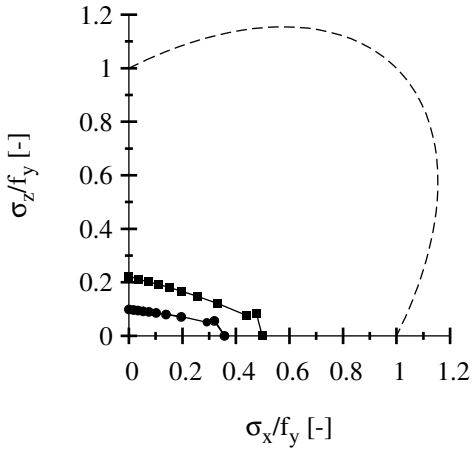

(d) $b/t = 100$

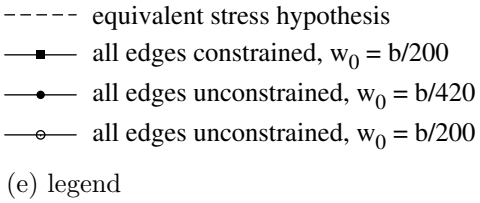

(e) legend

Figure 5.27: Effect of in-plane edge restraints ($\alpha = 3$, all edges hinged)

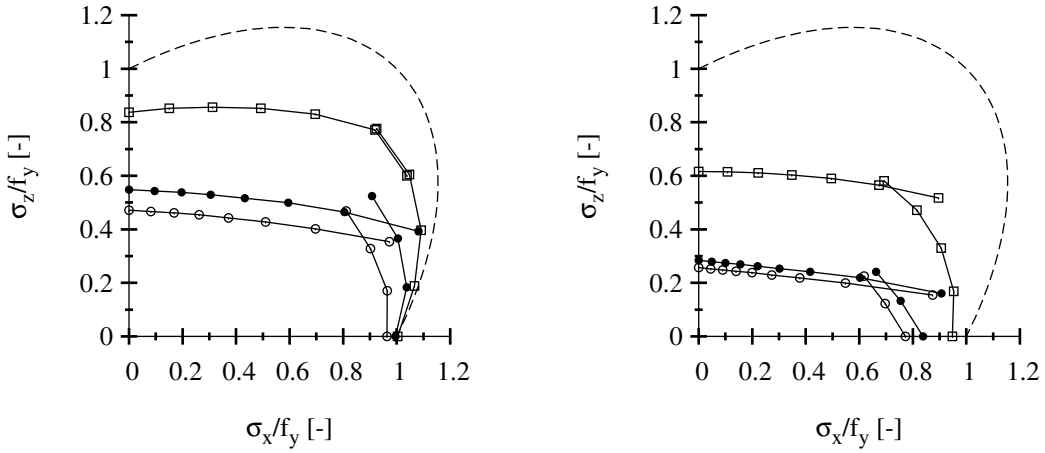

(a) $b/t = 30$

(b) $b/t = 45$

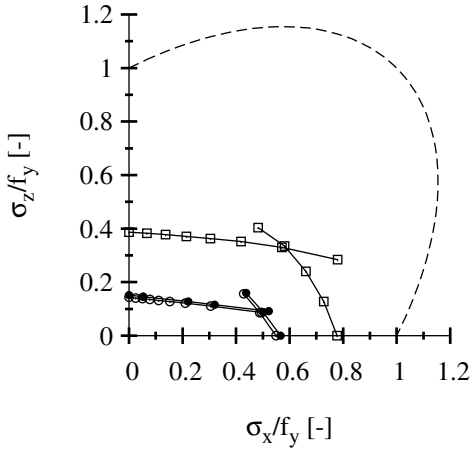

(c) $b/t = 65$

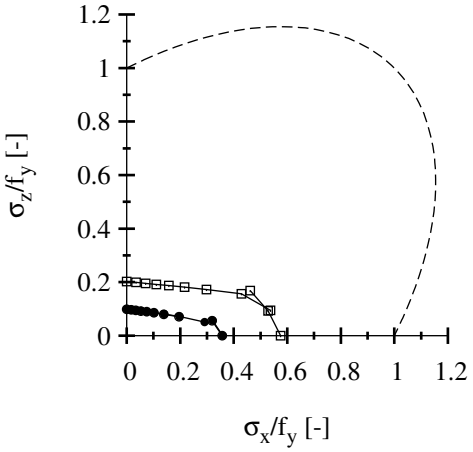

(d) $b/t = 100$

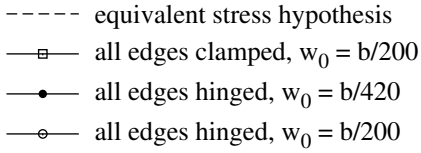

(e) legend

Figure 5.28: Effect of rotational edge restraints ($\alpha = 3$, all edges unconstrained)

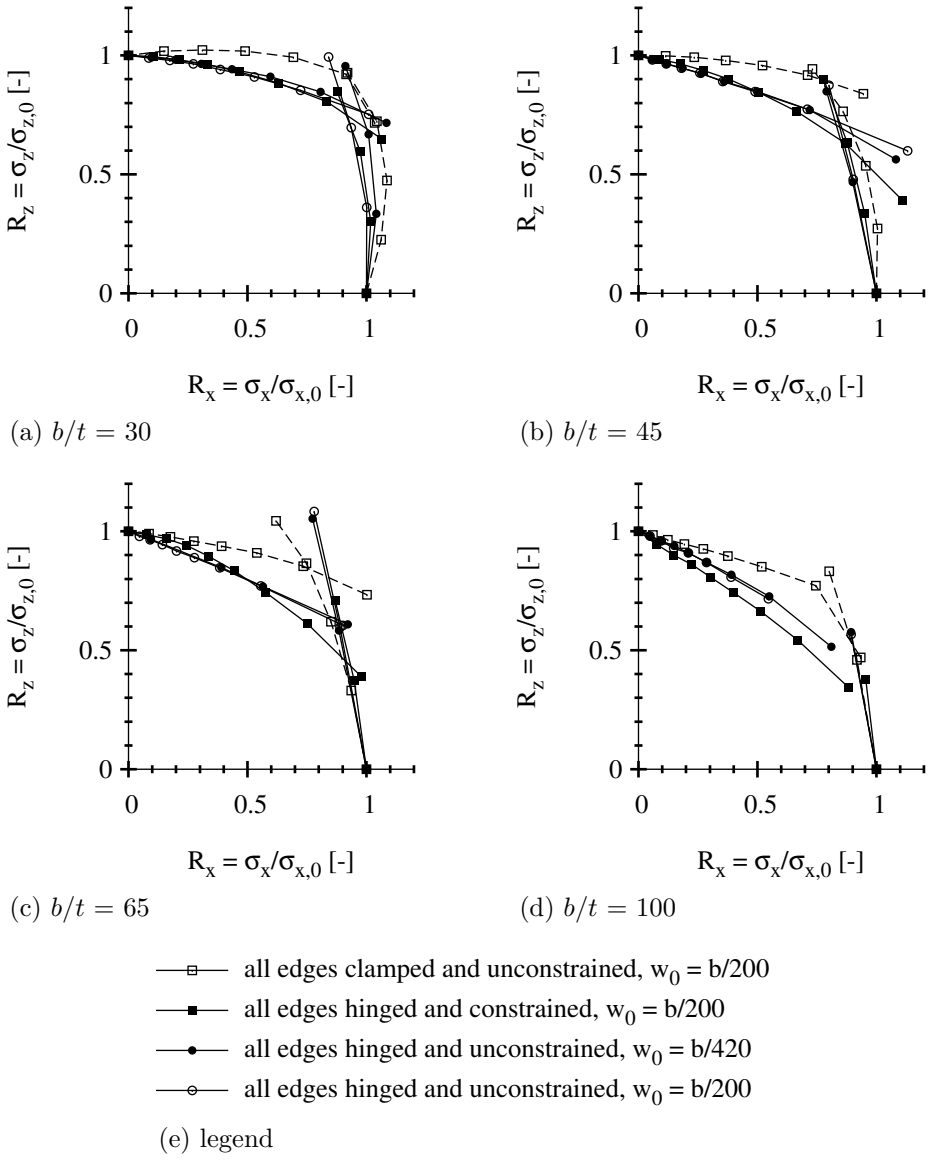

(a) $b/t = 30$ (b) $b/t = 45$

(c) $b/t = 65$ (d) $b/t = 100$

(e) legend

Figure 5.29: Effect of edge restraints, normalised values ($\alpha = 3$)

5.5 Girder web stability under transverse patch loading and shear force

5.5.1 General

Panels which are subjected to shear and patch loading may be classified into four classes for easier reference and better understanding. A schematic overview on this subdivision is illustrated in Fig. 5.30. On the basis of a partly edge loaded panel the reacting forces V_1 and V_2 are given on each adjacent side according to the sign convention for internal forces. The four classified cases are denoted from a. to d. and described below.

Case a. represents the pure patch loading situation where a plate is loaded partly along one edge and reacted by shear of equal magnitude on the adjacent sides. The relation between the forces V_1 and V_2 becomes -1.

Case b. corresponds to a patch loading situation where no additional shear force is present but where the patch loading is reacted by shear of different magnitude on the adjacent sides. This loading situation results e.g. when the supports are not symmetrical to the applied edge load. The ratio between the forces V_1 and V_2 lies in the range from -1 to 0.

Case c. is the typical loading situation if one speaks about combinations of shear- and patch loading. In addition to the edge loading the panel is also subjected to a shear force which leads to ratios of V_1 to V_2 in the range from 0 to +1. The sign of the internal shear force does not change if one follows the positive direction according to the sign convention.

Case d. shows a pure shear force in order to complete the above considerations. In this case the panel resists a constant internal shear force so that the resulting relation between V_1 and V_2 equals +1.

In order to widen the range of parameters which have been covered only in a very limited way in the experimental tests, parameter studies covering slenderness ratio, loading length, ratio of shear force to patch loading, end-post condition or longitudinal stiffener typ are conducted. The aim is especially to characterise the behaviour of panels subjected to combinations of shear- and patch loading more detailed. The set of investigated parameters which is based on the experimental layout is as follows:

- web panel dimensions $a = 2400\,\text{mm}$ and $h_w = 1200\,\text{mm}$
- slenderness ratios $h_w/t_w = 60$, 100 and 200
- relative loading lengths $s_s/h_w = 0.25$, 0.50, 0.75 and 1.00
- rigid and non-rigid end-posts
- varying level of shear stress
- longitudinal stiffeners: weak and strong

For the longitudinally stiffened girders open- and closed-section stiffeners in the con-

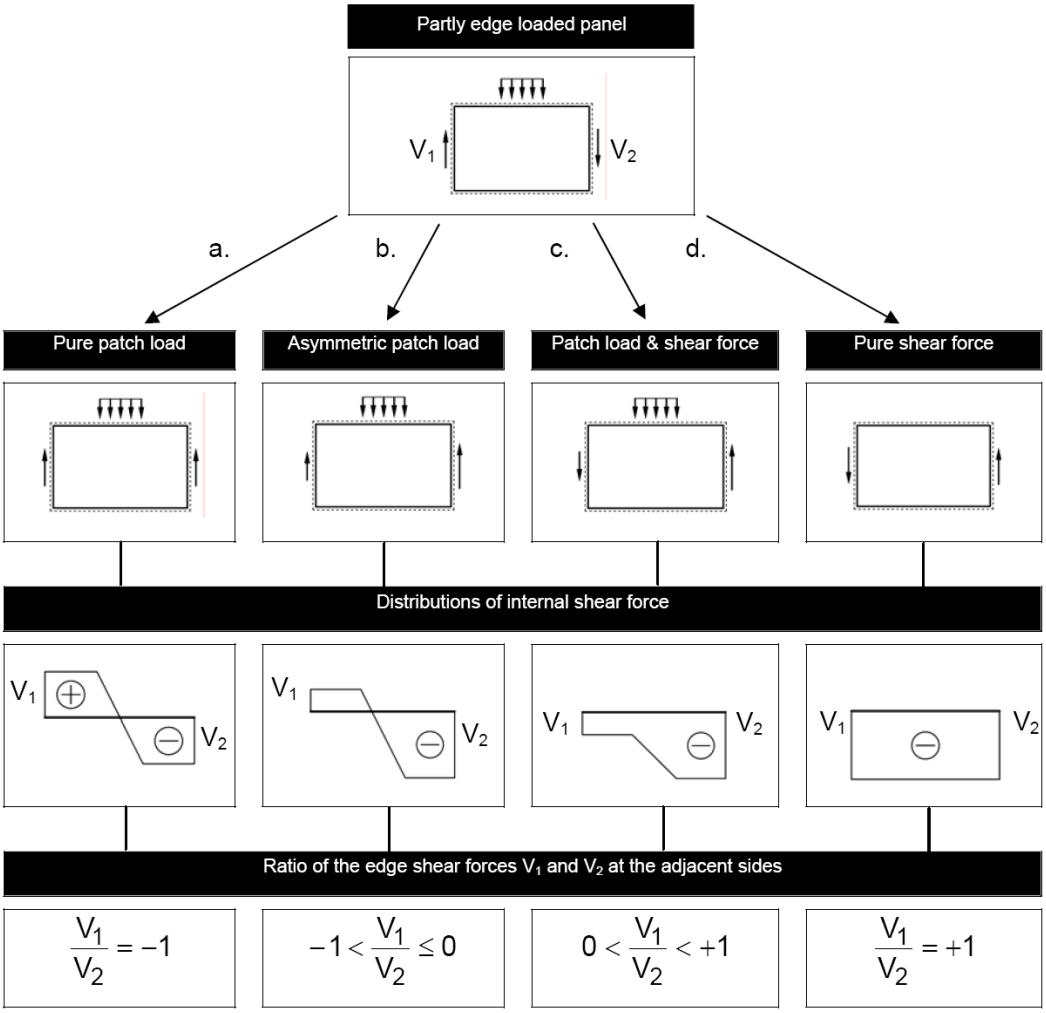

Figure 5.30: Cases with varying distributions of internal shear force

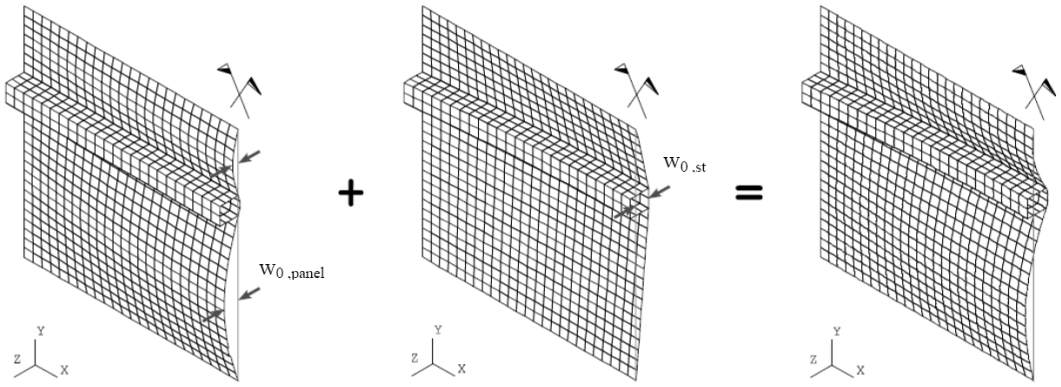

Figure 5.31: Combination of local and global imperfection shapes for modelling [114]

figuration “flat bar” and “trapezoidal shape” are studied. In each case a weak stiffener is used in order to study the global buckling behaviour of the stiffened panel and a strong stiffener which enforces local buckling of the subpanels. Firstly, the general behaviour of shear- and patch loaded panels is described in Sec. 5.5.2 whereas the effects of different parameters and the behaviour of panels with longitudinal stiffener are reported on in Secs. 5.5.3 to 5.5.6.

The numerical modelling is based on the assumptions which have been chosen for the recalculation of tests from literature, see Sec. 5.3.4. This section recalls the assumptions on material modelling and gives information on the modelling of imperfections. The nonlinear material behaviour is taken into account with the nominal yield strength and a linear strain hardening slope of $E/100$ with fracture at a strain of 0.05 according to Annex C.6, EN 1993-1-5 [46]. Concerning the influence of imperfections, the sensitivity of panels has been already studied in detail e.g. by Seitz [114] in case of patch loading and by Pavlovcic et al. [92] in case of shear force. Both studies conclude that the imperfection sensitivity for unstiffened panels and subpanels of stiffened panels is low. However, special attention has to be paid if a longitudinal stiffener is involved because it is also the direction of the imperfection amplitude which has influence on the ultimate load. Since the failure due to compressive stresses is more severe, a negative imperfection amplitude of $w_{0,st} = h_w/400$ for the longitudinal stiffener is chosen here according to Annex C.5 of EN 1993-1-5 [46]. This imperfection mode is added to the local imperfection shape as illustrated in Fig. 5.31. In general, simplified sinusoidal imperfection patterns are chosen for superposition because eigenmode shapes may not be sufficient in case of stiffened panels, see e.g. Seitz [114].

5.5.2 Structural behaviour

In Section 5.5.1 the shear- and patch loading behaviour has been pre-classified according to the ratio of the edge shear forces V_1 and V_2 at the adjacent sides. Based on this overview

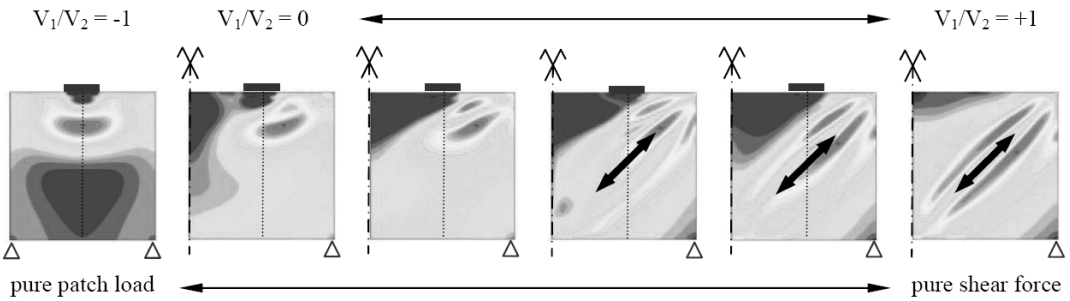

Figure 5.32: Principal tensile stresses at ultimate limit state

the general behaviour is studied on the basis of the experimental tests and the analysis of results of the numerical parametric study. In contrast to the behaviour of the basic load cases “pure patch loading” and “pure shear force” the interaction behaviour between these two has not been investigated in detail. The experimental test series of Roberts and Shahabian [101, 116] covers e.g. only a small number of parameters and rather short loading lengths.

The presentation of results obtained in this study distinguishes between the two ranges of V_1/V_2 which correspond to]-1;0] concerning an asymmetric patch loading condition with no additional shear force present and]0;+1[where a shear force is acting in addition to the patch loading. Although it facilitates an easier reference of load combinations, this differentiation should not be seen as strict separation of buckling phenomena as there is a smooth transition from pure patch loading to pure shear force acting. This transition is illustrated in Fig. 5.32 by the distribution of principal tensile stresses in a panel which is subjected to varying combinations of shear- and patch loading. The full symmetric stress distribution in case of a pure patch loading quickly changes if the patch stresses are not reacted by shear of equal magnitude on the adjacent edges. However, a typical patch loading failure still prevails. However, it is influenced by the additional shear stresses equilibrated mainly by one side. Vice versa a pure shear failure is dominated by the formation of a tension field when the elastic critical shear buckling stress has been reached. If an additional patch loading is introduced the orientation of the tension field remains but the maximum tensile stresses are shifted to the highly stressed areas. It is found that the typical shear failure mode consistently transforms into a typical patch loading collapse mode. This assumption is also supported by the study of the displacement shapes of the girders as it is exemplarily shown in Fig. 5.33.

In the following the behaviour of the panels is explained in more detail for the cases asymmetric patch loading as well as patch loading and additional shear force.

Asymmetric patch loading with $V_1/V_2 \in]-1;0]$. From Figs. 5.32 and 5.33 the principal tensile stresses and the out-of-plane deformations for the two ratios V_1/V_2 = -1.0 (pure patch loading) and V_1/V_2 = 0.0 (full asymmetric patch loading) can be compared at ultimate limit state. It can be seen that the asymmetry in loading results in a diagonalisation of the deformed shape for an increasing ratio of V_1/V_2. This corresponds

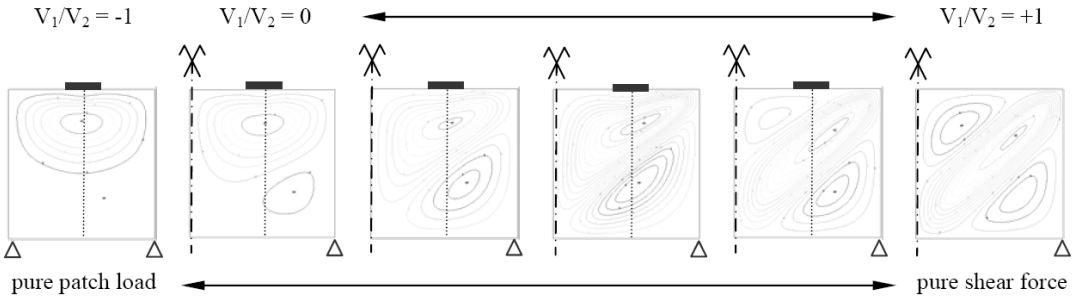

Figure 5.33: Out-of-plane displacments at ultimate limit state

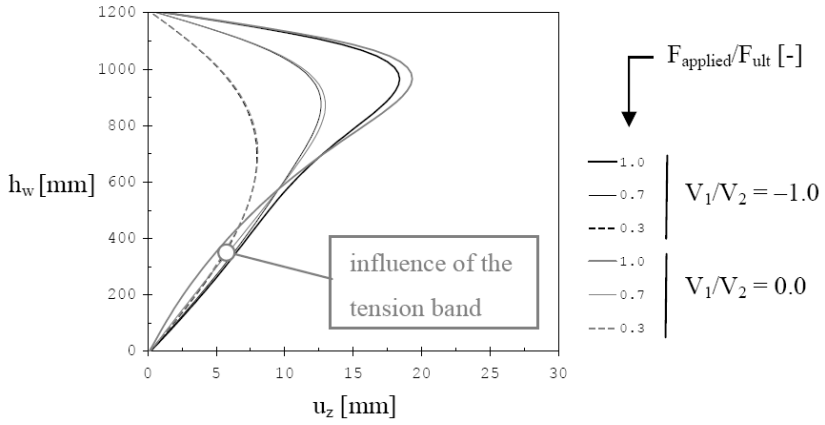

Figure 5.34: Out-of-plane panel deformations for V_1/V_2 = -1 and 0.0

to the development of a post-critical tension band. In contrast to the pure patch loading case, one of the vertical edges (here: the left-hand side) resists only a smaller part or no stresses at all if the patch loading acts asymmetrically. However, the patch stresses which are introduced at the top flange travel partly along this vertical edge and they are carried to the supporting edge (here: the right-hand side) via a tension band. This has also an influence on the out-of-plane deformations which are compared for different levels of the applied load $F_{applied}/F_{ult}$ in Fig. 5.34. In the figure the out-of-plane deformations at the panel's vertical centerline are compared for the three levels of loading $F_{applied}/F_{ult}$ = 0.3, 0.7 and 1.0 (ultimate limit state). In general the displacements grow similarily and match each other quite well. However, when approaching the ultimate limit state the tension band's straightening effect can be clearly identified by a decreasing displacement in this region, see boxed text in Fig. 5.34.

A limitation for this tensioning effect exists which explains why there is a higher reduction for longer loading lengths: with increasing length the pure patch loading resistance basically also increases. However, the asymmetry requires that the patch loading is reacted mainly at one vertical edge only which causes a complex state of stress in the panel where the load path along the tension band has to carry this increase in stress. The ability to carry the stresses is limited so that the advantages of longer load introduction

lengths are accompanied by a stronger interaction behaviour in the case of asymmetric patch loading.

Patch loading and additional shear force with $V_1/V_2 \in \,]\,0;+1\,[$. With an additional shear force acting, the patch loading resistance is significantly reduced as the interaction diagram in Fig. 5.35 shows. The closer the ratio V_1/V_2 gets to +1.0 (pure shear force) the stronger the interaction becomes and it is assumed that in case of a full utilization of the shear resistance no additional patch loading can be applied. Again, an influence is found for the parameter loading length showing a stronger interaction for longer loading lengths than for short ones. This will be further discussed in Sec. 5.5.5. For the failure mode in terms of panel deformations for patch loading with an additional shear force two basic failure shapes can be characterised: an asymmetric patch loading failure as described in the section before and a typical shear failure with the development of a tension field. The transition zone between these two types of failure has been observed to occur in the range between $V_1/V_2 = 0.5$ and 0.75. However, the transition is smooth: an increase of the applied shear force amplifies the tension band which is already developed due to the asymmetric patch loading. The additional stress further reduces the ability to carry parts of patch loading which have to be transferred to the supporting edge (here on the right-hand side, see Fig. 5.32). The higher the shear force gets, the more the tension field dominates the failure mode.

Although the classification of the general behaviour according to the ratio V_1/V_2 is useful and concise for the description of the general behaviour, it is not feasible for the representation in terms of an interaction diagram as described more detailed in Sec. 6.2. A suitable and common way is to subdivide the combined loading into two basic load cases as presented in Sec. 3.3. By doing this, the effect of shear stresses caused by the transverse forces can be better accounted for because it is already included in the patch loading model. In Fig. 5.35 the ratio V_1/V_2 is drawn in relation to the type of interaction diagram based on the aforementioned subdivision.

5.5.3 Effect of slenderness ratio

With regard to the general interaction behaviour the slenderness ratio plays only a minor role. The investigated slenderness comprises web height to thickness ratios of $h_w/t_w =$ 60, 100 and 200 which correspond to shear slendernesses of $\overline{\lambda}_w = 0.8$, 1.3 and 2.6. From the scatter that is evident in the interaction digram of Fig. 5.36 it can be concluded with regard to Fig. 5.39 that it is the influence of the loading length which causes dispersion.

5.5.4 Effect of end-post condition

End-posts do not only resist the reaction force at the support but they also provide a sufficient anchorage for the longitudinal component of the membrane stresses which develop due to tension field action. Depending on the stiffness of the end-post layout

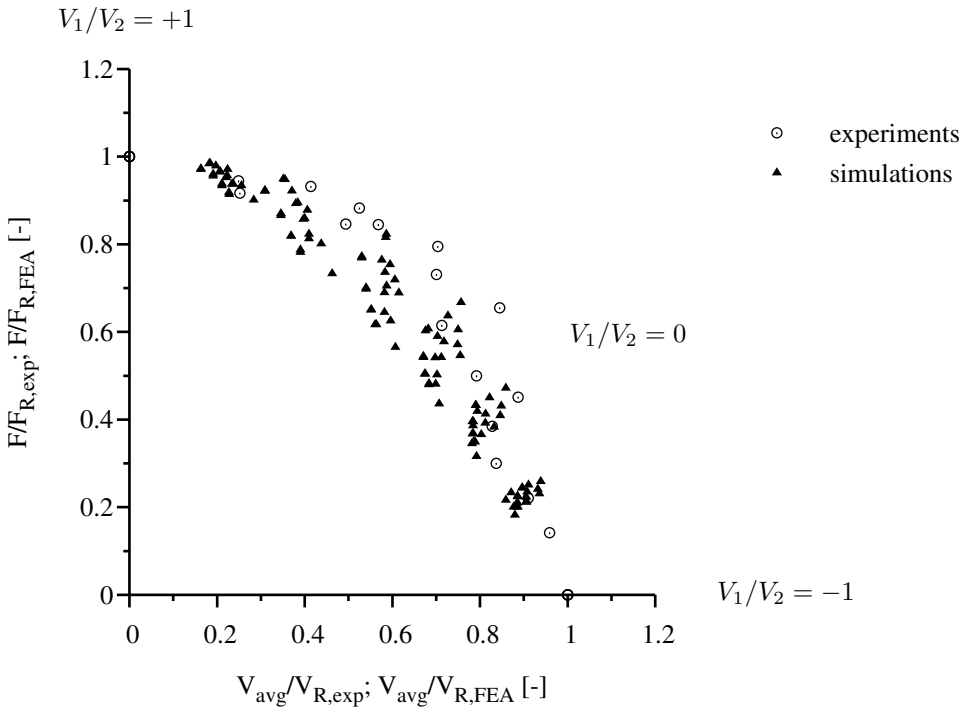

Figure 5.35: Approximate corresponding ratios V_1/V_2 shown in the interaction diagram, F_R and V_R according to experiments or based on FEA

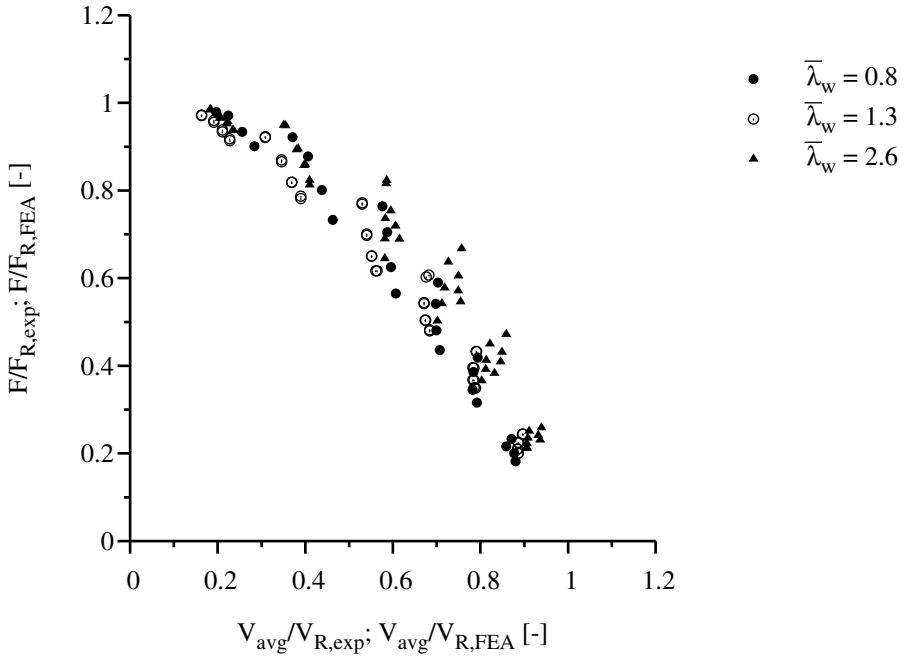

Figure 5.36: Effect of slenderness ratio, F_R and V_R according to experiments or based on FEA

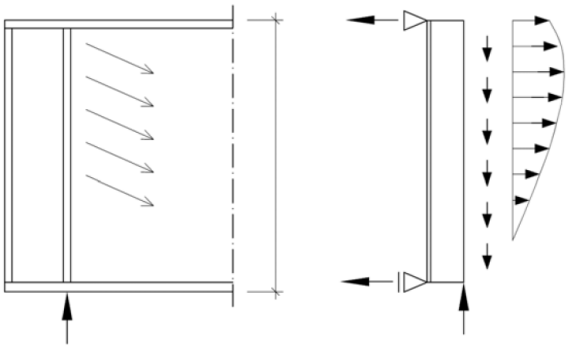

Figure 5.37: End-post loading condition scheme

they are classified as rigid or non-rigid according to Chapter 5, EN 1993-1-5 [46]. Rules allow to take the stiffness into account when a positive influence is noticeable which is assumed for shear slenderness ratios of $\overline{\lambda}_w$ larger than 1.08.

Figure 5.38 illustrates the influence of the end-post condition on the interaction behaviour of shear- and patch loaded panels for the slenderness ratios $\overline{\lambda}_w = 1.3$ and 2.6 which are greater than 1.08. For a small slenderness ratio of $\overline{\lambda}_w = 1.3$ the influence of the end-post configuration is almost negligible because the in-plane stiffness of the web panel is still sufficiently high. For higher slenderness ratios the influence increases because the in-plane stiffness of the web panel decreases so that the state of stress can benefit from a rigid end-post condition. In this case a larger component of the tensile membrane stresses can be taken which is a slightly more favourable with regard to the interaction behaviour in case of higher slenderness values.

5.5.5 Effect of loading length

The loading length has been found to be one of the most influential parameters. From Fig. 5.39 it can be concluded that with an increasing patch loading length the interaction between shear- and patch loading becomes stronger. As explained in Sec. 5.5.2, it goes back to the fact that for longer loading lengths also the basic patch loading resistance increases. The increase in stresses needs to be transferred to the edge which are in equilibrium with the applied patch loading and the shear force, if present. This also means that higher stresses are carried via the tension band which vice versa leads to a stronger interaction as for short loading lengths because the ability to carry this increase in stress is limited. In case the shear failure is governing it is also the patch loading that adds to an increase in displacement of the shear buckle. In Fig. 5.39 the numerically determined resistances are shown in an interaction diagram where the data points are grouped according to the parameter relative loading length $s_s/h_w = 0.25$, 0.50, 0.75 and 1.00. It can be identified that the interaction is getting stronger with increasing patch loading length. For comparison Eq. 5.6 of Roberts and Shahabian [101, 116] is also given.

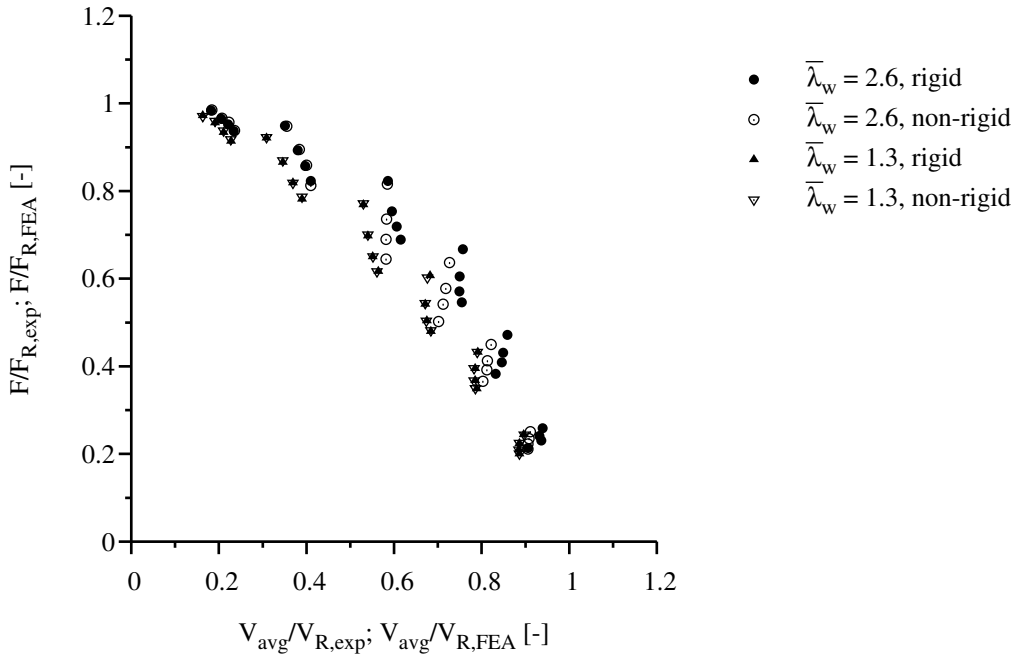

Figure 5.38: Effect of end-post condition, F_R and V_R according to experiments or based on FEA

$$\left(\frac{V - 0.5 \cdot F}{V_R}\right)^2 + \left(\frac{F}{F_R}\right) \leq 1.0 \tag{5.6}$$

For relative loading lengths up to $s_s/h_w = 0.25$ the numerically determined resistances lie on the safe side above the curve but for longer loading lengths data points start to fall below the interaction equation. This observation confirms the suitability of the interaction equation suggested by Roberts and Shahabian for relative loading lengths up to $s_s/h_w = 0.25$ although it has been based upon the test series which comprised rather short relative loading lengths up to $s_s/h_w = 0.10$. However, it has to be stated that it is not sufficient for longer loading lengths as the interaction criterion gets stronger. A new interaction equation which takes into account loading lengths which are longer than $s_s/h_w = 0.25$ is developed and proposed in Sec. 6.5.

5.5.6 Effect of longitudinal stiffener

The behaviour and design of thin-walled structures which are composed of several steel plated elements is usually governed by stability. In order to increase their stability, the plates are strengthened by additional sets of transversal and longitudinal stiffeners. In this section the interaction behaviour of girders with longitudinal stiffener subjected to patch loading and shear force is discussed based on the knowledge gained for the unstiffened cases. The investigation covers open- and closed-section stiffeners, see Fig. 5.40.

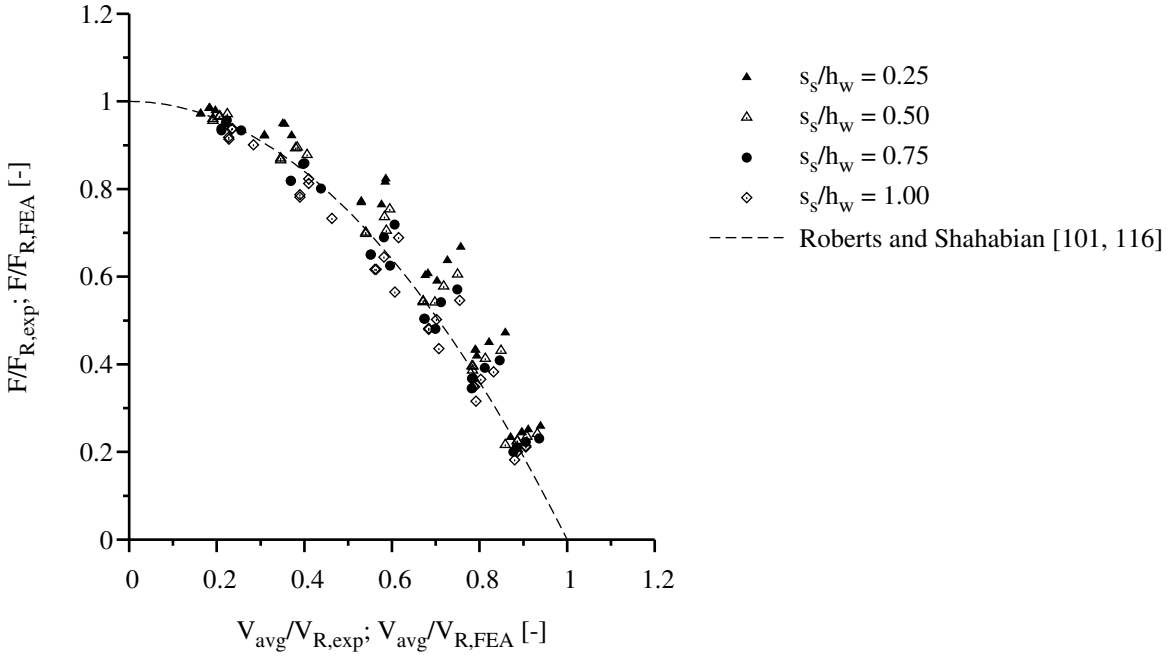

Figure 5.39: Effect of loading length, F_R and V_R according to experiments or based on FEA

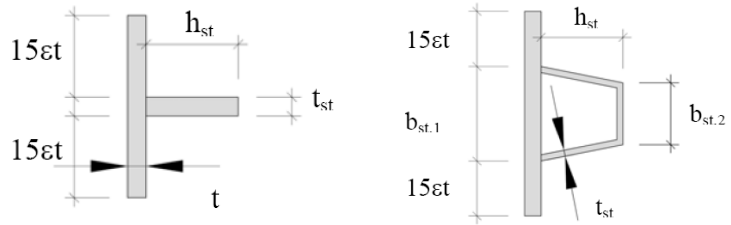

(a) open-section stiffener: flat bar

(b) closed-section stiffener: trapezoidal shape

Figure 5.40: Types of longitudinal stiffening with contributing plate width

Table 5.4: Weak stiffener dimensions

cross-section	$b_{st,1}$ [mm]	$b_{st,2}$ [mm]	h_{st} [mm]	t_{st} [mm]
open	n.a.	n.a.	100	13
closed	100	50	90	4

Table 5.5: Strong stiffener dimensions

cross-section	$b_{st,1}$ [mm]	$b_{st,2}$ [mm]	h_{st} [mm]	t_{st} [mm]
open	n.a.	n.a.	110	20
closed	100	100	100	6

In the past, stiffeners mostly were of open cross section with a negligible torsional rigidity. Nowadays, the improvement in welding techniques and the fabrication of thin-walled sections leads to an increased use of closed-section stiffeners in the longitudinal direction which possess a considerable torsional rigidity. Both section types are taken into account in the configuration of a weak or a strong stiffener with dimensions according to Tables 5.4 and 5.5.

Depending on the stiffness of the stiffener, failure of the stiffened panel may occur in two ways: global buckling of the whole stiffened panel or local buckling of individual subpanels as shown in Fig. 5.41. In the study these two possible failure types are addressed separately below, i.e. global buckling of the stiffened panel and local buckling of the subpanels.

Global buckling of the stiffened panel. The presence of a stiffener generally increases the web panel stiffness. In case the stiffener is not able to form a nodal line until ultimate state is reached global buckling including failure of the stiffener occurs. In Figs. 5.42 to 5.44 representative results of girders with longitudinal stiffener are compared to the corresponding unstiffened case for the basic load cases and for interaction. Both open-section and closed-section stiffeners have been used which reveal the differences in buckling behaviour. In contrast to the open-section stiffener the closed-section stiffener provides an additional amount of torsional rigidity to the web panel which produces a torsional restraint along the stiffener axis although the flexural rigidity is too small to enforce subpanel failure. It can be concluded that the torsional rigidity of the stiffener has an increased influence especially when patch loading is involved because then the clamping has the most favourable effect in terms of buckling behaviour and resistance. For the pure patch loading behaviour the positive influence of closed-section stiffeners has also been stated in Seitz [114]. It should be noted that for the interaction case the stiffener does not alter the failure shape, see Fig. 5.44. However, the out-of-plane deformations are significantly reduced due to the additional stiffness. The effectiveness of a stiffener for panels which are subjected to stress combinations is higher than for the basic load cases. As shown in Fig. 5.49, the data points based on the interaction behaviour in case of global

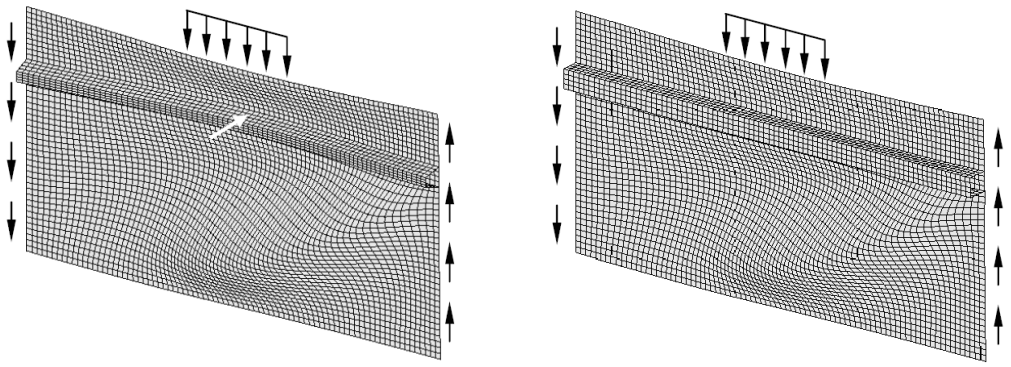

(a) global buckling (b) local buckling

Figure 5.41: Failure types of girder webs with longitudinal stiffener

buckling are covered by the data scatter of the unstiffened cases. Thus, the applicability of an interaction equation which is defined for girders without longitudinal stiffener is also valid for girders with longitudinal stiffener showing global buckling behaviour.

Local buckling of subpanels. If the stiffener is strong enough not to fail until the collapse load of the whole stiffened panel is reached then local buckling of subpanels occurs. To enforce this failure type the longitudinal stiffener needs to be designed in a sufficiently rigid manner, e.g. by second-order theory, in order to provide a nodal line for the web panel. In contrast to global buckling the potential post-critical strength reserve of the subpanel can be fully utilised in case of local buckling because the ultimate load is not determined by a sudden failure of the stiffener which cannot attain any post-critical strength. Figure 5.47 illustrates the local buckling behaviour when for failure of the directly or indirectly loaded subpanel the stiffener is able to form a nodal line. It should be noted that in addition to the nodal line, the torsional rigidity of the closed-section stiffener is also able to provide a clamping of the subpanels at the boundary edge adjacent to the stiffener.

A longitudinal stiffener, for which failure is excluded, breaks down a girder web into several subpanels so that generally it should be further distinguished which subpanel is decisive. The weakest subpanel governs the resistance of the whole panel. However, if the governing subpanels for the basic load cases “pure shear force” and “pure patch loading” are regarded they are not necessarily the same. For shear loading the subpanel with the largest dimensions usually determines the resistance, which for the example shown in Fig. 5.45 would correspond to subpanel 2. In case of patch loading, the decisive subpanel depends not only on its dimensions but also on the loading length over which the patch load is applied. In Seitz [114] it has been shown that for short load introduction lengths the directly loaded subpanel governs (subpanel 1) whereas for long loading lengths the indirectly loaded subpanel (subpanel 2) becomes decisive.

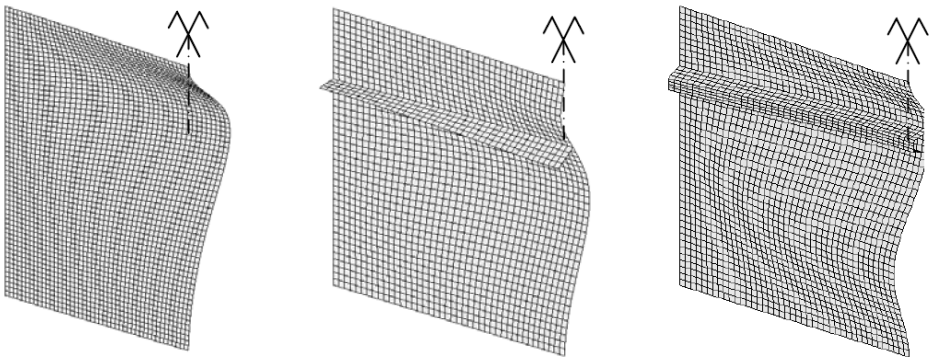

(a) unstiffened, $F_{ult,0}$ (b) open-section, $F_{ult} = 1.26 \cdot F_{ult,0}$ (c) closed-section, $F_{ult} = 1.39 \cdot F_{ult,0}$

Figure 5.42: Buckling behaviour under pure patch loading

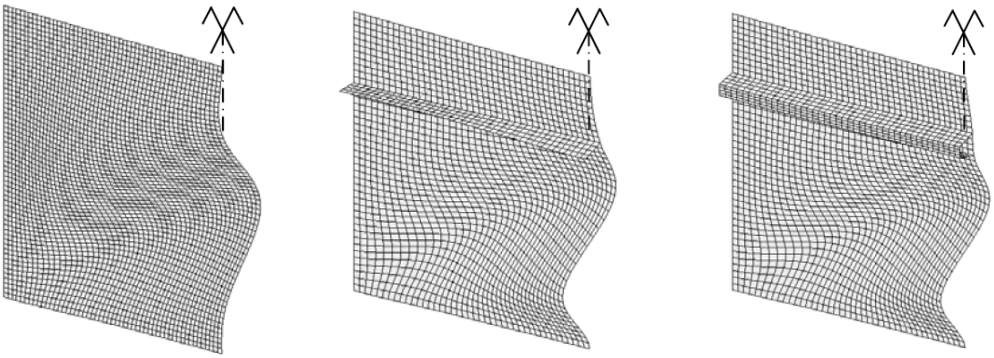

(a) unstiffened, $V_{ult,0}$ (b) open-section, $V_{ult} = 1.31 \cdot V_{ult,0}$ (c) closed-section, $V_{ult} = 1.37 \cdot V_{ult,0}$

Figure 5.43: Buckling behaviour under pure shear force

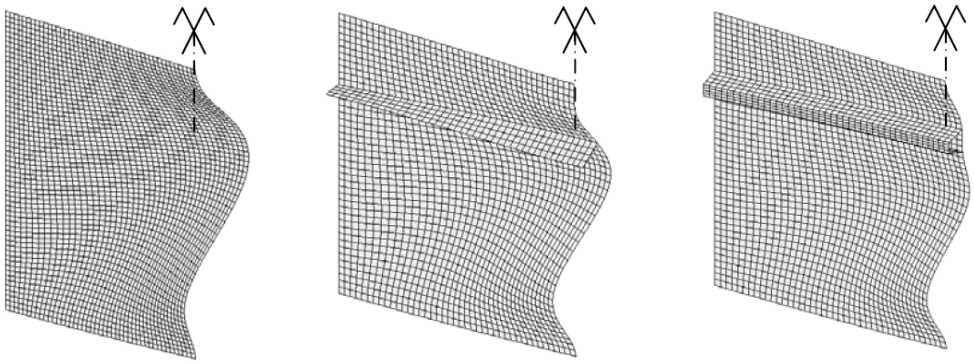

(a) unstiffened, $R_{ult,0}$ (b) open-section, $R_{ult} = 1.48 \cdot R_{ult,0}$ (c) closed-section, $R_{ult} = 1.56 \cdot R_{ult,0}$

Figure 5.44: Buckling behaviour under combined shear- and patch loading for $V_1/V_2 = 0.28$ (R = shear and patch loading resistance)

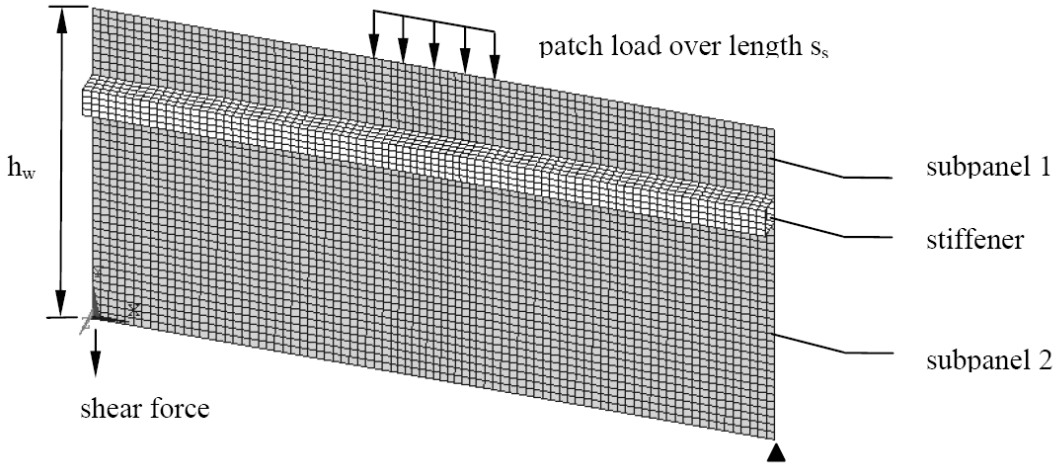

Figure 5.45: Example layout of a girder with a rigid longitudinal stiffener

If interaction is regarded, the governing subpanel coincides for long loading lengths (subpanel 2) but differs for short loading lengths. It is subpanel 1 which governs for patch loading whereas subpanel 2 is decisive for the shear force. The diagram in Fig. 5.46 depicts the interaction behaviour for different loading lengths for the example layout introduced in Fig. 5.45. The drawn curve represents as reference the lower bound which has been adjusted to the data scatter of the girders without longitudinal stiffner, see Sec. 6.5.3. It can be observed that for the long loading lengths $s_s/h_w = 0.50$ and 0.75 the points come close to this curve because subpanel 2 is the governing panel for both shear force and patch loading. The corresponding buckling shape at postultimate state is given in Fig. 5.47a for the example data point from the diagram. Assuming the same load combination of shear force and patch loading, Fig. 5.48 compares the out-of-plane deformations of a girder without a longitudinal stiffener to a girder with a sufficiently rigid longitudinal stiffener. The diagonalisation of the buckling shape due to asymmetric loading can be congruently observed so that a local buckling failure may be treated analogous to an girder without a longitudinal stiffener because the subpanel itself is represented as an unstiffened panel. The orientation of the buckle indicates in both cases a shear-influenced patch loading failure as described for the girder without a longitudinal stiffener.

As stated before, the decisive subpanel is not coincident for short loading lengths which leads to a shear-like failure of subpanel 2 if the shear force is dominating or to a patch-like failure of subpanel 1 for a dominating patch loading. Thus, an interdependent influence can be found for a shear force or patch loading which acts in addition to the dominating load. In comparison to a single failure-governing subpanel this interaction is less strong but still present as shown by the circles and diamonds in Fig. 5.46. However, this interaction is covered on the safe side within the lower bound curve of the unstiffened data points.

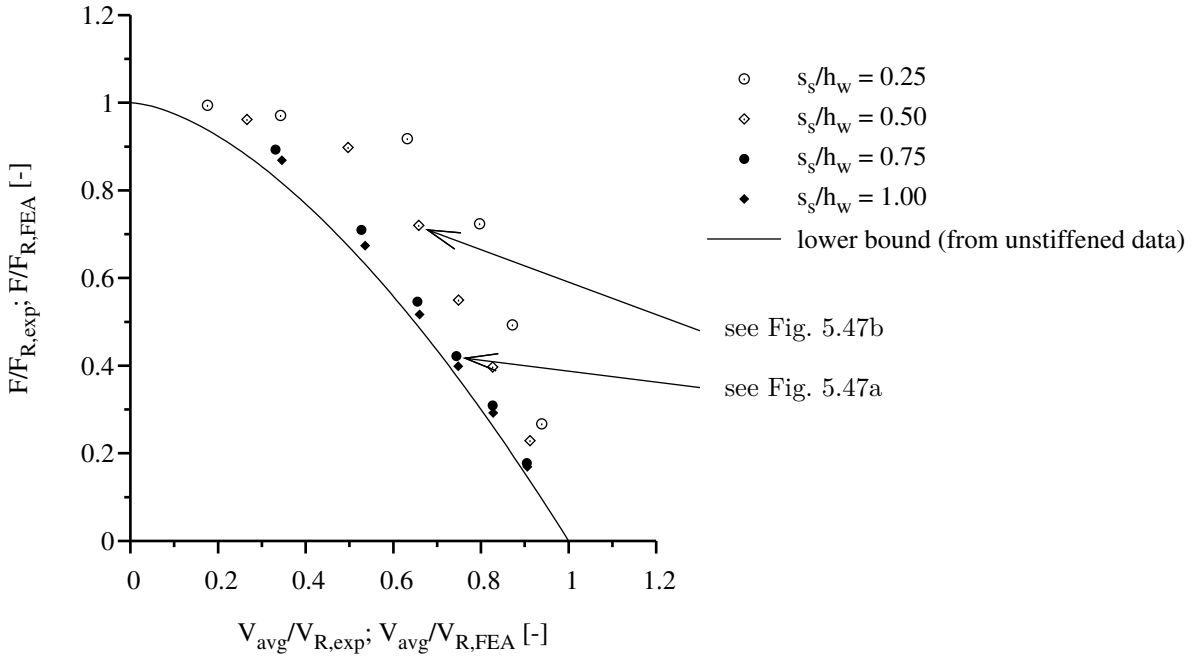

Figure 5.46: Interaction behaviour dependent on local or global failure mode, F_R and V_R based on FEA

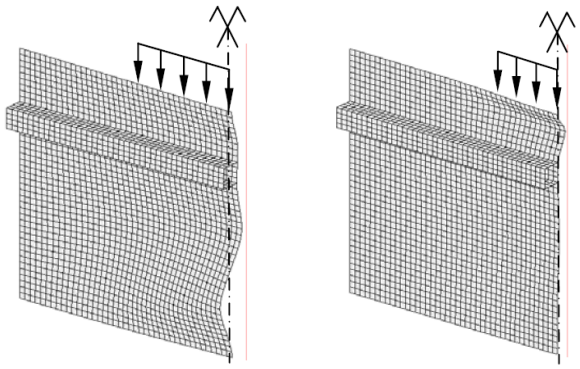

(a) $s_s/h_w = 0.75$ (b) $s_s/h_w = 0.50$

Figure 5.47: Local buckling behaviour at postultimate state

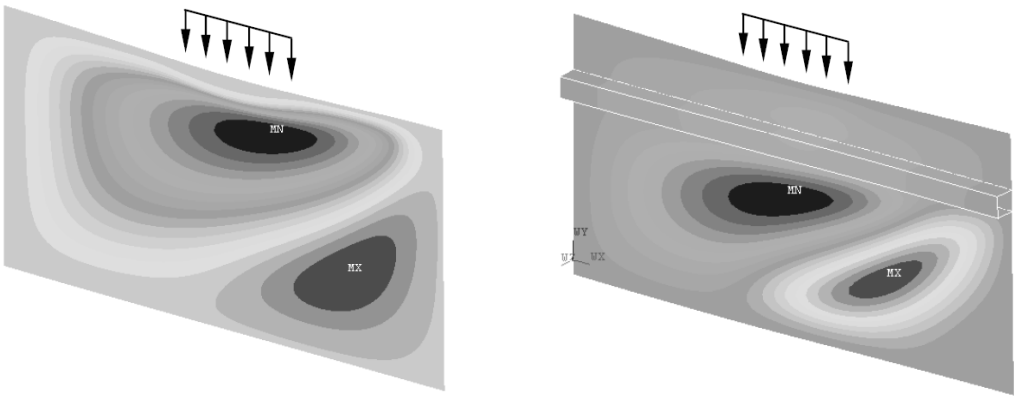

(a) girder web without longitudinal stiffener

(b) girder web with longitudinal stiffener showing local buckling behaviour

Figure 5.48: Comparison of out-of-plane deformations

5.5.7 Conclusions

The investigations of panels which are subjected to shear- and patch loading have shown that these two types of loading have an influence on each other which is not negligible. Based on earlier work, the subdivision into basic load cases is adopted for the presentation and comparison of interaction diagrams. Further observations lead to an introduction of the terms “asymmetric patch loading” and “shear- and patch loading” which classify the applied load combination more detailed. Asymmetric patch loading is referenced when no additional shear force is present and the patch loading is reacted by shear of different magnitude on the adjacent edges, whereas shear- and patch loading means that shear force and patch loading act together on the panel.

From the studies on the behaviour of the shear- and patch loaded panels a consistent transition from a pure shear force failure, including tension field action, to a pure patch loading failure is found. Corresponding to the two terms introduced above either a patch loading failure influenced only by the asymmetry in equilibration of the forces dominates, or a nearly pure shear force failure is governing. The parametric studies reveal that the loading length is one of the most influential factors on this interaction behaviour. The longer the loading length gets, the stronger the interaction is, however a limiting curve as lower bound for interaction is approached. A comparison of the interaction behaviour of girders without and with longitudinal stiffener shows that dependent on the global or local type of failure a similar behaviour exists either for the whole stiffened panel or the subpanels. Although stiffness is added to the panel the state of stress leading to failure is not significantly altered by the presence of the stiffener which leads to similar observations as for the girders without longitudinal stiffener.

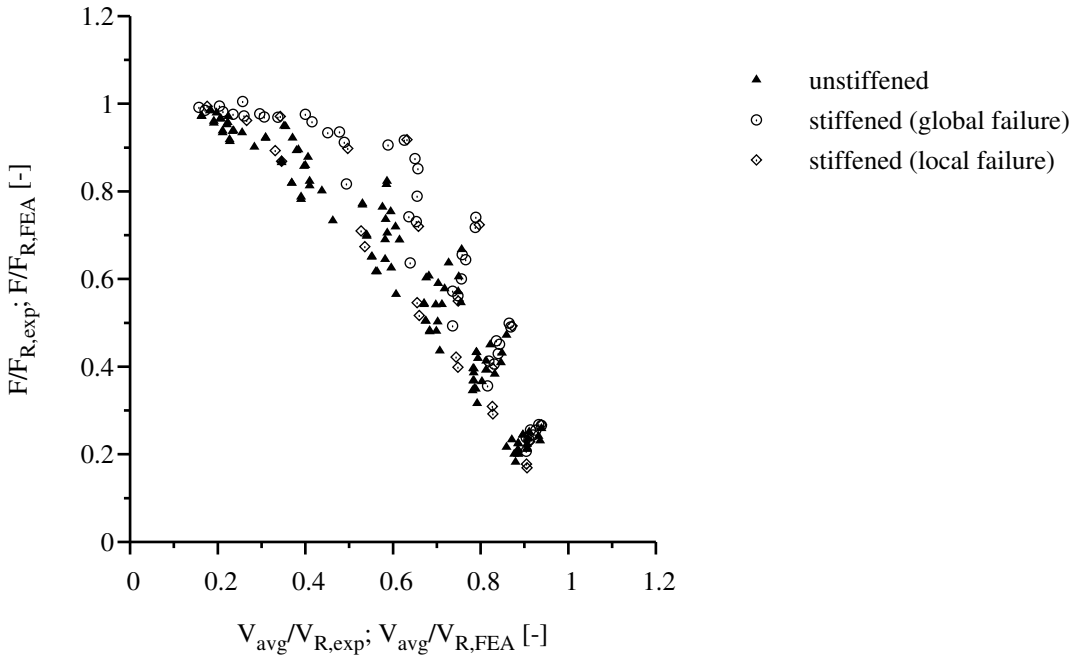

Figure 5.49: Comparison of girders without and with longitudinal stiffener, F_R and V_R according to experiments or based on FEA

5.6 Summary

The studies which have been carried out follow up earlier work. Comprehensive numerical studies have been conducted not only to understand the stability behaviour in these cases but also to identify starting points for improvement or even development of design rules which will be addressed in Chapter 6. The conclusions which have been drawn for plates under biaxial compression and plate I-girders subjected to transverse loading and shear force are summarised below.

Plate stability under biaxial compression. It is shown that for slender plates of which the slenderness theoretically approaches infinity a linear interaction is reached. For square plates such a linear relationship is true because the imperfection shapes of the basic loadings coincide. For rectangular plates the imperfection shape significantly alters the interaction curve due to the stiffening effects of the different shapes. One- and three-halfwave mode shapes are used to describe the interaction behaviour. Since the resulting favourable interaction behaviour relies on realistic imperfection shapes, it can be generally taken into account. It can be concluded that the panel aspect ratio is one of the most influential parameters for the interaction curvature.

Another important parameter which effects the interaction behaviour is the edge restraint, both in-plane and rotational. For high slendernesses, the in-plane restraint leads to favourable interaction curves in terms of absolute values. A normalisation however shows that the interaction shapes are very similar. This is an important observation since the slenderness is determined irrespective of the in-plane edge boundary condition which

only becomes relevant in large deformation analysis. Thus, similar interaction curves can be drawn over the same slenderness for both unconstrained and constrained in-plane restraints. The rotational edge restraint is even more favourable both in absolute values and after normalisation. Since clamping effects can be accounted for in linear buckling theory, the slenderness becomes smaller and this positive influence on the interaction behaviour can be accounted for in the determination of the slenderness.

It is concluded and assumed for the studies in Chapter 6 that a precise assessment of the reference strength facilitates the use of few interaction curves which are then able to account for different edge boundary conditions. Current design rules will be improved with regard to the following objectives: sound representation of the interaction behaviour by using precise reference strengths and, by doing this, enabling the use of advanced software solutions in determining elastic critical buckling stresses which is especially of advantage in full building models where the individual panel is analysed as part of the whole structure.

Girder web stability under transverse loading and shear force. The investigations of panels which are subjected to shear- and patch loading have shown that these two types of loading have an influence on each other which is not negligible. Based on earlier work the subdivision into basic load cases is adopted for the presentation and comparison of interaction diagrams. Further observations lead to an introduction of the terms "asymmetric patch loading" and "shear- and patch loading" which classify the applied load combination more detailed. Asymmetric patch loading is referenced when no additional shear force is present and the patch loading is reacted by shear of different magnitude on the adjacent edges, whereas shear- and patch loading means that shear force and patch loading act together on the panel.

From the studies on the behaviour of the shear- and patch loaded panels a consistent transition from a pure shear force failure, including tension field action, to a pure patch loading failure is found. Corresponding to the two terms introduced above either a patch loading failure influenced by asymmetry dominates, or a nearly pure shear force failure is governing. The parameter studies reveal that the loading length is one of the most influential factors on this interaction behaviour. The longer the loading length gets, the stronger the interaction is. However, a limiting curve as lower bound for interaction is approached. A comparison of the interaction behaviour of girders without and with longitudinal stiffener shows that dependent on the global or local type of failure a similar behaviour exists either for the whole stiffened panel or the subpanels. Although stiffness is added to the panel the state of stress leading to failure is not significantly altered by the presence of the stiffener which leads to similar observations as for the girders without longitudinal stiffener. As a result, the data scatter in the interaction diagrams as determined for the girders without longitudinal stiffener covers also the data range of girders with longitudinal stiffener which is relevant for the definition of an interaction equation.

6 Proposal and justification of improved design rules for EN 1993-1-5:2006

6.1 General

In the member states of the European Union and possibly beyond, the design of steel plates is already - or in the near future will be - covered by EN 1993-1-5 [46]. As design methods it offers both the reduced stress method and the effective width method. Both methods can be used to determine the resistance of steel plates under longitudinal, transverse and shear stresses and their interaction cases. As discussed in Chapters 2 and 3, improvements are necessary for the design of biaxially loaded plates when applying the reduced stress method based on a single slenderness. When applying the effective width method, a new proposal needs to be developed and introduced for the interaction between transverse loading and shear force. This proposal should be extended on the interaction with bending moment to facilitate application. In order to achieve the objectives for both methods, experimental and numerical studies were undertaken, see Chapters 4 and 5, in order to analyse the stability behaviour and to identify the influence of key parameters. This knowledge will now be implemented in improved design rules for Chapters 7 and 10, EN 1993-1-5 [46].

In the following the proposals are structured according to the two design methods: the reduced stress method, see Sec. 6.4, and the effective width method, see Sec. 6.5. Before current proposals are evaluated and improvements are proposed, considerations on the general formulation of an interaction equation, see Sec. 6.2, and on the choice of the verification point, see Sec. 6.3, are presented.

6.2 On the general formulation of an interaction equation

In addition to a development of a design method for a single load case, the formulation of an interaction equation puts additional difficulties, which are:

- **Limited number of available data.** In general, there is only a limited number of available data points particularly from experiments because the ratio of loading is added as an important parameter. In order to be able to identify the parameter variation within a given load ratio a similarly large number of specimens should be

tested than for a basic load scenario. In case of biaxially loaded plates, it can be shown that the reason for the limited number of data is not only the financial effort for experiments but also the difficulty to define clearly the edge boundary conditions of the plate.

- **Reference value for basic loading.** The reference strength for basic loading based on resistance models usually has a variation itself. It is desirable to know the experimental ultimate load from basic loading for each interaction test series, otherwise an assumption based on a resistance model has to be made. However, this assumption is only as good as the resistance model behind. This turns out to be a crucial issue, especially for the interaction criteria of the effective width models for which experimental data for the corresponding basic loading is hardly available.

In the following, the interaction between transverse patch loading and shear force (F-V) is exemplarily used to illustrate the aforementioned difficulties and to explain the decisions which were taken in the formulation of the proposals later on. Figure 6.1 shows the F-V-interaction with reference strengths based on basic loadings from experimental and numerical studies in which nothing else than the load parameter was varied in comparison to the interaction case. In contrast to this, Fig. 6.2 shows the same interaction data but with reference strengths according to Chapters 5 and 6, EN 1993-1-5 [46]. It can be shown that the data increasingly scatters for the EN reference strengths due to the variance of the resistance model. In order to draw a concise conclusion on the interaction behaviour, it would be necessary to eliminate the effect of the reference strength's resistance model. In the F-V parameter study, experimental and numerical reference strengths are referenced when studying the effect of parameters, see Sec. 5.5. It can be stated that Fig. 6.1 is better suited to analyse the interaction behaviour.

As the quality of the reference strength influences the interaction data, it is not the best choice to evaluate or define an interaction equation based on design models for reference strengths. Imagine that only the experimental data is available in Fig. 6.2. In that case only two data points lie in the quadrant which is relevant for interaction and the interaction equation would be less strict than in the case when the numerical data is additionally considered. The parameters of the experiments are covered rather by the means and upper fractiles of the resistance models which would lead to an underestimation of interaction. It can be shown that if parameters are chosen such that they also cover the lower tail of the resistance models variation, as done in the numerical simulation, interaction becomes more severe. Of course, if the definition of interaction equations is coupled to application ranges which restrict the use e.g. to the parameters of the experiments, interaction may be defined less strict. However, in view of general applicability and safety, the reference strengths should be based on corresponding experimental and numerical basic loadings whenever possible.

Although the considerations above are generally valid, they are most pronounced in the effective width method. The resistance functions of the reduced stress method are rather precise and it can be shown that boundary effects can be covered quite well. Nevertheless,

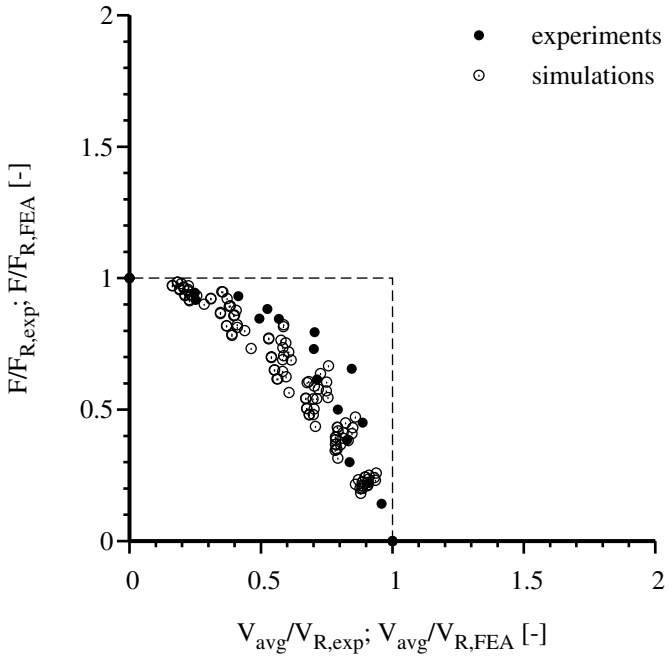

Figure 6.1: Evaluation of interaction data, F_R and V_R according to experiments or based on FEA

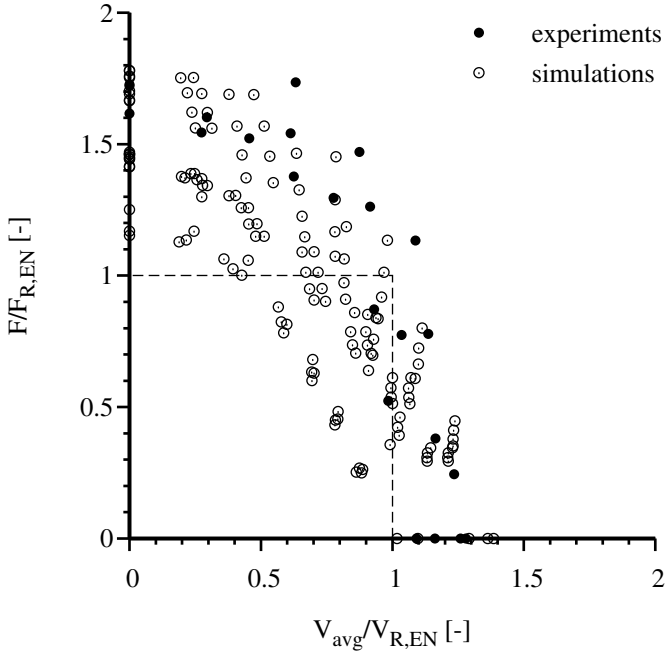

Figure 6.2: Evaluation of interaction data, F_R and V_R according to engineering model resistances (here: Chapters 5 and 6, EN 1993-1-5 [46])

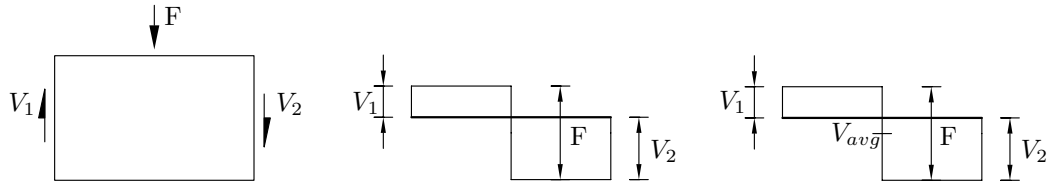

(a) load configuration (b) maximum shear force $V_{max} = V_2$ (c) average shear force V_{avg}

Figure 6.3: Choices for the reference load (shear force diagrams for $V_1/V_2 = 0.5$)

the question which resistance function is used and what applies in reality is important and will be discussed later on again. The characteristics of the reduced stress method is that it should be compatible to the equivalent stress hypothesis in case the slenderness reduces and stability becomes not relevant anymore. This condition for yielding is a formulation which agrees most closely with the test results of the large number of tests on steel made in this field.

6.3 On the choice of a verification point

A plate is usually not subjected to constant stresses but rather to stress gradients. For the basic loading under longitudinal stress and shear for example, Clause 4.6(3) of EN 1993-1-5 [46] allows to carry out the plate buckling verification at a distance of min(0.5·a; 0.5·b) from the panel end where the stresses are the greater. Focusing on the resistance to transverse patch loading, it is presumed that the worst case is when the patch loading is placed at the centerline of the plate. At this location also the bending stresses induced by the transverse loading usually become extremal. Thus, in Chapter 6, EN 1993-1-5 [46], the verification point is at this centerline. It can be shown that besides global bending, equilibrating shear stresses occur which change sign, being zero at the centerline in case of pure patch loading.

For the interaction between transverse patch loading and shear force, there are basically two choices which reference load can be assigned to each axis of an interaction diagram, see Fig. 6.3:

- The applied patch load F is related to the pure patch loading resistance F_R and the maximum internal shear force V_{max} is related to the pure shear resistance V_R
- The applied patch load F is related to the pure patch loading resistance F_R and the applied shear force is corrected by 0.5-times of the applied patch load, denoted average shear V_{avg} in the following.

In case the maximum internal shear force is taken as reference the corresponding distribution of data points is according to Fig. 6.4. Although the maximum value of the internal shear force can be easily attained from the distribution of internal forces, the

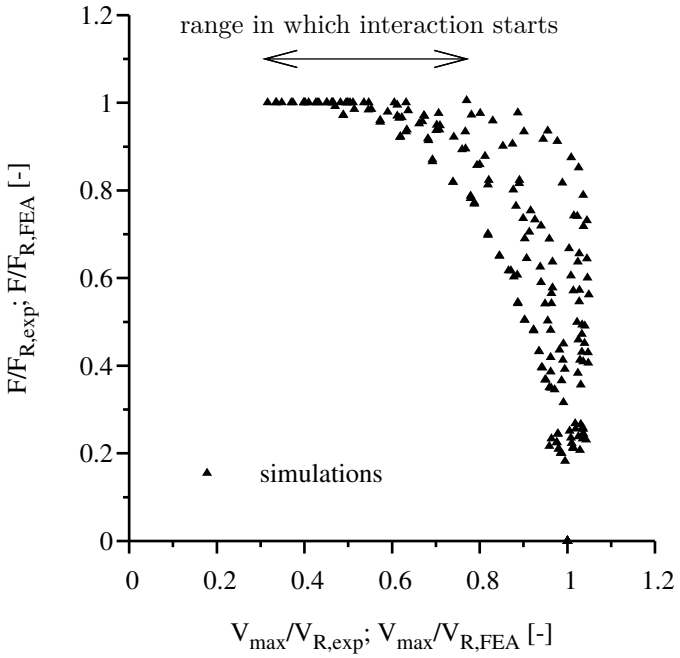

Figure 6.4: Use of the maximum shear force V_{max} as reference load, F_R and V_R according to experiments or based on FEA

use in the interaction diagram is disadvantageous for the following reasons. As the verification of the pure patch loading resistance already includes the shear force ($= 0.5 \cdot F$) which is induced by the patch loading, it is twice considered in the interaction diagram. However, depending on e.g. the slenderness ratio and the loading length, the shear force component of the patch loading has a certain part with regard to the shear resistance so that the ratio V_{max}/V_R ranges from 0.32 to 0.74, as marked in Fig. 6.4, which results in highly dispersed data. Moreover, the verification point usually does not coincide with the relevant location for bending moment.

The second approach subdivides the combined loading into two basic load cases "pure transverse patch loading" and "pure shear force" which can be composed to create the original load combination. Thus, the influence of shear stresses induced by the transverse force which is already included in the patch loading model can be better accounted for. The corresponding interaction diagram was already shown in Fig. 6.1 and despite the high number of studied parameters it shows a smaller scatter in comparison to Fig. 6.4. The verification point usually does coincide with the one for bending moment. For these reasons, the verification point at maximum bending moment and average shear is adopted.

The argumentation also applies to the reduced stress method. It should be noted here because questions from engineers in practice show that the interpretation of the most critical point of the plate, see Clause 10(2), EN 1993-1-5 [46], seems to be not fully clear. It can be concluded that for reasons of plausibility and consistency, the verification point is defined at the centerline of a transversely patch loaded plate.

6.4 Reduced stress method

6.4.1 General

The comparison of results from earlier plate analyses and own simulations with the reduced stress method based on a single plate slenderness indicates that in case of biaxial loading a revision of the procedure is absolutely reasonable and desirable. Existing results from literature will be discussed in Sec. 6.4.2 with regard to relevant boundary conditions. Based on this a modified proposal is developed in Sec. 6.4.3.

6.4.2 Evaluation of current design rules

In Figs. 6.5 and 6.6 the simulation results of plates under biaxial compression are compared to the design rules of DIN 18800-3 [28], DNV-RP-C201 [33] and Chapter 10, EN 1993-1-5 [46]. With regard to the many parameters involved in the interaction diagrams, a selection of simulation results and reference strengths has been made for which the discrepancies of current design rules can be representatively illustrated. In general, the idea is to compare the standard procedure of the relevant standard and simulation results which are based on input parameters corresponding to the de facto used boundary condition. Thus, simulation results are shown for an imperfection amplitude of $b/420$ in comparison to a value of $b/200$ which is relevant in the stocky to medium slenderness range. Rotational edge restraints are considered in the determination elastic critical stresses whereas in-plane edge restraints are only accessible by large deformation theory so that here a further differentiation is made between unconstrained and constrained edge boundary conditions. By doing this in general, a lower and upper bound to the design interaction curves is given.

In Fig. 6.5 the comparison is shown for a square plate ($\alpha = 1$) with b/t-ratios of 30, 45, 65 and 100. It should be noted that constrained in-plane edge restraints become only relevant for high slendernesses. In DIN 18800-3 [28], for a b/t-ratio of 30 a stability-induced reduction of the unaxial loading load case is not required. However, in case of biaxial loading, the simulations show that due to deviation forces interaction effects have to be taken into account. Instead DIN interaction curve and equivalent stress hypothesis coincide which becomes obvious since the interaction is determined based on the reduction factors of the basic loadings being 1.0. In contrast to this, both DNV-RP-C201 [33] and Chapter 10, EN 1993-1-5 [46] consider deviation forces. Thus, an agreement on the level of reduction cannot be found, Chapter 10, EN 1993-1-5 [46] being the most conservative design rule. However, the simulation results let assume that an even stronger interaction is required, in particular when it is recalled that the imperfection amplitude of $b/420$ instead of $b/200$ is used. With increasing slenderness the interaction shape of the simulation results approaches an almost straight line which is independent from the type of in-plane edge restraint. From a qualitative point of view only DIN 18800-3 [28] catches this interaction behaviour correctly. Both DNV-RP-C201 [33] and Chapter 10, EN 1993-1-5

[46] assume a much more favourable - almost circular - interaction. It can be shown e.g. for a b/t-ratio of 100 that the design rules may still be safe if the constrained edge boundary condition is not considered in the calculation of the reference strength. Nevertheless, from the author's point of view and for reasons of consistency, the interaction criterion should not rely on boundary conditions which are not taken into account by the reference strength. Thus, action is required in order to modify Chapter 10, EN 1993-1-5 [46] in such a way that the interaction behaviour can be followed adequately.

In Fig. 6.6 the comparison is shown for a plate with a panel aspect ratio of $\alpha = 3$ and b/t-ratios of 30, 45, 65 and 100. The influence of the column-like behaviour in the short direction is clearly noticeable. The large deviation of the reference strengths for column-like buckling makes it difficult retrieve as concise conclusions as it is the case for the square plate. Nevertheless, the observations which were made for the square plate are also valid here. The positive influence of the imperfection shape attenuates the discrepancies between simulations results, DNV-RP-C201 [33] and Chapter 10, EN 1993-1-5 [46]. But it can be shown that the linear interaction which DIN 18800-3 [28] assumes for non-square plates is too strong. On the other hand, the pronounced dents of Chapter 10, EN 1993-1-5 [46] for higher slendernesses is mechanically not comprehensible (see $\otimes$ in Figs. 6.6c and 6.6d). Thus, action is required in order to modify Chapter 10, EN 1993-1-5 [46] in such a way that the interaction behaviour can be followed adequately for the non-square plates as well.

The prominent conclusion is to separate the influence of the edge boundary condition from the interaction criterion and to return it to the reference strength. This could also open up the possibility to take into account favourable edge boundary conditions which would essentially contribute to a numerically assisted verification procedure in the future. A proposal for a modification of Chapter 10, EN 1993-1-5 [46] is studied in Sec. 6.4.3.

Besides that, in [110] a list of required and desirable conditions is itemised which a generalised buckling verification should fulfill. In the following the requirements are discussed with regard to the results of this work.

- **Compatibility to the equivalent stress hypothesis.** It has to be postulated that for plates which are not prone to buckling the method should become identical to the equivalent stress hypothesis according to the von Mises criterion.
- **Compatibility to basic loading.** It has to be postulated that in case of a single basic loading the buckling verification method should become identical to the buckling verification applied for the basic loading. It is assumed that buckling curves are provided for basic loadings and that these reduction factors are brought together with an interaction equation. Influences from both rotational and in-plane edge boundary conditions should be covered by the buckling curves. Thus, an interaction equation should not draw a positive influence of effects coming from boundary conditions to make the interaction equation more favourable. Instead it should properly describe the interaction behaviour and attribute effects from boundary conditions to the buckling curves.

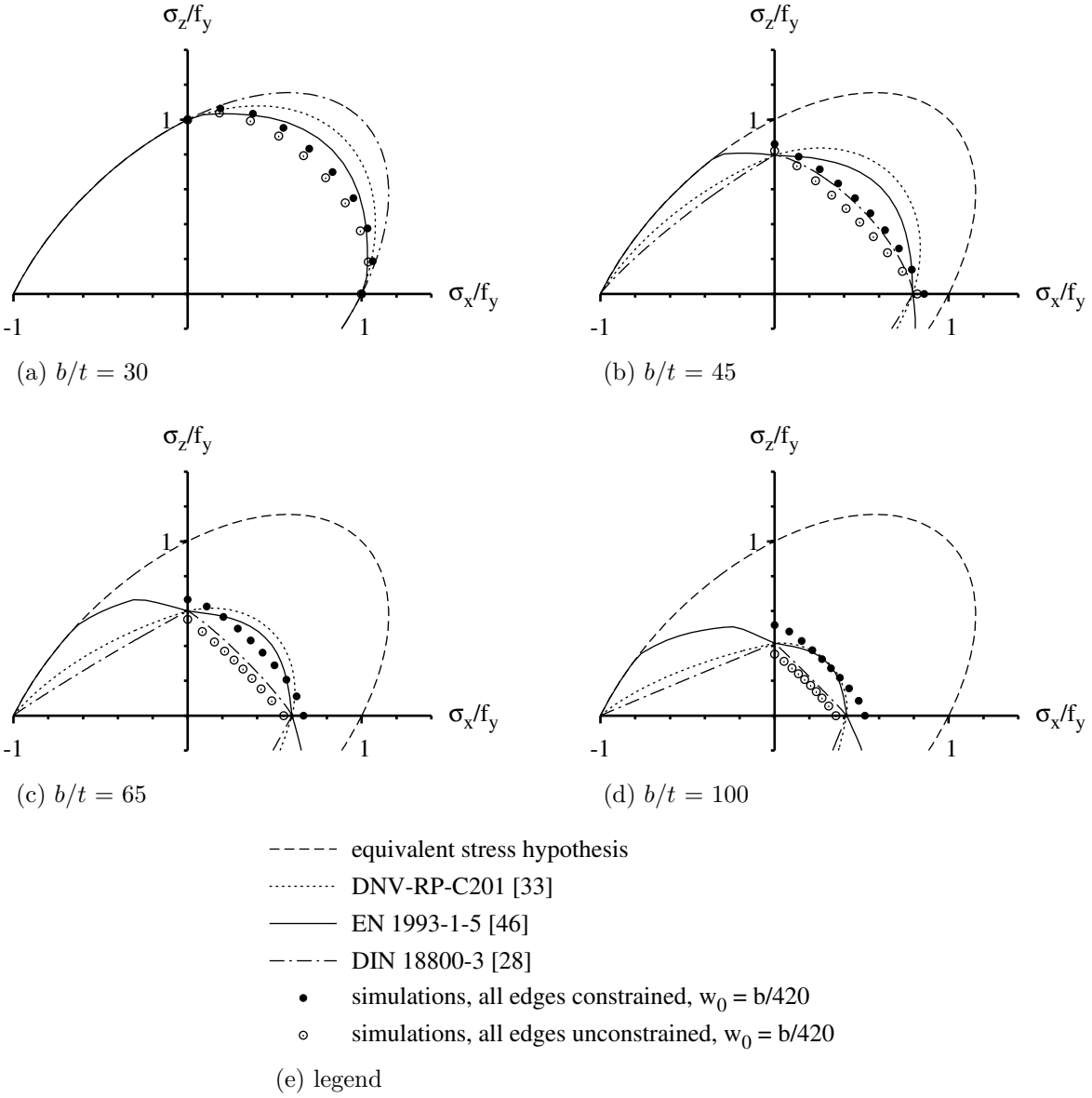

(a) $b/t = 30$

(b) $b/t = 45$

(c) $b/t = 65$

(d) $b/t = 100$

(e) legend

Figure 6.5: Comparison of interaction rules and simulations ($\alpha = 1$, all edges hinged, reference strengths according to the relevant standard)

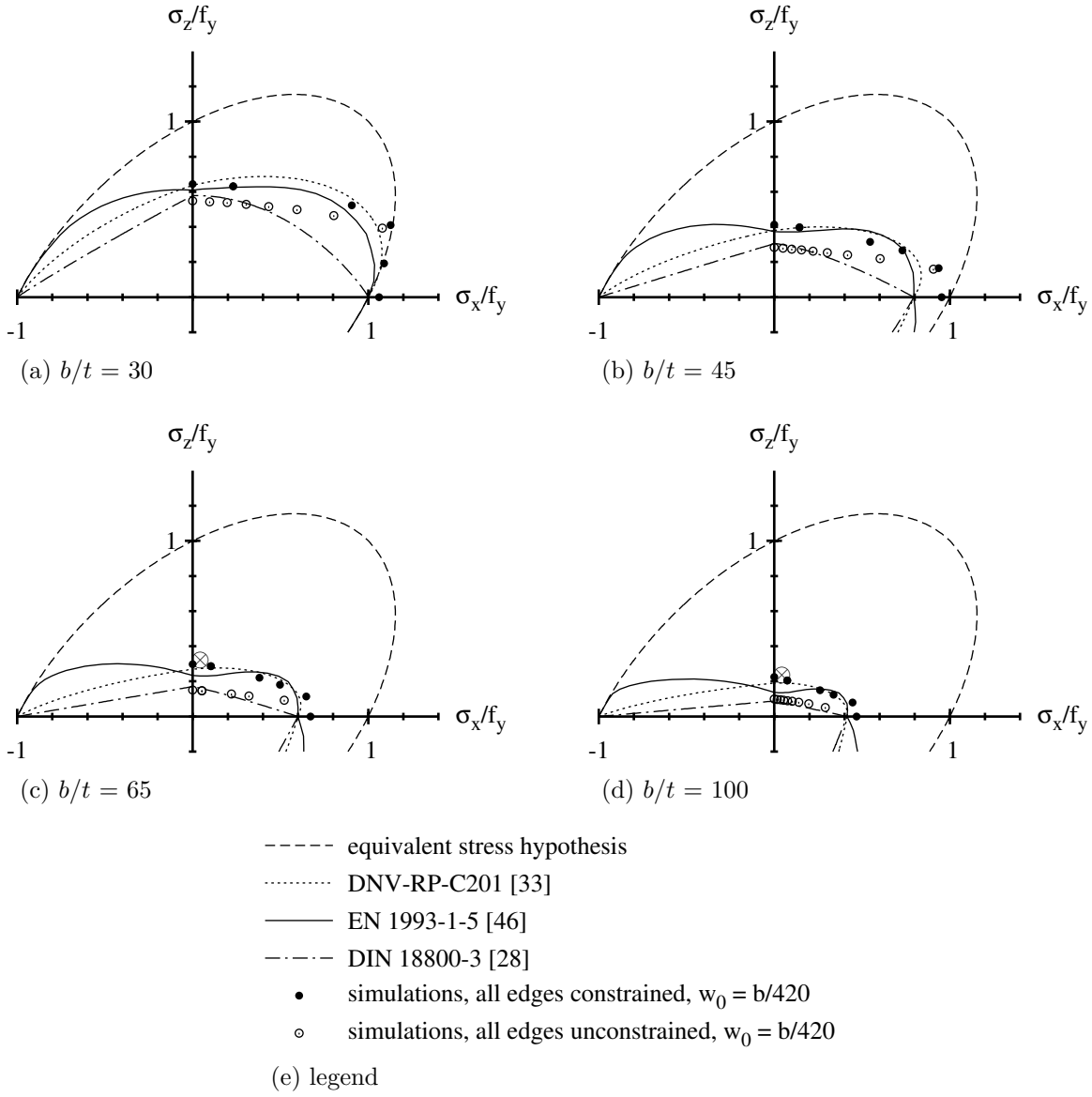

(a) $b/t = 30$ (b) $b/t = 45$

(c) $b/t = 65$ (d) $b/t = 100$

(e) legend

Figure 6.6: Comparison of interaction rules and simulations ($\alpha = 3$, all edges hinged, reference strengths according to the relevant standard)

- **Plausibility and safety of results.** Results have to be plausible and safe which is a application requirement sine qua non. Interestingly in [110] monotonically decreasing buckling loads for biaxial compression are postulated. However, this basic requirement is not fulfilled for rectangular plates other than square plates. And also for square plates, doubts about the favourably curved interaction shape exist.

In the following the desirable conditions are commented.

- **Use of a global slenderness.** According to linear buckling theory, only one decisive eigenmode shape associated with the lowest eigenvalue and its equivalent elastic critical stress exists for a given stress field i.e. a combined loading. A breakdown of such a stress field into basic loadings would be artificial and mechanically not correct because separate eigenmode shapes are associated with each basic loading. Nevertheless it has been done e.g. in DIN 18800-3 [28] because the determination of critical stresses for basic loadings is much simpler and can be done based on charts, e.g. [70, 71, 109]. Taking into account advanced software solutions which have become available today, the determination of an equivalent elastic critical stress for a given stress field usually causes no serious difficulties anymore. The use of a single plate slenderness based on an equivalent critical stress is supported because it allows to consider the mutual influence of all stress components.
- **Choice of interaction equation.** It is obvious to choose an interaction equation which is similar to the equivalent stress hypothesis because the method should become identical to this hypothesis for stocky plates. The use of a generalised equivalent stress hypothesis as in Chapter 10, EN 1993-1-5 [46], is straightforward but it was shown that it cannot properly describe the mechanical behaviour of a plate under biaxial compression.
- **Stabilising effect of tensile stress.** The stabilising influence of tensile stresses should be taken into account mainly for economic reasons. This item is mentioned in [110] because in DIN 18800-3 [28] this is not possible due to the breakdown of the stress field into separate basic loadings. This is a further development which is supported but not studied here.

The applicability of the von Mises based interaction equation is argued by Scheer and Nölke in [110, 111]. In [111] the two experimental test series by Becker [4] and Bradfield et al. [11] were neglected which have been used by Lindner and Habermann [78] for the justification of DIN 18800-3 [28]. It is argued that Lindner and Habermann [78] had to take assumptions for which Scheer and Nölke [111] think that the results are inapplicable. In [111] the conclusion is drawn that the experimental results cannot be used. The author is of the opinion that a reassessment of the experiments should be done in order to identify the possibility to use them. If there are no strong doubts they should be used, also in order to support the numerical simulations. In [111] also numerical calculations are doubted. For the ones done by Jungbluth [68] the argument is that no plausible interaction curve can be drawn. However, they fit to a straight line similar to Dunkerley's formula.

A point which should be discussed however is the fact that the edges are assumed to remain straight. Usually the numerically determined ultimate loads should then be higher than the calculated ones. Instead they are about 6 % smaller. Therefore, in [111] a limitation of their use is seen. The author could not clarifiy the assumption for the edge conditions, but if the longitudinal edges are assumed to move in-plane, the results match very well. The deviation of 6 % can be explained by the choice of the imperfection amplitude of b/200. As shown by Rusch and Lindner [108] and also by the author [74, 75] a recalculation of the buckling curve is only possible with a reduced imperfection amplitude of b/420. The calculations of Dinkler and Kröplin [31] are doubted by [111] because they vary between -6 % to +29 %. It is announced that in [110] further explanations will be given which is not the case. Besides that, a report on their numerical calculations [95] has never been published.

In DIN 18800-3 [28] the approach based on individual plate slendernesses has been used for reasons given by Lindner and Habermann [79]. Biaxial loading has been studied numerically by Dinkler [30] which showed the need to change the interpolation as proposed in E DIN 18800-3 [48]. For Chapter 10, EN 1993-1-5 [46], the reintroduction of the equivalent elastic critical stress is connected to the fact that in contrast to earlier years, it is nowadays quite easily possible to determine this stress value.

Although the results if Jungbluth [68] should be excluded in terms of their absolute values, they show an interaction behaviour which is qualitatively similar to all other data. What went wrong in the assumptions e.g. for edge boundary conditions could not be clarified afterwards but looking at the results as a closed system, they get the interaction behaviour right and support not only other data but also the conclusions drawn by the author.

6.4.3 Proposal for improved design rules

Following the principles which were set up in Secs. 6.2 and 6.3, an interaction equation which modifies Chapter 10, EN 1993-1-5 [46], is developed.

In Sec. 6.4.2 simulation results were compared to the interaction equation of Chapter 10, EN 1993-1-5 [46]. It was shown that a modification of the interaction equation is required in order to describe adequately the stability behaviour. In Eq. 6.1 the general format of an interaction equation based on the equivalent stress hypothesis is given. Parameters which influence the interaction curve shape are the factor V and, if required, the exponents $e_{i=1,2,3}$.

$$\left(\frac{\sigma_{x,Ed}}{\sigma_{x,Rd}}\right)^{e_1} + \left(\frac{\sigma_{z,Ed}}{\sigma_{z,Rd}}\right)^{e_2} - V \cdot \boxed{\left(\frac{\sigma_{x,Ed} \cdot \sigma_{z,Ed}}{\sigma_{x,Rd} \cdot \sigma_{z,Rd}}\right)} + 3 \cdot \left(\frac{\tau_{Ed}}{\tau_{Rd}}\right)^{e_3} \leq 1 \tag{6.1}$$

The factor V is usually expressed as given in Eq. 6.2.

$$V = (\rho_x \cdot \rho_z)^e \tag{6.2}$$

This approach has been used e.g. in DIN 18800-3 [28] where all parameters were calibrated against experimental and numerical results. DNV-RP-C201 [33] is also based on this approach but with simplified exponents. Existing applications of the reduced stress method are based on individual plate slendernesses [28, 33] whereas Chapter 10, EN 1993-1-5 [46] is based on a single plate slenderness which already considers an interaction on the level of the elastic critical stresses. Thus, existing factors cannot be adopted one-to-one. The approach of Chapter 10, EN 1993-1-5 [46] is sufficient for the interaction with shear stresses and it is assumed to be appropriate for biaxial loadings with tension in at least one direction. However, in the biaxial compression range discrepancies exist for which the curvature needs to be reassessed. Since this curvature is mainly influenced by the boxed term according to Eq. 6.1, the factor V will be studied based on its general format according to Eq. 6.2 in the following. The introduction of such a factor was also proposed e.g. in a recent article on plate buckling [66].

In order to study the effect of the factor V the square plate will be used since the imperfection shape of the basic loadings coincide so that it can be considered as worst case in terms of deviation forces. As it has been shown in Sec. 5.4, non-square panel aspect ratios become more favourable due to advantageous imperfection shapes. Due to the symmetry of the square plate, the curvature is defined by the points located at the bisecting plane under an angle of 45 degrees, see Fig. 6.7. Figures 6.8 to 6.10 show the evaluation of simulations, design rules and proposals in this plane. In all figures a discrimination is made between unconstrained and constrained in-plane edge restraints, shown at the top and bottom diagram respectively. The Winter curve (i.e. Sec. 4, EN 1993-1-5 [46]) is given throughout but not further considered since it represents loaded edges constrained and unloaded edges unconstrained for which it was shown in Sec. 5.4.4 that in case of biaxial loading a clear definition of edge boundary conditions is only possible when all edges are either unconstrained or constrained. The other buckling curve gives the interaction based on the relevant reference strength for unconstrained (i.e. Annex B, EN 1993-1-5 [46]) or constrained (i.e. based on Fig. 5.10) in-plane edge restraints. Simulations have been carried out with geometric imperfection values of b/200, b/420 and partly b/1000.

Calibration of the factor V. In Fig. 6.8 the calibration of the factor V is illustrated. It can be clearly shown that the EN interaction is not appropriate and action is required. For the calibration hinged boundary conditions are assumed. Fitting e according to Eq. 6.2 as lower bound to the simulations, e becomes 1.7. It is governed by the medium slendernesses and becomes slightly conservative for the high slendernesses. Having in mind that the recalculation of buckling curves in the medium slenderness range succeeds only with a reduced imperfection amplitude of b/420, it can be argued the same way for the calibration of the interaction equation. To achieve consistency one could simplify the

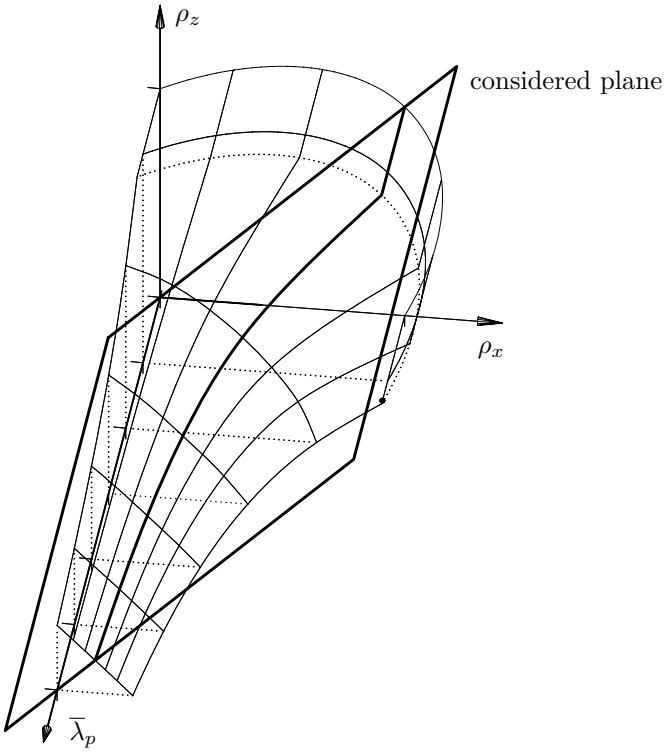

Figure 6.7: Plane under an angle of 45 degrees which is utilised in Figs. 6.8 to 6.10

equation to $e = 1$ then. The corresponding proposal can be written according to Eq. 6.3 in case of biaxial compression.

$$\left(\frac{\sigma_{x,Ed}}{\sigma_{x,Rd}}\right)^2 + \left(\frac{\sigma_{z,Ed}}{\sigma_{z,Rd}}\right)^2 - \rho_x \cdot \rho_z \cdot \left(\frac{\sigma_{x,Ed} \cdot \sigma_{z,Ed}}{\sigma_{x,Rd} \cdot \sigma_{z,Rd}}\right) \leq 1 \tag{6.3}$$

A comparison of the simulation results with the proposed $V = \rho_x \cdot \rho_z$ shows that a good agreement can be achieved. In the following the effects of in-plane and rotational edge restraints will be discussed.

Effect of in-plane edge restraints. The comparison of Figs. 6.8a and 6.8b shows that the interaction for plates with constrained edges is more favourable than for unconstrained edges. Nevertheless, it can be confirmed in both cases that the EN interaction is not appropriate and that the Winter curve (i.e. Chapter 4, EN 1993-1-5 [46]) should not be applied. But the EN interaction is particularly unsafe when the adequate reference strengths are chosen, i.e. Annex B, EN 1993-1-5 [46] for unconstrained edges and the determination based on Fig. 5.10 for constrained edges. A modification of the interaction equation based on the factor V is strongly required. By doing this, it can be shown that Eq. 6.3 equally fits to unconstrained and constrained in-plane edge restraints as long as the adequate reference strength is used. It should be noted that it would be safe to apply the proposal with reference strengths based on Chapter 4, EN 1993-1-5 [46] in case of constrained edges.

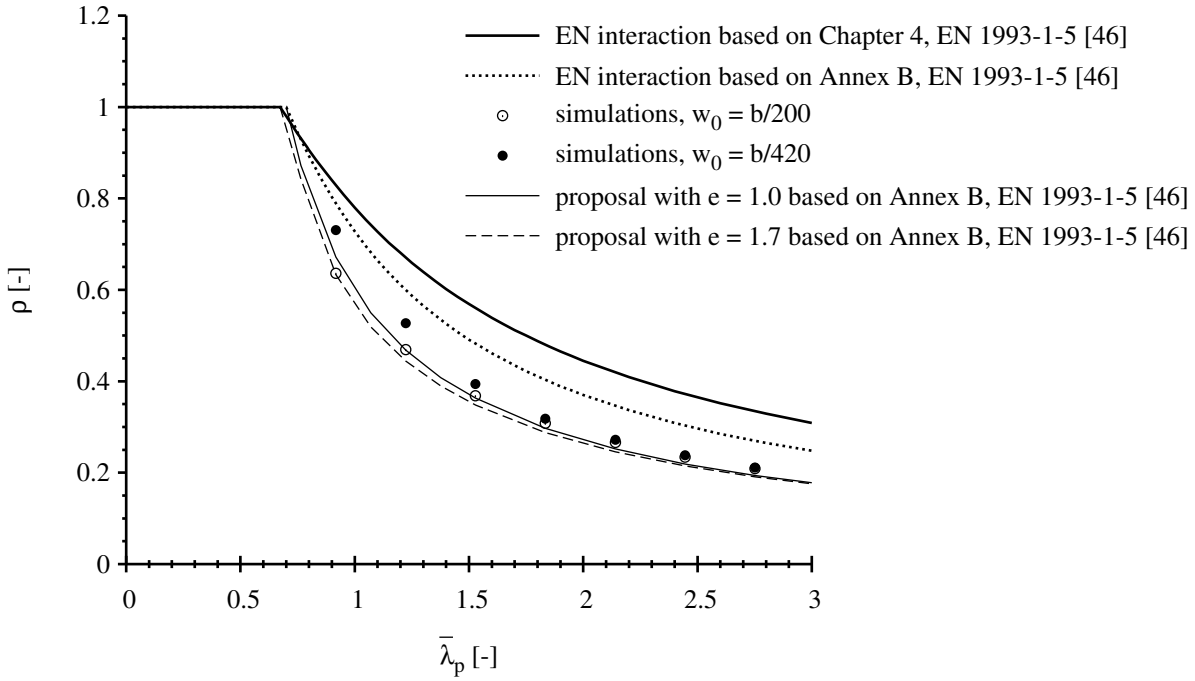

(a) all edges unconstrained

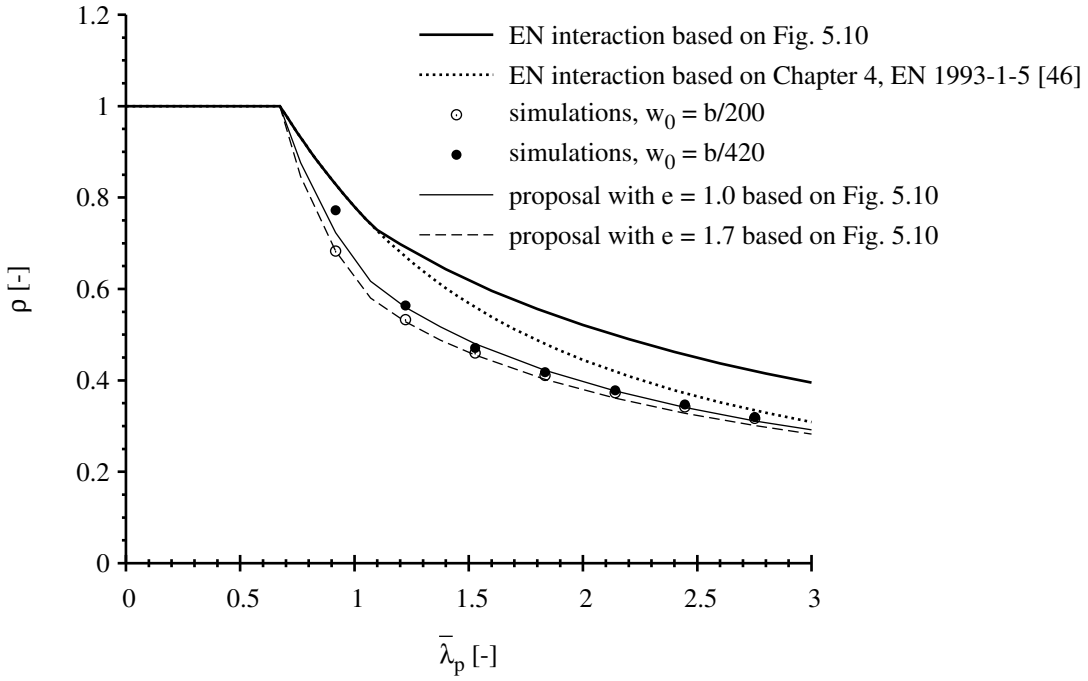

(b) all edges constrained

Figure 6.8: Calibration of V and effect of in-plane edge restraints ($\alpha = 1$, all edges hinged)

Effect of rotational edge restraints. Instead of hinged edges according to Fig. 6.8, the evaluation has been similarly done to study the effect of rotational edge restraints. In Fig. 6.9 the longitudinal edges are clamped and the transverse edges are hinged. In Fig. 6.10 all edges are clamped. In both cases the simulations have been evaluated with relevant edge boundary conditions, i.e. taking the clamping effects for the determination of the elastic critical stresses into account. Due to this the slenderness values are shifted to the left. In general, the observations which have been mentioned above for the effect of in-plane edge restraints are also valid here. With regard to the evaluation of the rotational edge restraints, the proposed interaction equation fits well for the medium to high slenderness range. For the plate with all edges unconstrained and clamped it is not fully matching but it is on the safe side, see Fig. 6.9a. In contrast to this, simulation results fall below the interaction curve in the stocky range. An explanation was searched and found when simulations were carried out with a significantly reduced imperfection amplitude of b/1000. It can be shown that in this parameter range there is a strong influence of the imperfection amplitude. Once again the question has to be put what the adequate value is that should be used in numerical calculations. However, it can be shown in general that the clamping effects can be adressed properly when using the proposed interaction equation and taking the clamping effects for the determination of the elastic critical stresses into account.

Transferability to panel aspect ratios other than square. The proposal according to Eq. 6.3 which has been derived from a square plate is evaluated for panel aspect ratios other than square. In Figs. 6.11 to 6.13 the proposal is compared to experiments with panel aspect ratios of $\alpha = 3$, 4 and 6. In the comparison also code rules are given. It can be shown that the proposal is the most appropriate interaction criterion, also for the tests from Bradfield et al. [11] which address panel aspect ratios of $\alpha \geq 4$. However, the scatter of the experimental data makes it difficult to draw concise conclusions. Besides that, in Fig. 6.14 the proposal is compared to simulation results of a plate with $\alpha = 3$. It can be shown that the reference strengths on the x-axis which are not influenced by column-like behaviour fit well to the simulations. In contrast to this, the reference strengths on the y-axis which are influenced by column like behaviour exhibit some discrepancy, see Sec. 5.3.2. However, the proposed interaction equation is able to follow the simulation results sufficiently well. Thus, it can be shown that the interaction criterion derived from a square plate can be transferred to describe the stability behaviour of non-square plates as well.

Transferability to other stress gradients and loadings. Assuming that the plate under biaxial uniform compression represents the worst case in terms of interaction behaviour, other stress gradients and loadings as e.g. biaxial bending stresses should be covered. However, in particular for transverse patch loading the choice of the appropriate buckling curve as reference strength is relevant. It has been shown that usually unconstrained conditions apply so that Annex B should be used, see German National Annex to EN 1993-1-5 [47] and DIN-Fachbericht 103 [29]. Thus, it can be shown that by choosing the adequate reference strength the proposed interaction criterion applies in general.

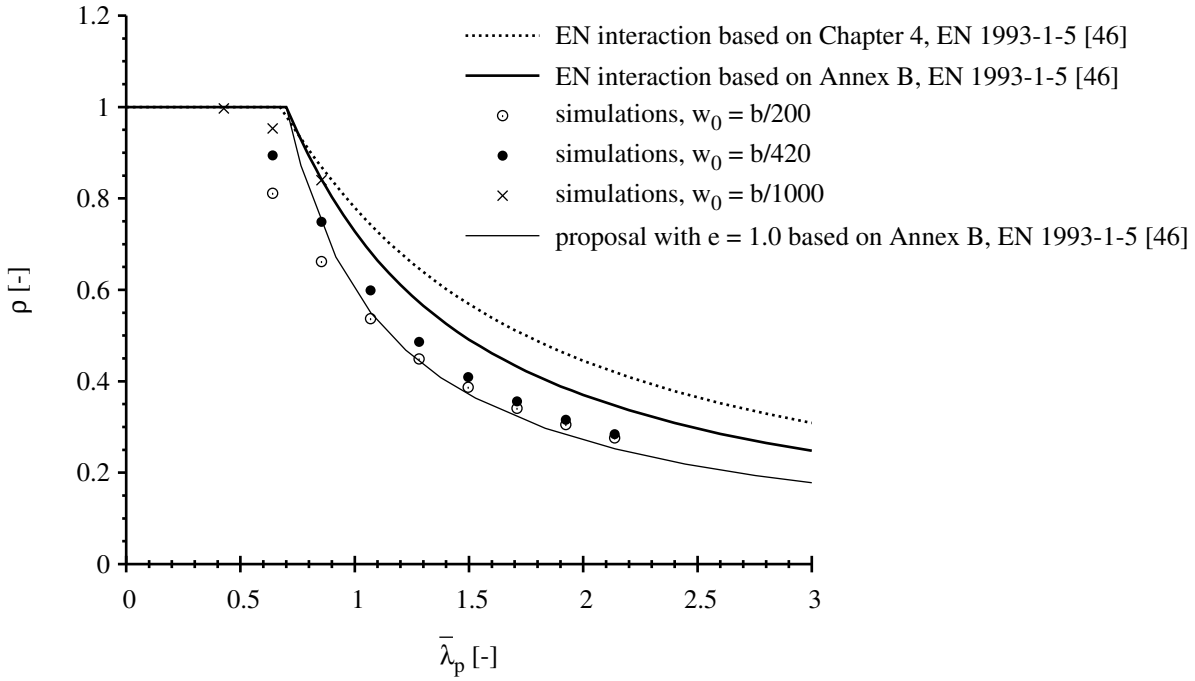

(a) all edges unconstrained

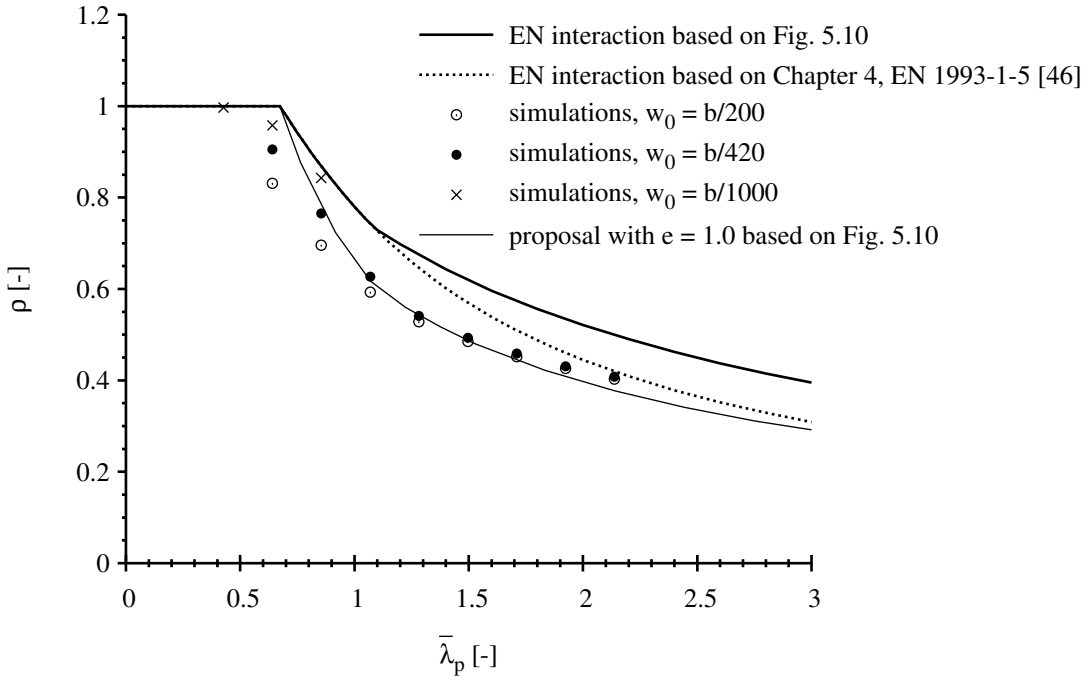

(b) all edges constrained

Figure 6.9: Calibration of V and effect of rotational edge restraints ($\alpha = 1$, longitudinal edges clamped, transversal edges hinged)

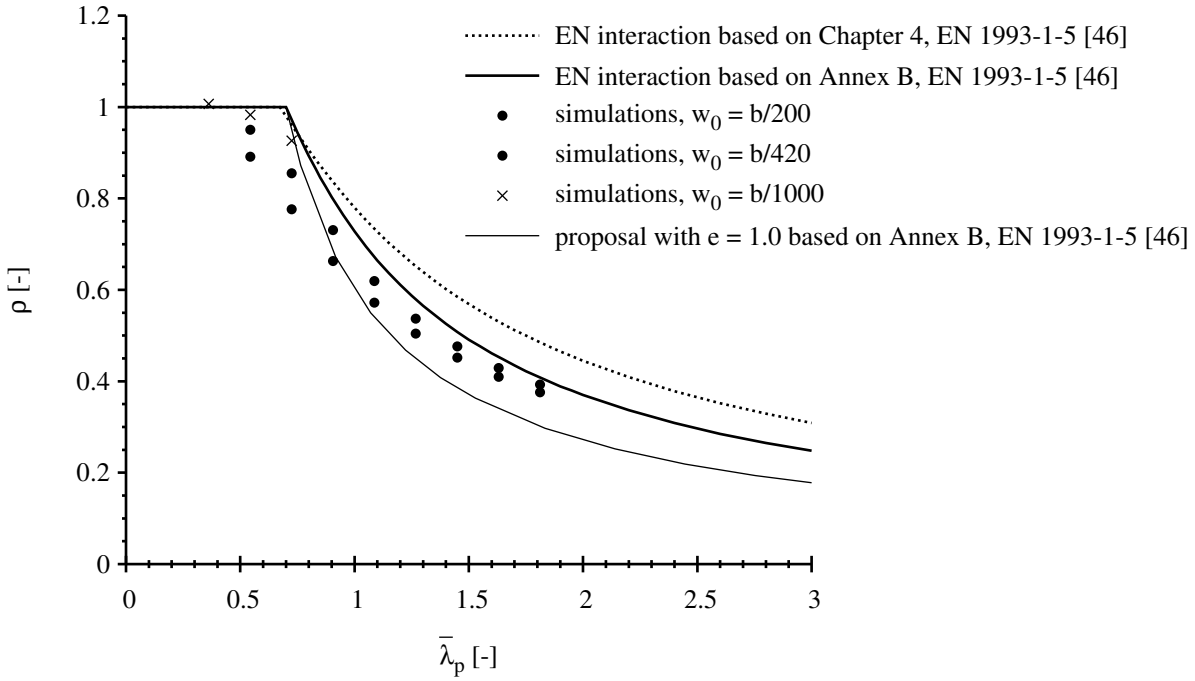

(a) all edges unconstrained

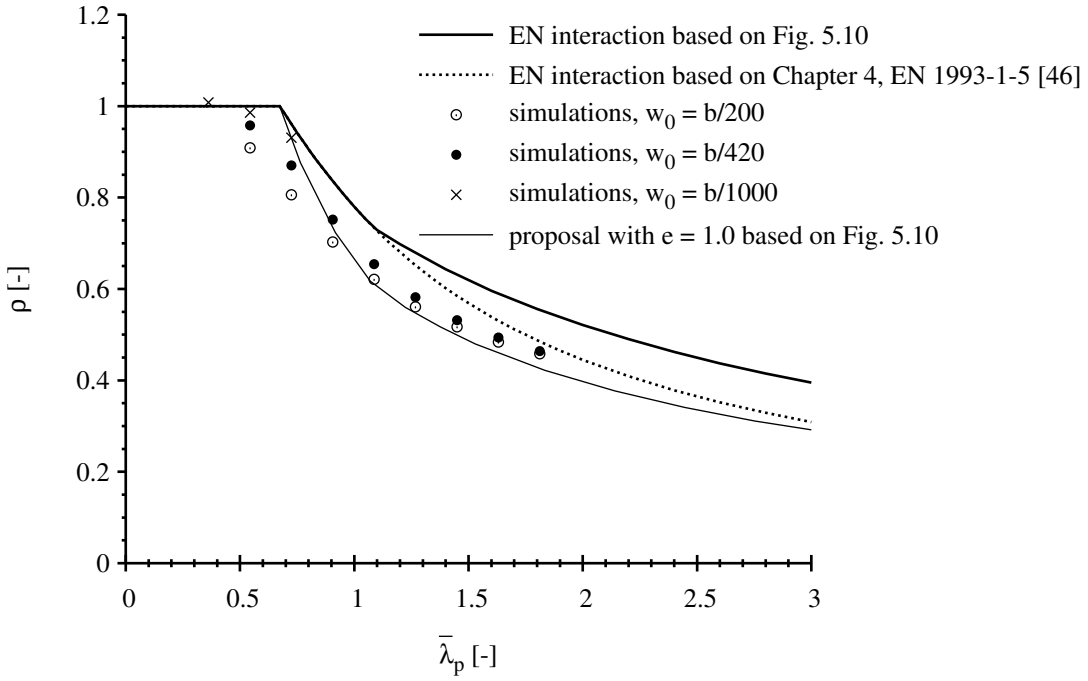

(b) all edges constrained

Figure 6.10: Calibration of V and effect of rotational edge restraints ($\alpha = 1$, all edges clamped)

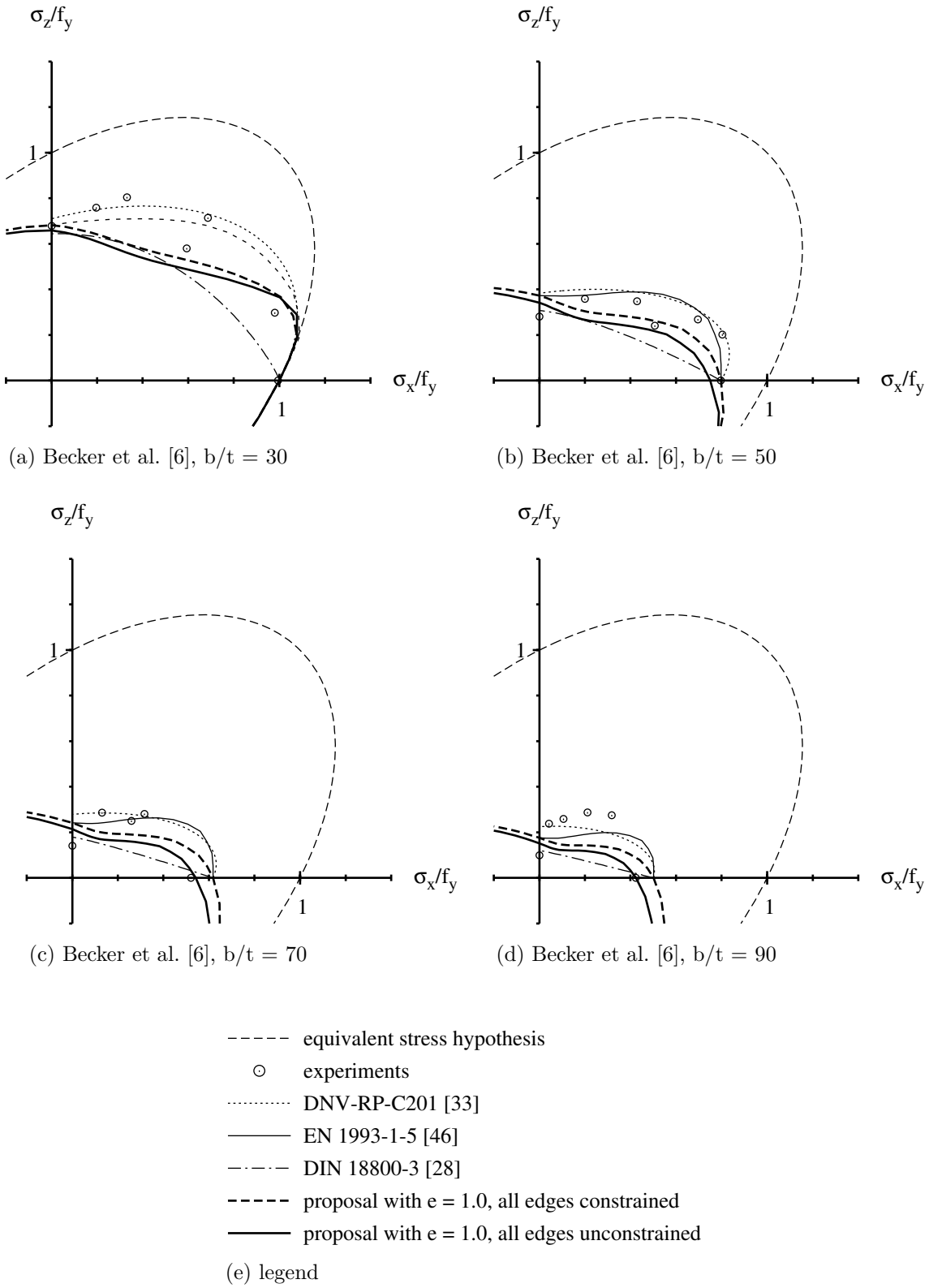

(a) Becker et al. [6], b/t = 30

(b) Becker et al. [6], b/t = 50

(c) Becker et al. [6], b/t = 70

(d) Becker et al. [6], b/t = 90

(e) legend

Figure 6.11: Comparison of interaction rules, proposal and experiments, Becker et al. [6] ($\alpha = 3$)

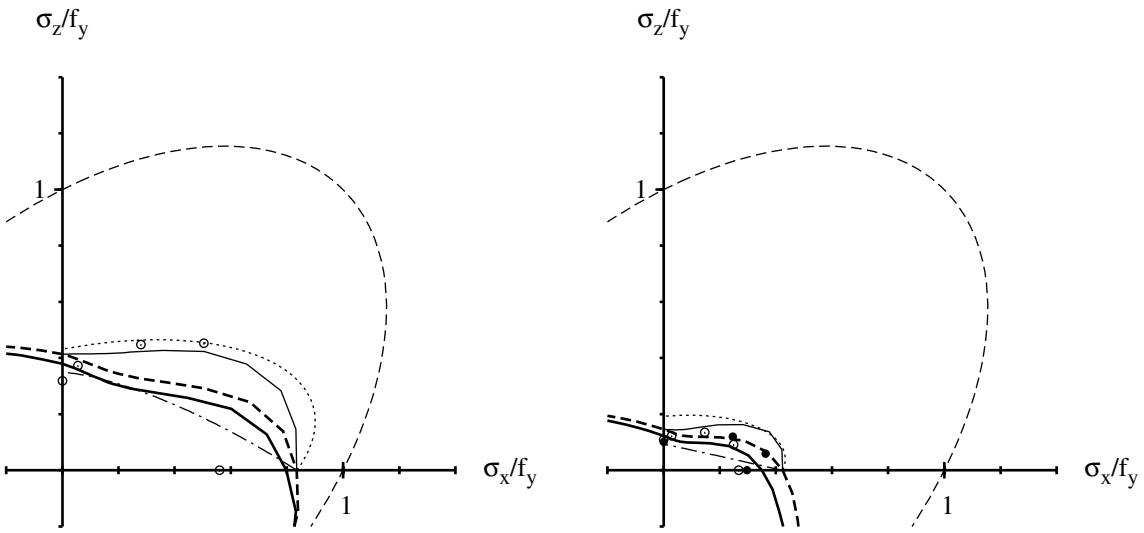

(a) Becker and Colao [5], b/t = 30

(b) Becker and Colao [5], b/t = 70

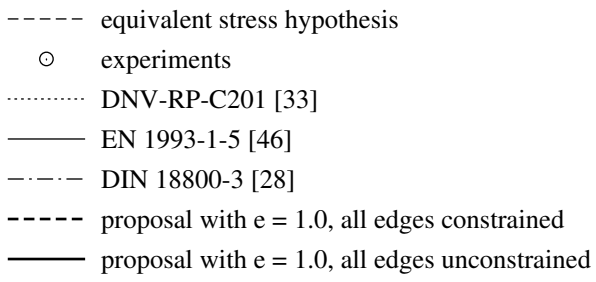

(c) legend

Figure 6.12: Comparison of interaction rules, proposal and experiments, Becker and Colao [5] ($\alpha = 3$)

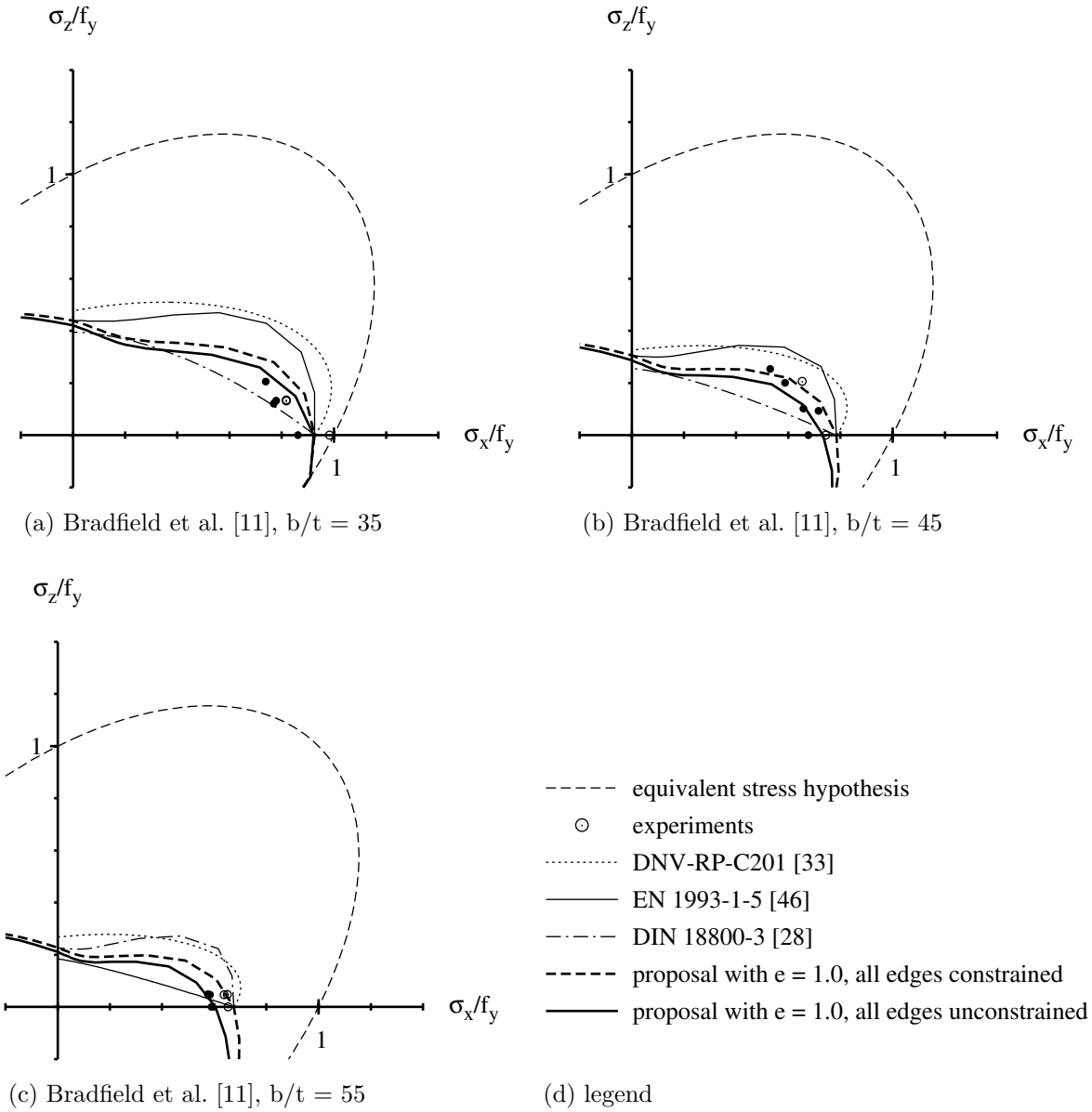

(a) Bradfield et al. [11], b/t = 35

(b) Bradfield et al. [11], b/t = 45

(c) Bradfield et al. [11], b/t = 55

(d) legend

Figure 6.13: Comparison of interaction rules, proposal and experiments, Bradfield et al. (1993) ($\alpha = 4$ and 6)

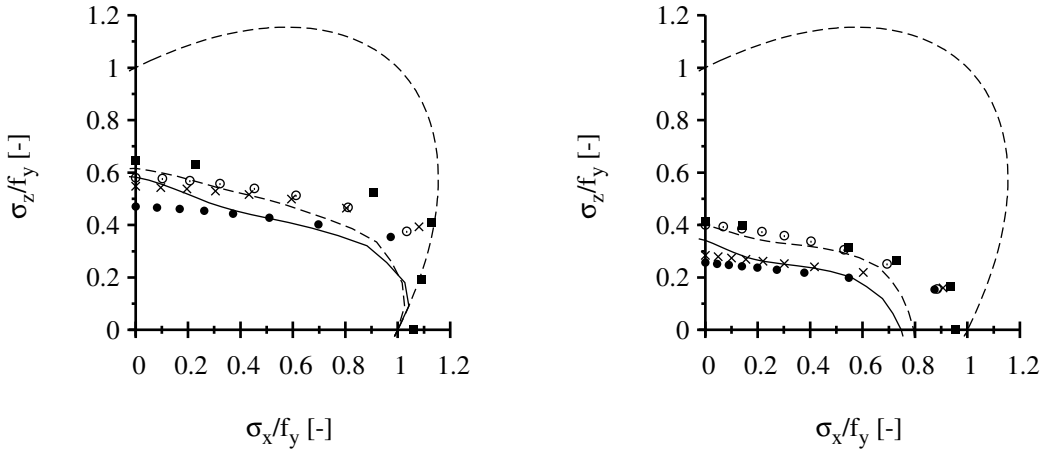

(a) $b/t = 30$

(b) $b/t = 45$

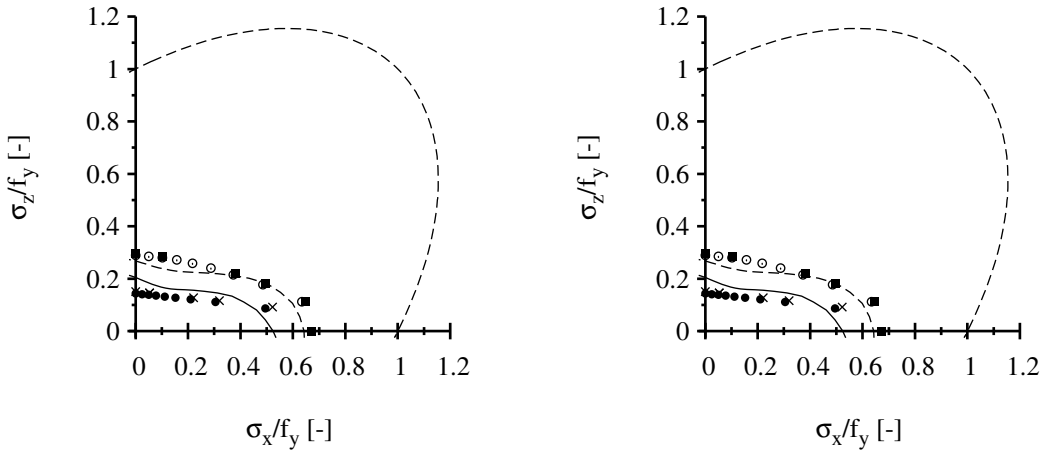

(c) $b/t = 65$

(d) $b/t = 100$

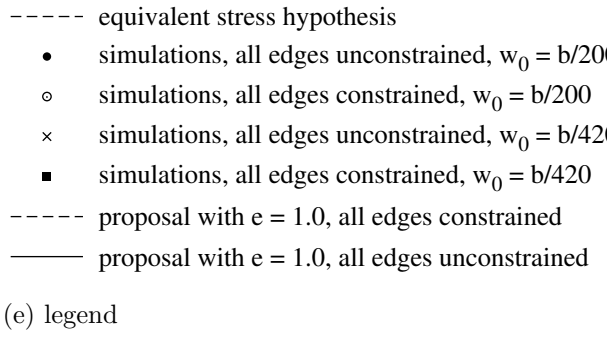

(e) legend

Figure 6.14: Comparison of interaction rules, proposal and simulations ($\alpha = 3$, all edges hinged)

Final comparison to current code rules. In Figs. 6.15 and 6.16 the proposal is compared to the rules of DIN 18800-3 [28], DNV-RP-C201 [33] and Chapter 10, EN 1993-1-5 [46]. In general the proposal gives consistent interaction curvatures if the continuation in compression-tension quadrants is also taken into consideration. In contrast to this, it was shown that Chapter 10, EN 1993-1-5 [46] may even lead to an increase of the resistance if the biaxial compression quadrant is entered. Nevertheless, the consideration of favourable tensile stresses in case of compression-tension and of deviation forces in case of small slendernesses are clearly two advantages of Chapter 10, EN 1993-1-5 [46] in comparison to DIN 18800-3 [28] and DNV-RP-C201 [33]. In particular the deviation forces for small slendernesses turn out to be a requirement which has been completely neglected in DIN 18800-3 [28].

According to Fig. 6.15 it can be shown that for square plates a linear interaction is approached the more slender the plate becomes. As a result the proposed interaction curves coincide with DIN 18800-3 [28]. However, for small slendernesses a stronger interaction needs to be taken into account so that the proposed interaction equation is now the most conservative one.

According to Fig. 6.16 for panel aspect ratios other than square the imperfection shape has a strong influence on the curvature of the interaction curves. It has been shown that the linear interaction which DIN 18800-3 [28] assumes is too conservative. In contrast to this, Chapter 10, EN 1993-1-5 [46] is too favourable. Here, the proposed interaction equation is successfully able to take the positive influence of the imperfection shape into account.

A formulation for an implementation in a future revision of EN 1993-1-5 has been prepared and is given in Annex C.

6.5 Effective width method

6.5.1 General

The lack of a design rule in Chapter 7, EN 1993-1-5 [46], for the interaction between transverse patch loading and shear force (F-V) and the results from the experimental and numerical studies indicate that the formulation of an appropriate interaction equation is required. Existing proposals from literature will be discussed in Sec. 6.5.2.1 with regard to the applicability to the enhanced parameter range which was studied in this work. Based on this analysis a new proposal is developed in Sec. 6.5.3.1.

An evaluation of the interaction equation between transverse patch loading and bending moment (F-M) is performed in Sec. 6.5.2.2. It can be shown that the development of new patch loading resistance models requires a reassessment of the F-M interaction equation. By doing this, the targeted merging of F-V and F-M interaction rules is considered in the general format of the equation.

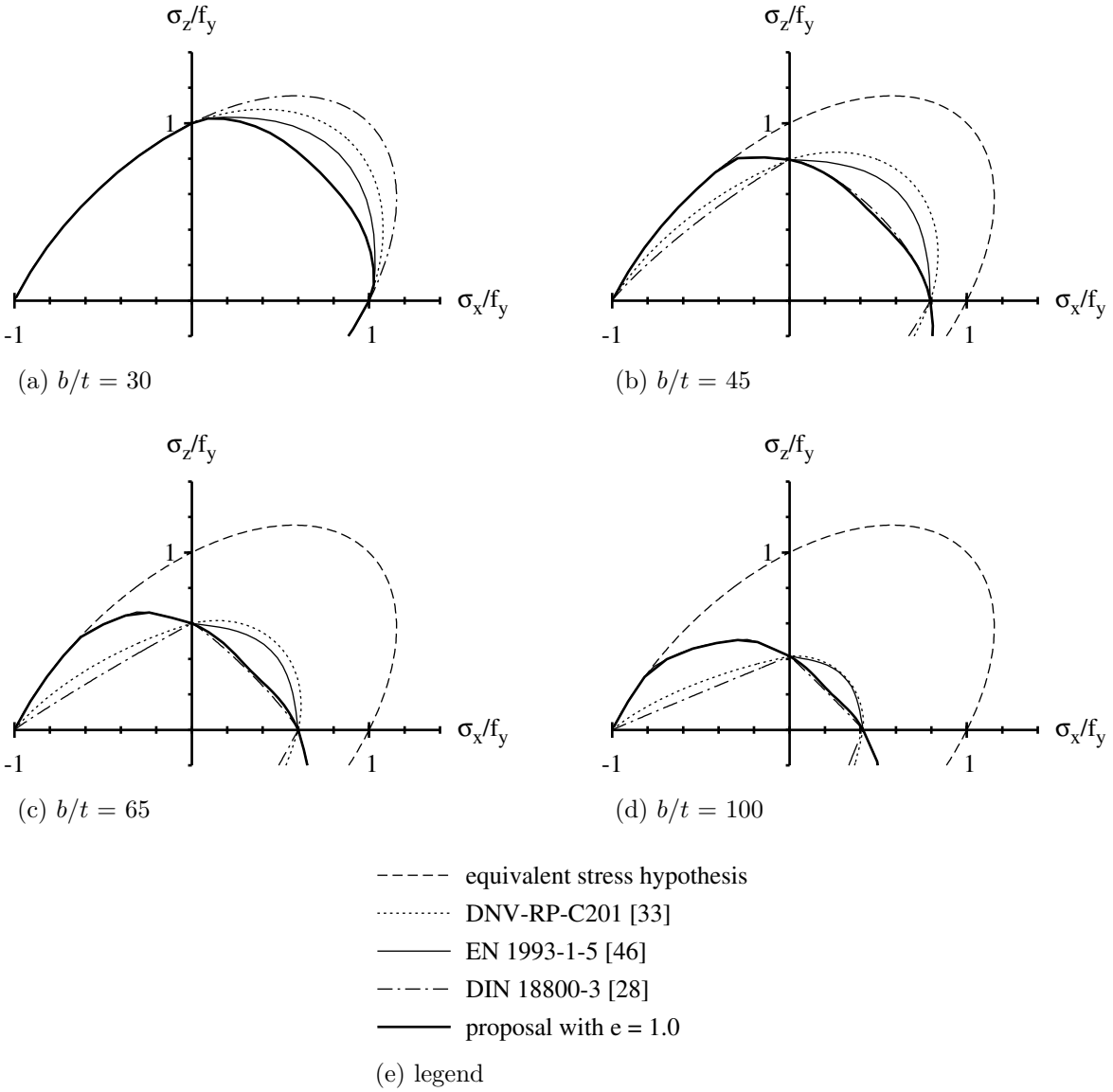

(a) $b/t = 30$

(b) $b/t = 45$

(c) $b/t = 65$

(d) $b/t = 100$

(e) legend

Figure 6.15: Comparison of interaction rules and proposal ($\alpha = 1$, reference strengths according to the relevant standard)

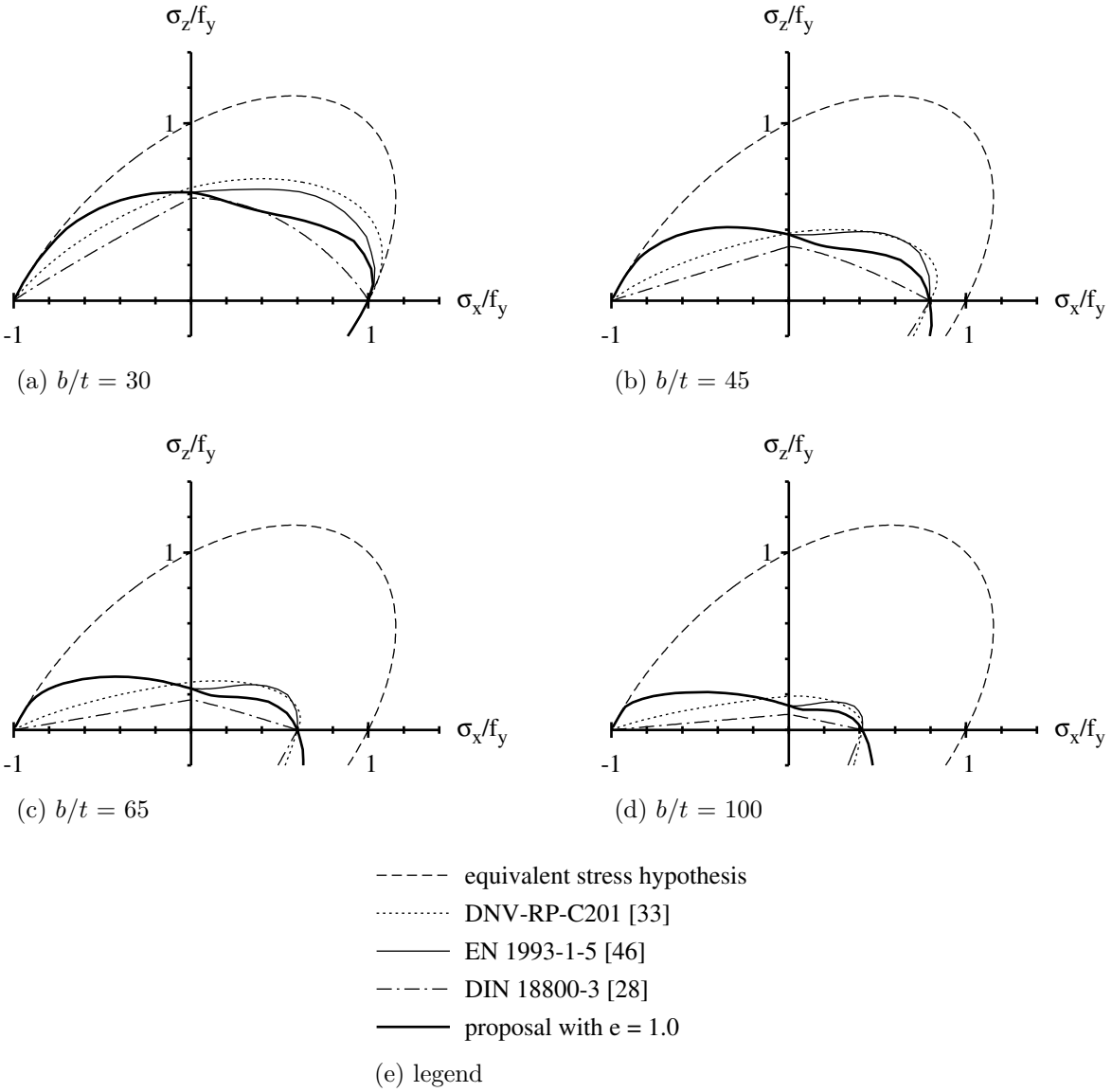

(a) $b/t = 30$

(b) $b/t = 45$

(c) $b/t = 65$

(d) $b/t = 100$

(e) legend

Figure 6.16: Comparison of interaction rules and proposal ($\alpha = 3$, reference strengths according to the relevant standard)

The reference strengths are important parameters and a lot of progress has been made for the patch loading resistance models as summarised in Sec. 2.4. Besides Chapter 6, EN 1993-1-5 [46], the following advanced patch loading resistance models are compared:

- The proposal for girders without longitudinal stiffener according to Gozzi [56] which follows the general procedure as proposed by Lagerqvist [77] for Chapter 6, EN 1993-1-5 [46], but which has been further developed with regard to the yield load and the reduction function.
- The modified resistance model for girders with longitudinal stiffener according to Davaine [24] which improves current Chapter 6, EN 1993-1-5 [46], by adding the elastic critical load of the directly loaded subpanel and modifiying the reduction curve.
- The resistance model for girders with longitudinal stiffener according to Clarin [19] which is based on and harmonised with the improved resistance model for girders without longitudinal stiffener according to Gozzi [56]. It uses the elastic critical load of the directly loaded subpanel according to Davaine [24]. The reduction curve proposed by Gozzi [56] is also used for girders with longitudinal stiffener.

For all girders, the bending moment resistance is determined according to Chapter 4, EN 1993-1-5 [46] and the shear force resistance is determined according to Chapter 5, EN 1993-1-5 [46].

In order to evaluate the quality of the proposed interaction equation with regard to the different resistance models for patch loading statistical analyses are performed. For the statistical evaluation, the test result R_e, which can be of experimental and numerical origin, is consistently compared to the calculated resistance R_t of the chosen engineering model for a defined ratio of patch loading, bending moment and shear force. From a constant ratio of shear force to patch loading two scalar load amplification factors can be determined. One factor is coming from the experimental or numerical data base whereas the corresponding second factor results from the calculated resistance of the chosen engineering model. The quotient of the two scalar load amplification factors represents a key figure on the basis of a vectorial comparison which can be then determined for each pair of tested and calculated resistance. The procedure is schematically illustrated in Fig. 6.17.

6.5.2 Evaluation of current proposals

6.5.2.1 Transverse patch loading and shear force

An interaction equation calibrated for slender steel-plated girders has been proposed so far only by Roberts and Shahabian [101, 116]. The proposals by Elgaaly [41] and Zoetemeijer [126] do not meet the requirements of steel plated girders because they have been proposed either for cold-formed trapezoidal beams or European rolled sections. The comparison with existing data from the literature review shows that they are not appropriate for

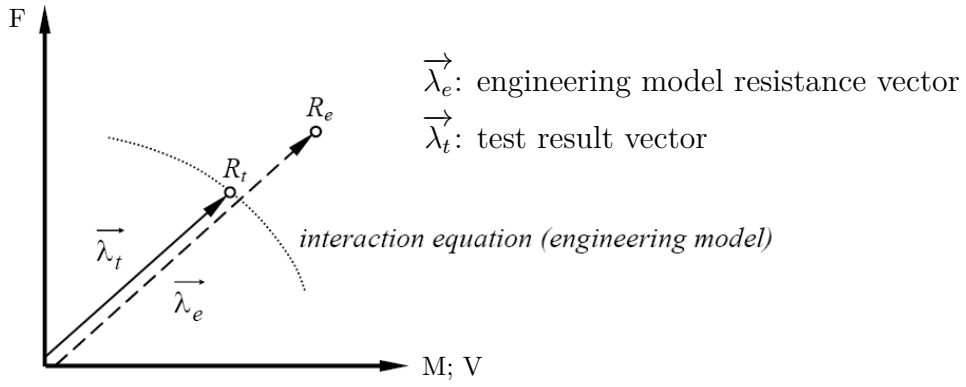

Figure 6.17: Vectorial comparison of test result R_e and engineering model resistance R_t

Table 6.1: Statistical evaluation of interaction equations from literature

interaction equation model	mean value	standard deviation	lower 5 %-fractile
Zoetemeijer [126]	0.930	0.054	0.842
Elgaaly [41]	0.954	0.053	0.867
Roberts and Shahabian [101, 116]	1.025	0.054	0.936

slender plates. In fact, Oxfort and Gauger [87] dealt with slender girders but there have been only few data points available making a reasonable proposal virtually impossible. For high levels of shear the recommendation is overconservative whereas for high levels of patch loading the resistance becomes unsafe due to overestimation. From Fig. 6.18 it becomes obvious that the proposals of Elgaaly [41], Zoetemeijer [126] and Oxfort and Gauger [87] are not suitable to describe properly the interaction behaviour of plated I-girders.

The interaction equations as proposed by Zoetemeijer [126] and Elgaaly [41] underestimate the interaction behaviour so that the mean value of the data cloud is below the curves drawn in Fig. 6.18. Although the interaction equation as defined by Roberts and Shahabian [101, 116] underestimates in some cases the interaction behaviour, it will be compared to the experimental and numerical results which have been gained in this project and the reasons for the discrepancy of values which are not on the safe side will be given. According to Eq. 6.4 the proposal of Roberts and Shahabian [101, 116] reads:

$$\left(\frac{V - 0.5 \cdot F}{V_R}\right)^2 + \frac{F}{F_R} \leq 1 \tag{6.4}$$

This interaction equation is drawn in Fig. 6.18 along with the experimental data available from literature and the own experimental studies. In addition, the results from the numerical study are split in this diagram into short relative loading lengths up to $s_s/h_w \leq 0.25$ and for relative loading lengths with $s_s/h_w > 0.25$. The existing curve has

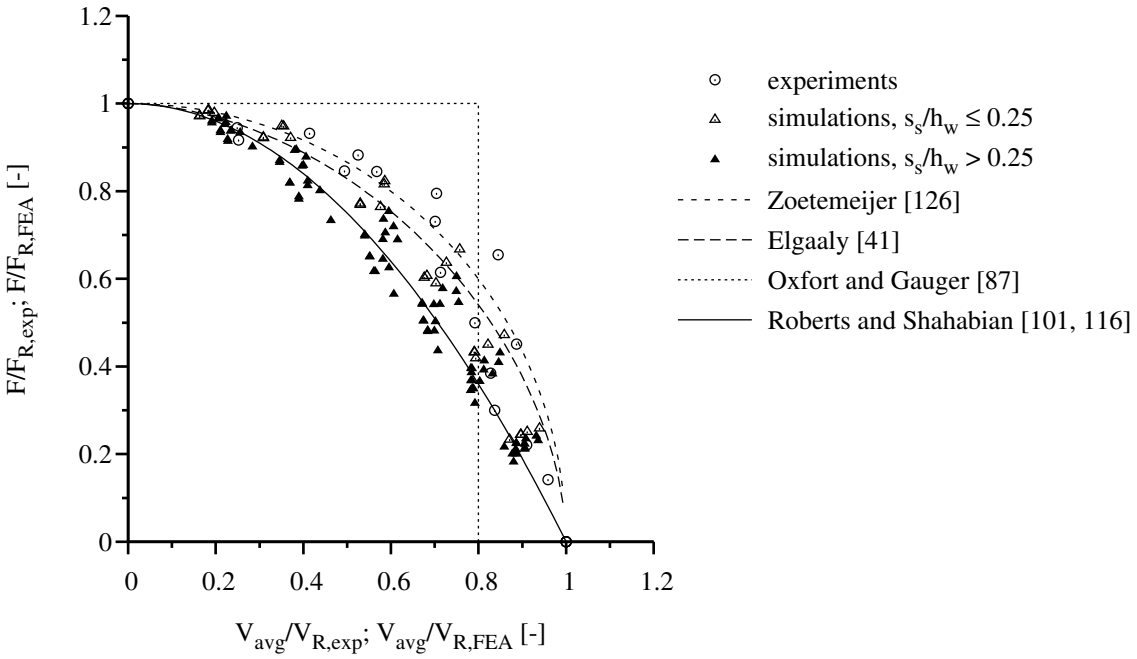

Figure 6.18: Comparison of F-V interaction equations, F_R and V_R according to experiments or based on FEA

been adopted on the basis of the test series of Roberts and Shahabian [101, 116] but it can be approved also for the numerical parameter study if the loading length does not exceed $s_s/h_w = 0.25$. This is the main limitation which applies to the interaction equation as defined by Roberts and Shahabian [101, 116].

6.5.2.2 Transverse patch loading and bending moment

Plates under transverse patch loading are unavoidably subjected to bending moment. Since the interaction between transverse patch loading and bending moment (F-M) generally governs the dimensioning, this interaction already was the topic in a number of research works, e.g. [8, 42, 65, 96, 119]. Several interaction equations were proposed. A comprehensive summary of interaction equations can be found e.g. in [77] and a good description of the interaction behaviour is given e.g. in [24]. The following proposals exist:

- Ungermann [119]

$$\frac{F}{F_R} + \frac{M}{M_R} \leq 1.4 \tag{6.5}$$

- Elgaaly [42]

$$\left(\frac{F}{F_R}\right)^3 + \left(\frac{M}{M_R}\right)^3 \leq 1 \tag{6.6}$$

- Bergfelt [8]

$$\left(\frac{F}{F_R}\right)^8 + \left(\frac{M}{M_R}\right)^2 \leq 1 \tag{6.7}$$

- Roberts [96]

$$\left(\frac{F}{F_R}\right)^2 + \left(\frac{M}{M_R}\right)^2 \leq 1 \tag{6.8}$$

- Johansson and Lagerqvist [65]

$$\frac{F}{F_R} + 1.25 \cdot \frac{M}{M_R} \leq 1.75 \tag{6.9}$$

- Section 7.2, EN 1993-1-5 [46]

$$\frac{F}{F_R} + 0.8 \cdot \frac{M}{M_R} \leq 1.4 \tag{6.10}$$

Equation 6.10 has been adopted in Sec. 7.2, EN 1993-1-5 [46], for both rolled and welded sections. Figure 6.19 exemplarily shows the equations given and the bending moment reference strength according to Chapter 4, EN 1993-1-5 [46], for girders without longitudinal stiffener. They have in common that they have been formulated based on reference strengths according to resistance models and not according to experimental and numerical basic loadings. Results of the statistical evaluation are given in Tables 6.2 to 6.4 for welded and rolled sections. Although all proposals refer to EN reference strengths here, which might not have been the case when they were proposed, it can be seen that they lead to similar statistical parameters such as mean value, standard deviation and fractile values. The proposal of Roberts, see Eq. 6.8, is the most conservative one, whereas the proposal of Bergfelt, see Eq. 6.7 is the most favourable one. Moreover, it can be shown that the trilinear approach of Sec. 7.2, EN 1993-1-5 [46], see Eq. 6.10, is a justifiable though simple approach. In [67] it was adopted for both rolled and welded section although the statistical data gives a rather small 5 %-fractile of 0.902 for rolled girders, see Table 6.4. The fact that a lot of uncertainty is associated with the tests on rolled girders and that only one data point clearly falls inside the interaction curve led to this decision. In the overall evaluation the high number of welded sections dominates and increases the 5 %-fractile to become larger than 1, see Table 6.2. Two questions remain: how does the interaction equation perform for girders with longitudinal stiffener and what effect does the use of advanced resistance models for patch loading have?

Figure 6.20 shows the EN interaction equation in relation to EN reference strengths for girders with longitudinal stiffener. It can be shown that the interaction equation is generally applicable. The data points inside the interaction curve are a result of the inadequate patch loading resistance model. Statistical parameters are given in Table 6.5.

Table 6.2: Statistical evaluation of interaction equations for girders without longitudinal stiffener, all sections, F_R and M_R according to Chapters 4 and 6, EN 1993-1-5 [46], see Fig. 6.19

interaction equation model	mean value	standard deviation	lower 5 %-fractile
Bergfelt [8]	1.496	0.284	1.029
Johansson and Lagerqvist [65]	1.499	0.278	1.042
Elgaaly [42]	1.508	0.274	1.058
Ungermann [119]	1.523	0.262	1.092
Roberts [96]	1.543	0.257	1.120
Sec. 7.2, EN 1993-1-5 [46]	1.503	0.276	1.050

Table 6.3: Statistical evaluation of interaction equations for girders without longitudinal stiffener, welded sections, F_R and M_R according to Chapters 4 and 6, EN 1993-1-5 [46], see Fig. 6.19

interaction equation model	mean value	standard deviation	lower 5 %-fractile
Bergfelt [8]	1.541	0.264	1.107
Johansson and Lagerqvist [65]	1.544	0.258	1.120
Elgaaly [42]	1.552	0.254	1.134
Ungermann [119]	1.567	0.239	1.174
Roberts [96]	1.584	0.237	1.193
Sec. 7.2, EN 1993-1-5 [46]	1.548	0.255	1.128

The quality of the resistance models for transverse patch loading was a topic in research works over the last years and improvements were proposed as summarised in Sec. 2.4. In Figs. 6.21 to 6.23 the advanced resistance models are compared to the EN interaction equation. For girders without longitudinal stiffener, see Fig. 6.21, the improvements of Gozzi's resistance model clearly lead to a smaller mean value and standard deviation if the bottom lines of Tables 6.2 to 6.4 are compared to Table 6.6. It gives a justifiable 5 %-fractile for the welded sections. For rolled sections, however, the interaction is not appropriate anymore. Since rolled section are not in the scope of this work, they will be disregarded in the following but this is an important conclusion which should be noted.

For girders with longitudinal stiffener both Davaine's and Clarin's resistance model lead to a similar improvement as Gozzi's resistance model for girders without longitudinal stiffener. It should be noted that some unsafe results which were existent when the EN reference strength was used are corrected. The statistical evaluation according to Tables 6.22 and 6.23 indicate an improved mean value and standard deviation, with slightly better results for Clarin's resistance model. In both cases the EN interaction equation is still on the safe side and may be in principle further used for welded sections.

A small numerical study in [24] compared the interaction cases of girders with longitudinal stiffener to basic loadings which have been determined by simulations in the same

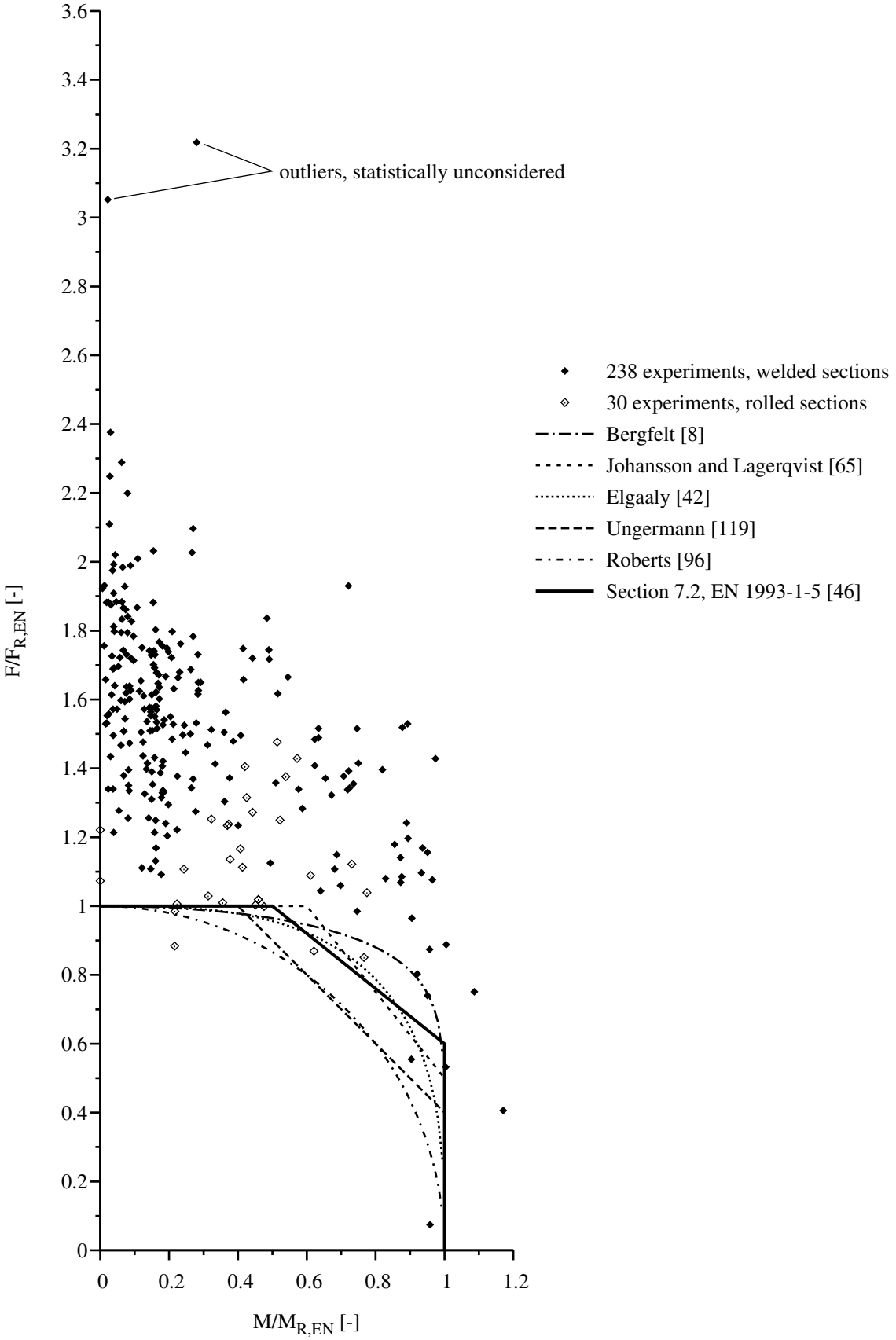

Figure 6.19: Comparison of F-M interaction equations, girders without longitudinal stiffener, F_R and M_R according to Chapters 4 and 6, EN 1993-1-5 [46]

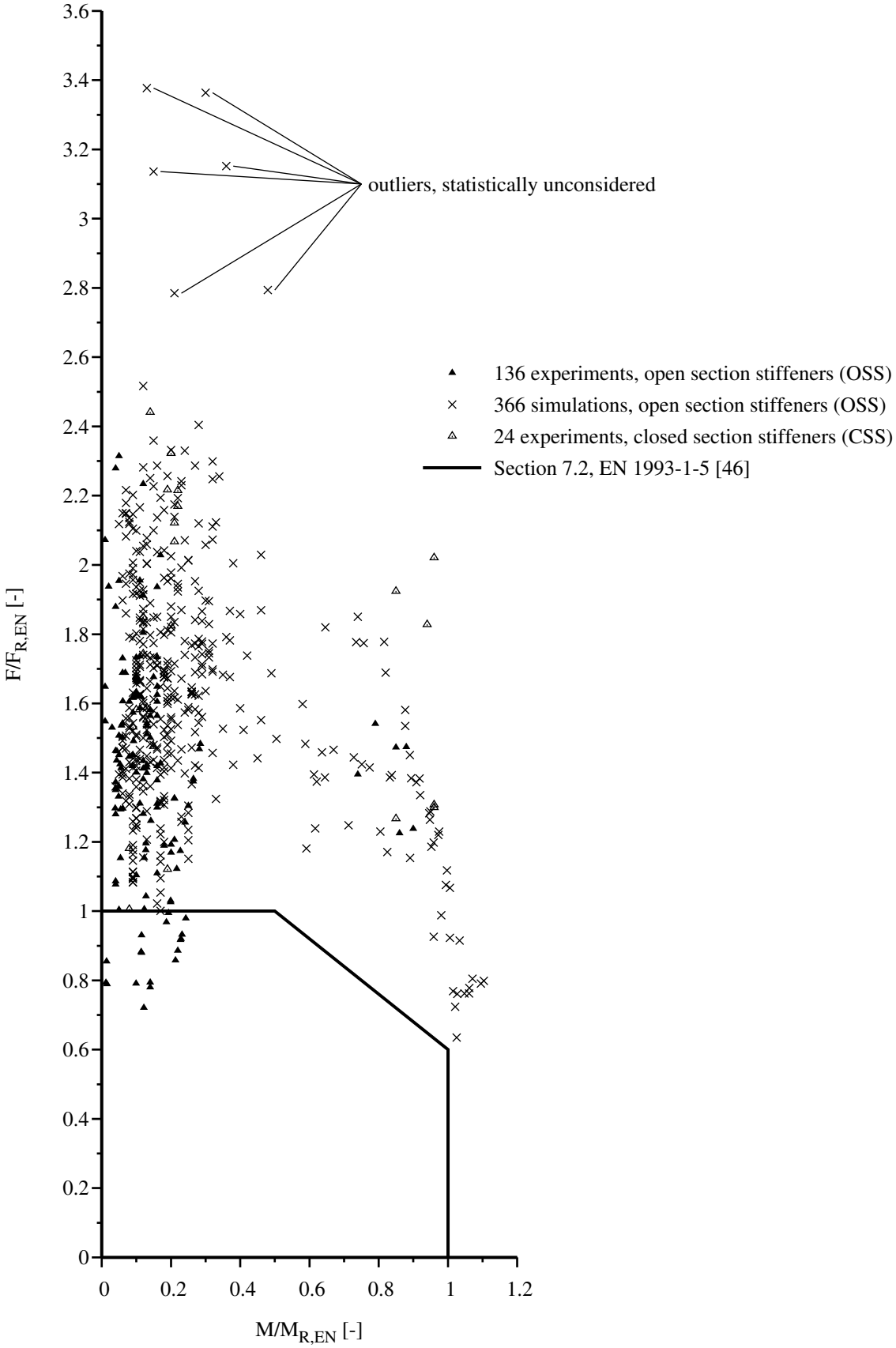

Figure 6.20: F-M interaction according to EN 1993-1-5 [46], girders with longitudinal stiffener, F_R and M_R according to Chapters 4 and 6, EN 1993-1-5 [46]

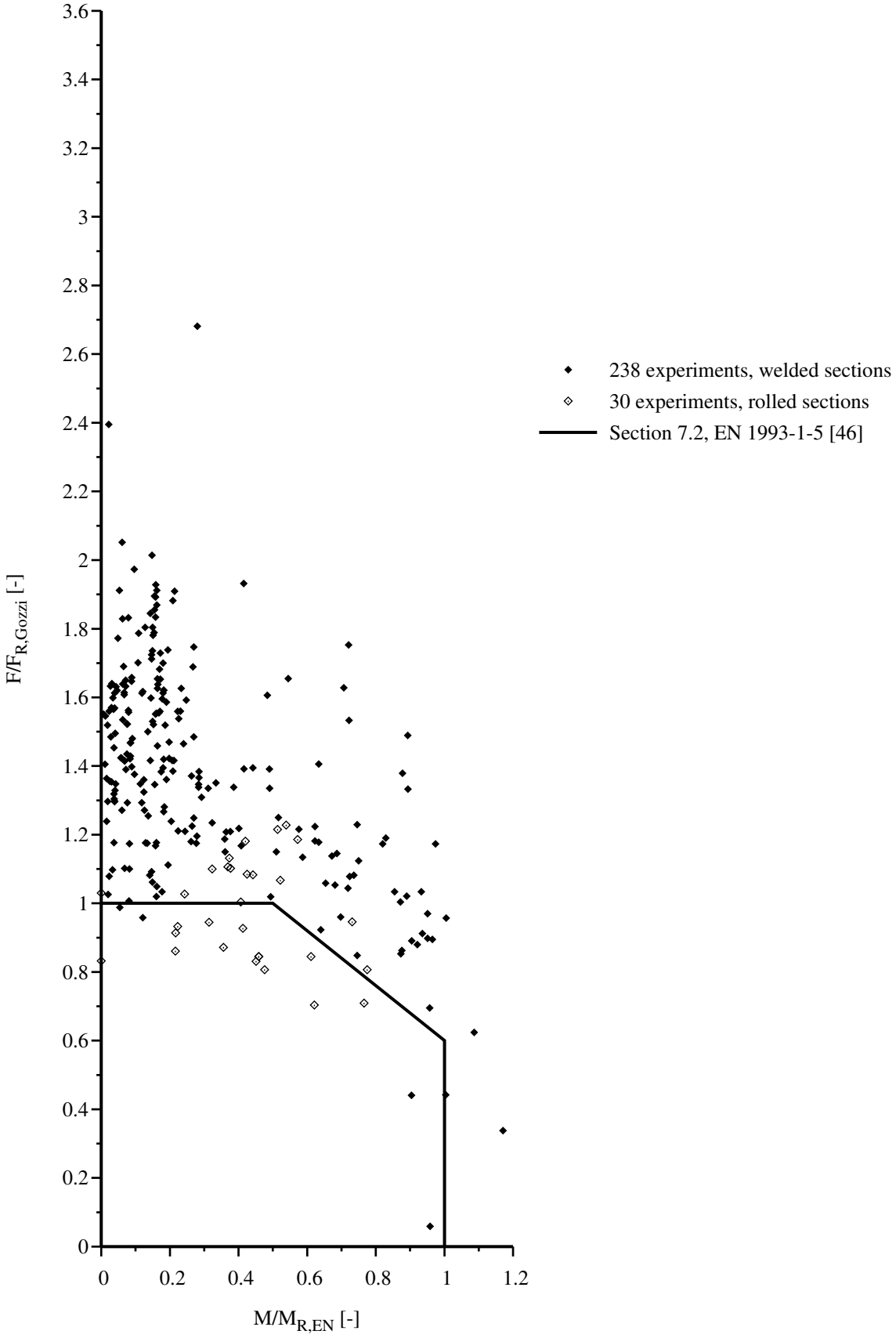

Figure 6.21: F-M interaction according to EN 1993-1-5 [46], girders without longitudinal stiffener, F_R according to Gozzi [56], M_R according to Chapter 4, EN 1993-1-5 [46]

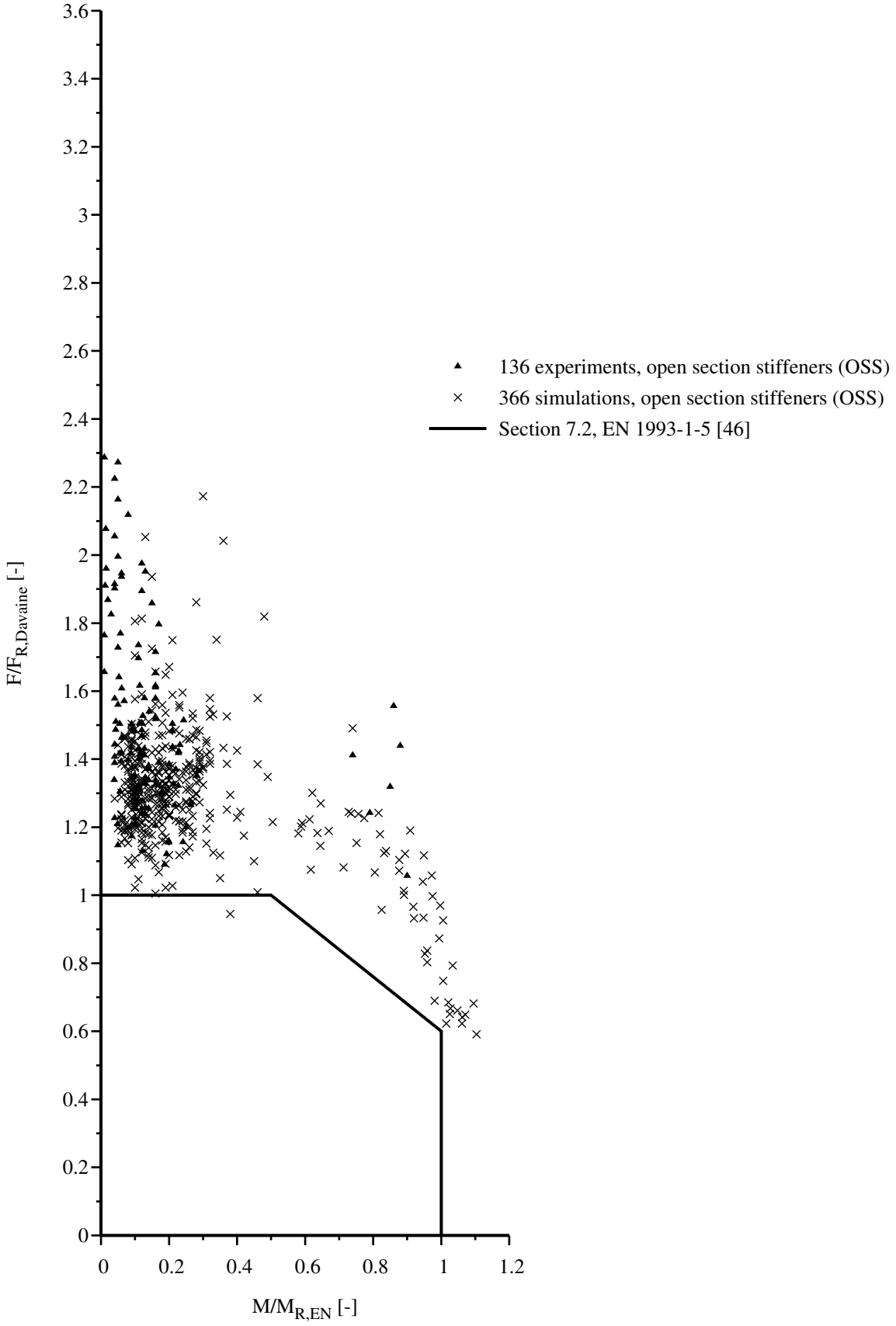

Figure 6.22: F-M interaction according to EN 1993-1-5 [46], girders with longitudinal stiffener, F_R according to Davaine [24], M_R according to Chapter 4, EN 1993-1-5 [46]

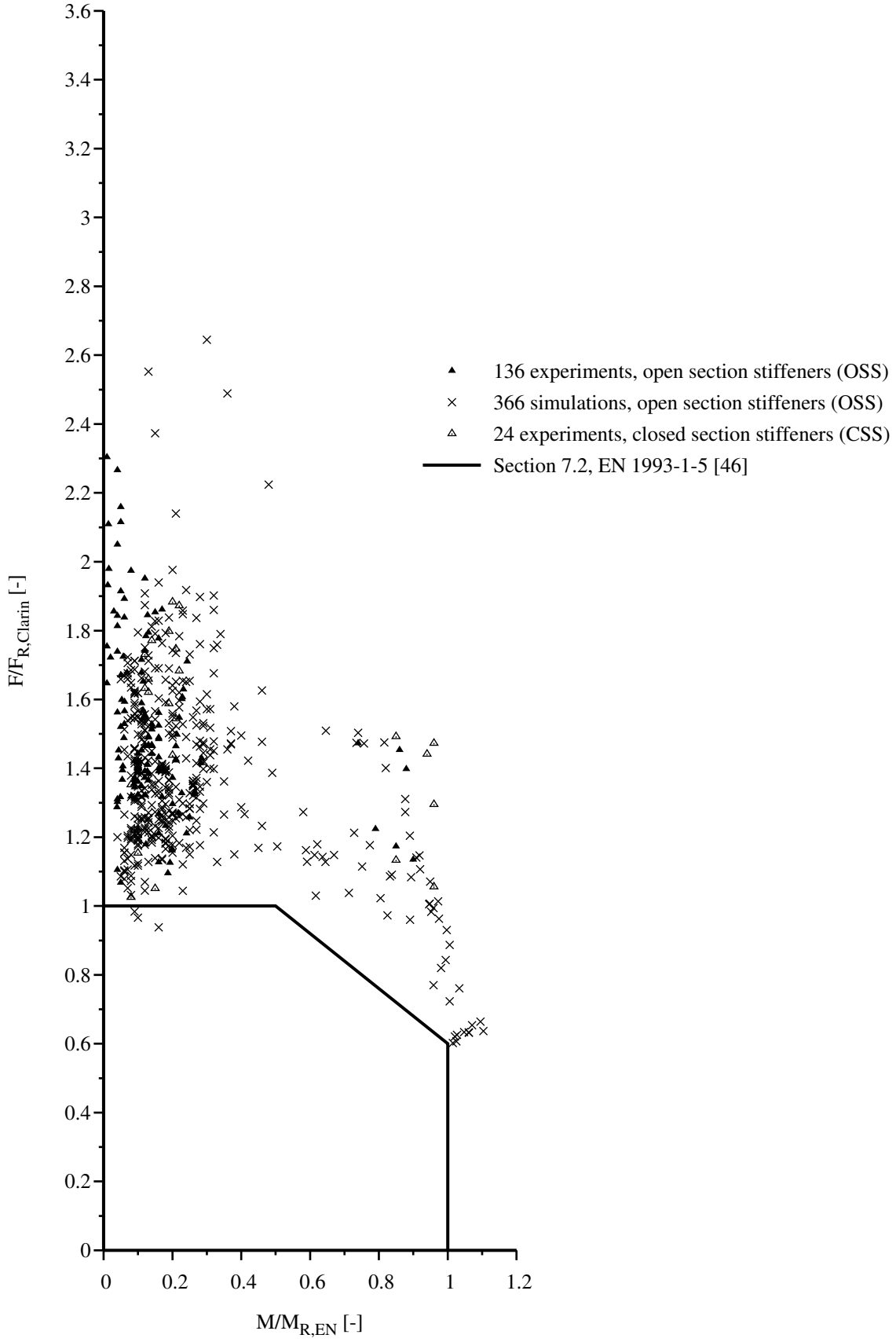

Figure 6.23: F-M interaction according to EN 1993-1-5 [46], girders with longitudinal stiffener, F_R according to Clarin [19], M_R according to Chapter 4, EN 1993-1-5 [46]

Table 6.4: Statistical evaluation of interaction equations for girders without longitudinal stiffener, rolled sections, F_R and M_R according to Chapters 4 and 6, EN 1993-1-5 [46], see Fig. 6.19

interaction equation model	mean value	standard deviation	lower 5 %-fractile
Bergfelt [8]	1.141	0.159	0.880
Johansson and Lagerqvist [65]	1.146	0.154	0.893
Elgaaly [42]	1.164	0.156	0.908
Ungermann [119]	1.175	0.148	0.932
Roberts [96]	1.223	0.163	0.955
Sec. 7.2, EN 1993-1-5 [46]	1.152	0.152	0.902

Table 6.5: Statistical evaluation of the EN interaction equation for girders with longitudinal stiffener, F_R and M_R according to Chapters 4 and 6, EN 1993-1-5 [46], see Fig. 6.20

type of longitudinal stiffening	mean value	standard deviation	lower 5 %-fractile
OSS, experiments	1.403	0.322	0.873
OSS, simulations	1.638	0.305	1.136
CSS	1.756	0.393	1.110
all	1.587	0.330	1.045
OSS, simulations*	1.659	0.350	1.083
all*	1.603	0.363	1.006

* including the six outliers

Table 6.6: Statistical evaluation of the EN interaction equation for girders without longitudinal stiffener, F_R according to Gozzi [56], M_R according to Chapter 4, EN 1993-1-5 [46], see Fig. 6.21

type of section	mean value	standard deviation	lower 5 %-fractile
welded	1.453	0.232	1.072
rolled	1.077	0.137	0.852
all	1.411	0.253	0.995

Table 6.7: Statistical evaluation of the EN interaction equation for girders with longitudinal stiffener, F_R according to Davaine [24], M_R according to Chapter 4, EN 1993-1-5 [46], see Fig. 6.22

type of longitudinal stiffening	mean value	standard deviation	lower 5 %-fractile
OSS, experiments	1.494	0.264	1.061
OSS, simulations	1.307	0.137	1.082
CSS	1.661	0.287	1.189
all	1.366	0.208	1.024
OSS, simulations*	1.316	0.157	1.057
all*	1.372	0.216	1.017

* including the six outliers

Table 6.8: Statistical evaluation of the EN interaction equation for girders with longitudinal stiffener, F_R according to Clarin [19], M_R according to Chapter 4, EN 1993-1-5 [46], see Fig. 6.23

type of longitudinal stiffening	mean value	standard deviation	lower 5 %-fractile
OSS, experiments	1.515	0.245	1.112
OSS, simulations	1.381	0.206	1.041
CSS	1.523	0.247	1.118
all	1.419	0.226	1.047
OSS, simulations*	1.396	0.239	1.002
all	1.429	0.246	1.024

* including the six outliers

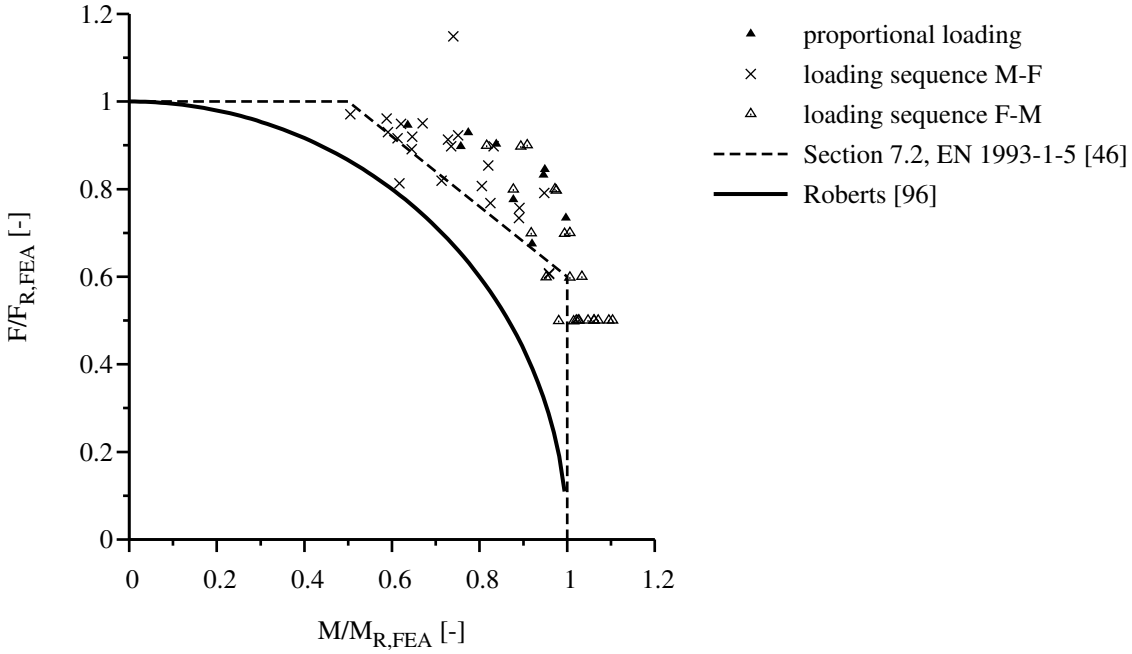

Figure 6.24: F-M interaction according to a small study by Davaine [24], girders with longitudinal stiffener, reference strengths based on FEA

study. It is concluded that the interaction criterion according to Sec. 7.2, EN 1993-1-5 [46], should be only used with values for F_R and M_R which are calculated according to Chapters 4 and 6, EN 1993-1-5 [46]. When numerically based results are used for the determination of F_R, it is concluded that the Roberts criterion, see Eq. 6.8, seems to be more appropriate. Figure 6.24 shows the results of the study. It can be shown that though different loading paths were studied, the data points are rather homogenous except for two outliers. The Roberts interaction which is recommended in [24] is definitely conservative and may be too strict.

It is assumed that mainly due to the large number of test results no experimental reference strengths have been determined as this has been done for the F-V test series by Roberts and Shahabian [101, 116] which makes it difficult to draw a concise conclusion. Therefore, Sec. 6.5.3.2 aims to improve the F-M interaction equation with focus on its consistency with the F-V interaction.

6.5.3 Proposal for improved design rules

6.5.3.1 Transverse patch loading and shear force (F-V)

Following the principles which were set up in Secs. 6.2 and 6.3, an interaction equation which is applicable in the framework of EN 1993-1-5 is developed.

In Fig. 6.25 the interaction diagram with reference strengths based on experimental and numerical basic loadings and average shear force definition is given. It was shown that

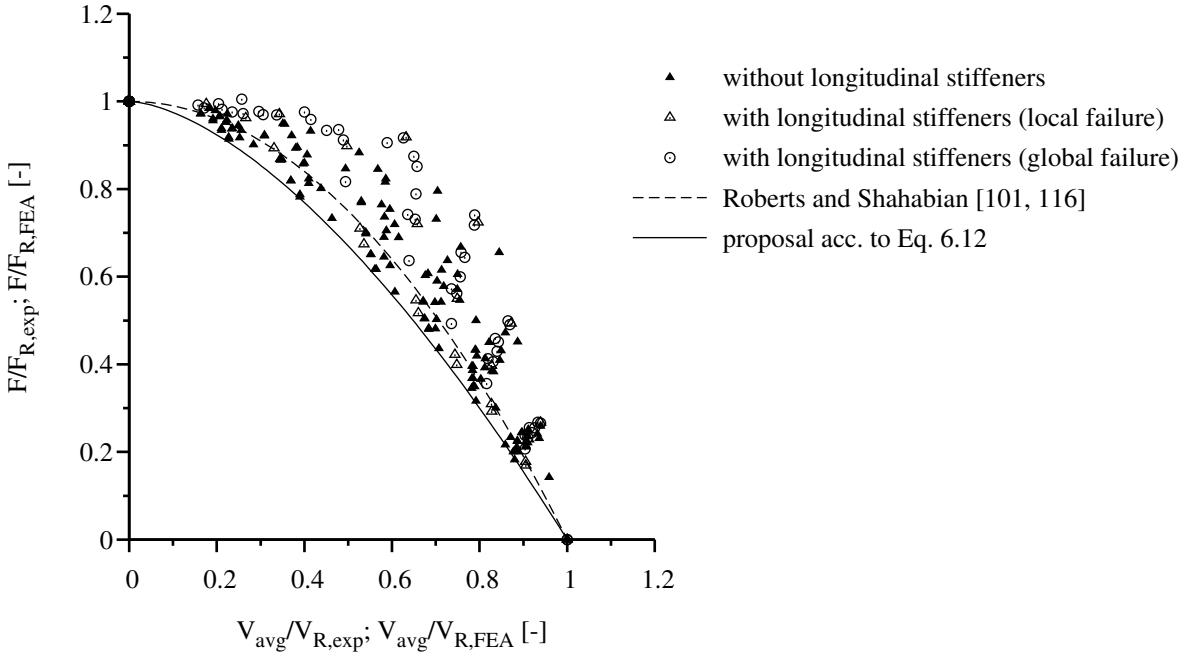

Figure 6.25: Curve fitting of the F-V interaction equation, F_R and V_R according to experiments or based on FEA

the proposed interaction equation of Roberts and Shahabian [101, 116] is only valid for relative loading lengths up to $s_s/h_w \leq 0.25$ so that the formulation of a new interaction equation is required to ensure e.g. the applicability to bridge launching situations with long loading lengths. Based on the least squares error method a new curve is fitted as lower bound to the data. The interaction equation is based on the general format as given in Eq. 6.11.

$$\left(\frac{F}{F_R}\right)^b + \left(\frac{V - 0.5 \cdot F}{V_R}\right)^a \leq 1.0 \tag{6.11}$$

The parameters a and b are determined and rounded off to a single decimal place. The values $a = 1.6$ and $b = 1.0$ turn out to be appropriate so that:

$$\frac{F}{F_R} + \left(\frac{V - 0.5 \cdot F}{V_R}\right)^{1.6} \leq 1.0 \tag{6.12}$$

Equation 6.12 is shown in Fig. 6.25. The analysis in Sec. 5.5 showed that a further differentiation between girders without and with longitudinal stiffener, as well as other key parameters, is not feasible so that a single interaction criterion is kept. The proposal of Roberts and Shahabian [101, 116] is not explicitely considered in the following but it could be used for short loading lengths when the limit of $s_s/h_w \leq 0.25$ applies.

The appropriateness for girders without longitudinal stiffener as well as for the global and local buckling behaviour of girders with longitudinal stiffener will be justified by

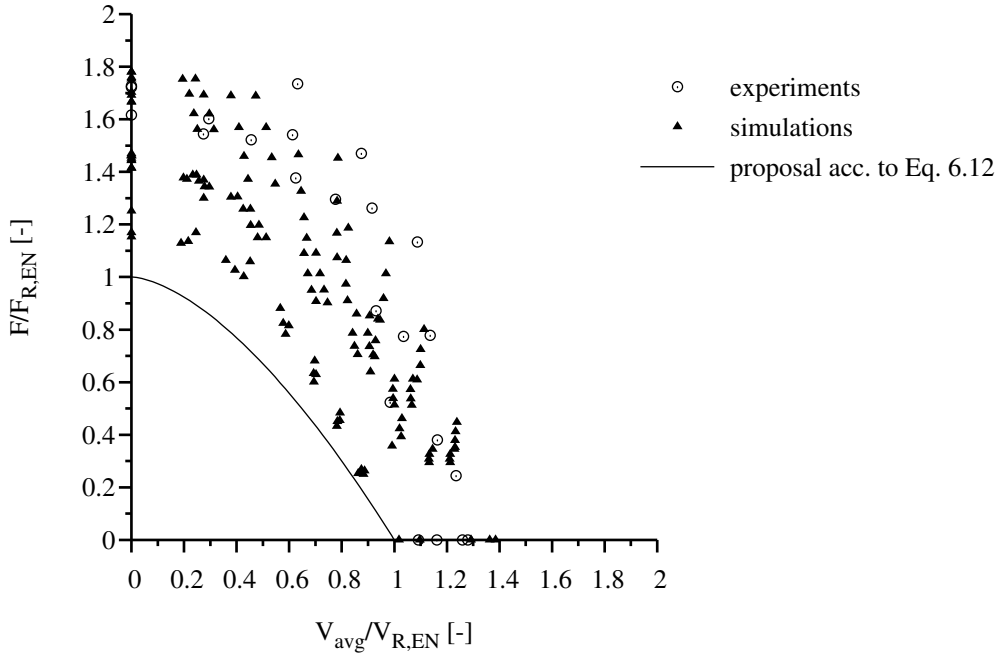

Figure 6.26: F-V interaction proposal, girders without longitudinal stiffener, F_R and V_R according to Chapters 5 and 6, EN 1993-1-5 [46]

a statistical analysis of the interaction equation with regard to the use with different resistance models for the transverse loading. With the statistics for a comparison between experimentally or numerically determined resistance R_e and calculated resistance R_t the different approaches are evaluated in the following.

Girders without longitudinal stiffener. The evaluation with EN reference strengths is given in Fig. 6.26. The data scatter for the shear resistance is low whereas the patch loading resistance is characterised by a wide dispersion of data.

Although the inaccuracy of the patch loading resistance model for slender girders shifts the data scatter along the x-axis, the high standard deviation leads to a lower 5 %-fractile of 1.099, see Table 6.9. It indicates that the interaction equation is approved, slightly on the safe side.

The question is whether the improved patch loading resistance model as proposed by Gozzi [56] still leads to appropriate results. Fig. 6.27 shows the results of the improved resistance model in the interaction diagram. It can be seen that the scatter is reduced for patch loading, thus resulting in a smaller standard deviation and shifting the data points closer to the interaction curve. The evaluation of the interaction equation gives a lower 5 %-fractile of 1.007, see Table 6.9. Thus, the proposed interaction equation can be taken as approved also for the improved resistance model by Gozzi [56].

Girders with longitudinal stiffener. In Fig. 6.28 the resistances according to EN 1993-1-5 [46] are compared to the proposed interaction equation for girders with longitudinal stiffener. Due to the high mean values of the patch loading resistance model based

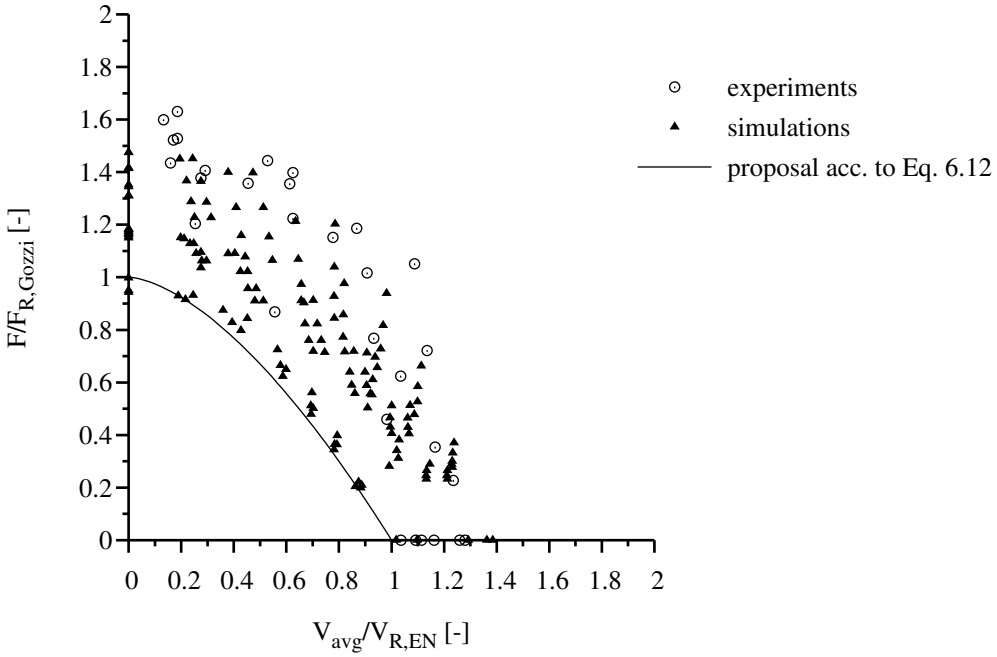

Figure 6.27: F-V interaction proposal, girders without longitudinal stiffener, F_R according to Gozzi [56], V_R according to Chapter 5, EN 1993-1-5 [46]

Table 6.9: Statistical evaluation of the F-V interaction proposal for girders without longitudinal stiffener

patch loading resistance model	mean value	standard deviation	lower 5 %-fractile
Chapter 6, EN 1993-1-5 [46]	1.458	0.219	1.099
Gozzi [56]	1.309	0.184	1.007

Table 6.10: Statistical evaluation of the F-V interaction proposal for girders with longitudinal stiffener

patch loading resistance model	mean value	standard deviation	lower 5 %-fractile
Chapter 6, EN 1993-1-5 [46]	1.752	0.215	1.398
Davaine [24]	1.574	0.139	1.346
Clarin [19]	1.556	0.126	1.348

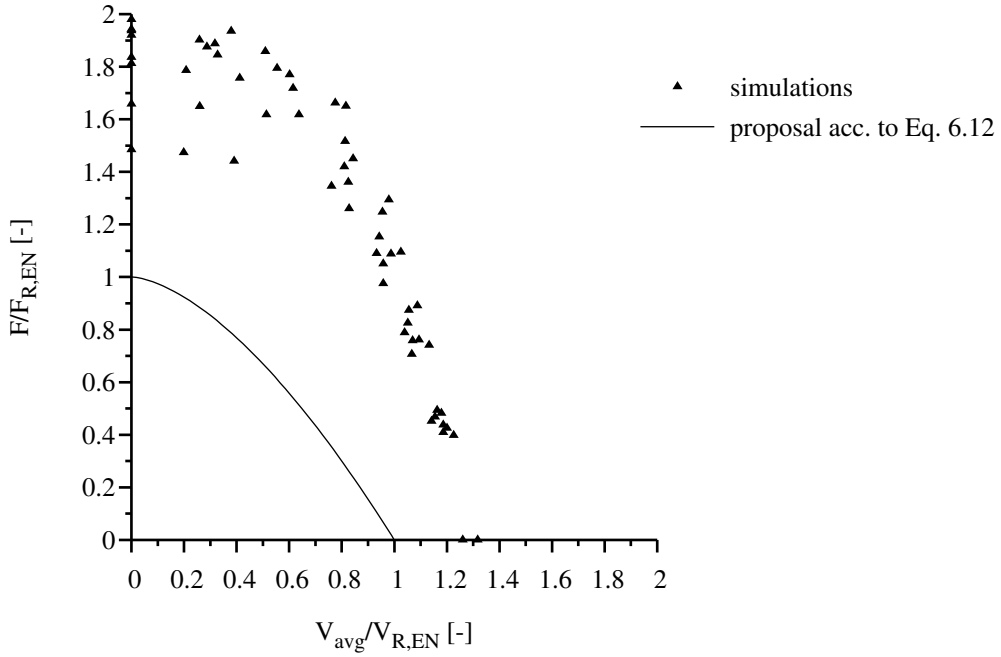

Figure 6.28: F-V interaction proposal, girders with longitudinal stiffener, F_R and V_R according to Chapters 5 and 6, EN 1993-1-5 [46]

on Graciano [57], the data scatter is significantly shifted away from the interaction curve. An improvement of the resistance function may shift the data closer to the interaction curve so that it becomes more relevant. However, as it has been shown in the studies on interaction behaviour, the global and local buckling phenomena are covered within the interaction range for the unstiffened cases so that it should be fulfilled even for more advantageous resistance models which will be studied below.

In Fig. 6.29 the interaction diagram is shown with the patch loading reference strength according to Davaine [24]. The improvement of the resistance model can be clearly seen because not only the points are shifted closer to the interaction curve but also the data scatter has been significantly reduced. However, the interaction equation is still on the safe side. Due to the fact that also girders with closed-section stiffeners are included in the calculation of the patch loading resistance, the data scatter is rather conservative because the torsional rigidities are not considered in the design procedures. Figure 6.30 shows the interaction diagram with the patch loading resistances according to Clarin [19]. Here, the improvement of the resistance model leads to a shift of the data scatter closer to the interaction curve. However, the results are still on the safe side. As the improvement in the design procedure of Clarin [19] is about the same as of Davaine [24], a very similar data scatter is found, see Table 6.10.

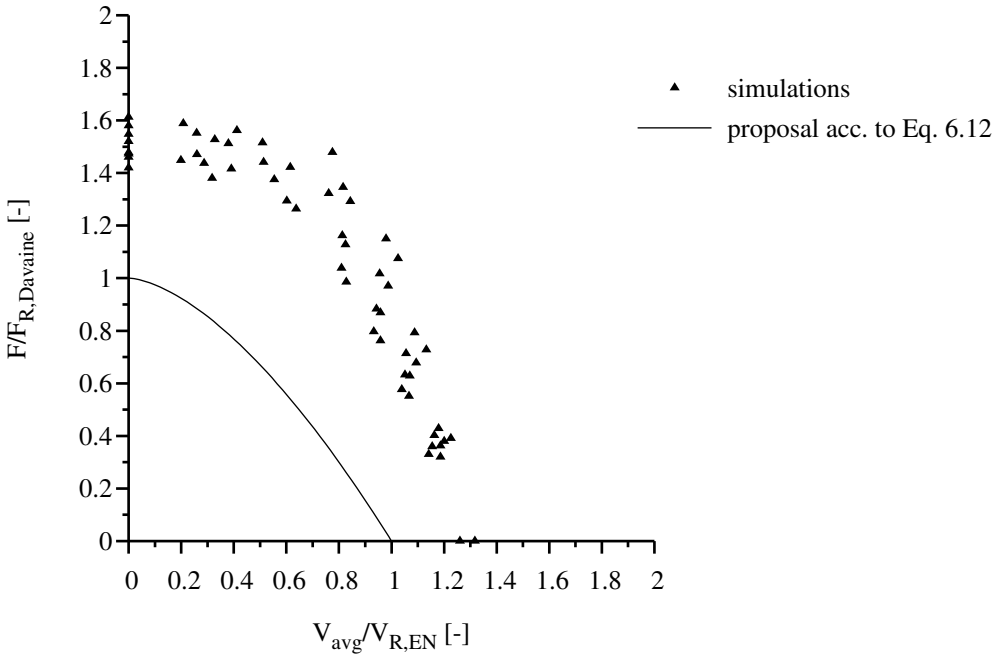

Figure 6.29: F-V interaction proposal, girders with longitudinal stiffener, F_R according to Davaine [24], V_R according to Chapter 5, EN 1993-1-5 [46]

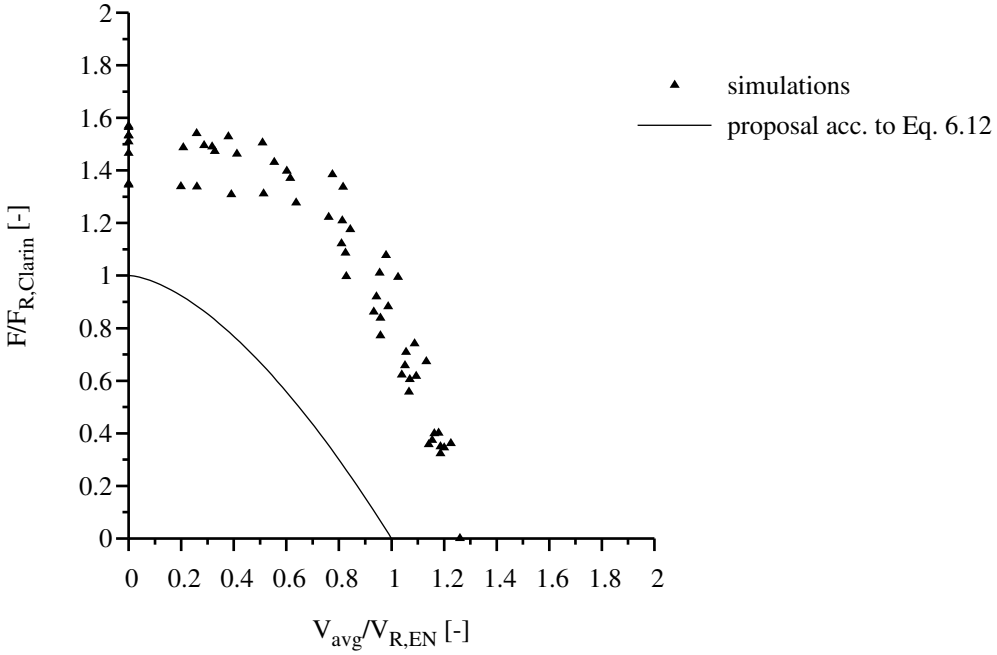

Figure 6.30: F-V interaction proposal, girders with longitudinal stiffener, F_R according to Clarin [19], V_R according to Chapter 5, EN 1993-1-5 [46]

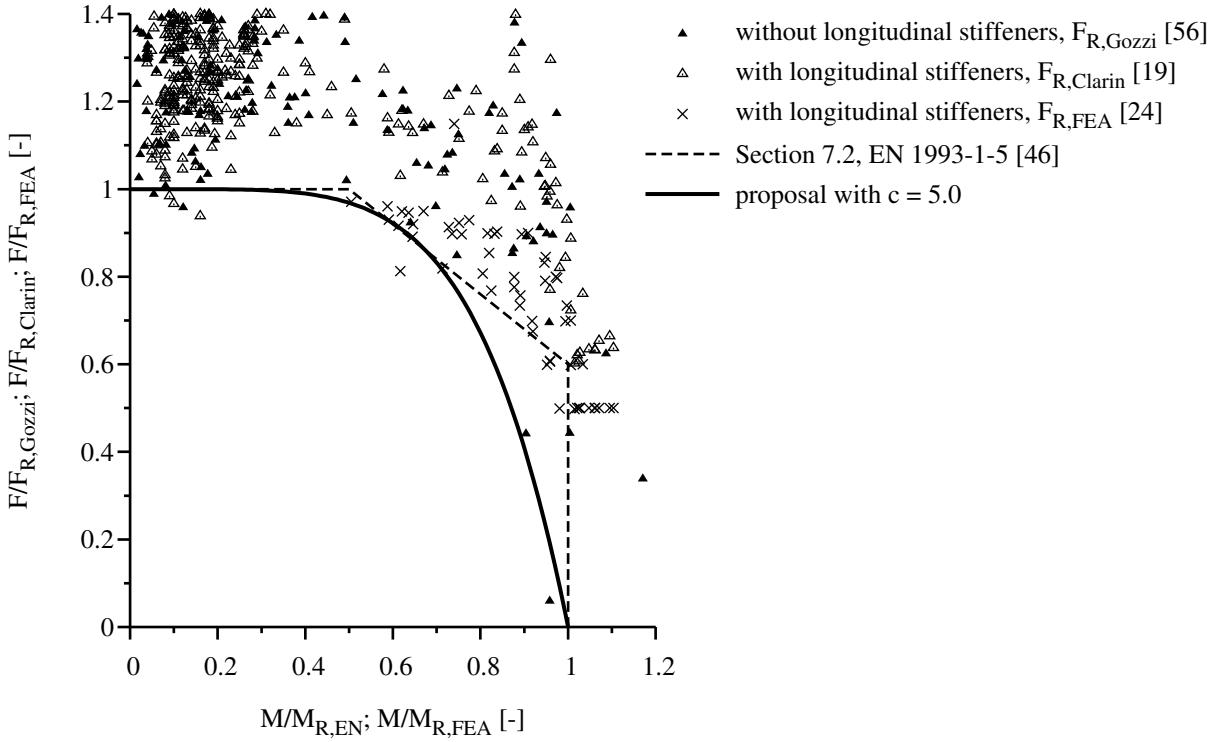

Figure 6.31: F-M interaction proposal, F_R according to the legend, M_R based on the relevant cross-section class

6.5.3.2 Enhancement of the F-V proposal with bending moment

Following the principles which were set up in Secs. 6.2 and 6.3, an interaction equation which can be consistently merged with the F-V proposal is derived on the basis of the general format according to Eq. 6.13 for the F-M interaction.

$$\frac{F}{F_R} + \left(\frac{M}{M_R}\right)^c \leq 1.0 \tag{6.13}$$

Equation 6.13 is fitted as lower bound curve to the data for welded girders without longitudinal stiffener based on Gozzi's resistance model, girders with longitudinal stiffener based on Clarin's resistance model and the results of Davaine's small study with numerically based reference strengths. The comparison is shown in Figs. 6.31 and 6.32. The difference between both figures is the reference strength which has been chosen as bending moment resistance. Data points inside the interaction curve are disregarded since they are close to the basic loading cases so that their deviation is considered as inherent to the resistance models for the reference strengths.

In Fig. 6.31 the reference strength for the bending moment resistance is based on the relevant cross-section class. The parameter c is determined and rounded off to a single decimal place so that $c = 5.0$. It can be shown that for high levels of bending moment the interaction curve hardly catches the distribution of data points. For that reason, the

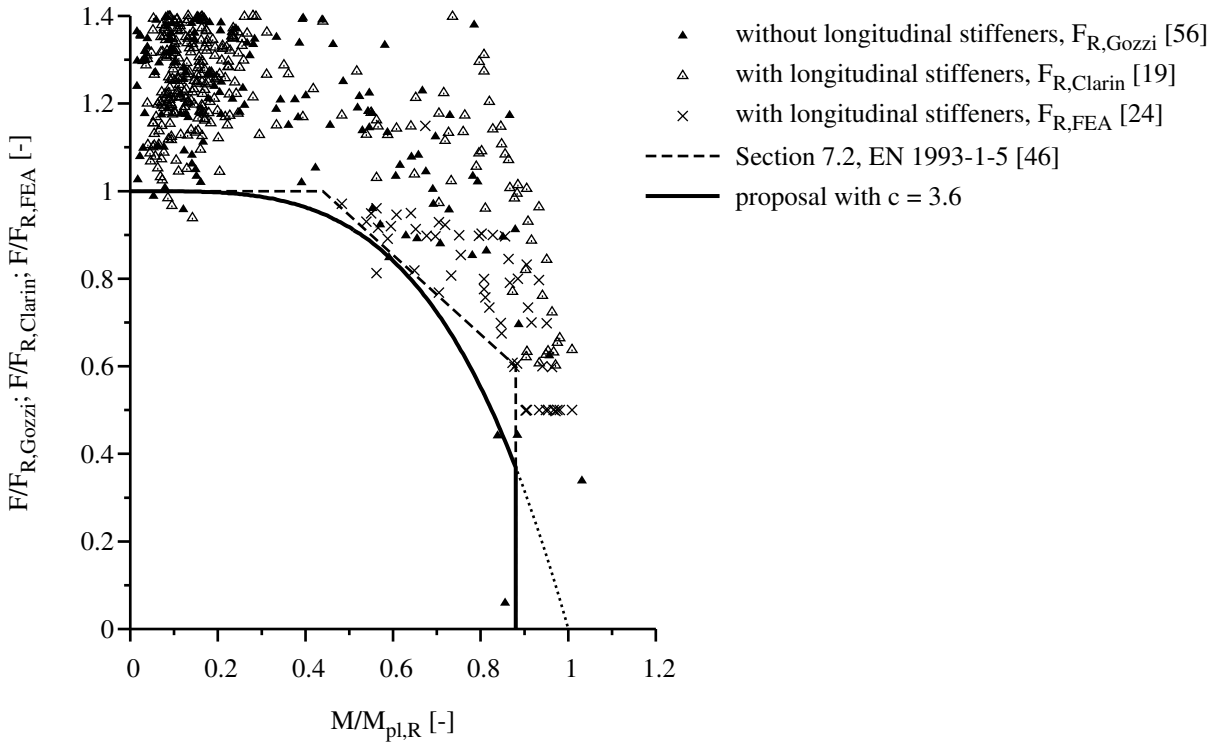

Figure 6.32: F-M interaction proposal, F_R according to the legend, $M_R = M_{pl,R}$ irrespective of the cross-section class (here: $M_{el,R}/M_{pl,R} = 0.88$)

plastic moment resistance irrespective of the cross-section class was chosen as reference strength as it is similarly used in the M-V interaction of Sec. 7.1, EN 1993-1-5 [46]. The parameter c is determined and rounded off to a single decimal place so that $c = 3.6$. The results are given in Fig. 6.32. It can be shown that the data is slightly more homogeneous though it is hardly perceptible. The statistical evaluation of both proposals which is given in Tables 6.12 and 6.13 supports this. In Table 6.11 the results when applying Sec. 7.1, EN 1993-1-5 [46] are given and a comparison shows that in both cases an improvement exists which can be identified by comparing especially the standard deviation. It should be noted that in terms of statistical quality both proposals are almost identical.

However, there are two advantages of the proposal based on the plastic bending moment resistance. The first one is the compatibility to Sec. 7.1, EN 1993-1-5 [46]. The second one is that for Class 1 and Class 2 cross-sections interaction becomes more strict. It can be seen from Fig. 6.33 that there is no cut-off since Class 1 and Class 2 cross-sections use the plastic bending moment resistance by themselves. When comparing test results for high levels of bending moment, Fig. 6.33 shows that in fact no results are available and a more favourable curve might be nothing else than a good guess. This consistency and the data scatter which is perceived to be slightly more homogeneous leads to the adoption of the plastic bending moment resistance as reference value.

Finally, the consistent definition of the F-V and F-M interaction equations as continuous function enables the merging of both criteria. The full F-M-V interaction equation may

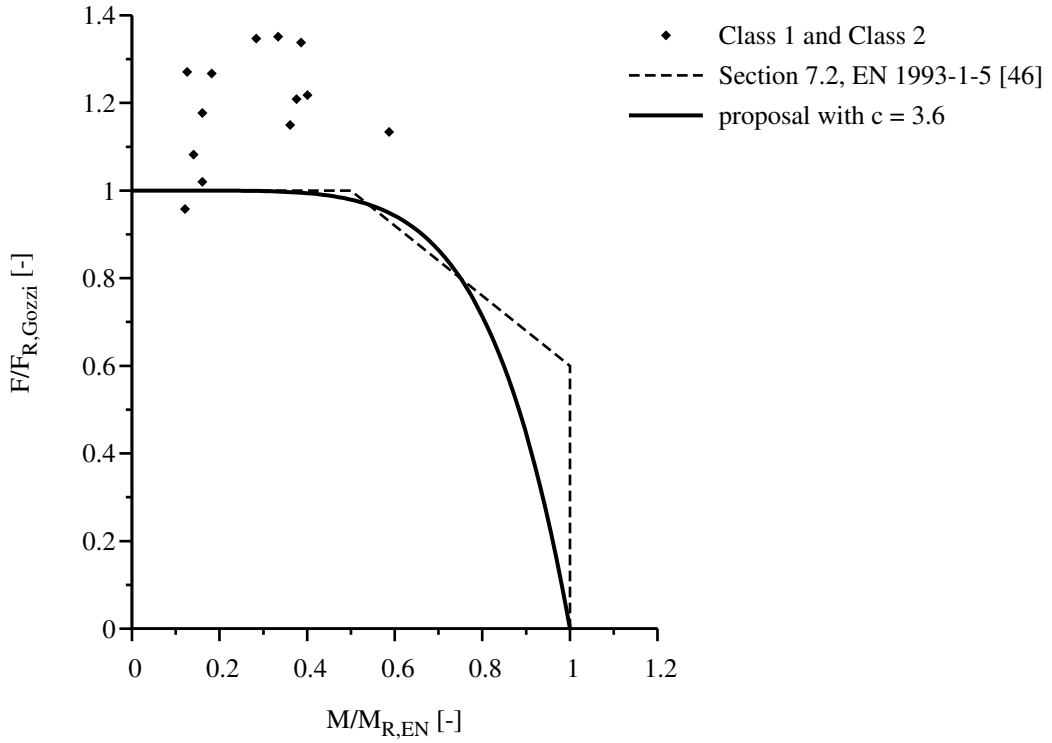

Figure 6.33: F-M interaction proposal applied to Class 1 and Class 2 cross-sections, F_R according to Gozzi [56], $M_R = M_{pl,R}$

Table 6.11: Statistical evaluation of the EN interaction equation, F_R and M_R according to EN 1993-1-5 [46]

type of longitudinal stiffening	mean value	standard deviation	lower 5 %-fractile
unstiffened	1.548	0.255	1.128
stiffened	1.598	0.315	1.080
all	1.583	0.300	1.090

Table 6.12: Statistical evaluation of the proposal with $c = 5.0$, F_R according to the table, $M_R = M_{R,EN}$ based on the relevant cross-section class

type of longitudinal stiffening	mean value	standard deviation	lower 5 %-fractile
unstiffened, $F_{R,Gozzi}$ [56]	1.462	0.243	1.063
stiffened, $F_{R,Clarin}$ [19]	1.456	0.224	1.088
all	1.458	0.229	1.081

Table 6.13: Statistical evaluation of the proposal with $c = 3.6$, F_R according to the table, $M_R = M_{pl,R}$ irrespective of the cross-section class

type of longitudinal stiffening	mean value	standard deviation	lower 5 %-fractile
unstiffened, $F_{R,Gozzi}$ [56]	1.466	0.242	1.068
stiffened, $F_{R,Clarin}$ [19]	1.466	0.224	1.098
all	1.466	0.229	1.089

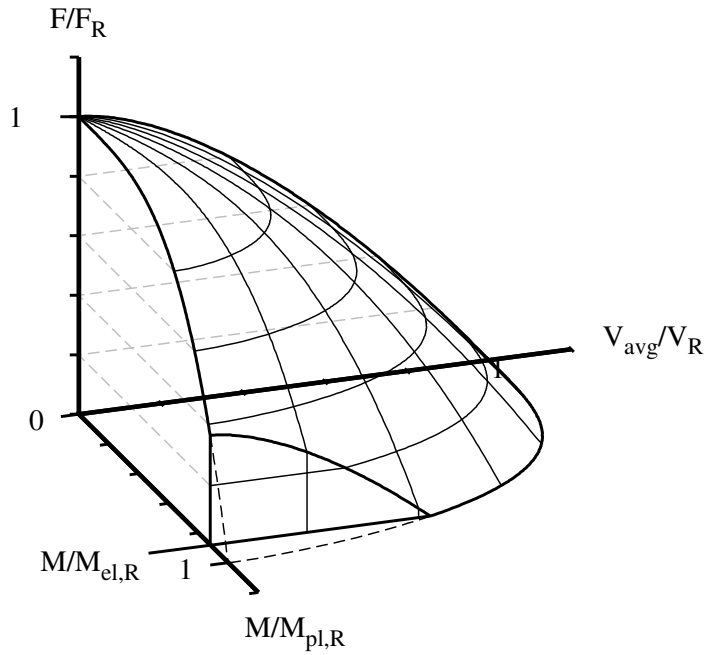

Figure 6.34: F-M-V interaction surface (here: $M_{el,R}/M_{pl,R} = 0.88$)

be written according to Eq. 6.14. The interaction surface is shown in Figure 6.34.

$$\frac{F}{F_R} + \left(\frac{M}{M_{pl,R}}\right)^{3.6} + \left(\frac{V_{avg}}{V_R}\right)^{1.6} \leq 1.0 \tag{6.14}$$

A formulation for an implementation in a future revision of EN 1993-1-5 has been prepared and is given in Annex C.

6.6 Conclusions

Based on the work of the previous chapters, evident and necessary improvements regarding the interaction criteria of steel plates were developed in this chapter. At the beginning, considerations on the formulation of interaction criteria and verification points were made in general. In detail, a modification of the reduced stress method based on a single plate

slenderness for biaxially loaded steel plates and a new interaction equation for the effective width method in case of transverse patch loading, bending moment and shear force have been proposed. A formulation for an implementation in a future revision of EN 1993-1-5 has been prepared and is given in Annex C. Both proposals are summarised below.

Reduced stress method. The consideration of favourable tensile stresses and influence of deviation forces for small slendernesses are clear advantages of Chapter 10, EN 1993-1-5 [46], in comparison to DIN 18800-3 [28] and DNV-RP-C201 [33]. The effect of tensile stresses has not been studied in this work, however, the latter issue turns out to be a requirement which has been neglected in DIN 18800-3 [28] so far.

For square plates it can be shown that a linear interaction is approached the more slender the plate becomes. As a result the proposed interaction curves coincide with DIN 18800-3 [28]. However, for small slendernesses a stronger interaction needs to be taken into account so that the proposed interaction equation becomes the most conservative one. For panel aspect ratios other than square the imperfection shape has a strong influence on the curvature of the interaction curves. It has been shown that the linear interaction which DIN 18800-3 [28] assumes is too conservative there. On the other hand, the interaction according to Chapter 10, EN 1993-1-5 [46] is too favourable. Here, the proposed interaction equation is successfully able to take the positive influence of the imperfection shape into account. A formulation for an implementation in a future revision of EN 1993-1-5 has been prepared and is given in Annex C.

Effective width method. A comparison of the experimental and numerical F-V results with known tests from literature shows that the interaction between transverse patch loading and shear force is not negligible. The evaluation of interaction equations from literature leads to the conclusion that the proposals on the basis of cold-formed trapezoidal beams [41] and hot rolled sections [126] are not applicable to slender steel plates. Also the recommendation of Oxfort and Gauger [87] turns out to be inappropriate which is mainly due to the insufficient number of tested girders. On the other hand the interaction equation proposed by Roberts and Shahabian [101, 116] can be approved for short relative loading lengths of $s_s/h_w \leq 0.25$. For longer loading lengths their equation does not lead to safe results which requires the formulation of a new interaction equation. By choosing the verification point at the centerline of the transverse loading the part of the shear force which is induced by the transverse loading and which is already included in the resistance model can be accounted for. As a result not only the lowest data scatter is found but also a conclusive subdivision of the interaction cases into the basic loadings “transverse patch loading” and “shear force” is possible which makes an interaction verification for a pure transverse patch loading obsolete.

Plates under transverse patch loading are unavoidably subjected to bending moment so that this interaction has been already addressed in a number of research works. The performance of all proposals is similar and it could be shown that the trilinear approach of Sec. 7.2, EN 1993-1-5 [46] is simple though appropriate. However, the objective to propose a single F-M-V interaction equation leads to the development of an F-M interaction

equation which can be consistently merged with the F-V proposal. The verification point is naturally chosen at the centerline of the transverse loading which is usually also the location where the maximum bending moment occurs.

The proposed interaction criterion is based on the experimental and numerical data set from own work and from literature and a statistical evaluation proves the applicability of the equation not only to current EN resistance models but also to the improved resistance models developed by Gozzi [56], Davaine [24] and Clarin [19] for girders without and with longitudinal stiffener. A formulation for an implementation in a future revision of EN 1993-1-5 has been prepared and is given in Annex C. Chacon [16] developed a proposal for hybrid girders which is currently in the process of harmonisation with the proposal of Gozzi [56]. The applicability of the proposed interaction criterion should be finally checked with the relevant data.

7 Summary and outlook

7.1 Summary

In the frame of this work the stability behaviour of steel plates under selected load combinations was analysed and improved design rules were proposed for the following cases:

- Plates under biaxial compression and application of the reduced stress method based on a single plate slenderness
- Plate I-girder webs under transverse patch loading, bending moment and shear force (F-M-V) and application of the effective width method

In the initial step shortcomings of these two topics were identified in a review of design methods, code rules and earlier research work. Based on experimental studies, a numerical model was developed and its applicability was proven by the recalculation of buckling curves, own experiments and experiments from literature. The numerical model was then used for parameter studies in which key parameters were varied in order to develop improved design rules. The results of the studies are summarised below.

Plates under biaxial compression and application of the reduced stress method based on a single plate slenderness. The reduced stress method based on a single plate slenderness is contradictory to existing knowledge and simulation results on the stability behaviour of plates under biaxial compression for medium to high slendernesses. However, its application still leads to acceptable strengths in case both in-plane and rotational edge boundary conditions are conservatively considered as unconstrained and hinged. Nevertheless, reference strengths should consider boundary conditions as accurate as possible for several reasons. If certain effects are deliberately neglected on the side of the reference strengths, it is the author's opinion that the interaction criterion also should not take them into account. Thus, an improved interaction equation based on Chapter 10, EN 1993-1-5 [46], was developed which reflects the mechanically correct stability behaviour. As a result, reference strengths for the biaxial compression load case may now be used to account for actual edge boundary conditions, e.g. by using numerical methods to determine elastic critical loads more precisely, which fully contributes to numerically assisted verification procedures in the future.

On the other hand, it could be also shown that the reduced stress method based on a single plate slenderness is a step in the right direction for small slendernesses because the transition from the equivalent stress hypothesis to the reduction which is required for stocky plates becomes more consistent with simulation results.

Plate I-girder webs under transverse patch loading, bending moment and shear force (F-M-V) and application of the effective width method. The interaction between transverse patch loading and shear force is not negligible and the results from the small experimental study in [115] were confirmed. It was shown that the loading length is the most influential factor on the interaction behaviour which is not adequately considered in [115] so that a modification of the interaction criterion was required. By doing this, the transferability of the results to girders with longitudinal stiffener has been also checked for key parameters and their behaviour which may show global or local buckling is found to be covered by the interaction criterion proposed for girders without longitudinal stiffener.

A feasible use of an interaction criterion is only possible if all relevant internal forces are considered such as transverse loading and shear force as well as bending moment. Thus, the proposed F-V interaction criterion was finally enhanced with bending moment and an F-M-V interaction criterion was proposed which is intended to replace the F-M interaction criterion of Sec. 7.2, EN 1993-1-5 [46]. A reevaluation of F-M results showed that a partial plastic stress redistribution is admissible so that as reference value the plastic bending moment resistance is proposed. In turn, this decision is more conservative for Class 1 and Class 2 cross-sections which is judged to be adequate because in the relevant range a sufficient number of results does not exist to draw further conclusions.

7.2 Outlook

In the near future finite element based design procedures similar to the combination of LBA and MNA analyses in shell design will further spread and new questions will definitely appear. A basic issue which could be concluded from this work is the need for a consistent definition of imperfection shapes and amplitudes which relate to fabrication and buckling curves used in design and numerical modelling. Nevertheless, reduced stress method and effective width method remain the main design procedures and will also be further developed. Future questions for both methods are summarised below.

Reduced stress method based on a single plate slenderness. A major drawback of the reduced stress method is that a redistribution of stresses between cross-sectional elements is currently neither allowed nor reasonably feasible to do so that efforts are undertaken to overcome this [86]. A very basic requirement has to be, however, that the interaction equation describes the behaviour of a single plate sufficiently well. In case of a biaxial loading including compressive and tensile stresses, the stabilising influence of the tensile stresses is taken into account according to Chapter 10, EN 1993-1-5 [46], which is a clear improvement over DIN 18800-3 [28]. However, it is felt that only few pilot studies have looked at this effect. Further work should also study the plastic destabilising influence of these tensile stresses.

Recent tendencies in the formulation of buckling curves aim at harmonisation in order to reduce their overall number and to achieve a general format, e.g. by developing "generalised buckling curves" [84]. The latter development can be similarly observed in the field of shell buckling. The former, however, inevitably neglects the specific characteristics of loadings and boundary conditions. It was shown in [76] that a further increase of resistance is possible if the membrane in-plane restraint condition is considered. Thus, further work should reassess the reference strengths not only with regard to an improved description of edge boundary conditions but also with regard to a consistent definition of imperfections.

Effective width method. The F-M interaction criterion according to Sec. 7.2, EN 1993-1-5 [46], can be applied so far to both rolled and welded cross-sections provided that the transverse patch loading resistance model according to Chapter 6, EN 1993-1-5 [46], is used. It is shown in this work that the criterion does not apply to rolled sections any longer when using e.g. the improved transverse patch loading resistance model developed by Gozzi [56]. In general, results of Class 1 and Class 2 cross-sections exist mainly for M/M_R-ratios less than 0.4. The conservative approach in this work could possibly be improved in the future when data including high utilisation levels of bending moment become available. Since experimental and numerical data on rolled girders and on Class 1 and Class 2 cross-sections are few and not sufficiently conclusive further work is required in this field.

In general, an existing interaction criterion requires at least a critical reevaluation when a new resistance model is introduced as reference strength. Chacon [16] developed a proposal for hybrid girders which is currently in the process of harmonisation with the proposal of Gozzi [56]. The applicability of the proposed interaction criterion should be finally checked with the relevant data.

The herein proposed F-M-V interaction criterion presumes that a transverse patch loading is present. Since in general the interaction surface is also able to comprise the interaction between bending moment and shear force, it appears to be possible and desirable to harmonise the F-M-V interaction criterion with the M-V interaction criterion according to Sec. 7.1, EN 1993-1-5 [46], in the future.

Bibliography

[1] ANSYS releases 10 and 11. Ansys Inc., Canonsburg, USA.

[2] D. Bamm, J. Lindner, and R.-P. Voss. Traglastversuche an ausgesteiften Trägerauflagern. *Stahlbau*, 52(10):296–300, 1983.

[3] K.-J. Bathe. *Finite Element Procedures.* Prentice Hall, 2nd edition, 1995.

[4] H. Becker. *Steel plated structures, paper 24: Instability strength of polyaxially loaded plates and relation to design*, pages 559–580. Crosby Lockwood Staples, 1977.

[5] H. Becker and A. Colao. Compressive strength of ship hull girders. Part III - Theory and additional experiments. Technical report, Ship Structure Committee Report 267, 1977.

[6] H. Becker, R. Goldman, and J. Prozerycki. Compressive strength of ship hull girders. Part I - Unstiffened Plates. Technical report, Ship Structure Committee Report 217, 1970.

[7] D. Beg, U. Kuhlmann, L. Davaine, and B. Braun. *Eurocode Design Manual - Design of Plated Structures.* ECCS, 2010.

[8] A. Bergfelt. Studies and tests on slender plate girders without stiffeners - shear strength and local web crippling. In *IABSE Colloquium, London*, pages 67–83, 1971.

[9] A. Bergfelt. *Patch loading on a slender web - Influence of horizontal and vertical web stiffeners on the load carrying capacity.* Publication S79:1, Institutionen för Konstruktionsteknik, Stål- och Träbyggnad, Göteborg, Sweden, 1979.

[10] A. Bergfelt. Girder web stiffening for patch loading. Technical report, Report S83:1, Chalmers University of Technology, Department of Structural Engineering, Division of Steel and Timber Structures, Göteborg, 1983.

[11] C. D. Bradfield, R. W. P. Stonor, and K. E. Moxham. Test of long plates under biaxial compression. *Journal of Constructional Steel Research*, 24(1):25–56, 1993.

[12] B. Braun. *Numerische Berechnung von kreiszylindrischen Siloanlagen.* Diploma Thesis, Universität Stuttgart, Mitteilung des Instituts für Konstruktion und Entwurf Nr. 2004-4X, 2004.

[13] B. Braun. *Combined shear- and patch loading: test report.* Background document COMBRI-Report-LTU-002, RFCS project RFS-CR-03018, 2007.

[14] BSK. *Boverkets Handbok om Stålkonstruktioner, BSK 07, November 2007.*

[15] A. Carratero and J.-P. Lebet. Introduction de forces concentrées dans les poutres élancées. *Construction Métallique*, 35(1):5–18, 1998.

[16] R. Chacon. *Resistance of transversally stiffened hybrid steel plate girders to concentrated loads.* PhD thesis, Universitat Politècnica de Catalunya, Departament d´Enginyeria de la Construcció, 2009.

[17] R. Chacon, E. Mirambell, and E. Real. Resistance of transversally stiffened hybrid steel girders under concentrated loads. In D. Camotim, editor, *Stability and Ductility of Steel Structures, Lisbon, Portugal, September 6-8, 2006*, 2006.

[18] R. Chacon, E. Mirambell, and E. Real. A mechanism solution for predicting the collapse loads of girders subjected to patch loading. In *Eurosteel 2008, 3-5 September 2008, Graz, Austria*, 2008.

[19] M. Clarin. *Plate Buckling Resistance - Patch Loading of Longitudinally Stiffened Webs and Local Buckling.* PhD thesis, No. 2007:31, Luleå University of Technology, Department of Civil, Mining and Environmental Engineering, Division of Structural Engineering - Steel Structures, 2007.

[20] R.D. Cook, D.S. Malkus, M.E. Plesha, and R.J. Witt. *Concepts and Applications of Finite Element Analysis.* Wiley, 4th edition, 2001.

[21] W. Cui and A.E. Mansour. Effects of welding distortions and residual stresses on the ultimate strength of long rectangular plates under uniaxial compression. *Marine Structures*, 11(6):251–269, 1998.

[22] W. Cui, Y. Wang, and P.T. Pedersen. Strength of ship plates under combined loading. *Marine Structures*, 15(1):75–97, 2002.

[23] W.C. Cui and A.E. Mansour. Generalization of a simplified method for predicting ultimate compressive strength of ship panels. *International Shipbuilding Progress*, 46(6):291–303, 1999.

[24] L. Davaine. *Formulation de la résistance au lancement d'une âme métallique de pont raidie longitudinalement - Résistance dite de "Patch Loading".* PhD thesis, L'Institut National des Sciences Appliquées de Rennes, 2005.

[25] P.C. Davidson, J.C. Chapman, C.S. Smith, and P.J. Dow. The design of plate panels subject to in-plane shear and biaxial compression. *Transaction of the Royal Institution of Naval Architects*, 132(B):267–286, 1990.

[26] A.F. Dier and P.S. Dowling. *Plates under combined loading and lateral compression.* CESLIC Report SP8, Department of Civil Engineering, Imperial College, London, 1980.

[27] A.F. Dier and P.S. Dowling. The strength of plates subjected to biaxial forces. In J. Rhodes and J. Spence, editors, *Behaviour of thin-walled structures*, pages 329–353, 1984.

[28] DIN 18800 Teil 3. *Stahlbauten - Stabilitätsfälle, Plattenbeulen*, 11.1990.

[29] DIN-Fb 103. *DIN-Fachbericht 103: Stahlbrücken, 2009.*

[30] D. Dinkler. Rechnerische Traglasten für gestauchte Platten. Untersuchungen am Institut für Statik der TU Braunschweig (unpublished), 1987.

[31] D. Dinkler and B. Kröplin. Zum Tragsicherheitsnachweis für quadratische, scheibenartig beanspruchte Einzelfelder aus Stahl. *Stahlbau*, 53(6):174–178, 1984.

[32] DnV. *Det norske Veritas. Rules for the Design, Construction and Inspection of Offshore Structures. Appendix C - Steel Structures*, 1977.

[33] DnV RP-C201. *Det norske Veritas RP-C201: Buckling strength of plated structures. Recommended practice*, 2002.

[34] M. Dogaki, M. Murata, Y. Nishijima, T. Okumura, and H. Yonezawa. Ultimate strength of plate girders with longitudinal stiffeners under patch loading. *Technology reports of Kansai University*, 33:121–132, 1990.

[35] M. Dogaki, N Kishigami, and H. Yonezawa. Ultimate strength analysis of plate girder webs under patch loading. In *International Conference on Steel and Aluminium Structures (ICSAS), Singapore, 22-24 May 1991*, 1991.

[36] P.S. Dowling, J.E. Harding, and J.E. Slatford. *Strength of Ships Plating - Plates in biaxial compression. Final Report for the Admiralty Marine Technology Establishment.* CESLIC Report SP4, Department of Civil Engineering, Imperial College, London, 1979.

[37] M. Drdácký and R. Novotný. Partial edge load-carrying capacity tests of thick plate girder webs. *Acta Technica*, 87(5):614–620, 1977.

[38] P. Dubas and E. Gehri, editors. *Behaviour and design of steel plated structures.* ECCS, 1986.

[39] P. Dubas and H. Tschamper. Stabilité des âmes soumises à une charge concentrée et à une flexion globale. *Construction Métallique*, 27(2):25–39, 1990.

[40] N.A. Dumont. *Traglastberechnung beulgefährdeter Rechteckplatten im elastisch-plastischen Bereich nach der geometrisch nichtlinearen Theorie unter Berücksichtigung geometrischer und werkstofflicher Imperfektionen.* PhD thesis, D17, TH Darmstadt, 1978.

[41] M. Elgaaly. Failure of thin-walled members under patch loading and shear. In W. W. Yu, editor, *Proceedings of the 3rd International Specialty Conference on Cold Formed Structures, Missouri, 1975*, volume 1, pages 357–381, 1975.

[42] M. Elgaaly. Web design under compressive edge loads. *Engineering Journal*, 20(4): 153–171, 1983.

[43] M. Elgaaly and W. L. Nunan. Behavior of rolled section web under eccentric edge compressive load. *Journal of Structural Engineering*, 115(7):1561–1578, 1989.

[44] M. Elgaaly and R. K. Salkar. Web crippling under edge loading. In *Proceedings of the National Steel Construction Conference, Washingten D. C., USA, June 5-7, 1991*, 1991.

[45] EN 1990-2. *Execution of steel structures and aluminium structures - Part 2: Technical requirements for steel structures*, 07.2008.

[46] EN 1993-1-5. *Eurocode 3: Design of steel structures - Part 1-5: Plated Structural Elements*, 02.2007.

[47] EN 1993-1-5/NA. *German National Annex to Eurocode 3: Design of steel structures - Part 1-5: Plated Structural Elements*, 01.2010.

[48] Entwurf DIN 18800 Teil 3. *Stahlbauten - Stabilitätsfälle, Plattenbeulen*, märz 1988 edition, 1988.

[49] D. Faulkner. A review of effective plating for use in the analysis of stiffened plating in bending and compression. *Journal of Ship Research*, 19(1):1–17, 1975.

[50] D. Faulkner, J. C. Adamschak, G. J. Snyder, and M. F. Vetter. Synthesis of welded grillages to withstand compression and normal loads. *Computers & Structures*, 3 (2):221–246, 1973.

[51] M. Fischer, R. Grube, H. Rieger, and P. Wenk. *Messungen der Vorverformungen von beulgefährdeten Stahlblechen mit und ohne Steifen.* Universität Dortmund, 1989.

[52] P.A. Frieze, P.J. Dowling, and R.W. Hobbs. *Steel plated structures, paper 2: Ultimate load behaviour of plates in compression*, pages 24–50. Crosby Lockwood Staples, 1977.

[53] Y. Fujita, T. Nomoto, and O. Niho. Ultimate strength of stiffened plates subjected to compression (1st report). Technical report, Journal of the Society of Naval Architects of Japan, 1977.

[54] Y. Fujita, T. Nomoto, and O. Niho. Ultimate strength of stiffened plates subjected to compression (2nd report). Technical report, Journal of the Society of Naval Architects of Japan, 1979.

[55] Y. Galéa, B. Godart, I. Radouant, and J. Raoul. Tests of buckling of panels subjected to in-plane patch loading. In *ECCS Colloquium on Stability of Plate and Shell Structures, Ghent University, 6-8 April 1987*, 1987.

[56] J. Gozzi. *Patch loading resistance of plated girders - Ultimate and serviceability limit state*. PhD thesis, No. 2007:30, Luleå University of Technology, Department of Civil, Mining and Environmental Engineering, Division of Structural Engineering - Steel Structures, 2007.

[57] C. Graciano. *Patch loading - Resistance of longitudinally stiffened steel girder webs*. PhD thesis, No. 2002:18, Luleå University of Technology, Department of Civil and Mining Engineering, Division of Steel Structures, 2002.

[58] C. A. Granholm. Tests on girders with extremely thin web plates. Technical report, Report 202, Institutionen för Byggnadsteknik, Göteborg, 1960.

[59] C. Guedes Soares and J. M. Gordo. Compressive strength of rectangular plates under biaxial load and lateral pressure. *Thin-Walled Structures*, 24(3):231–259, 1996.

[60] J.E. Harding. *Bolted spliced panels and stress redistribution in box girder components up to collapse*. PhD thesis, University of London, 1975.

[61] J.E. Harding. *The interaction of direct and shear stresses on plate panels*, chapter 8, pages 221–255. Applied Science Publishers, London & New York, 1983.

[62] T. Höglund. Local buckling of steel bridge girder webs during launching. In *Proceedings of the Nordic Steel Colloquium, Odense, Denmark, 9-11 September 1991*, pages 531–535, 1991.

[63] H. Isami. A new approach to predict the strength of steel rectangular plates under biaxial in-plane compression. *Journal of Structural Engineering, Japan Society of Civil Engineers*, 37A:219–228, 1991.

[64] K. Janus, I. Kárniková, and M. Skaloud. Experimental investigation into the ultimate load behaviour of longitudinally stiffened steel webs under partial edge loading. *Acta Technica CSAV*, (2):158–195, 1988.

[65] B. Johansson and O. Lagerqvist. Resistance of plate edges to concentrated forces. *Journal of Constructional Steel Research*, 32(1):69–105, 1995.

[66] B. Johansson and M. Veljkovic. Review of plate buckling rules in EN 1993-1-5. *Steel Construction - Design and Research*, 2(4):228–234, 2009.

[67] B. Johansson, R. Maquoi, G. Sedlacek, C. Müller, and D. Beg. *Commentary and worked examples to EN 1993-1-5 "Plated Structural Elements"*. European Commission, 2007.

[68] O. Jungbluth. *Beulnachweise bei gleichzeitiger Wirkung von σ_x, σ_y, τ mit Interaktionsdiagrammen*. Arbeitspapier 4/XXI/DIN 18800 (unpublished), 1980.

[69] O. Jungbluth, H. Friemann, and G. Kubsch. *Experimentelle und theoretische Ermittlungen der Beullasten unversteifter Stahlbleche unter Berücksichtigung von Vorverformungen und Eigenspannungen*. No. 14/1985, Stahlbau Verlagsgesellschaft, Köln, 1985.

[70] K. Klöppel, J. Scheer, and H. Möller. *Beulwerte ausgesteifter Rechteckplatten, Bd. 1*. Ernst & Sohn, 1960.

[71] K. Klöppel, J. Scheer, and H. Möller. *Beulwerte ausgesteifter Rechteckplatten, Bd. 2*. Ernst & Sohn, 1968.

[72] U. Kuhlmann, editor. *Competitive Steel and Composite Bridges by Improved Steel Plated Structures (COMBRI)*. RFCS, European Commission, 2007.

[73] U. Kuhlmann, editor. *Valorisation of Knowledge for Competitive Steel and Composite Bridges*. 2009.

[74] U. Kuhlmann and B. Braun. Untersuchung des Einflusses von Vorbeulen auf die Tragfähigkeit von stählernen Leichtbau-Hallenkonstruktionen - Reine Biegung. Technical report, Universität Stuttgart, Mitteilung des Instituts für Konstruktion und Entwurf Nr. 2007-37X, 2007.

[75] U. Kuhlmann and B. Braun. Untersuchung des Einflusses von Vorbeulen auf die Tragfähigkeit von stählernen Leichtbau-Hallenkonstruktionen - Längs- und Schubspannungen. Technical report, Universität Stuttgart, Mitteilung des Instituts für Konstruktion und Entwurf Nr. 2008-17X, 2008.

[76] U. Kuhlmann, H.-P. Günther, and B. Braun. Improved buckling curves for the design of compressed steel plated elements. In *6th International Symposium on Steel Bridges, Prague, Czech Republic*, 2006.

[77] O. Lagerqvist. *Patch loading - Resistance of steel girders subjected to concentrated forces*. PhD thesis, No. 1994:159, Luleå University of Technology, Department of Civil and Mining Engineering, Division of Steel Structures, 1994.

[78] J. Lindner and W. Habermann. Zur mehrachsigen Beanspruchung beim Plattenbeulen. In *Festschrift Prof. Dr.-Ing. Joachim Scheer zu seinem sechzigsten Geburtstag*, 1987.

[79] J. Lindner and W. Habermann. Zur Weiterentwicklung des Beulnachweises für Platten bei mehrachsiger Beanspruchung. *Stahlbau*, 57(11):333–339, 1988.

[80] J. Lindner and W. Habermann. Berichtigung zu: Zur Weiterentwicklung des Beulnachweises für Platten bei mehrachsiger Beanspruchung. *Stahlbau*, 58(11):349–351, 1989.

[81] J. Lindner and A. Rusch. *Grenz(b/t)-Verhältnisse in Abhängigkeit der Belastung unter besonderer Berücksichtigung von Imperfektionen.* Schlussbericht zum DIBt-Forschungsvorhaben P 32-5-16.91.32-965/00, Berlin, 2000.

[82] MathCAD release 12.1. PTC, Needham, USA.

[83] A.M.H. Max. Simple design formulas for unstiffened and stiffened plates in uniaxial compression. Technical report, Consulting Engineers, Aarau, Switzerland, 1971.

[84] C. Müller. *Zum Nachweis ebener Tragwerke aus Stahl gegen seitliches Ausweichen.* PhD thesis, RWTH Aachen, 2003.

[85] R. Narayanan and N.E. Shanmugan. *Compressive Strength of Biaxially Loaded Plates*, chapter 7, pages 195–219. Applied Science Publishers, London & New York, 1983.

[86] J. Naumes, M. Feldmann, and G. Sedlacek. Gemeinsame Grundlagen von Methode 1 (wirksame Breiten) und Methode 2 (Beulspannungsbegrenzung) beim Plattenbeulnachweis nach Eurocode 3, Teil 1-5. *Stahlbau*, 78(3):139–147, 2009.

[87] J. Oxfort and H.-U. Gauger. Beultraglast von Vollwandträgern unter Einzellasten. *Stahlbau*, 58(11):331–339, 1989.

[88] J. Oxfort and N. Weber. Versuche zum Beul- und Krüppelverhalten von Trägerstegblechen bei zentrischer und exzentrischer Belastung. Technical report, 6/1979, Institut für Stahlbau und Holzbau, Universität Stuttgart, 1979.

[89] J. Oxfort and N. Weber. Versuche zum Stegblechbeulen bei Einzellasteinleitung und Biegung oder Querkraft. Technical report, 7/1981, Institut für Stahlbau und Holzbau, Universität Stuttgart, 1981.

[90] J. K. Paik and A. K. Thayamballi. *Ultimate Limit State Design of Steel-Plated Structures.* Wiley, 2003.

[91] J.K. Paik and P.T. Pedersen. A simplified method for predicting ultimate compressive strength of ship panels. *International Shipbuilding Progress*, 43:139–157, 1996.

[92] L. Pavlovcic, A. Detzel, U. Kuhlmann, and D. Beg. Shear resistance of longitudinally stiffened panels - Part 1: Tests and numerical analysis of imperfections. *Journal of Constructional Steel Research*, 63(3):337–350, 2007.

[93] E. Ramm and H. Stegmüller. The displacement finite element method in nonlinear buckling analysis of shells. In E. Ramm, editor, *Buckling of Shells: proceedings of a state-of-the-art colloquium, Universität Stuttgart, Germany, 6-7 May 1982*, pages 201–235. Springer, 1982.

[94] J. Raoul, I. Schaller, and J.-N. Theillout. Tests of buckling of panels subjected to in-plane patch loading. In *IUTAM Symposium, Prague 1990*, pages 173–183, 1990.

[95] M. Reininghaus and A. Gehrke. Zur Berechnung von Tragspannungen beulgefährdeter, unversteifter quadratischer Platten. (announced in [106], but unpublished).

[96] T. M. Roberts. Slender plate girders subjected to edge loading. *Proceedings of the Institution of Civil Engineers*, 71:805–819, September 1981.

[97] T. M Roberts and C. K. Chong. Collapse of plate girders under edge loading. *Journal of the Structural Division*, 107(8):1503–1509, August 1981.

[98] T. M. Roberts and B. Coric. Collapse of plate girders subjected to patch loading. *Miscellany Dedicated to the 65th Birthday of Academian Professor Dr. Nicola Haijdin*, pages 203–209, 1988.

[99] T. M. Roberts and N. Markovic. Stocky plate girders subjected to edge loading. *Proceedings of the Institution of Civil Engineers*, pages 539–550, 1983.

[100] T. M Roberts and K. C. Rockey. A mechanism solution for predicting the collapse loads of slender plate girders when subjected to in-plate patch loading. *Proceedings of the Institution of Civil Engineers*, 67:155–175, March 1979.

[101] T.M. Roberts and F. Shahabian. Design procedures for combined shear and patch loading of plate girders. *Proceedings of the Institution of Civil Engineers, Structures & Buildings*, 140:219–225, 2000.

[102] T.M. Roberts and F. Shahabian. Resistance of slender web panels to combinations of in-plane loading. In *Proceedings of the 3rd International Conference on Coupled Instabilities in Metal Structures, CIMS 2000, Lisbon, 21-23 September 2000*, pages 349–357, 2000.

[103] T.M. Roberts and F. Shahabian. Ultimate resistance of slender web panels to combined bending shear and patch loading. *Journal of Constructional Steel Research*, 57(7):779–790, 2001.

[104] K. C. Rockey, A. Bergfelt, and L. Larsson. Behaviour of longitudinally reinforced plate girders when subjected to inplane patch loading. Technical report, Publication S78:19, Department of Structural Engineering, Division of Steel and Timber Structures, Chalmers University of Technology, Göteborg, 1978.

[105] K.C. Rockey and M. Skaloud. The ultimate load behaviour of plate girders loaded in shear. *The Structural Engineer*, 50(1):29–47, 1972.

[106] D. C. Ruff and U. Schulz. Der Einfluss von Imperfektionen auf das Tragverhalten von Platten. *Stahlbau*, 68(10):829–834, 1999.

[107] D. C. Ruff and U. Schulz. Ergänzende Stellungnahme zum Einfluss von Imperfektionen auf das Tragverhalten von Platten. *Stahlbau*, 69(6):503, 2000.

[108] A. Rusch and J. Lindner. Tragfähigkeit von beulgefährdeten Querschnittselementen unter Berücksichtigung von Imperfektionen. *Stahlbau*, 70(10):765–774, 2001.

[109] J. Scheer. Beulwerte für schubbeanspruchte Rechteckplatten. *Der Stahlbau*, 7(7): 208–211, 1962.

[110] J. Scheer and H. Nölke. Zum Nachweis der Beulsicherheit von Platten bei gleichzeitiger Wirkung mehrerer Randspannungen. *Stahlbau*, 70(9):718–729, 2001.

[111] J. Scheer and H. Nölke. Neuer Vorschlag zum Nachweis der Beulsicherheit von Platten unter mehreren Randspannungen. In *Festschrift G. Valtinat*, pages 261–274, 2001.

[112] J. Scheer, X.L. Liu, J. Falke, and U. Peil. Traglastversuche zur Lasteinleitung an I-förmigen geschweißten Biegeträgern ohne Steifen. *Stahlbau*, 57(4):115–121, 1988.

[113] H. Schmidt. Stability of steel shell structures: General report. *Journal of Constructional Steel Research*, 55(1-3):159–181, 2000.

[114] M. Seitz. *Tragverhalten längsversteifter Blechträger unter quergerichteter Krafteinleitung*. PhD thesis, Universität Stuttgart, Mitteilung des Instituts für Konstruktion und Entwurf Nr. 2005-2, 2005.

[115] F. Shahabian and T.M. Roberts. Buckling of slender web plates subjected to combinations of in-plane loading. *Journal of Constructional Steel Research*, 51(2):99–121, 1999.

[116] F. Shahabian and T.M. Roberts. Combined shear-and-patch loading of plate girders. *Journal of Structural Engineering*, 126(3):316–321, 2000.

[117] S. Shimizu, S. Yoshida, and H. Okuhara. An experimental study on patch-loaded web plates. In *ECCS Colloquium on stability of plate and shell structures, Ghent University, 6-8 April 1987*, pages 85–94, 1987.

[118] R.W.P. Stonor, C.D. Bradfield, K. E. Moxham, and J.B. Dwight. Tests on plates under biaxial compression. Technical report, Cambridge University Engineering Department, CUED/D-STRUCT/TR.98, 1983.

[119] D. Ungermann. *Bemessungsverfahren für Vollwand- und Kastenträger unter besonderer Berücksichtigung des Stegverhaltens*. PhD thesis, RWTH Aachen, 1990.

[120] T. Usami. Effective width of locally buckled plates in compression and bending. *Journal of Structural Engineering*, 119(5):1358–1373, 1993.

[121] S. Valsgard. Ultimate capacity of plates in biaxial inplane compression. Technical report, Det Norske Veritas report 76-678 (revised 1979), 1978.

[122] S. Valsgard. Numerical design prediction of the capacity of plates in biaxial inplane compression. *Computers & Structures*, 12(5):729–739, 1980.

[123] S. Walbridge and J.-P. Lebet. Patch loading tests of bridge girders with longitudinal web stiffeners. Technical report, Rapport d'essais EPL Lausanne, ICOM 447, 2001.

[124] O.C. Zienkiewicz and R.L. Taylor. *Finite Element Method, volume 1: The Basis*. Butterworth-Heinemann, 5th edition, 2000.

[125] O.C. Zienkiewicz and R.L. Taylor. *Finite Element Method, volume 2: Solid Mechanics*. Butterworth-Heinemann, 5th edition, 2000.

[126] P. Zoetemeijer. The influence of normal-, bending- and shear stresses on the ultimate compression force exerted laterally to european rolled sections. Technical report, Report 6-80-5, Department of Civil Engineering, Delft University of Technology, 1980.

A Specimen data of girders under transverse patch loading and shear force

A.1 Girders without longitudinal stiffeners

In Table A.1 experimental data is given for 26 girders. References are listed below according to the consecutive numbering:

- 1-24: Shahabian and Roberts [116]
- 25-26: Tests by the author, see Chapter 4

In Table A.2 numerical data is given for 145 girders. The simulations were solely carried out by the author.

Table A.1: Experimental data

#	Specimen	f_{yw} [N/mm^2]	f_{yf} [N/mm^2]	a [mm]	h_w [mm]	t_w [mm]	b_f [mm]	t_f [mm]	s_s [mm]	F_u [kN]	V_{avg} [kN]
1	PG1-1S	343	257	600	600	4.1	200	12.5	n.a.	n.a.	373
2	PG1-1P	343	257	600	600	4.1	200	12.5	50	220	0
3	PG1-2SP1	339	250	600	600	4.1	200	12.3	50	205	158
4	PG1-2SP2	339	250	600	600	4.1	200	12.3	50	208	97
5	PG1-3SP1	338	251	600	600	4.1	200	12.5	50	175	266
6	PG1-3SP2	338	251	600	600	4.1	200	12.5	50	186	215
7	PG2-1S	285	254	900	900	3.1	300	10.2	n.a.	n.a.	271
8	PG2-1P	285	254	900	900	3.1	300	10.2	50	113	0
9	PG2-2SP1	284	256	900	900	3.1	300	10.2	50	51	241
10	PG2-2SP2	284	256	900	900	3.1	300	10.2	50	25	247
11	PG2-3SP1	282	253	900	900	3.1	300	10.2	50	74	230
12	PG2-3SP2	282	253	900	900	3.1	300	10.2	50	16	260
13	PG3-1S	282	264	900	600	3.2	200	10.1	n.a.	n.a.	202
14	PG3-1P	282	264	900	600	3.2	200	10.1	50	120	0
15	PG3-2SP1	273	263	900	600	3.2	200	10.2	50	36	169
16	PG3-2SP2	273	263	900	600	3.2	200	10.2	50	110	52
17	PG3-3SP1	275	258	900	600	3.2	200	10.2	50	60	161
18	PG3-3SP2	275	258	900	600	3.2	200	10.2	50	106	107
19	PG4-1S	250	293	1000	500	1.9	200	9.9	n.a.	n.a.	87
20	PG4-1P	250	293	1000	500	1.9	200	9.9	50	52	0
21	PG4-2SP1	247	313	1000	500	1.9	200	9.8	50	38	61
22	PG4-2SP2	247	313	1000	500	1.9	200	9.8	50	20	72
23	PG4-3SP1	236	294	1000	500	1.9	200	10.0	50	32	62
24	PG4-3SP2	236	294	1000	500	1.9	200	10.0	50	44	43
25	SP600	383	354	2390	600	6.0	450	20.0	200	423	317
26	SP1200	383	354	2390	1200	6.0	450	20.0	200	515	386

Table A.2: Numerical data

#	Specimen	f_{yw} [N/mm^2]	f_{yf} [N/mm^2]	a [mm]	h_w [mm]	t_w [mm]	b_f [mm]	t_f [mm]	s_s [mm]	F_u [kN]	V_{avg} [kN]
1	R-60-V	355	355	2400	1200	20.0	600	50.0	n.a.	n.a.	5598
2	R-60-025	355	355	2400	1200	20.0	600	50.0	300	4502	0
3	R-60-050	355	355	2400	1200	20.0	600	50.0	600	5178	0
4	R-60-075	355	355	2400	1200	20.0	600	50.0	900	6129	0
5	R-60-025-050	355	355	2400	1200	20.0	600	50.0	300	4405	1101
6	R-60-025-0	355	355	2400	1200	20.0	600	50.0	300	4149	2075
7	R-60-025-18	355	355	2400	1200	20.0	600	50.0	300	3438	3226
8	R-60-025-36	355	355	2400	1200	20.0	600	50.0	300	2658	3935
9	R-60-025-54	355	355	2400	1200	20.0	600	50.0	300	1885	4442
10	R-60-025-72	355	355	2400	1200	20.0	600	50.0	300	1048	4873
11	R-60-050-050	355	355	2400	1200	20.0	600	50.0	600	5026	1257
12	R-60-050-0	355	355	2400	1200	20.0	600	50.0	600	4545	2272
13	R-60-050-18	355	355	2400	1200	20.0	600	50.0	600	3651	3287
14	R-60-050-36	355	355	2400	1200	20.0	600	50.0	600	2803	3909
15	R-60-050-54	355	355	2400	1200	20.0	600	50.0	600	1999	4388
16	R-60-050-72	355	355	2400	1200	20.0	600	50.0	600	1120	4806
17	R-60-075-050	355	355	2400	1200	20.0	600	50.0	900	5726	1431
18	R-60-075-0	355	355	2400	1200	20.0	600	50.0	900	4909	2454
19	R-60-075-18	355	355	2400	1200	20.0	600	50.0	900	3831	3336
20	R-60-075-36	355	355	2400	1200	20.0	600	50.0	900	2947	3914
21	R-60-075-54	355	355	2400	1200	20.0	600	50.0	900	2116	4380
22	R-60-075-72	355	355	2400	1200	20.0	600	50.0	900	1225	4912
23	R-60-100	355	355	2400	1200	20.0	600	50.0	900	7071	0
24	R-60-100-050	355	355	2400	1200	20.0	600	50.0	900	6368	1592
25	R-60-100-0	355	355	2400	1200	20.0	600	50.0	900	5181	2591
26	R-60-100-18	355	355	2400	1200	20.0	600	50.0	900	3993	3398
27	R-60-100-36	355	355	2400	1200	20.0	600	50.0	900	3080	3958
28	R-60-100-54	355	355	2400	1200	20.0	600	50.0	900	2232	4434
29	R-60-100-72	355	355	2400	1200	20.0	600	50.0	900	1288	4928
30	N-100-V	355	355	2400	1200	12.0	450	30.0	n.a.	n.a.	2692
31	N-100-025	355	355	2400	1200	12.0	450	30.0	300	1803	0
32	N-100-050	355	355	2400	1200	12.0	450	30.0	600	2142	0
33	N-100-075	355	355	2400	1200	12.0	450	30.0	900	2428	0
34	N-100-025-050	355	355	2400	1200	12.0	450	30.0	300	1750	438
35	N-100-025-0	355	355	2400	1200	12.0	450	30.0	300	1665	833
36	N-100-025-18	355	355	2400	1200	12.0	450	30.0	300	1391	1427
37	N-100-025-36	355	355	2400	1200	12.0	450	30.0	300	1087	1819
38	N-100-025-54	355	355	2400	1200	12.0	450	30.0	300	781	2127
39	N-100-025-72	355	355	2400	1200	12.0	450	30.0	300	441	2414
40	N-100-050-050	355	355	2400	1200	12.0	450	30.0	600	2057	514
41	N-100-050-0	355	355	2400	1200	12.0	450	30.0	600	1864	932
42	N-100-050-18	355	355	2400	1200	12.0	450	30.0	600	1501	1454
43	N-100-050-36	355	355	2400	1200	12.0	450	30.0	600	1165	1805
44	N-100-050-54	355	355	2400	1200	12.0	450	30.0	600	847	2109
45	N-100-050-72	355	355	2400	1200	12.0	450	30.0	600	482	2386
46	N-100-075-050	355	355	2400	1200	12.0	450	30.0	900	2276	569
47	N-100-075-0	355	355	2400	1200	12.0	450	30.0	900	1989	994
48	N-100-075-18	355	355	2400	1200	12.0	450	30.0	900	1581	1485
49	N-100-075-36	355	355	2400	1200	12.0	450	30.0	900	1224	1815
50	N-100-075-54	355	355	2400	1200	12.0	450	30.0	900	893	2109
51	N-100-075-72	355	355	2400	1200	12.0	450	30.0	900	511	2382
52	N-100-100	355	355	2400	1200	12.0	450	30.0	1200	2666	0
53	N-100-100-050	355	355	2400	1200	12.0	450	30.0	1200	2448	612
54	N-100-100-0	355	355	2400	1200	12.0	450	30.0	1200	2098	1049
55	N-100-100-18	355	355	2400	1200	12.0	450	30.0	1200	1646	1509
56	N-100-100-36	355	355	2400	1200	12.0	450	30.0	1200	1286	1841
57	N-100-100-54	355	355	2400	1200	12.0	450	30.0	1200	934	2116
58	N-100-100-72	355	355	2400	1200	12.0	450	30.0	1200	536	2385
59	R-100-V	355	355	2400	1200	12.0	450	30.0	n.a.	n.a.	2692
60	R-100-025	355	355	2400	1200	12.0	450	30.0	300	1807	0
61	R-100-050	355	355	2400	1200	12.0	450	30.0	600	2151	0
62	R-100-075	355	355	2400	1200	12.0	450	30.0	900	2430	0
63	R-100-025-050	355	355	2400	1200	12.0	450	30.0	300	1756	439
64	R-100-025-0	355	355	2400	1200	12.0	450	30.0	300	1663	832
65	R-100-025-18	355	355	2400	1200	12.0	450	30.0	300	1390	1426
66	R-100-025-36	355	355	2400	1200	12.0	450	30.0	300	1096	1836
67	R-100-025-54	355	355	2400	1200	12.0	450	30.0	300	780	2128
68	R-100-025-72	355	355	2400	1200	12.0	450	30.0	300	440	2412
69	R-100-050-050	355	355	2400	1200	12.0	450	30.0	600	2057	514
70	R-100-050-0	355	355	2400	1200	12.0	450	30.0	600	1864	932
71	R-100-050-18	355	355	2400	1200	12.0	450	30.0	600	1501	1454
72	R-100-050-36	355	355	2400	1200	12.0	450	30.0	600	1165	1805
73	R-100-050-54	355	355	2400	1200	12.0	450	30.0	600	849	2113
74	R-100-050-72	355	355	2400	1200	12.0	450	30.0	600	482	2386
75	R-100-075-050	355	355	2400	1200	12.0	450	30.0	900	2269	567
76	R-100-075-0	355	355	2400	1200	12.0	450	30.0	900	1989	994
77	R-100-075-18	355	355	2400	1200	12.0	450	30.0	900	1580	1484
78	R-100-075-36	355	355	2400	1200	12.0	450	30.0	900	1226	1818

continued on next page

continued from previous page

#	Specimen	f_{yw} [N/mm^2]	f_{yf} [N/mm^2]	a [mm]	h_w [mm]	t_w [mm]	b_f [mm]	t_f [mm]	s_s [mm]	F_u [kN]	V_{avg} [kN]
79	R-100-075-54	355	355	2400	1200	12.0	450	30.0	900	895	2114
80	R-100-075-72	355	355	2400	1200	12.0	450	30.0	900	510	2383
81	R-100-100	355	355	2400	1200	12.0	450	30.0	1200	2681	0
82	R-100-100-050	355	355	2400	1200	12.0	450	30.0	1200	2450	613
83	R-100-100-0	355	355	2400	1200	12.0	450	30.0	1200	2098	1049
84	R-100-100-18	355	355	2400	1200	12.0	450	30.0	1200	1655	1517
85	R-100-100-36	355	355	2400	1200	12.0	450	30.0	1200	1286	1842
86	R-100-100-54	355	355	2400	1200	12.0	450	30.0	1200	937	2123
87	R-100-100-72	355	355	2400	1200	12.0	450	30.0	1200	536	2385
88	N-200-V	355	355	2400	1200	6.0	300	25.0	n.a.	n.a.	750
89	N-200-025	355	355	2400	1200	6.0	300	25.0	300	561	0
90	N-200-050	355	355	2400	1200	6.0	300	25.0	600	644	0
91	N-200-075	355	355	2400	1200	6.0	300	25.0	900	698	0
92	N-200-025-050	355	355	2400	1200	6.0	300	25.0	300	552	138
93	N-200-025-0	355	355	2400	1200	6.0	300	25.0	300	532	266
94	N-200-025-18	355	355	2400	1200	6.0	300	25.0	300	458	438
95	N-200-025-36	355	355	2400	1200	6.0	300	25.0	300	357	545
96	N-200-025-54	355	355	2400	1200	6.0	300	25.0	300	253	616
97	N-200-025-72	355	355	2400	1200	6.0	300	25.0	300	141	683
98	N-200-050-050	355	355	2400	1200	6.0	300	25.0	600	622	155
99	N-200-050-0	355	355	2400	1200	6.0	300	25.0	600	576	288
100	N-200-050-18	355	355	2400	1200	6.0	300	25.0	600	473	437
101	N-200-050-36	355	355	2400	1200	6.0	300	25.0	600	372	538
102	N-200-050-54	355	355	2400	1200	6.0	300	25.0	600	266	610
103	N-200-050-72	355	355	2400	1200	6.0	300	25.0	600	151	680
104	N-200-075-050	355	355	2400	1200	6.0	300	25.0	900	669	167
105	N-200-075-0	355	355	2400	1200	6.0	300	25.0	900	600	300
106	N-200-075-18	355	355	2400	1200	6.0	300	25.0	900	482	436
107	N-200-075-36	355	355	2400	1200	6.0	300	25.0	900	379	533
108	N-200-075-54	355	355	2400	1200	6.0	300	25.0	900	274	609
109	N-200-075-72	355	355	2400	1200	6.0	300	25.0	900	156	679
110	N-200-100	355	355	2400	1200	6.0	300	25.0	1200	755	0
111	N-200-100-050	355	355	2400	1200	6.0	300	25.0	1200	708	177
112	N-200-100-0	355	355	2400	1200	6.0	300	25.0	1200	614	307
113	N-200-100-18	355	355	2400	1200	6.0	300	25.0	1200	487	437
114	N-200-100-36	355	355	2400	1200	6.0	300	25.0	1200	379	526
115	N-200-100-54	355	355	2400	1200	6.0	300	25.0	1200	276	602
116	N-200-100-72	355	355	2400	1200	6.0	300	25.0	1200	160	679
117	R-200-V	355	355	2400	1200	6.0	300	25.0	n.a.	n.a.	758
118	R-200-025	355	355	2400	1200	6.0	300	25.0	300	561	0
119	R-200-050	355	355	2400	1200	6.0	300	25.0	600	645	0
120	R-200-075	355	355	2400	1200	6.0	300	25.0	900	703	0
121	R-200-025-050	355	355	2400	1200	6.0	300	25.0	300	552	138
122	R-200-025-0	355	355	2400	1200	6.0	300	25.0	300	532	266
123	R-200-025-18	355	355	2400	1200	6.0	300	25.0	300	462	444
124	R-200-025-36	355	355	2400	1200	6.0	300	25.0	300	374	574
125	R-200-025-54	355	355	2400	1200	6.0	300	25.0	300	265	651
126	R-200-025-72	355	355	2400	1200	6.0	300	25.0	300	146	712
127	R-200-050-050	355	355	2400	1200	6.0	300	25.0	600	623	156
128	R-200-050-0	355	355	2400	1200	6.0	300	25.0	600	576	288
129	R-200-050-18	355	355	2400	1200	6.0	300	25.0	600	487	451
130	R-200-050-36	355	355	2400	1200	6.0	300	25.0	600	390	569
131	R-200-050-54	355	355	2400	1200	6.0	300	25.0	600	278	644
132	R-200-050-72	355	355	2400	1200	6.0	300	25.0	600	155	706
133	R-200-075-050	355	355	2400	1200	6.0	300	25.0	900	669	167
134	R-200-075-0	355	355	2400	1200	6.0	300	25.0	900	602	301
135	R-200-075-18	355	355	2400	1200	6.0	300	25.0	900	506	460
136	R-200-075-36	355	355	2400	1200	6.0	300	25.0	900	401	568
137	R-200-075-54	355	355	2400	1200	6.0	300	25.0	900	288	642
138	R-200-075-72	355	355	2400	1200	6.0	300	25.0	900	162	710
139	R-200-100	355	355	2400	1200	6.0	300	25.0	1200	756	0
140	R-200-100-050	355	355	2400	1200	6.0	300	25.0	1200	709	177
141	R-200-100-0	355	355	2400	1200	6.0	300	25.0	1200	622	311
142	R-200-100-18	355	355	2400	1200	6.0	300	25.0	1200	521	466
143	R-200-100-36	355	355	2400	1200	6.0	300	25.0	1200	413	572
144	R-200-100-54	355	355	2400	1200	6.0	300	25.0	1200	290	631
145	R-200-100-72	355	355	2400	1200	6.0	300	25.0	1200	162	687

A.2 Girders with longitudinal stiffeners

In Table A.3 experimental data is given for one girder. The test was carried out by Seitz [114].

In Table A.4 numerical data is given for 58 girders with closed-section stiffeners and in Table A.5 for 29 girders with open-section stiffeners. The simulations were solely carried out by the author.

Table A.3: Experimental data, girder with closed-section stiffeners

#	Specimen	f_{yw} [N/mm^2]	f_{yf} [N/mm^2]	a [mm]	h_w [mm]	b_1 [mm]	t_w [mm]	b_f [mm]	t_f [mm]	s_s [mm]	$I_{s\ell,1}$ [cm^4]	F_u [kN]	V_{avg} [kN]
1	IV-2	373	378	2400	1200	250	6.0	260	20.0	700	343.99	987	370

Table A.4: Numerical data, girders with closed-section stiffeners

#	Specimen	f_{yw} [N/mm^2]	f_{yf} [N/mm^2]	a [mm]	h_w [mm]	b_1 [mm]	t_w [mm]	b_f [mm]	t_f [mm]	s_s [mm]	$I_{s\ell,1}$ [cm^4]	F_u [kN]	V_{avg} [kN]
1	Cg-200-V-025	355	355	2400	1200	250	6.0	300	25.0	n.a.	271.00	n.a.	1035
2	Cg-200-025-025	355	355	2400	1200	250	6.0	300	25.0	300	271.00	719	0
3	Cg-200-050-025	355	355	2400	1200	250	6.0	300	25.0	600	271.00	896	0
4	Cg-200-075-025	355	355	2400	1200	250	6.0	300	25.0	900	271.00	998	0
5	Cg-200-025-025-05	355	355	2400	1200	250	6.0	300	25.0	300	271.00	709	177
6	Cg-200-025-025-0	355	355	2400	1200	250	6.0	300	25.0	300	271.00	697	349
7	Cg-200-025-025-18	355	355	2400	1200	250	6.0	300	25.0	300	271.00	660	648
8	Cg-200-025-225-36	355	355	2400	1200	250	6.0	300	25.0	300	271.00	517	815
9	Cg-200-025-025-54	355	355	2400	1200	250	6.0	300	25.0	300	271.00	354	899
10	Cg-200-025-025-72	355	355	2400	1200	250	6.0	300	25.0	300	271.00	191	971
11	Cg-200-050-025-05	355	355	2400	1200	250	6.0	300	25.0	600	271.00	879	220
12	Cg-200-050-025-0	355	355	2400	1200	250	6.0	300	25.0	600	271.00	859	429
13	Cg-200-050-025-18	355	355	2400	1200	250	6.0	300	25.0	600	271.00	763	680
14	Cg-200-050-025-36	355	355	2400	1200	250	6.0	300	25.0	600	271.00	576	793
15	Cg-200-050-025-54	355	355	2400	1200	250	6.0	300	25.0	600	271.00	404	873
16	Cg-200-050-025-72	355	355	2400	1200	250	6.0	300	25.0	600	271.00	228	958
17	Cg-200-075-025-05	355	355	2400	1200	250	6.0	300	25.0	900	271.00	974	244
18	Cg-200-075-025-0	355	355	2400	1200	250	6.0	300	25.0	900	271.00	932	466
19	Cg-200-075-025-18	355	355	2400	1200	250	6.0	300	25.0	900	271.00	788	678
20	Cg-200-075-025-36	355	355	2400	1200	250	6.0	300	25.0	900	271.00	599	783
21	Cg-200-075-025-54	355	355	2400	1200	250	6.0	300	25.0	900	271.00	429	869
22	Cg-200-075-025-72	355	355	2400	1200	250	6.0	300	25.0	900	271.00	243	952
23	Cg-200-100-025	355	355	2400	1200	250	6.0	300	25.0	1200	271.00	1109	0
24	Cg-200-100-025-05	355	355	2400	1200	250	6.0	300	25.0	1200	271.00	1078	270
25	Cg-200-100-025-0	355	355	2400	1200	250	6.0	300	25.0	1200	271.00	1011	506
26	Cg-200-100-025-18	355	355	2400	1200	250	6.0	300	25.0	1200	271.00	811	675
27	Cg-200-100-025-36	355	355	2400	1200	250	6.0	300	25.0	1200	271.00	623	774
28	Cg-200-100-025-54	355	355	2400	1200	250	6.0	300	25.0	1200	271.00	450	860
29	Cg-200-100-025-72	355	355	2400	1200	250	6.0	300	25.0	1200	271.00	258	942
30	Cl-200-V-025	355	355	2400	1200	250	6.0	300	25.0	n.a.	595.00	n.a.	1047
31	Cl-200-025-025	355	355	2400	1200	250	6.0	300	25.0	300	595.00	740	0
32	Cl-200-050-025	355	355	2400	1200	250	6.0	300	25.0	600	595.00	1158	0
33	Cl-200-075-025	355	355	2400	1200	250	6.0	300	25.0	900	595.00	1552	0
34	Cl-200-025-025-05	355	355	2400	1200	250	6.0	300	25.0	300	595.00	736	184
35	Cl-200-025-025-0	355	355	2400	1200	250	6.0	300	25.0	300	595.00	719	360
36	Cl-200-025-18	355	355	2400	1200	250	6.0	300	25.0	300	595.00	680	661
37	Cl-200-025-36	355	355	2400	1200	250	6.0	300	25.0	300	595.00	536	835
38	Cl-200-025-54	355	355	2400	1200	250	6.0	300	25.0	300	595.00	365	913
39	Cl-200-025-72	355	355	2400	1200	250	6.0	300	25.0	300	595.00	198	983
40	Cl-200-050-025-05	355	355	2400	1200	250	6.0	300	25.0	600	595.00	1114	279
41	Cl-200-050-025-0	355	355	2400	1200	250	6.0	300	25.0	600	595.00	1040	520
42	Cl-200-050-025-18	355	355	2400	1200	250	6.0	300	25.0	600	595.00	833	689
43	Cl-200-050-025-36	355	355	2400	1200	250	6.0	300	25.0	600	595.00	637	784
44	Cl-200-050-025-54	355	355	2400	1200	250	6.0	300	25.0	600	595.00	460	866
45	Cl-200-050-025-72	355	355	2400	1200	250	6.0	300	25.0	600	595.00	265	954
46	Cl-200-075-025-05	355	355	2400	1200	250	6.0	300	25.0	900	595.00	1387	347

continued on next page

continued from previous page

#	Specimen	f_{yw} [N/mm^2]	f_{yf} [N/mm^2]	a [mm]	h_w [mm]	b_1 [mm]	t_w [mm]	b_f [mm]	t_f [mm]	s_s [mm]	$I_{s\ell,1}$ [cm^4]	F_u [kN]	V_{avg} [kN]
47	Cl-200-075-025-0	355	355	2400	1200	250	6.0	300	25.0	900	595.00	1103	551
48	Cl-200-075-18	355	355	2400	1200	250	6.0	300	25.0	900	595.00	848	685
49	Cl-200-075-36	355	355	2400	1200	250	6.0	300	25.0	900	595.00	655	778
50	Cl-200-075-54	355	355	2400	1200	250	6.0	300	25.0	900	595.00	479	866
51	Cl-200-075-72	355	355	2400	1200	250	6.0	300	25.0	900	595.00	277	947
52	Cl-200-100-025	355	355	2400	1200	250	6.0	300	25.0	1200	595.00	1666	0
53	Cl-200-100-025-05	355	355	2400	1200	250	6.0	300	25.0	1200	595.00	1449	362
54	Cl-200-100-025-0	355	355	2400	1200	250	6.0	300	25.0	1200	595.00	1123	561
55	Cl-200-100-18	355	355	2400	1200	250	6.0	300	25.0	1200	595.00	861	691
56	Cl-200-100-36	355	355	2400	1200	250	6.0	300	25.0	1200	595.00	665	783
57	Cl-200-100-54	355	355	2400	1200	250	6.0	300	25.0	1200	595.00	486	867
58	Cl-200-100-72	355	355	2400	1200	250	6.0	300	25.0	1200	595.00	281	949

Table A.5: Numerical data, girders with open-section stiffeners

#	Specimen	f_{yw} [N/mm^2]	f_{yf} [N/mm^2]	a [mm]	h_w [mm]	b_1 [mm]	t_w [mm]	b_f [mm]	t_f [mm]	s_s [mm]	$I_{s\ell,1}$ [cm^4]	F_u [kN]	V_{avg} [kN]
1	O-200-V-025	355	355	2400	1200	300	6.0	300	25.0	n.a.	278.00	n.a.	990
2	O-200-025-025	355	355	2400	1200	300	6.0	300	25.0	300	278.00	625	0
3	O-200-050-025	355	355	2400	1200	300	6.0	300	25.0	600	278.00	813	0
4	O-200-075-025	355	355	2400	1200	300	6.0	300	25.0	900	278.00	1011	0
5	O-200-025-025-05	355	355	2400	1200	300	6.0	300	25.0	300	278.00	620	155
6	O-200-025-025-0	355	355	2400	1200	300	6.0	300	25.0	300	278.00	606	303
7	O-200-025-18	355	355	2400	1200	300	6.0	300	25.0	300	278.00	566	583
8	O-200-025-36	355	355	2400	1200	300	6.0	300	25.0	300	278.00	463	781
9	O-200-025-54	355	355	2400	1200	300	6.0	300	25.0	300	278.00	312	856
10	O-200-025-72	355	355	2400	1200	300	6.0	300	25.0	300	278.00	167	924
11	O-200-050-025-05	355	355	2400	1200	300	6.0	300	25.0	600	278.00	808	202
12	O-200-050-025-0	355	355	2400	1200	300	6.0	300	25.0	600	278.00	793	396
13	O-200-050-025-18	355	355	2400	1200	300	6.0	300	25.0	600	278.00	711	644
14	O-200-050-025-36	355	355	2400	1200	300	6.0	300	25.0	600	278.00	533	750
15	O-200-050-025-54	355	355	2400	1200	300	6.0	300	25.0	600	278.00	373	828
16	O-200-050-025-72	355	355	2400	1200	300	6.0	300	25.0	600	278.00	208	905
17	O-200-075-025-05	355	355	2400	1200	300	6.0	300	25.0	900	278.00	1016	254
18	O-200-075-025-0	355	355	2400	1200	300	6.0	300	25.0	900	278.00	946	473
19	O-200-075-18	355	355	2400	1200	300	6.0	300	25.0	900	278.00	750	630
20	O-200-075-36	355	355	2400	1200	300	6.0	300	25.0	900	278.00	578	729
21	O-200-075-54	355	355	2400	1200	300	6.0	300	25.0	900	278.00	418	810
22	O-200-075-72	355	355	2400	1200	300	6.0	300	25.0	900	278.00	241	895
23	O-200-100-025	355	355	2400	1200	300	6.0	300	25.0	1200	278.00	1199	0
24	O-200-100-025-05	355	355	2400	1200	300	6.0	300	25.0	1200	278.00	1172	293
25	O-200-100-025-0	355	355	2400	1200	300	6.0	300	25.0	1200	278.00	979	490
26	O-200-100-18	355	355	2400	1200	300	6.0	300	25.0	1200	278.00	763	632
27	O-200-100-36	355	355	2400	1200	300	6.0	300	25.0	1200	278.00	591	729
28	O-200-100-54	355	355	2400	1200	300	6.0	300	25.0	1200	278.00	427	808
29	O-200-100-72	355	355	2400	1200	300	6.0	300	25.0	1200	278.00	248	895

B Specimen data of girders under transverse patch loading and bending moment

B.1 Girders without longitudinal stiffeners

The specimen data is mainly taken from Lagerqvist [77] and Gozzi [56]. Tests which have been already excluded according to Sec. 7.3 in [77] and Sec. 5.3 in [56] are not shown here.

In Table B.1 experimental data is given for 238 welded girders. References are listed below according to the consecutive numbering:

- 1-4: Bamm et al. [2]
- 5-10: Granholm [58]
- 11: Galéa et al. [55]
- 12-41: Scheer et al. [112]
- 42-45: Shimizu et al. [117]
- 46-47: Oxfort and Gauger [87]
- 48-95: Dubas and Tschamper [39]
- 96-97: Höglund [62]
- 98-99: Dogaki et al. [35]
- 100-115: Drdácký and Novotný [37]
- 116-144: Bergfelt [9]
- 145-162: Bergfelt [10]
- 163-183: Skaloud and Novak, data taken from Roberts and Rockey [100]
- 184-186: Bagchi and Rockey, data taken from Roberts and Rockey [100]
- 187-200: Roberts [96]
- 201-205: Roberts and Coric [98]
- 206-210: Bossert and Ostapenko, data taken from Roberts and Chong [97]
- 211-220: Roberts and Markovic [99]
- 221: Raoul et al. [94]
- 222-230: Lagerqvist [77]
- 231-234: Shahabian and Roberts [116]
- 235: Seitz [114]
- 236-238: Gozzi [56]

Specimens 167 and 211 are not considered in the statistical evaluation because they have been classified as outliers according to Fig. 6.19, Sec. 6.5.2.2, which adulterate the statistical parameters. They are highlighted with a grey background in Table B.1.

In Table B.2 experimental data is given for 30 rolled girders. References are listed below according to the consecutive numbering:

- 1-11: Zoetemeijer [126]
- 12-15: Elgaaly and Nunan [43]
- 16-30: Elgaaly and Salkar [44]

Table B.1: Experimental data, welded girders

#	Ref. in [56, 77]	Specimen	f_{yw} [N/mm^2]	f_{yf} [N/mm^2]	a [mm]	h_w [mm]	t_w [mm]	b_f [mm]	t_f [mm]	s_s [mm]	F_u [kN]	M_u [kNm]
1	2001	77	305	427	1840	558	8.0	150	16.0	38	652	300
2	2002	78	305	427	1840	558	8.0	150	16.0	75	610	281
3	2003	79	305	305	1840	558	8.0	300	8.0	75	525	242
4	2004	80	286	427	1840	558	8.0	150	16.0	75	625	288
5	2006	E21	275	343	8000	580	4.6	180	9.0	120	170	339
6	2007	E23	275	343	8000	580	4.6	180	9.0	0	178	354
7	2008	E31	275	343	8000	580	3.1	180	9.0	120	91	182
8	2009	34	275	343	8000	580	3.1	180	9.0	0	83	313
9	2010	E36	275	343	8000	580	3.1	180	9.0	0	106	257
10	2011	E43	275	343	8000	580	3.1	200	10.0	0	105	210
11	2023	P1	276	250	1800	1274	6.0	230	40.0	690	530	2040
12	2024	A11	341	363	2300	800	3.7	200	20.2	280	176	925
13	2025	A12	341	363	2300	800	3.7	200	20.2	280	10	1204
14	2026	A13	341	363	2300	800	3.7	201	20.3	280	228	622
15	2027	A14	341	363	2300	800	3.7	200	20.3	280	139	1102
16	2028	A15	352	363	2300	800	4.1	199	20.3	280	217	922
17	2029	A16	341	363	2300	800	3.7	200	20.3	140	178	943
18	2030	A17	341	363	2300	800	3.7	199	20.3	140	201	556
19	2031	A21	341	329	2300	800	3.8	298	30.3	280	236	916
20	2032	A22	341	329	2300	800	3.8	300	30.2	280	264	716
21	2033	A23	341	329	2300	800	3.8	301	30.1	280	244	1302
22	2034	A24	341	329	2300	800	3.7	301	30.3	280	262	397
23	2035	A25	341	329	2300	800	3.7	301	30.2	280	205	1656
24	2036	A26	341	329	2300	800	3.7	299	30.4	140	238	1243
25	2037	A27	352	329	2300	800	4.1	299	30.1	140	258	702
26	2038	B11	329	335	1700	800	6.3	201	20.4	280	439	1156
27	2039	B12	328	335	1700	800	6.0	201	20.4	140	397	1051
28	2040	B13	325	327	2700	800	6.1	201	20.2	280	469	1219
29	2041	B21	332	329	2300	800	5.1	299	30.4	280	309	2421
30	2042	B22	332	329	2300	800	5.1	300	30.2	280	357	1854
31	2043	B23	332	329	2300	800	5.1	300	30.1	280	396	1047
32	2044	C11	378	363	2300	800	7.4	201	20.3	280	544	1412
33	2045	C12	378	363	2300	800	7.3	198	20.3	280	267	1450
34	2046	C13	378	363	2300	800	7.3	200	20.2	280	375	1574
35	2047	C14	378	363	2300	800	7.3	200	20.2	280	204	1698
36	2048	C15	373	363	2300	800	6.4	199	20.1	280	572	859
37	2049	C21	378	329	2300	800	7.4	299	30.9	280	806	2072
38	2050	C22	378	329	2300	800	7.4	301	30.3	280	314	2466
39	2051	C23	378	329	2300	800	7.5	299	30.3	280	623	2378
40	2052	C24	378	329	2300	800	7.5	298	30.2	280	500	2581
41	2053	C25	373	329	2300	800	6.3	300	30.2	280	631	951
42	2054	AL-1	319	320	1000	1000	6.0	300	9.0	300	332	747
43	2055	AL-2	320	320	1000	1000	6.0	300	9.0	500	355	799
44	2056	AS-1	320	320	1000	1000	6.0	300	9.0	300	353	529
45	2057	AS-2	325	320	1000	1000	6.0	300	9.0	500	480	720
46	2062	V1	215	195	2000	1300	11.8	302	38.3	100	888	2334
47	2063	V2	339	329	2000	1300	7.7	261	38.1	100	663	2975
48	2064	T01-1	360	281	2400	990	4.0	150	10.0	40	120	450
49	2065	T01-2	360	281	1800	990	4.0	150	10.0	40	177	80
50	2066	T01-3	360	281	1800	990	4.0	150	10.0	40	174	78
51	2067	T01-5	360	274	1800	990	4.0	150	10.0	40	173	78
52	2068	T01-6	360	274	1800	990	4.0	150	10.0	40	165	74
53	2069	T02-1	349	293	2400	990	4.0	150	8.0	40	134	309
54	2070	T02-2	349	293	1800	990	4.0	150	8.0	40	157	71
55	2071	T02-3	349	293	1800	990	4.0	150	8.0	40	154	69
56	2072	T02-5	349	298	1800	990	4.0	150	8.0	40	150	67
57	2073	T02-6	349	298	1800	990	4.0	150	8.0	40	161	72
58	2074	T03-1	317	294	2400	990	5.0	150	8.0	40	107	466

continued on next page

continued from previous page

#	Ref. in [56, 77]	Specimen	f_{yw} [N/mm^2]	f_{yf} [N/mm^2]	a [mm]	h_w [mm]	t_w [mm]	b_f [mm]	t_f [mm]	s_s [mm]	F_u [kN]	M_u [kNm]
59	2075	T03-2	317	294	1800	990	5.0	150	8.0	40	196	88
60	2076	T03-3	317	294	1800	990	5.0	150	8.0	40	194	87
61	2077	T03-5	317	294	1800	990	5.0	150	8.0	40	197	89
62	2078	T03-6	317	294	1800	990	5.0	150	8.0	40	197	89
63	2079	VT01-1	369	293	2480	1000	3.8	150	8.4	240	125	305
64	2080	VT01-2	369	293	1760	1000	3.8	150	8.4	40	146	64
65	2081	VT01-3	369	293	1760	1000	3.8	150	8.4	240	193	85
66	2082	VT01-4	369	327	2480	1000	3.8	150	8.5	240	124	466
67	2083	VT01-5	369	327	1760	1000	3.8	150	8.5	240	191	84
68	2084	VT01-6	369	327	1760	1000	3.8	150	8.5	40	146	64
69	2085	VT02-1	352	292	2480	1000	3.8	100	11.9	40	97	356
70	2086	VT02-2	352	292	1760	1000	3.8	100	11.9	40	143	63
71	2087	VT02-3	352	292	1760	1000	3.8	100	11.9	40	145	64
72	2088	VT02-4	352	292	2480	1000	3.8	100	11.9	40	125	310
73	2089	VT02-5	352	292	1760	1000	3.8	100	11.9	40	144	63
74	2090	VT03-1	305	286	2480	1000	5.2	150	12.0	40	140	668
75	2091	VT03-2	305	286	1760	1000	5.2	150	12.0	40	259	114
76	2092	VT03-3	305	286	1760	1000	5.2	150	12.0	240	353	155
77	2093	VT03-5	305	277	1760	1000	5.2	150	12.0	40	231	102
78	2094	VT03-6	305	277	1760	1000	5.2	150	12.0	240	333	146
79	2095	VT04-1	300	279	2480	1000	5.2	150	12.0	240	187	588
80	2096	VT04-2	300	279	1760	1000	5.2	150	12.0	40	243	107
81	2097	VT04-3	300	279	1760	1000	5.2	150	12.0	640	421	185
82	2098	VT04-4	300	284	2480	1000	5.2	150	12.0	640	292	628
83	2099	VT04-5	300	284	1760	1000	5.2	150	12.0	40	246	108
84	2100	VT04-6	300	284	1760	1000	5.2	150	12.0	640	427	188
85	2101	VT05-1	292	300	2480	800	5.0	150	8.4	40	114	382
86	2102	VT05-2	292	300	1760	800	5.0	150	8.4	40	179	79
87	2103	VT05-3	292	300	1760	800	5.0	150	8.4	240	250	110
88	2104	VT05-5	292	300	1760	800	5.0	150	8.4	40	187	82
89	2105	VT05-6	292	300	1760	800	5.0	150	8.4	240	255	112
90	2106	VT06-1	301	291	2480	800	5.0	150	12.0	40	172	364
91	2107	VT06-2	301	291	1760	800	5.0	150	12.0	40	211	93
92	2108	VT06-3	301	286	1760	800	5.0	150	12.0	240	266	117
93	2109	VT06-4	301	286	2480	800	5.0	150	12.0	240	217	455
94	2110	VT06-5	301	286	1760	800	5.0	150	12.0	40	216	95
95	2111	VT06-6	301	291	1760	800	5.0	150	12.0	640	388	171
96	2112	1	422	355	3150	830	4.9	200	10.0	170	250	197
97	2113	5	422	355	3150	830	4.9	200	10.0	0	224	176
98	2114	1	255	308	900	900	3.2	80	5.0	90	110	25
99	2115	2	306	308	900	900	6.0	80	5.0	90	298	67
100	2135	TTG1	285	269	300	300	4.0	49	10.0	30	130	10
101	2136	TTG2	270	288	300	300	4.0	50	9.9	30	148	11
102	2137	TTG3	281	265	300	300	4.0	50	15.9	30	170	13
103	2138	TTG4	267	267	450	450	4.0	49	10.0	45	120	14
104	2139	TTG6	249	265	450	450	4.0	50	15.8	45	150	17
105	2140	TTG7	257	274	600	600	3.6	50	10.0	60	140	21
106	2141	TTG8	282	279	600	600	3.6	50	10.1	60	148	22
107	2142	TTG9	306	282	600	600	3.7	49	16.0	60	150	22
108	2143	TTG'1	285	269	300	300	4.0	49	10.0	45	150	11
109	2144	TTG'2	270	288	300	300	4.0	50	9.9	60	146	11
110	2145	TTG'3	281	265	300	300	4.0	49	15.9	30	150	11
111	2146	TTG'4	267	267	450	450	4.0	49	10.0	60	136	15
112	2147	TTG'6	249	265	450	450	4.0	50	15.8	45	160	18
113	2148	TTG'7	257	274	600	600	3.6	50	10.0	30	119	18
114	2149	TTG'8	282	279	600	600	3.6	50	10.1	45	138	21
115	2150	TTG'9	306	282	600	600	3.7	49	16.0	60	146	22
116	2168	B23	325	347	9400	700	3.3	150	6.1	0	95	57
117	2169	B1	325	347	2400	700	3.3	150	6.1	100	106	64
118	2170	B2	325	235	2400	700	3.3	200	8.5	0	110	66
119	2171	B3	325	235	2400	700	3.3	200	8.5	100	122	73
120	2172	B4	325	243	2400	700	3.3	250	10.1	0	121	72
121	2173	B5	325	243	2400	700	3.3	250	10.1	100	133	80
122	2174	B6	325	232	2400	700	3.3	250	11.9	0	135	81
123	2175	B7	325	232	2400	700	3.3	250	11.9	100	139	84
124	2176	B8	325	305	2400	700	3.3	300	15.3	0	151	91
125	2177	B9	325	305	2400	700	3.3	300	15.3	100	156	94
126	2178	R1	266	295	800	800	2.1	300	15.5	40	60	12
127	2179	R12	266	295	800	800	2.1	300	15.5	40	66	13
128	2180	R3	266	285	800	800	2.0	120	5.1	40	38	8
129	2181	R32	266	285	800	800	2.0	120	5.1	40	41	8
130	2182	A11	300	295	2500	800	2.1	300	15.4	40	64	8
131	2183	A13	300	295	1200	800	2.1	300	15.4	40	66	20
132	2184	A21	245	265	2500	800	3.0	250	12.0	40	84	17
133	2185	A23	245	265	1200	800	3.0	250	12.0	40	85	26
134	2186	A31	354	290	2200	680	2.1	120	5.1	40	47	56
135	2187	A33	354	290	1020	680	2.1	120	5.1	40	51	13
136	2188	B8	285	290	800	800	2.1	120	5.0	40	48	10
137	2189	B6	285	290	800	600	2.1	120	5.0	40	42	8

continued on next page

continued from previous page

#	Ref. in [56, 77]	Specimen	f_{yw} [N/mm^2]	f_{yf} [N/mm^2]	a [mm]	h_w [mm]	t_w [mm]	b_f [mm]	t_f [mm]	s_s [mm]	F_u [kN]	M_u [kNm]
138	2190	B4	285	290	800	400	2.1	120	5.0	40	48	10
139	2191	B3	285	290	800	300	2.1	120	5.0	40	49	10
140	2192	B41	285	290	400	400	2.1	120	5.0	40	53	5
141	2193	B31	285	290	400	300	2.1	120	5.0	40	51	5
142	2194	B83	328	298	800	800	2.9	250	12.4	40	121	24
143	2195	B63	328	298	800	600	2.9	250	12.4	40	120	24
144	2196	B43	328	298	800	400	2.9	250	12.4	40	119	24
145	2288	324	207	277	2400	300	2.0	100	6.1	40	40	24
146	2289	325	207	277	900	300	2.0	100	6.1	40	34	8
147	2290	326	207	277	900	300	2.0	100	6.1	120	38	9
148	2291	624	206	284	2400	600	2.0	100	6.1	40	35	21
149	2292	625	206	284	900	600	2.0	100	6.1	40	31	7
150	2293	626	206	284	900	600	2.0	100	6.1	120	38	8
151	2294	424	205	278	3000	400	2.0	100	12.2	40	41	30
152	2295	425	205	278	1100	400	2.0	100	12.2	40	37	10
153	2296	426	205	278	1100	400	2.0	100	12.2	120	42	12
154	2297	824	205	277	3000	800	2.0	100	12.1	40	42	31
155	2298	825	205	277	1100	800	2.0	100	12.1	40	41	11
156	2299	826	205	277	1100	800	2.0	100	12.1	120	47	13
157	2300	827	206	273	3000	800	2.0	250	12.3	40	38	29
158	2301	828	206	273	1100	800	2.0	250	12.3	40	41	11
159	2302	829	206	273	1100	800	2.0	250	12.3	120	41	11
160	2303	837	215	268	3000	800	3.0	250	12.0	40	82	61
161	2304	838	215	268	1100	800	3.0	250	12.0	40	91	25
162	2305	839	215	268	1100	800	3.0	250	12.0	120	93	25
163	2306	TG1	298	342	1000	1000	2.5	160	5.5	100	52	13
164	2307	TG2	299	253	1000	1000	2.5	200	10.1	100	64	16
165	2308	TG3	251	266	1000	1000	2.5	200	16.2	100	69	17
166	2309	TG4	254	231	1000	1000	2.5	200	20.2	100	88	22
167	2310	TG5	289	261	1000	1000	2.5	250	30.5	100	179	45
168	2311	TG6	290	294	2000	1000	3.0	160	6.3	100	82	41
169	2312	TG7	297	253	2000	1000	3.0	200	10.0	100	98	49
170	2313	TG8	308	266	2000	1000	3.0	200	16.6	100	118	59
171	2314	TG9	300	231	2000	1000	3.0	200	19.8	100	126	63
172	2315	TG10	299	261	2000	1000	3.0	250	30.0	100	147	74
173	2316	TG11	290	294	2000	1000	3.0	160	6.3	200	93	47
174	2317	TG12	297	253	2000	1000	3.0	200	10.0	200	118	59
175	2318	TG13	308	266	2000	1000	3.0	200	16.6	200	132	66
176	2319	TG14	300	231	2000	1000	3.0	200	19.8	200	152	76
177	2320	TG15	299	261	2000	1000	3.0	250	30.0	200	158	79
178	2321	STG12	243	294	500	500	2.0	50	6.0	50	37	5
179	2322	STG34	243	261	500	500	2.0	45	16.2	50	54	7
180	2323	STG56	243	225	500	500	2.0	50	24.6	50	76	10
181	2324	STG78	280	294	1000	500	2.0	50	5.0	100	36	9
182	2325	STG910	280	261	1000	500	2.0	45	15.9	100	49	12
183	2326	STG1112	280	225	1000	500	2.0	60	24.8	100	56	14
184	2327	BR1	250	250	660	635	3.3	152	12.7	75	141	23
185	2328	BR2	250	250	864	635	3.3	152	12.7	50	124	27
186	2329	BR3	250	250	1270	635	3.3	152	12.7	50	89	28
187	2333	A2-3	224	221	600	250	2.1	149	3.1	50	33	5
188	2334	A2-7	224	279	600	250	2.1	149	6.8	50	42	6
189	2335	A2-12	224	305	600	250	2.1	149	11.8	50	53	8
190	2336	A3-3	221	221	600	250	3.1	149	3.1	50	80	12
191	2337	A3-7	221	279	600	250	3.1	149	6.8	50	101	15
192	2338	A3-12	221	305	600	250	3.1	149	11.8	50	129	19
193	2342	B2-2	224	221	600	500	2.1	149	3.1	50	34	5
194	2343	B2-7	224	279	600	500	2.1	149	6.8	50	38	6
195	2344	B2-12	224	305	600	500	2.1	149	11.8	50	44	7
196	2345	B2-20	224	305	600	500	2.1	149	20.1	50	85	13
197	2346	B3-3	221	221	600	500	3.1	149	3.1	50	71	11
198	2347	B3-7	221	279	600	500	3.1	149	6.8	50	91	14
199	2348	B3-12	221	305	600	500	3.1	149	11.8	50	111	17
200	2349	B3-20	221	305	600	500	3.1	149	20.1	50	131	20
201	2356	D2-2	178	272	760	380	2.0	80	3.1	50	34	6
202	2357	D3-6	245	298	760	380	3.0	80	6.3	50	84	16
203	2358	D5-10	292	305	760	380	4.9	100	10.0	50	253	48
204	2359	D2-3S	178	272	760	380	2.0	80	3.1	50	32	18
205	2360	D3-6S	245	298	760	380	3.0	80	6.3	50	84	48
206	2365	EG2.1	252	300	1092	914	2.9	203	15.9	1092	134	18
207	2367	EG2.3	252	300	1092	914	2.9	203	15.9	1092	205	28
208	2368	EG2.4	252	300	1092	914	2.9	203	15.9	1092	194	26
209	2369	EG3.1	236	300	1448	914	3.1	203	15.9	1448	201	36
210	2370	EG3.2	236	300	1448	914	3.1	203	15.9	1448	170	31
211	2371	E10-1/1	222	240	500	500	10.0	150	10.0	0	716	90
212	2372	E10-2/1	247	250	500	500	10.0	150	10.0	100	787	98
213	2373	E10-1/2	222	240	500	500	10.0	150	10.0	50	698	87
214	2374	E10-2/2	247	250	500	500	10.0	150	10.0	50	738	92
215	2375	E6-1/1	253	250	500	500	6.0	150	10.0	0	304	38
216	2376	E6-1/2	253	250	500	500	6.0	150	10.0	50	378	47

continued on next page

continued from previous page

#	Ref. in [56, 77]	Specimen	f_{yw} [N/mm^2]	f_{yf} [N/mm^2]	a [mm]	h_w [mm]	t_w [mm]	b_f [mm]	t_f [mm]	s_s [mm]	F_u [kN]	M_u [kNm]
217	2377	E6-2/1	253	237	500	500	6.0	150	10.0	100	399	50
218	2378	E6-2/2	253	237	500	500	6.0	150	10.0	50	344	43
219	2379	F3-1/1	242	308	500	500	3.0	150	5.9	50	89	11
220	2380	F3-1/2	242	308	500	500	3.0	150	5.9	50	89	11
221	2384	1	362	286	1780	1274	6.0	230	40.0	230	610	271
222	2385	A13p	830	844	1008	240	3.8	119	12.0	40	323	81
223	2386	A14p	830	844	1004	240	3.8	119	12.0	80	346	87
224	2387	A22p	830	844	1260	278	3.8	120	12.0	80	357	113
225	2388	A32p	832	844	1404	320	3.9	120	12.0	40	334	117
226	2389	A41p	832	844	1315	360	3.8	121	11.9	40	311	102
227	2390	A51p	830	844	1690	398	3.8	120	12.0	40	310	147
228	2391	A61p	830	844	1626	440	3.8	120	12.0	40	293	119
229	2392	A71p	762	844	1405	321	7.9	121	11.9	40	931	327
230	2393	A81p	762	844	1684	401	8.0	120	12.0	40	929	391
231	2394	PG1-1	343	257	600	600	4.1	200	12.5	50	220	33
232	2395	PG2-1	285	254	900	900	3.1	300	10.2	50	113	25
233	2396	PG3-1	282	264	900	600	3.2	200	10.1	50	120	27
234	2397	PG4-1	250	293	1000	500	1.9	200	9.9	50	52	13
235	2403	I	367	396	2400	1200	6.0	260	20.0	700	659	395
236	2404	P200	394	354	2401	1198	5.9	449	20.0	200	544	327
237	2405	P700	394	354	2400	1200	5.9	450	20.0	700	660	396
238	2406	P1400	394	354	2400	1200	5.9	450	20.0	1440	808	485

Table B.2: Experimental data, rolled girders

#	Ref. in [77]	Specimen	f_y [N/mm^2]	$0.8 \cdot f_y$ [N/mm^2]	a [mm]	h_w [mm]	h_1 [mm]	t_w [mm]	b_f [mm]	t_f [mm]	s_s [mm]	F_u [kN]	M_u [kNm]
1	2012	1	367	293.6	900	220	190	6.2	120	9.8	40	380	0
2	2013	2	367	293.6	900	220	190	6.2	120	9.8	40	349	78
3	2014	26	317	253.6	900	206	164	7.5	240	12.0	40	480	108
4	2015	27	317	253.6	1200	206	164	7.5	240	12.0	40	458	137
5	2016	31	317	253.6	800	206	164	7.5	240	12.0	40	473	0
6	2017	A1	357	285.6	1000	262	208	8.5	300	14.0	40	660	165
7	2018	A2	357	285.6	2000	262	208	8.5	300	14.0	40	560	280
8	2019	A11	357	285.6	1067	262	208	8.5	300	14.0	40	670	168
9	2020	A12	357	285.6	1067	262	208	8.5	300	14.0	40	670	168
10	2021	B1	286	228.8	1800	444	390	12.0	300	23.0	40	1000	450
11	2022	B2	286	228.8	2700	444	390	12.0	300	23.0	40	870	587
12	2116	I:1	352	281.6	305	291	268	6.1	99	8.2	61	294	22
13	2117	II:1	476	380.8	305	291	268	6.5	102	9.0	61	492	37
14	2118	II:2	476	380.8	305	291	268	6.5	102	9.0	61	447	34
15	2119	II:3	476	380.8	305	291	268	6.5	102	9.0	61	438	33
16	2120	1	348	278.4	482	291	267	5.1	104	5.4	61	234	28
17	2121	2	348	278.4	482	291	267	5.1	104	5.4	121	331	40
18	2122	3	368	294.4	479	291	267	5.0	103	5.3	182	335	40
19	2123	4	356	284.8	562	332	305	6.2	130	8.5	70	396	56
20	2124	5	356	284.8	562	332	305	6.2	130	8.5	140	432	61
21	2125	6	320	256.0	559	332	305	5.8	130	8.4	210	384	54
22	2126	7	389	311.2	644	381	346	6.7	140	10.9	81	498	80
23	2127	8	389	311.2	644	381	346	6.7	140	10.9	162	645	104
24	2128	9	363	290.4	644	381	346	6.8	143	10.9	243	754	121
25	2129	10	331	264.8	717	428	394	7.7	154	11.0	90	489	88
26	2130	11	331	264.8	717	428	394	7.7	154	11.0	180	556	100
27	2131	12	421	336.8	721	428	394	7.3	154	10.9	270	823	148
28	2132	13	399	319.2	840	502	434	8.9	169	13.4	106	863	181
29	2133	14	399	319.2	840	502	434	8.9	169	13.4	213	1032	217
30	2134	15	392	313.6	840	502	434	9.0	169	13.4	319	1316	277

B.2 Girders with longitudinal stiffeners

The specimen data is mainly taken from Graciano [57], Clarin [19] and Davaine [24]. Tests which have been already excluded according to Sec. 4.5 in [19] are not shown here.

In Table B.3 experimental data is given for 24 girders with closed-section stiffeners. References are listed below according to the consecutive numbering:

- 1-12: Dubas and Tschamper [39]
- 13-18: Carratero and Lebet [15]
- 19-22: Seitz [114]
- 23-24: Walbridge and Lebet [123]

In Table B.4 experimental data is given for 136 girders with open-section stiffeners. References are listed below according to the consecutive numbering:

- 1-98: Janus et al. [64]
- 99-100: Rockey et al. [104]
- 101-111: Bergfelt [9]
- 112-113: Dogaki et al. [34]
- 114-115: Galéa et al. [55]
- 116-121: Bergfelt [10]
- 122-133: Dubas and Tschamper [39]
- 134-136: Walbridge and Lebet [123]

In Table B.5 numerical data is given for 421 girders with open-section stiffeners. The simulations were solely carried out by Davaine [24]. Specimens 187 to 189 and 193 to 195 are not considered in the statistical evaluation because they have been classified as outliers according to Fig. 6.20, Sec. 6.5.2.2, which adulterate the statistical parameters. They are highlighted with a grey background in Table B.4.

Table B.3: Experimental data, girders with closed-section stiffeners

#	Specimen	f_{yw} [N/mm^2]	f_{yf} [N/mm^2]	a [mm]	h_w [mm]	b_1 [mm]	t_w [mm]	b_f [mm]	t_f [mm]	s_s [mm]	$I_{s\ell,1}$ [cm^4]	F_u [kN]	M_u [kNm]
1	VT07-1	375	296	2480	1000	150	3.8	150	8.4	40	62.40	130	582
2	VT07-2	375	296	1760	1000	150	3.8	150	8.4	40	62.40	176	77
3	VT07-3	375	296	1760	1000	150	3.8	150	8.4	40	62.40	172	76
4	VT08-1	358	292	2480	1000	150	3.8	150	8.3	240	62.74	160	558
5	VT08-2	358	292	1760	1000	150	3.8	150	8.3	240	62.74	280	123
6	VT08-3	358	292	1760	1000	150	3.8	150	8.3	240	62.74	300	132
7	VT09-1	371	286	2480	1000	150	3.8	150	12.0	40	62.49	130	635
8	VT09-2	371	286	1760	1000	150	3.8	150	12.0	40	62.49	198	87
9	VT09-3	371	286	1760	1000	150	3.8	150	12.0	40	62.49	210	92
10	VT10-1	380	282	2480	1000	150	3.8	150	12.0	240	62.30	247	617
11	VT10-2	380	282	1760	1000	150	3.8	150	12.0	240	62.30	330	145
12	VT10-3	380	282	1760	1000	150	3.8	150	12.0	240	62.30	315	139
13	Panel 1-5	483	399	1050	800	230	6.0	300	20.0	200	129.55	645	169
14	Panel 2-1	405	371	1200	800	160	4.0	160	10.0	300	102.12	437	131
15	Panel 2-2	447	364	1200	800	300	6.0	200	15.0	300	130.53	632	190
16	Panel 2-6	483	399	1050	800	160	6.0	300	20.0	200	129.55	778	204
17	Panel 4-4	483	399	1200	800	230	6.0	300	20.0	300	129.55	590	177
18	Panel 6-4	483	399	1800	800	160	6.0	300	20.0	300	129.55	698	314
19	Träger II	367	396	2400	1200	250	6.0	260	20.0	700	344.45	1034	517
20	Träger III	367	378	2400	1200	310	6.0	260	20.0	700	344.45	949	475

continued on next page

continued from previous page

#	Specimen	f_{yw} [N/mm^2]	f_{yf} [N/mm^2]	a [mm]	h_w [mm]	b_1 [mm]	t_w [mm]	b_f [mm]	t_f [mm]	s_s [mm]	$I_{s\ell,1}$ [cm^4]	F_u [kN]	M_u [kNm]
21	Träger IV	373	378	2400	1200	250	6.0	260	20.0	700	343.99	991	2731
22	Träger V	373	378	2400	1200	310	6.0	260	20.0	700	343.99	958	2653
23	Panel 2-C1	392	355	1000	700	75	5.0	225	20.0	200	118.25	699	175
24	Panel 3-C2	392	355	1000	700	125	5.0	225	20.0	200	118.25	507	127

Table B.4: Experimental data, girders with open-section stiffeners

#	Specimen	f_{yw} [N/mm^2]	f_{yf} [N/mm^2]	a [mm]	h_w [mm]	b_1 [mm]	t_w [mm]	b_f [mm]	t_f [mm]	s_s [mm]	$I_{s\ell,1}$ [cm^4]	F_u [kN]	M_u [kNm]
1	TG 2-1	234	453	505	505	100	2.0	50	5.0	50	0.28	37	5
2	TG 2-2	232	446	505	505	100	2.0	50	5.0	50	1.02	36	4
3	TG 2-3	233	458	505	505	100	2.0	50	5.0	50	2.92	41	5
4	TG 3-1(1)	236	485	505	505	50	2.0	50	5.0	50	0.28	35	4
5	TG 3-1(2)	234	466	505	505	50	2.0	50	5.0	50	0.28	42	5
6	TG 3-2(1)	239	467	505	505	50	2.0	50	5.0	50	1.02	39	5
7	TG 3-2(2)	232	471	505	505	50	2.0	50	5.0	50	1.02	42	5
8	TG 3-3(1)	231	461	505	505	50	2.0	50	5.0	50	2.92	48	6
9	TG 3-3(2)	233	481	505	505	50	2.0	50	5.0	50	2.92	43	5
10	TG 11-1	191	293	1005	503	250	2.0	50	5.0	100	0.28	32	8
11	TG 11-2	210	472	1005	503	250	2.0	50	5.0	100	1.02	34	9
12	TG 11-3	215	476	1005	503	250	2.0	50	5.0	100	2.92	38	9
13	TG 12-1	204	295	1005	503	100	2.0	50	5.0	100	0.28	33	8
14	TG 12-2	218	461	1005	503	100	2.0	50	5.0	100	1.02	38	10
15	TG 12-3	218	470	1005	503	100	2.0	50	5.0	100	2.92	38	10
16	TG 13-1(1)	191	303	1005	503	50	2.0	50	5.0	100	0.28	29	7
17	TG 13-1(2)	204	293	1005	503	50	2.0	50	5.0	100	0.28	33	8
18	TG 13-2(1)	210	475	1005	503	50	2.0	50	5.0	100	1.02	44	11
19	TG 13-2(2)	218	469	1005	503	50	2.0	50	5.0	100	1.02	34	9
20	TG 13-3(1)	215	478	1005	503	50	2.0	50	5.0	100	2.92	43	11
21	TG 13-3(2)	218	473	1005	503	50	2.0	50	5.0	100	2.92	40	10
22	TG 31-1	256	242	623	500	200	6.0	120	12.0	62	11.89	315	49
23	TG 31-1'	256	242	623	500	200	6.0	120	12.0	62	11.89	300	47
24	TG 31-2	256	242	623	500	125	6.0	120	12.0	62	11.89	342	53
25	TG 31-2'	256	242	623	500	125	6.0	120	12.0	62	11.89	327	51
26	TG 31-3	256	242	623	500	75	6.0	120	12.0	62	11.75	370	58
27	TG 31-3'	256	242	623	500	75	6.0	120	12.0	62	11.75	395	61
28	TG 32-1	256	242	623	500	200	6.0	120	12.0	62	11.89	285	44
29	TG 32-1'	256	242	623	500	200	6.0	120	12.0	62	11.89	295	46
30	TG 32-2	256	242	623	500	125	6.0	120	12.0	62	11.89	290	45
31	TG 32-2'	256	242	623	500	125	6.0	120	12.0	62	11.89	299	47
32	TG 32-3	256	242	623	500	75	6.0	120	12.0	62	11.75	351	55
33	TG 32-3'	256	242	623	500	75	6.0	120	12.0	62	11.75	338	53
34	TG 33-1	256	242	623	500	200	6.0	120	12.0	62	11.89	296	46
35	TG 33-1'	256	242	623	500	200	6.0	120	12.0	62	11.89	276	43
36	TG 33-2	256	242	623	500	125	6.0	120	12.0	62	11.89	300	47
37	TG 33-2'	256	242	623	500	125	6.0	120	12.0	62	11.89	282	44
38	TG 33-3	256	242	623	500	75	6.0	120	12.0	62	11.75	372	58
39	TG 33-3'	256	242	623	500	75	6.0	120	12.0	62	11.75	399	62
40	TG 021-0	224	292	500	500	100	2.4	100	5.1	50	0.42	40	5
41	TG 021-1	238	309	500	500	100	2.2	120	6.1	50	3.63	55	7
42	TG 021-2	238	309	500	500	100	2.2	120	6.0	50	6.78	58	7
43	TG 021-3	238	309	500	500	100	2.2	120	6.0	50	12.34	62	8
44	TG 022-1	238	239	500	500	100	2.2	120	11.7	50	3.68	65	8
45	TG 022-2	238	239	500	500	100	2.2	119	11.9	50	6.78	67	8
46	TG 022-3	238	239	500	500	100	2.2	120	11.9	50	11.96	59	7
47	TG 041-0	362	262	500	500	100	4.4	119	8.5	50	1.16	192	24
48	TG 041-1	360	262	500	500	100	4.0	119	8.4	50	13.83	190	24
49	TG 041-2	360	262	500	500	100	4.0	119	7.8	50	23.52	202	25
50	TG 041-3	360	262	500	500	100	4.0	119	8.5	50	39.84	194	24
51	TG 042-1	360	285	500	500	100	4.0	121	20.0	50	12.30	315	39
52	TG 042-2	360	285	500	500	100	4.0	121	20.0	50	25.03	290	36
53	TG 042-3	360	285	500	500	100	4.0	120	20.0	50	39.35	276	35
54	TG 061-0	426	239	500	500	100	5.6	120	11.9	50	3.90	339	42
55	TG 061-1	426	277	500	500	100	5.6	90	12.3	50	11.04	387	48
56	TG 061-2	455	277	500	500	100	5.5	90	12.3	50	37.58	408	51
57	TG 061-3	455	277	500	500	100	5.5	89	12.1	50	52.83	420	53
58	TG 062-1	426	254	500	500	100	5.6	99	30.4	50	11.22	564	71
59	TG 062-2	426	254	500	500	100	5.6	100	30.5	50	35.09	592	74
60	TG 062-3	426	254	500	500	100	5.6	100	30.0	50	55.33	610	76
61	TG 121-1	244	274	500	500	100	2.0	120	6.0	50	0.65	55	7
62	TG 121-2	244	274	500	500	100	2.0	120	6.0	50	1.07	50	6

continued on next page

continued from previous page

#	Specimen	f_{yw} [N/mm^2]	f_{yf} [N/mm^2]	a [mm]	h_w [mm]	b_1 [mm]	t_w [mm]	b_f [mm]	t_f [mm]	s_s [mm]	$I_{s\ell,1}$ [cm^4]	F_u [kN]	M_u [kNm]
63	TG 121-3	244	274	500	500	100	2.0	120	6.1	50	1.84	57	7
64	TG 122-1	244	254	500	500	100	2.0	121	12.1	50	0.56	84	11
65	TG 122-2	244	254	500	500	100	2.0	121	12.1	50	1.07	72	9
66	TG 122-3	244	254	500	500	100	2.0	121	12.1	50	1.87	76	10
67	TG 141-1	283	294	500	500	100	4.0	120	8.4	50	2.40	171	21
68	TG 141-2	283	294	500	500	100	4.0	120	8.5	50	6.98	156	20
69	TG 141-3	283	294	500	500	100	4.0	120	8.3	50	9.26	185	23
70	TG 142-1	283	270	500	500	100	4.0	121	20.3	50	2.30	257	32
71	TG 142-2	283	270	500	500	100	4.0	121	20.4	50	6.81	248	31
72	TG-142-3	283	270	500	500	100	4.0	121	20.2	50	10.24	257	32
73	TG-161-1	396	272	500	500	100	5.4	91	12.4	50	5.78	336	42
74	TG-161-2	396	272	500	500	100	5.4	91	12.3	50	9.95	388	48
75	TG 161-3	396	272	500	500	100	5.4	91	12.4	50	14.10	399	50
76	TG 162-1	396	269	500	500	100	5.4	100	30.4	50	6.13	610	76
77	TG 162-2	396	269	500	500	100	5.4	99	30.6	50	10.03	600	75
78	TG 162-3	396	269	500	500	100	5.4	100	30.6	50	13.29	605	76
79	TG 241-1	304	278	500	500	50	4.1	120	8.3	50	0.94	201	25
80	TG241-1'	304	278	500	500	50	4.1	120	8.3	50	0.93	196	25
81	TG 241-2	304	278	500	500	50	4.1	121	8.2	50	2.56	186	23
82	TG 241-2'	304	278	500	500	50	4.1	121	8.1	50	2.78	199	25
83	TG 241-3	304	278	500	500	50	4.1	120	8.2	50	4.35	199	25
84	TG 241-3'	304	278	500	500	50	4.1	121	8.2	50	4.31	186	23
85	TG 241-4	304	278	500	500	50	4.1	121	8.1	50	6.67	187	23
86	TG 241-4'	304	278	500	500	50	4.1	121	8.4	50	6.73	210	26
87	TG 241-5	304	278	500	500	50	4.1	121	8.1	50	9.46	192	24
88	TG 241-6	304	278	500	500	50	4.1	121	8.2	50	13.92	208	26
89	TG 242-1	304	244	500	500	50	4.1	118	19.7	50	0.86	243	30
90	TG 242-1'	304	244	500	500	50	4.1	119	19.7	50	0.92	237	30
91	TG 242-2	304	244	500	500	50	4.1	119	19.8	50	2.50	267	33
92	TG 242-2'	304	244	500	500	50	4.1	118	19.9	50	2.44	259	32
93	TG 242-3	304	244	500	500	50	4.1	119	19.8	50	3.97	255	32
94	TG 242-3'	304	244	500	500	50	4.1	119	19.9	50	3.93	261	33
95	TG 242-4	304	244	500	500	50	4.1	119	19.7	50	6.68	264	33
96	TG 242-4'	304	244	500	500	50	4.1	118	19.6	50	7.02	266	33
97	TG 242-5	304	244	500	500	50	4.1	118	19.6	50	9.55	270	34
98	TG 242-6	304	244	500	500	50	4.1	118	19.6	50	13.83	285	36
99	R2	266	286	802	798	168	2.1	301	15.6	40	20.61	71	14
100	R4	266	285	800	798	162	2.0	120	5.1	40	5.17	45	9
101	R22ss	266	295	800	800	168	2.0	300	15.0	40	20.61	69	14
102	R42ss	266	285	800	800	162	2.0	120	5.0	40	5.17	43	9
103	A12s	300	295	2500	800	160	2.0	300	15.0	40	19.37	80	50
104	A14s	300	295	1200	800	160	2.0	300	15.0	40	19.37	78	23
105	A16s	300	295	600	800	160	2.0	300	15.0	40	19.37	92	14
106	A22s	245	265	2500	800	160	3.0	250	12.0	40	26.53	133	83
107	A24s	245	265	1200	800	160	3.0	250	12.0	40	26.53	98	29
108	A26s	245	265	600	800	160	3.0	250	12.0	40	26.53	121	18
109	A32s	354	290	2200	680	136	2.0	120	5.0	40	4.94	46	25
110	A34s	354	290	1020	680	136	2.0	120	5.0	40	4.94	54	14
111	A36s	354	290	510	680	136	2.0	120	5.0	40	4.94	55	7
112	Model 4	270	266	897	899	180	3.2	181	8.0	90	3.63	105	24
113	Model 5	270	266	892	902	180	3.2	180	8.0	90	7.03	110	25
114	P2	279	244	1780	1274	327	6.0	230	40.0	690	331.52	720	2772
115	P3	286	267	1780	1274	264	6.0	230	40.0	690	330.27	730	2811
116	731	252	277	3000	735	250	3.0	250	12.0	40	26.42	93	70
117	732	252	277	1100	735	250	3.0	250	12.0	40	26.42	92	25
118	733	252	277	1100	735	250	3.0	250	12.0	120	26.42	101	28
119	734	252	277	3000	735	150	3.0	250	12.0	40	26.42	105	79
120	735	252	277	1100	735	150	3.0	250	12.0	40	26.42	102	28
121	736	252	277	1100	735	150	3.0	250	12.0	120	26.42	106	29
122	VT07-4	375	281	2480	1000	200	3.8	150	8.4	40	84.44	135	502
123	VT07-5	375	281	1760	1000	200	3.8	150	8.4	40	84.44	165	73
124	VT07-6	375	281	1760	1000	200	3.8	150	8.4	40	84.44	170	75
125	VT08-4	358	328	2480	1000	200	3.8	150	8.3	240	84.44	199	553
126	VT08-5	358	328	1760	1000	200	3.8	150	8.3	240	84.44	229	101
127	VT08-6	358	328	1760	1000	200	3.8	150	8.3	240	84.44	235	103
128	VT09-4	371	283	2480	1000	150	3.8	150	12.0	40	84.44	145	552
129	VT09-5	371	283	1760	1000	150	3.8	150	12.0	40	84.44	184	81
130	VT09-6	371	283	1760	1000	150	3.8	150	12.0	40	84.44	180	79
131	VT10-4	380	275	2480	1000	150	3.8	150	12.0	240	84.44	161	655
132	VT10-5	380	275	1760	1000	150	3.8	150	12.0	240	84.44	275	121
133	VT10-6	380	275	1760	1000	150	3.8	150	12.0	240	84.44	288	127
134	Panel 4-C2	392	355	1000	700	125	5.0	225	20.0	200	106.52	521	130
135	Panel 5-C3	392	355	1000	700	75	5.0	225	20.0	200	106.52	560	140
136	Panel 6-C3	392	355	1000	700	100	5.0	225	20.0	200	106.52	582	146

Table B.5: Numerical data, girders with open-section stiffeners

#	Specimen	f_{yw} [N/mm^2]	f_{yf} [N/mm^2]	a [mm]	h_w [mm]	b_1 [mm]	t_w [mm]	b_f [mm]	t_f [mm]	s_s [mm]	$I_{s\ell,1}$ [cm^4]	F_u [kN]	M_u [kNm]
1	P101	355	355	8000	3000	285	20.0	900	60.0	1000	19116.00	6948	13896
2	P102	355	355	8000	3000	435	20.0	900	60.0	1000	19116.00	6987	13974
3	P103	355	355	8000	3000	585	20.0	900	60.0	1000	19116.00	6558	13116
4	P104	355	355	8000	3000	735	20.0	900	60.0	1000	19116.00	6348	12696
5	P105	355	355	8000	3000	885	20.0	900	60.0	1000	19116.00	6009	12018
6	P106	355	355	8000	3000	1035	20.0	900	60.0	1000	19116.00	5770	11540
7	P107	355	355	8000	3000	1185	20.0	900	60.0	1000	19116.00	5714	11428
8	P111	355	355	4000	3000	285	20.0	900	60.0	1000	19116.00	7906	7906
9	P112	355	355	4000	3000	435	20.0	900	60.0	1000	19116.00	7646	7646
10	P113	355	355	4000	3000	585	20.0	900	60.0	1000	19116.00	7045	7045
11	P114	355	355	4000	3000	735	20.0	900	60.0	1000	19116.00	6705	6705
12	P115	355	355	4000	3000	885	20.0	900	60.0	1000	19116.00	6290	6290
13	P116	355	355	4000	3000	1035	20.0	900	60.0	1000	19116.00	6100	6100
14	P117	355	355	4000	3000	1185	20.0	900	60.0	1000	19116.00	6061	6061
15	P121	355	355	12000	3000	285	20.0	900	60.0	1000	19116.00	6385	19155
16	P122	355	355	12000	3000	435	20.0	900	60.0	1000	19116.00	6652	19956
17	P123	355	355	12000	3000	585	20.0	900	60.0	1000	19116.00	6559	19677
18	P124	355	355	12000	3000	735	20.0	900	60.0	1000	19116.00	6499	19497
19	P125	355	355	12000	3000	885	20.0	900	60.0	1000	19116.00	6212	18636
20	P126	355	355	12000	3000	1035	20.0	900	60.0	1000	19116.00	5945	17835
21	P127	355	355	12000	3000	1185	20.0	900	60.0	1000	19116.00	5568	16704
22	P131	355	355	8000	3000	288	20.0	900	60.0	1000	10369.10	6691	13382
23	P132	355	355	8000	3000	438	20.0	900	60.0	1000	10369.10	6838	13676
24	P133	355	355	8000	3000	588	20.0	900	60.0	1000	10369.10	6479	12958
25	P134	355	355	8000	3000	738	20.0	900	60.0	1000	10369.10	6326	12652
26	P135	355	355	8000	3000	888	20.0	900	60.0	1000	10369.10	6068	12136
27	P136	355	355	8000	3000	1038	20.0	900	60.0	1000	10369.10	5869	11738
28	P137	355	355	8000	3000	1188	20.0	900	60.0	1000	10369.10	5715	11430
29	P141	355	355	4000	3000	288	20.0	900	60.0	1000	10369.10	7649	7649
30	P142	355	355	4000	3000	438	20.0	900	60.0	1000	10369.10	7456	7456
31	P143	355	355	4000	3000	588	20.0	900	60.0	1000	10369.10	6888	6888
32	P144	355	355	4000	3000	738	20.0	900	60.0	1000	10369.10	6584	6584
33	P145	355	355	4000	3000	888	20.0	900	60.0	1000	10369.10	6228	6228
34	P146	355	355	4000	3000	1038	20.0	900	60.0	1000	10369.10	6097	6097
35	P147	355	355	4000	3000	1188	20.0	900	60.0	1000	10369.10	6071	6071
36	P151	355	355	12000	3000	288	20.0	900	60.0	1000	10369.10	6222	18666
37	P152	355	355	12000	3000	438	20.0	900	60.0	1000	10369.10	6466	19398
38	P153	355	355	12000	3000	588	20.0	900	60.0	1000	10369.10	6472	19416
39	P154	355	355	12000	3000	738	20.0	900	60.0	1000	10369.10	6478	19434
40	P155	355	355	12000	3000	888	20.0	900	60.0	1000	10369.10	6334	19002
41	P156	355	355	12000	3000	1038	20.0	900	60.0	1000	10369.10	6332	18996
42	P157	355	355	12000	3000	1188	20.0	900	60.0	1000	10369.10	5664	16992
43	P161	355	355	8000	3000	290	20.0	900	60.0	1000	4840.37	6469	12938
44	P162	355	355	8000	3000	440	20.0	900	60.0	1000	4840.37	6688	13376
45	P163	355	355	8000	3000	590	20.0	900	60.0	1000	4840.37	6414	12828
46	P164	355	355	8000	3000	740	20.0	900	60.0	1000	4840.37	6334	12668
47	P165	355	355	8000	3000	890	20.0	900	60.0	1000	4840.37	6134	12268
48	P166	355	355	8000	3000	1040	20.0	900	60.0	1000	4840.37	6030	12060
49	P167	355	355	8000	3000	1190	20.0	900	60.0	1000	4840.37	5674	11348
50	P171	355	355	4000	3000	290	20.0	900	60.0	1000	4840.37	7441	7441
51	P172	355	355	4000	3000	440	20.0	900	60.0	1000	4840.37	7304	7304
52	P173	355	355	4000	3000	590	20.0	900	60.0	1000	4840.37	6779	6779
53	P174	355	355	4000	3000	740	20.0	900	60.0	1000	4840.37	6510	6510
54	P175	355	355	4000	3000	890	20.0	900	60.0	1000	4840.37	6192	6192
55	P176	355	355	4000	3000	1040	20.0	900	60.0	1000	4840.37	6092	6092
56	P177	355	355	4000	3000	1190	20.0	900	60.0	1000	4840.37	6077	6077
57	P181	355	355	12000	3000	290	20.0	900	60.0	1000	4840.37	6088	18264
58	P182	355	355	12000	3000	440	20.0	900	60.0	1000	4840.37	6299	18897
59	P183	355	355	12000	3000	590	20.0	900	60.0	1000	4840.37	6387	19161
60	P184	355	355	12000	3000	740	20.0	900	60.0	1000	4840.37	6458	19374
61	P185	355	355	12000	3000	890	20.0	900	60.0	1000	4840.37	6474	19422
62	P186	355	355	12000	3000	1040	20.0	900	60.0	1000	4840.37	6144	18432
63	P187	355	355	12000	3000	1190	20.0	900	60.0	1000	4840.37	5835	17505
64	P1101	355	355	8000	3000	298	20.0	900	60.0	1000	67.96	6043	12086
65	P1102	355	355	8000	3000	448	20.0	900	60.0	1000	67.96	6113	12226
66	P1103	355	355	8000	3000	598	20.0	900	60.0	1000	67.96	6064	12128
67	P1104	355	355	8000	3000	748	20.0	900	60.0	1000	67.96	6126	12252
68	P1105	355	355	8000	3000	898	20.0	900	60.0	1000	67.96	6118	12236
69	P1106	355	355	8000	3000	1048	20.0	900	60.0	1000	67.96	6139	12278
70	P1107	355	355	8000	3000	1198	20.0	900	60.0	1000	67.96	6155	12310
71	P1201	355	355	8000	3000	270	20.0	900	60.0	1000	30979.60	7840	15680
72	P1202	355	355	8000	3000	420	20.0	900	60.0	1000	30979.60	7640	15280
73	P1203	355	355	8000	3000	570	20.0	900	60.0	1000	30979.60	7109	14218
74	P1204	355	355	8000	3000	720	20.0	900	60.0	1000	30979.60	6767	13534
75	P1205	355	355	8000	3000	870	20.0	900	60.0	1000	30979.60	6148	12296
76	P1206	355	355	8000	3000	1020	20.0	900	60.0	1000	30979.60	5672	11344
77	P1207	355	355	8000	3000	1170	20.0	900	60.0	1000	30979.60	5700	11400
78	P1301	355	355	8000	3000	275	20.0	900	60.0	1000	57562.80	7760	15520

continued on next page

continued from previous page

#	Specimen	f_{yw} [N/mm^2]	f_{yf} [N/mm^2]	a [mm]	h_w [mm]	b_1 [mm]	t_w [mm]	b_f [mm]	t_f [mm]	s_s [mm]	$I_{s\ell,1}$ [cm^4]	F_u [kN]	M_u [kNm]
79	P1302	355	355	8000	3000	425	20.0	900	60.0	1000	57562.80	7568	15136
80	P1303	355	355	8000	3000	575	20.0	900	60.0	1000	57562.80	7022	14044
81	P1304	355	355	8000	3000	725	20.0	900	60.0	1000	57562.80	6662	13324
82	P1305	355	355	8000	3000	875	20.0	900	60.0	1000	57562.80	6076	12152
83	P1306	355	355	8000	3000	1025	20.0	900	60.0	1000	57562.80	5673	11346
84	P1307	355	355	8000	3000	1175	20.0	900	60.0	1000	57562.80	5698	11396
85	P1401	355	355	4000	3000	298	20.0	900	60.0	1000	67.96	6596	6596
86	P1402	355	355	4000	3000	448	20.0	900	60.0	1000	67.96	6690	6690
87	P1403	355	355	4000	3000	598	20.0	900	60.0	1000	67.96	6615	6615
88	P1404	355	355	4000	3000	748	20.0	900	60.0	1000	67.96	6702	6702
89	P1405	355	355	4000	3000	898	20.0	900	60.0	1000	67.96	6639	6639
90	P1406	355	355	4000	3000	1048	20.0	900	60.0	1000	67.96	6723	6723
91	P1407	355	355	4000	3000	1198	20.0	900	60.0	1000	67.96	6677	6677
92	P1501	355	355	4000	3000	270	20.0	900	60.0	1000	30979.60	8685	8685
93	P1502	355	355	4000	3000	420	20.0	900	60.0	1000	30979.60	8385	8385
94	P1503	355	355	4000	3000	570	20.0	900	60.0	1000	30979.60	7855	7855
95	P1504	355	355	4000	3000	720	20.0	900	60.0	1000	30979.60	7533	7533
96	P1505	355	355	4000	3000	870	20.0	900	60.0	1000	30979.60	6758	6758
97	P1506	355	355	4000	3000	1020	20.0	900	60.0	1000	30979.60	6005	6005
98	P1507	355	355	4000	3000	1170	20.0	900	60.0	1000	30979.60	6001	6001
99	P1601	355	355	4000	3000	275	20.0	900	60.0	1000	57562.80	8633	8633
100	P1602	355	355	4000	3000	425	20.0	900	60.0	1000	57562.80	8311	8311
101	P1603	355	355	4000	3000	575	20.0	900	60.0	1000	57562.80	7757	7757
102	P1604	355	355	4000	3000	725	20.0	900	60.0	1000	57562.80	7402	7402
103	P1605	355	355	4000	3000	875	20.0	900	60.0	1000	57562.80	6669	6669
104	P1606	355	355	4000	3000	1025	20.0	900	60.0	1000	57562.80	6011	6011
105	P1607	355	355	4000	3000	1175	20.0	900	60.0	1000	57562.80	6006	6006
106	P1701	355	355	12000	3000	298	20.0	900	60.0	1000	67.96	5766	17298
107	P1702	355	355	12000	3000	448	20.0	900	60.0	1000	67.96	5828	17484
108	P1703	355	355	12000	3000	598	20.0	900	60.0	1000	67.96	5796	17388
109	P1704	355	355	12000	3000	748	20.0	900	60.0	1000	67.96	5824	17472
110	P1705	355	355	12000	3000	898	20.0	900	60.0	1000	67.96	5812	17436
111	P1706	355	355	12000	3000	1048	20.0	900	60.0	1000	67.96	5835	17505
112	P1707	355	355	12000	3000	1198	20.0	900	60.0	1000	67.96	5844	17532
113	P1801	355	355	12000	3000	270	20.0	900	60.0	1000	30979.60	7255	21765
114	P1802	355	355	12000	3000	420	20.0	900	60.0	1000	30979.60	7377	22131
115	P1803	355	355	12000	3000	570	20.0	900	60.0	1000	30979.60	7021	21063
116	P1804	355	355	12000	3000	720	20.0	900	60.0	1000	30979.60	6871	20613
117	P1805	355	355	12000	3000	870	20.0	900	60.0	1000	30979.60	6443	19329
118	P1806	355	355	12000	3000	1020	20.0	900	60.0	1000	30979.60	5642	16926
119	P1807	355	355	12000	3000	1170	20.0	900	60.0	1000	30979.60	5569	16707
120	P1901	355	355	12000	3000	275	20.0	900	60.0	1000	57562.80	7169	21507
121	P1902	355	355	12000	3000	425	20.0	900	60.0	1000	57562.80	7304	21912
122	P1903	355	355	12000	3000	575	20.0	900	60.0	1000	57562.80	6898	20694
123	P1904	355	355	12000	3000	725	20.0	900	60.0	1000	57562.80	6642	19926
124	P1905	355	355	12000	3000	875	20.0	900	60.0	1000	57562.80	6119	18357
125	P1906	355	355	12000	3000	1025	20.0	900	60.0	1000	57562.80	5519	16557
126	P1907	355	355	12000	3000	1175	20.0	900	60.0	1000	57562.80	5548	16644
127	P2001	355	355	4000	2000	485	14.0	900	40.0	500	14887.40	2923	2923
128	P2002	355	355	4000	2000	485	16.0	900	40.0	500	16376.70	3494	3494
129	P2003	355	355	4000	2000	485	20.0	900	40.0	500	19116.00	4709	4709
130	P2004	355	355	8000	2000	485	14.0	900	40.0	500	14887.40	2830	5660
131	P2005	355	355	8000	2000	485	16.0	900	40.0	500	16376.70	3452	6904
132	P2006	355	355	8000	2000	485	20.0	900	40.0	500	19116.00	4896	9792
133	P2007	355	355	4000	2000	485	14.0	900	120.0	500	14887.40	4487	4487
134	P2008	355	355	4000	2000	485	16.0	900	120.0	500	16376.70	5457	5457
135	P2009	355	355	4000	2000	485	20.0	900	120.0	500	19116.00	7618	7618
136	P2010	355	355	8000	2000	485	14.0	900	120.0	500	14887.40	4377	8754
137	P2011	355	355	8000	2000	485	16.0	900	120.0	500	16376.70	5359	10718
138	P2012	355	355	8000	2000	485	20.0	900	120.0	500	19116.00	7482	14964
139	P2013	355	355	4000	2000	485	14.0	900	40.0	1000	14887.40	4031	4031
140	P2014	355	355	4000	2000	485	16.0	900	40.0	1000	16376.70	4910	4910
141	P2015	355	355	4000	2000	485	20.0	900	40.0	1000	19116.00	6779	6779
142	P2016	355	355	8000	2000	485	14.0	900	40.0	1000	14887.40	3817	7634
143	P2017	355	355	8000	2000	485	16.0	900	40.0	1000	16376.70	5152	10304
144	P2018	355	355	8000	2000	485	20.0	900	40.0	1000	19116.00	7294	14588
145	P2019	355	355	4000	2000	485	14.0	900	120.0	1000	14887.40	4939	4939
146	P2020	355	355	4000	2000	485	16.0	900	120.0	1000	16376.70	6035	6035
147	P2021	355	355	4000	2000	485	20.0	900	120.0	1000	19116.00	8414	8414
148	P2022	355	355	8000	2000	485	14.0	900	120.0	1000	14887.40	4684	9368
149	P2023	355	355	8000	2000	485	16.0	900	120.0	1000	16376.70	5765	11530
150	P2024	355	355	8000	2000	485	20.0	900	120.0	1000	19116.00	8119	16238
151	P2025	355	355	4000	2000	485	14.0	900	40.0	2000	14887.40	8048	8048
152	P2026	355	355	4000	2000	485	16.0	900	40.0	2000	16376.70	9812	9812
153	P2027	355	355	4000	2000	485	20.0	900	40.0	2000	19116.00	13558	13558
154	P2028	355	355	8000	2000	485	14.0	900	40.0	2000	14887.40	5195	10390
155	P2029	355	355	8000	2000	485	16.0	900	40.0	2000	16376.70	6635	13270
156	P2030	355	355	8000	2000	485	20.0	900	40.0	2000	19116.00	8570	17140
157	P2031	355	355	4000	2000	485	14.0	900	120.0	2000	14887.40	9837	9837

continued on next page

continued from previous page

#	Specimen	f_{yw} [N/mm^2]	f_{yf} [N/mm^2]	a [mm]	h_w [mm]	b_1 [mm]	t_w [mm]	b_f [mm]	t_f [mm]	s_s [mm]	$I_{s\ell,1}$ [cm^4]	F_u [kN]	M_u [kNm]
158	P2032	355	355	4000	2000	485	16.0	900	120.0	2000	16376.70	12039	12039
159	P2033	355	355	4000	2000	485	20.0	900	120.0	2000	19116.00	16788	16788
160	P2034	355	355	8000	2000	485	14.0	900	120.0	2000	14887.40	5810	11620
161	P2035	355	355	8000	2000	485	16.0	900	120.0	2000	16376.70	7164	14328
162	P2036	355	355	8000	2000	485	20.0	900	120.0	2000	19116.00	10006	20012
163	P2037	355	355	4000	2000	185	14.0	900	40.0	500	14887.40	3611	3611
164	P2038	355	355	4000	2000	185	16.0	900	40.0	500	16036.20	4303	4303
165	P2039	355	355	4000	2000	185	20.0	900	40.0	500	18223.60	5728	5728
166	P2040	355	355	8000	2000	185	14.0	900	40.0	500	14887.40	3427	6854
167	P2041	355	355	8000	2000	185	16.0	900	40.0	500	16036.20	4121	8242
168	P2042	355	355	8000	2000	185	20.0	900	40.0	500	18223.60	5483	10966
169	P2043	355	355	4000	2000	185	14.0	900	120.0	500	14887.40	4906	4906
170	P2044	355	355	4000	2000	185	16.0	900	120.0	500	16036.20	5922	5922
171	P2045	355	355	4000	2000	185	20.0	900	120.0	500	18223.60	8047	8047
172	P2046	355	355	8000	2000	185	14.0	900	120.0	500	14887.40	4406	8812
173	P2047	355	355	8000	2000	185	16.0	900	120.0	500	16036.20	5324	10648
174	P2048	355	355	8000	2000	185	20.0	900	120.0	500	18223.60	7418	14836
175	P2049	355	355	4000	2000	185	14.0	900	40.0	1000	14887.40	4394	4394
176	P2050	355	355	4000	2000	185	16.0	900	40.0	1000	16036.20	5323	5323
177	P2051	355	355	4000	2000	185	20.0	900	40.0	1000	18223.60	7253	7253
178	P2052	355	355	8000	2000	185	14.0	900	40.0	1000	14887.40	3905	7810
179	P2053	355	355	8000	2000	185	16.0	900	40.0	1000	16036.20	4692	9384
180	P2054	355	355	8000	2000	185	20.0	900	40.0	1000	18223.60	6252	12504
181	P2055	355	355	4000	2000	185	14.0	900	120.0	1000	14887.40	5142	5142
182	P2056	355	355	4000	2000	185	16.0	900	120.0	1000	16036.20	6230	6230
183	P2057	355	355	4000	2000	185	20.0	900	120.0	1000	18223.60	8517	8517
184	P2058	355	355	8000	2000	185	14.0	900	120.0	1000	14887.40	4508	9016
185	P2059	355	355	8000	2000	185	16.0	900	120.0	1000	16036.20	5482	10964
186	P2060	355	355	8000	2000	185	20.0	900	120.0	1000	18223.60	7748	15496
187	P2061	355	355	4000	2000	185	14.0	900	40.0	2000	14887.40	8668	8668
188	P2062	355	355	4000	2000	185	16.0	900	40.0	2000	16036.20	10552	10552
189	P2063	355	355	4000	2000	185	20.0	900	40.0	2000	18223.60	14441	14441
190	P2064	355	355	8000	2000	185	14.0	900	40.0	2000	14887.40	4328	8656
191	P2065	355	355	8000	2000	185	16.0	900	40.0	2000	16036.20	5604	11208
192	P2066	355	355	8000	2000	185	20.0	900	40.0	2000	18223.60	6926	13852
193	P2067	355	355	4000	2000	185	14.0	900	120.0	2000	14887.40	10158	10158
194	P2068	355	355	4000	2000	185	16.0	900	120.0	2000	16036.20	12321	12321
195	P2069	355	355	4000	2000	185	20.0	900	120.0	2000	18223.60	16910	16910
196	P2070	355	355	8000	2000	185	14.0	900	120.0	2000	14887.40	4842	9684
197	P2071	355	355	8000	2000	185	16.0	900	120.0	2000	16036.20	5912	11824
198	P2072	355	355	8000	2000	185	20.0	900	120.0	2000	18223.60	8574	17148
199	P3001	355	355	6000	3000	735	16.0	1000	40.0	1000	16376.70	4167	6251
200	P3002	355	355	6000	3000	735	20.0	1000	40.0	1000	19116.00	5888	8832
201	P3003	355	355	6000	3000	735	25.0	1000	40.0	1000	22045.10	8455	12683
202	P3004	355	355	6000	3000	735	16.0	1000	120.0	1000	16376.70	5311	7967
203	P3005	355	355	6000	3000	735	20.0	1000	120.0	1000	19116.00	7598	11397
204	P3006	355	355	6000	3000	735	25.0	1000	120.0	1000	22045.10	10733	16100
205	P3007	355	355	8000	3000	735	16.0	1000	40.0	1000	16376.70	4075	8150
206	P3008	355	355	8000	3000	735	20.0	1000	40.0	1000	19116.00	6027	12054
207	P3009	355	355	8000	3000	735	25.0	1000	40.0	1000	22045.10	10295	20590
208	P3010	355	355	8000	3000	735	16.0	1000	120.0	1000	16376.70	5287	10574
209	P3011	355	355	8000	3000	735	20.0	1000	120.0	1000	19116.00	7532	15064
210	P3012	355	355	8000	3000	735	25.0	1000	120.0	1000	22045.10	10595	21190
211	P3013	355	355	6000	3000	735	16.0	1000	40.0	2000	16376.70	5433	8150
212	P3014	355	355	6000	3000	735	20.0	1000	40.0	2000	19116.00	7835	11753
213	P3015	355	355	6000	3000	735	25.0	1000	40.0	2000	22045.10	11791	17687
214	P3016	355	355	6000	3000	735	16.0	1000	120.0	2000	16376.70	6384	9576
215	P3017	355	355	6000	3000	735	20.0	1000	120.0	2000	19116.00	9524	14286
216	P3018	355	355	6000	3000	735	25.0	1000	120.0	2000	22045.10	14188	21282
217	P3019	355	355	8000	3000	735	16.0	1000	40.0	2000	16376.70	5211	10422
218	P3020	355	355	8000	3000	735	20.0	1000	40.0	2000	19116.00	8474	16948
219	P3021	355	355	8000	3000	735	25.0	1000	40.0	2000	22045.10	11398	22796
220	P3022	355	355	8000	3000	735	16.0	1000	120.0	2000	16376.70	6415	12830
221	P3023	355	355	8000	3000	735	20.0	1000	120.0	2000	19116.00	9595	19190
222	P3024	355	355	8000	3000	735	25.0	1000	120.0	2000	22045.10	13787	27574
223	P3025	355	355	6000	3000	735	16.0	1000	40.0	3000	16376.70	6635	9953
224	P3026	355	355	6000	3000	735	20.0	1000	40.0	3000	19116.00	9528	14292
225	P3027	355	355	6000	3000	735	25.0	1000	40.0	3000	22045.10	14774	22161
226	P3028	355	355	6000	3000	735	16.0	1000	120.0	3000	16376.70	7650	11475
227	P3029	355	355	6000	3000	735	20.0	1000	120.0	3000	19116.00	11555	17333
228	P3030	355	355	6000	3000	735	25.0	1000	120.0	3000	22045.10	17734	26601
229	P3031	355	355	8000	3000	735	16.0	1000	40.0	3000	16376.70	6060	12120
230	P3032	355	355	8000	3000	735	20.0	1000	40.0	3000	19116.00	10666	21332
231	P3033	355	355	8000	3000	735	25.0	1000	40.0	3000	22045.10	12424	24848
232	P3034	355	355	8000	3000	735	16.0	1000	120.0	3000	16376.70	7473	14946
233	P3035	355	355	8000	3000	735	20.0	1000	120.0	3000	19116.00	11606	23212
234	P3036	355	355	8000	3000	735	25.0	1000	120.0	3000	22045.10	15939	31878
235	P3037	355	355	6000	3000	285	16.0	1000	40.0	1000	16376.70	5389	8084
236	P3038	355	355	6000	3000	285	20.0	1000	40.0	1000	19116.00	7319	10979

continued on next page

continued from previous page

#	Specimen	f_{yw} [N/mm^2]	f_{yf} [N/mm^2]	a [mm]	h_w [mm]	b_1 [mm]	t_w [mm]	b_f [mm]	t_f [mm]	s_s [mm]	$I_{s\ell,1}$ [cm^4]	F_u [kN]	M_u [kNm]
237	P3039	355	355	6000	3000	285	25.0	1000	40.0	1000	21729.40	9832	14748
238	P3040	355	355	6000	3000	285	16.0	1000	120.0	1000	16376.70	6503	9755
239	P3041	355	355	6000	3000	285	20.0	1000	120.0	1000	19116.00	8708	13062
240	P3042	355	355	6000	3000	285	25.0	1000	120.0	1000	21729.40	11609	17414
241	P3043	355	355	8000	3000	285	16.0	1000	40.0	1000	16376.70	5093	10186
242	P3044	355	355	8000	3000	285	20.0	1000	40.0	1000	19116.00	6833	13666
243	P3045	355	355	8000	3000	285	25.0	1000	40.0	1000	21729.40	8927	17854
244	P3046	355	355	8000	3000	285	16.0	1000	120.0	1000	16376.70	5991	11982
245	P3047	355	355	8000	3000	285	20.0	1000	120.0	1000	19116.00	7998	15996
246	P3048	355	355	8000	3000	285	25.0	1000	120.0	1000	21729.40	10922	21844
247	P3049	355	355	6000	3000	285	16.0	1000	40.0	2000	16376.70	6443	9665
248	P3050	355	355	6000	3000	285	20.0	1000	40.0	2000	19116.00	8840	13260
249	P3051	355	355	6000	3000	285	25.0	1000	40.0	2000	21729.40	11738	17607
250	P3052	355	355	6000	3000	285	16.0	1000	120.0	2000	16376.70	7093	10640
251	P3053	355	355	6000	3000	285	20.0	1000	120.0	2000	19116.00	9770	14655
252	P3054	355	355	6000	3000	285	25.0	1000	120.0	2000	21729.40	13203	19805
253	P3055	355	355	8000	3000	285	16.0	1000	40.0	2000	16376.70	5801	11602
254	P3056	355	355	8000	3000	285	20.0	1000	40.0	2000	19116.00	7692	15384
255	P3057	355	355	8000	3000	285	25.0	1000	40.0	2000	21729.40	9813	19626
256	P3058	355	355	8000	3000	285	16.0	1000	120.0	2000	16376.70	6514	13028
257	P3059	355	355	8000	3000	285	20.0	1000	120.0	2000	19116.00	8742	17484
258	P3060	355	355	8000	3000	285	25.0	1000	120.0	2000	21729.40	12071	24142
259	P3061	355	355	6000	3000	285	16.0	1000	40.0	3000	16376.70	7129	10694
260	P3062	355	355	6000	3000	285	20.0	1000	40.0	3000	19116.00	9860	14790
261	P3063	355	355	6000	3000	285	25.0	1000	40.0	3000	21729.40	13124	19686
262	P3064	355	355	6000	3000	285	16.0	1000	120.0	3000	16376.70	7822	11733
263	P3065	355	355	6000	3000	285	20.0	1000	120.0	3000	19116.00	10821	16232
264	P3066	355	355	6000	3000	285	25.0	1000	120.0	3000	21729.40	14761	22142
265	P3067	355	355	8000	3000	285	16.0	1000	40.0	3000	16376.70	6290	12580
266	P3068	355	355	8000	3000	285	20.0	1000	40.0	3000	19116.00	8272	16544
267	P3069	355	355	8000	3000	285	25.0	1000	40.0	3000	21729.40	10531	21062
268	P3070	355	355	8000	3000	285	16.0	1000	120.0	3000	16376.70	7027	14054
269	P3071	355	355	8000	3000	285	20.0	1000	120.0	3000	19116.00	9536	19072
270	P3072	355	355	8000	3000	285	25.0	1000	120.0	3000	21729.40	13149	26298
271	P4001	355	355	6000	4000	985	20.0	1200	60.0	1000	19116.00	6161	9242
272	P4002	355	355	6000	4000	985	25.0	1200	60.0	1000	22045.10	8607	12911
273	P4003	355	355	6000	4000	985	30.0	1200	60.0	1000	24503.70	11236	16854
274	P4004	355	355	6000	4000	985	20.0	1200	150.0	1000	19116.00	7731	11597
275	P4005	355	355	6000	4000	985	25.0	1200	150.0	1000	22045.10	10952	16428
276	P4006	355	355	6000	4000	985	30.0	1200	150.0	1000	24503.70	14490	21735
277	P4007	355	355	8000	4000	985	20.0	1200	60.0	1000	19116.00	5970	11940
278	P4008	355	355	8000	4000	985	25.0	1200	60.0	1000	22045.10	8465	16930
279	P4009	355	355	8000	4000	985	30.0	1200	60.0	1000	24503.70	11366	22732
280	P4010	355	355	8000	4000	985	20.0	1200	150.0	1000	19116.00	7594	15188
281	P4011	355	355	8000	4000	985	25.0	1200	150.0	1000	22045.10	10874	21748
282	P4012	355	355	8000	4000	985	30.0	1200	150.0	1000	24503.70	14393	28786
283	P4013	355	355	6000	4000	985	20.0	1200	60.0	2000	19116.00	7911	11867
284	P4014	355	355	6000	4000	985	25.0	1200	60.0	2000	22045.10	11469	17204
285	P4015	355	355	6000	4000	985	30.0	1200	60.0	2000	24503.70	15487	23231
286	P4016	355	355	6000	4000	985	20.0	1200	150.0	2000	19116.00	8890	13335
287	P4017	355	355	6000	4000	985	25.0	1200	150.0	2000	22045.10	13009	19514
288	P4018	355	355	6000	4000	985	30.0	1200	150.0	2000	24503.70	17766	26649
289	P4019	355	355	8000	4000	985	20.0	1200	60.0	2000	19116.00	7546	15092
290	P4020	355	355	8000	4000	985	25.0	1200	60.0	2000	22045.10	11194	22388
291	P4021	355	355	8000	4000	985	30.0	1200	60.0	2000	24503.70	16122	32244
292	P4022	355	355	8000	4000	985	20.0	1200	150.0	2000	19116.00	8693	17386
293	P4023	355	355	8000	4000	985	25.0	1200	150.0	2000	22045.10	13046	26092
294	P4024	355	355	8000	4000	985	30.0	1200	150.0	2000	24503.70	17868	35736
295	P4025	355	355	6000	4000	985	20.0	1200	60.0	3000	19116.00	9630	14445
296	P4026	355	355	6000	4000	985	25.0	1200	60.0	3000	22045.10	14119	21179
297	P4027	355	355	6000	4000	985	30.0	1200	60.0	3000	24503.70	19244	28866
298	P4028	355	355	6000	4000	985	20.0	1200	150.0	3000	19116.00	10439	15659
299	P4029	355	355	6000	4000	985	25.0	1200	150.0	3000	22045.10	15528	23292
300	P4030	355	355	6000	4000	985	30.0	1200	150.0	3000	24503.70	21678	32517
301	P4031	355	355	8000	4000	985	20.0	1200	60.0	3000	19116.00	8851	17702
302	P4032	355	355	8000	4000	985	25.0	1200	60.0	3000	22045.10	13409	26818
303	P4033	355	355	8000	4000	985	30.0	1200	60.0	3000	24503.70	20504	41008
304	P4034	355	355	8000	4000	985	20.0	1200	150.0	3000	19116.00	9887	19774
305	P4035	355	355	8000	4000	985	25.0	1200	150.0	3000	22045.10	15514	31028
306	P4036	355	355	8000	4000	985	30.0	1200	150.0	3000	24503.70	21913	43826
307	P4037	355	355	6000	4000	385	20.0	1200	60.0	1000	19116.00	7481	11222
308	P4038	355	355	6000	4000	385	25.0	1200	60.0	1000	22045.10	10028	15042
309	P4039	355	355	6000	4000	385	30.0	1200	60.0	1000	24503.70	12884	19326
310	P4040	355	355	6000	4000	385	20.0	1200	150.0	1000	19116.00	9676	14514
311	P4041	355	355	6000	4000	385	25.0	1200	150.0	1000	22045.10	13278	19917
312	P4042	355	355	6000	4000	385	30.0	1200	150.0	1000	24503.70	17009	25514
313	P4043	355	355	8000	4000	385	20.0	1200	60.0	1000	19116.00	7119	14238
314	P4044	355	355	8000	4000	385	25.0	1200	60.0	1000	22045.10	9826	19652
315	P4045	355	355	8000	4000	385	30.0	1200	60.0	1000	24503.70	12777	25554

continued on next page

continued from previous page

#	Specimen	f_{yw} [N/mm^2]	f_{yf} [N/mm^2]	a [mm]	h_w [mm]	b_1 [mm]	t_w [mm]	b_f [mm]	t_f [mm]	s_s [mm]	$I_{s\ell,1}$ [cm^4]	F_u [kN]	M_u [kNm]
316	P4046	355	355	8000	4000	385	20.0	1200	150.0	1000	19116.00	9252	18504
317	P4047	355	355	8000	4000	385	25.0	1200	150.0	1000	22045.10	12528	25056
318	P4048	355	355	8000	4000	385	30.0	1200	150.0	1000	24503.70	15973	31946
319	P4049	355	355	6000	4000	385	20.0	1200	60.0	2000	19116.00	10017	15026
320	P4050	355	355	6000	4000	385	25.0	1200	60.0	2000	22045.10	13626	20439
321	P4051	355	355	6000	4000	385	30.0	1200	60.0	2000	24503.70	17522	26283
322	P4052	355	355	6000	4000	385	20.0	1200	150.0	2000	19116.00	11017	16526
323	P4053	355	355	6000	4000	385	25.0	1200	150.0	2000	22045.10	15204	22806
324	P4054	355	355	6000	4000	385	30.0	1200	150.0	2000	24503.70	19421	29132
325	P4055	355	355	8000	4000	385	20.0	1200	60.0	2000	19116.00	9085	18170
326	P4056	355	355	8000	4000	385	25.0	1200	60.0	2000	22045.10	12415	24830
327	P4057	355	355	8000	4000	385	30.0	1200	60.0	2000	24503.70	15914	31828
328	P4058	355	355	8000	4000	385	20.0	1200	150.0	2000	19116.00	10239	20478
329	P4059	355	355	8000	4000	385	25.0	1200	150.0	2000	22045.10	13844	27688
330	P4060	355	355	8000	4000	385	30.0	1200	150.0	2000	24503.70	17690	35380
331	P4061	355	355	6000	4000	385	20.0	1200	60.0	3000	19116.00	11175	16763
332	P4062	355	355	6000	4000	385	25.0	1200	60.0	3000	22045.10	15478	23217
333	P4063	355	355	6000	4000	385	30.0	1200	60.0	3000	24503.70	20088	30132
334	P4064	355	355	6000	4000	385	20.0	1200	150.0	3000	19116.00	12079	18119
335	P4065	355	355	6000	4000	385	25.0	1200	150.0	3000	22045.10	16882	25323
336	P4066	355	355	6000	4000	385	30.0	1200	150.0	3000	24503.70	21818	32727
337	P4067	355	355	8000	4000	385	20.0	1200	60.0	3000	19116.00	10119	20238
338	P4068	355	355	8000	4000	385	25.0	1200	60.0	3000	22045.10	13831	27662
339	P4069	355	355	8000	4000	385	30.0	1200	60.0	3000	24503.70	17578	35156
340	P4070	355	355	8000	4000	385	20.0	1200	150.0	3000	19116.00	11156	22312
341	P4071	355	355	8000	4000	385	25.0	1200	150.0	3000	22045.10	15202	30404
342	P4072	355	355	8000	4000	385	30.0	1200	150.0	3000	24503.70	19480	38960
343	P5001	355	355	8000	5000	1235	25.0	1200	60.0	1000	22045.10	8283	16566
344	P5002	355	355	8000	5000	1235	30.0	1200	60.0	1000	24503.70	10860	21720
345	P5003	355	355	8000	5000	1235	25.0	1200	150.0	1000	22045.10	10551	21102
346	P5004	355	355	8000	5000	1235	30.0	1200	150.0	1000	24503.70	13976	27952
347	P5005	355	355	8000	5000	1235	25.0	1200	60.0	2000	22045.10	10304	20608
348	P5006	355	355	8000	5000	1235	30.0	1200	60.0	2000	24503.70	13924	27848
349	P5007	355	355	8000	5000	1235	25.0	1200	150.0	2000	22045.10	12135	24270
350	P5008	355	355	8000	5000	1235	30.0	1200	150.0	2000	24503.70	16767	33534
351	P5009	355	355	8000	5000	1235	25.0	1200	60.0	3000	22045.10	11851	23702
352	P5010	355	355	8000	5000	1235	30.0	1200	60.0	3000	24503.70	16158	32316
353	P5011	355	355	8000	5000	1235	25.0	1200	150.0	3000	22045.10	13784	27568
354	P5012	355	355	8000	5000	1235	30.0	1200	150.0	3000	24503.70	19750	39500
355	P5013	355	355	8000	5000	485	25.0	1200	60.0	1000	22045.10	9643	19286
356	P5014	355	355	8000	5000	485	30.0	1200	60.0	1000	24503.70	12528	25056
357	P5015	355	355	8000	5000	485	25.0	1200	150.0	1000	22045.10	12698	25396
358	P5016	355	355	8000	5000	485	30.0	1200	150.0	1000	24503.70	16353	32706
359	P5017	355	355	8000	5000	485	25.0	1200	60.0	2000	22045.10	12946	25892
360	P5018	355	355	8000	5000	485	30.0	1200	60.0	2000	24503.70	16808	33616
361	P5019	355	355	8000	5000	485	25.0	1200	150.0	2000	22045.10	14560	29120
362	P5020	355	355	8000	5000	485	30.0	1200	150.0	2000	24503.70	18644	37288
363	P5021	355	355	8000	5000	485	25.0	1200	60.0	3000	22045.10	14710	29420
364	P5022	355	355	8000	5000	485	30.0	1200	60.0	3000	24503.70	18751	37502
365	P5023	355	355	8000	5000	485	25.0	1200	150.0	3000	22045.10	16171	32342
366	P5024	355	355	8000	5000	485	30.0	1200	150.0	3000	24503.70	20684	41368
367	P4020-1	355	355	8000	4000	985	25.0	1200	60.0	2000	22045.10	9101	78202
368	P4020-2	355	355	8000	4000	985	25.0	1200	60.0	2000	22045.10	9167	90334
369	P4020-3	355	355	8000	4000	985	25.0	1200	60.0	2000	22045.10	9035	102071
370	P4020-4	355	355	8000	4000	985	25.0	1200	60.0	2000	22045.10	8478	112956
371	P4020-5	355	355	8000	4000	985	25.0	1200	60.0	2000	22045.10	6802	121604
372	P4020-6	355	355	8000	4000	985	25.0	1200	60.0	2000	22045.10	5600	132842
373	P4020-7	355	355	8000	4000	985	25.0	1200	60.0	2000	22045.10	6720	131125
374	P4020-8	355	355	8000	4000	985	25.0	1200	60.0	2000	22045.10	7840	127540
375	P4020-9	355	355	8000	4000	985	25.0	1200	60.0	2000	22045.10	8960	123234
376	P4020-10	355	355	8000	4000	985	25.0	1200	60.0	2000	22045.10	10080	115256
377	P4020-11	355	355	8000	4000	985	25.0	1200	60.0	2000	22045.10	9463	120321
378	P4020-12	355	355	8000	4000	985	25.0	1200	60.0	2000	22045.10	8215	126451
379	P4020-13	355	355	8000	4000	985	25.0	1200	60.0	2000	22045.10	10395	98124
380	P4023-1	355	355	8000	4000	985	25.0	1200	150.0	2000	22045.10	12667	145335
381	P4023-2	355	355	8000	4000	985	25.0	1200	150.0	2000	22045.10	12539	169078
382	P4023-3	355	355	8000	4000	985	25.0	1200	150.0	2000	22045.10	12395	192789
383	P4023-4	355	355	8000	4000	985	25.0	1200	150.0	2000	22045.10	12039	216078
384	P4023-5	355	355	8000	4000	985	25.0	1200	150.0	2000	22045.10	11718	239437
385	P4023-6	355	355	8000	4000	985	25.0	1200	150.0	2000	22045.10	6500	292060
386	P4023-7	355	355	8000	4000	985	25.0	1200	150.0	2000	22045.10	7800	289464
387	P4023-8	355	355	8000	4000	985	25.0	1200	150.0	2000	22045.10	9100	285943
388	P4023-9	355	355	8000	4000	985	25.0	1200	150.0	2000	22045.10	10400	280622
389	P4023-10	355	355	8000	4000	985	25.0	1200	150.0	2000	22045.10	11700	257257
390	P4023-11	355	355	8000	4000	985	25.0	1200	150.0	2000	22045.10	11781	241050
391	P4023-12	355	355	8000	4000	985	25.0	1200	150.0	2000	22045.10	10848	272039
392	P4023-13	355	355	8000	4000	985	25.0	1200	150.0	2000	22045.10	12337	182827
393	P4056-1	355	355	8000	4000	385	25.0	1200	60.0	2000	22045.10	11418	82836
394	P4056-2	355	355	8000	4000	385	25.0	1200	60.0	2000	22045.10	11151	94301

continued on next page

continued from previous page

#	Specimen	f_{yw} [N/mm^2]	f_{yf} [N/mm^2]	a [mm]	h_w [mm]	b_1 [mm]	t_w [mm]	b_f [mm]	t_f [mm]	s_s [mm]	$I_{s\ell,1}$ [cm^4]	F_u [kN]	M_u [kNm]
395	P4056-3	355	355	8000	4000	385	25.0	1200	60.0	2000	22045.10	10597	105194
396	P4056-4	355	355	8000	4000	385	25.0	1200	60.0	2000	22045.10	9108	114215
397	P4056-5	355	355	8000	4000	385	25.0	1200	60.0	2000	22045.10	7519	123038
398	P4056-6	355	355	8000	4000	385	25.0	1200	60.0	2000	22045.10	6200	125805
399	P4056-7	355	355	8000	4000	385	25.0	1200	60.0	2000	22045.10	7440	122143
400	P4056-8	355	355	8000	4000	385	25.0	1200	60.0	2000	22045.10	8680	117783
401	P4056-9	355	355	8000	4000	385	25.0	1200	60.0	2000	22045.10	9920	112489
402	P4056-10	355	355	8000	4000	385	25.0	1200	60.0	2000	22045.10	11160	104652
403	P4056-11	355	355	8000	4000	385	25.0	1200	60.0	2000	22045.10	9634	112496
404	P4056-12	355	355	8000	4000	385	25.0	1200	60.0	2000	22045.10	8375	118067
405	P4056-13	355	355	8000	4000	385	25.0	1200	60.0	2000	22045.10	11134	97085
406	P5005-1	355	355	8000	5000	1235	25.0	1200	60.0	2000	22045.10	5152	167052
407	P5005-2	355	355	8000	5000	1235	25.0	1200	60.0	2000	22045.10	9780	101560
408	P3021-1	355	355	8000	3000	735	25.0	1000	40.0	2000	22045.10	5699	57230
409	P3021-2	355	355	8000	3000	735	25.0	1000	40.0	2000	22045.10	8759	44518
410	P2030-1	355	355	8000	2000	485	20.0	900	40.0	2000	19116.00	4285	33474
411	P2030-2	355	355	8000	2000	485	20.0	900	40.0	2000	19116.00	6778	28755
412	P4019-1	355	355	8000	4000	985	20.0	1200	60.0	2000	19116.00	3773	125493
413	P4019-2	355	355	8000	4000	985	20.0	1200	60.0	2000	19116.00	6914	74829
414	P4021-1	355	355	8000	4000	985	30.0	1200	60.0	2000	24503.70	8061	143586
415	P4021-2	355	355	8000	4000	985	30.0	1200	60.0	2000	24503.70	14718	95435
416	P4032-1	355	355	8000	4000	985	25.0	1200	60.0	3000	22045.10	6705	135774
417	P4032-2	355	355	8000	4000	985	25.0	1200	60.0	3000	22045.10	15404	93807
418	P4002-1	355	355	6000	4000	985	25.0	1200	60.0	1000	22045.10	4304	130036
419	P4002-2	355	355	6000	4000	985	25.0	1200	60.0	1000	22045.10	8009	75014
420	P4026-1	355	355	6000	4000	985	25.0	1200	60.0	3000	22045.10	7060	134648
421	P4026-2	355	355	6000	4000	985	25.0	1200	60.0	3000	22045.10	12585	81877

C Proposal for a modification of EN 1993-1-5:2006

C.1 Reduced stress method

Based on the results from Chapter 6 it is proposed to modify Clause (5) of Chapter 10, EN 1993-1-5 [46]. In order to improve in general the layout of the verification procedure of Chapter 10, EN 1993-1-5, it is proposed to merge Clause (5) without replacement into Clause (2) as follows:

10 Reduced stress method

(2) For unstiffened or stiffened panels subjected to combined stresses $\sigma_{x,Ed}$, $\sigma_{z,Ed}$ and τ_{Ed} the resistance should satisfy:

$$\left(\frac{\sigma_{x,Ed}}{\rho_x \cdot f_y/\gamma_{M1}}\right)^2+\left(\frac{\sigma_{z,Ed}}{\rho_z \cdot f_y/\gamma_{M1}}\right)^2-V\cdot\left(\frac{\sigma_{x,Ed}}{\rho_x \cdot f_y/\gamma_{M1}}\right)\cdot\left(\frac{\sigma_{z,Ed}}{\rho_z \cdot f_y/\gamma_{M1}}\right)+3\cdot\left(\frac{\tau_{Ed}}{\chi_w \cdot f_y/\gamma_{M1}}\right)^2 \leq 1$$

where

$V = \rho_x \cdot \rho_z$ when $\sigma_{x,Ed}$ and $\sigma_{z,Ed}$ are both compression, else $V = 1$;

ρ_x is the reduction factor for longitudinal stresses from 4.5.4(1) taking into account column-like behaviour where relevant;

ρ_z is the reduction factor for transverse stresses from 4.5.4(1) taking into account column-like behaviour where relevant;

χ_w is the reduction factor for shear stresses from 5.3(1);

each calculated for the slenderness $\overline{\lambda}_p$ according to equation (10.2).

C.2 Effective width method

Based on the results from Chapter 6 it is proposed to modify Clause (1) of Sec. 7.2, EN 1993-1-5 [46], as follows:

7.2 Interaction between transverse force, bending moment and shear force

(1) If the girder is subjected to a concentrated transverse force acting on the compression flange in conjunction with bending moment and shear force, the resistance should satisfy:

$$\eta_2 + \overline{\eta}_1{}^{3.6} + \eta_{3,avg}{}^{1.6} \leq 1$$

where

$$\eta_2 = \frac{F_{Ed}}{F_{Rd}}$$

$$\overline{\eta}_1 = \frac{M_{Ed}}{M_{pl,Rd}}$$

$$\eta_{3,avg} = \frac{V_{Ed,avg}}{V_{b,Rd}} = \frac{|V_{Ed,max}| - 0.5 \cdot F_{Ed}}{V_{b,Rd}}$$

$M_{pl,Rd}$ is the design plastic resistance of the cross section consisting of the effective area of the flanges and the fully effective web irrespective of its section class.

$V_{Ed,avg}$ is the absolute value of the maximum design shear force adjacent to the centerline of the transverse loading less half of the design transverse force.

NOTE: If no transverse force is present section 7.1 should be applied.

In addition the requirements in sections 4.6, 5.5 and 6.6 should be met.